Volume 15, No. 5

November, 1963

SOVIET ATOMIC ENERGY

АТОМНАЯ ЭНЕРГИЯ
(ATOMNAYA ÉNERGIYA)

TRANSLATED FROM RUSSIAN

CONSULTANTS BUREAU

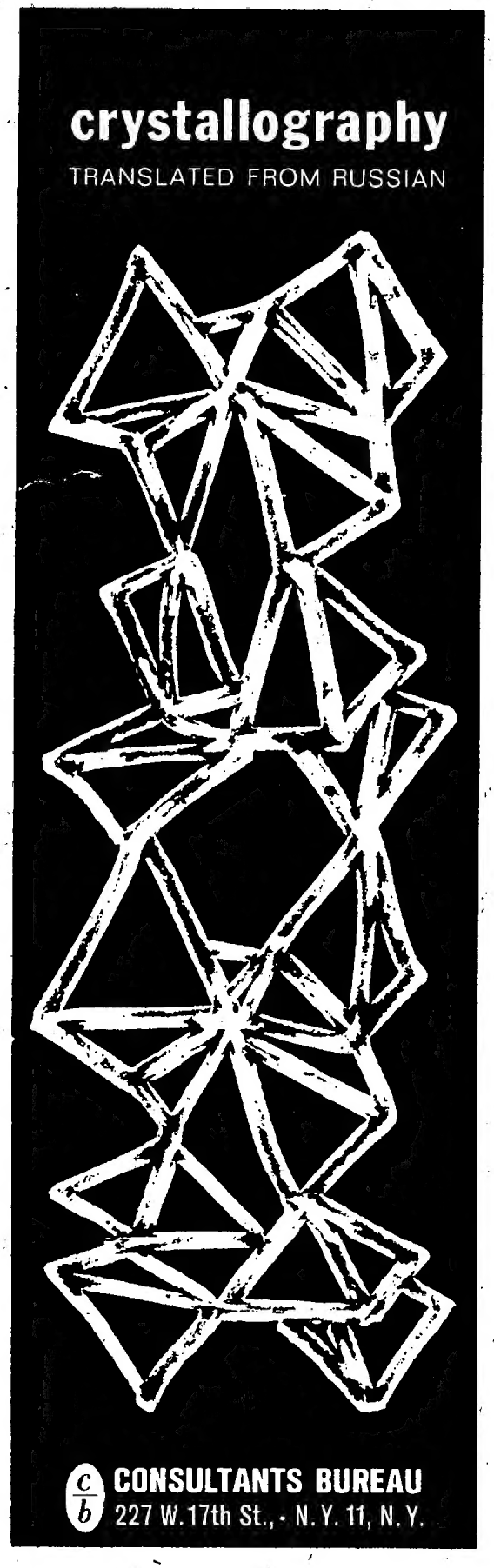

MECHANICAL TWINNING OF CRYSTALS

by M.V. Klassen-Neklyudova

In addition to studies of reorientation in response to mechanical stress, this comprehensive new work includes many effects related to mechanical twinning such as formation of reoriented regions in response to high temperatures, and to electric and magnetic fields. Discussions include experimental evidence on twinning with and without change of shape, lattice reconstruction in martensite type transformations, formation of twins by recrystallization, formation of reoriented regions in inhomogeneous deformation, and the macroscopic and microscopic theories of twinning.

228 pages **$19.50**

EFFECTS OF ULTRASOUND ON THE KINETICS OF CRYSTALLIZATION

by A.P. Kapustin

The first detailed survey of the more important experimental aspects of crystallization and dissolution in ultrasonic fields. Topics covered embrace all aspects of the effects of various frequencies and strengths of ultrasound on crystallization, emphasis being on experiments and methods that provide an understanding of the mechanisms involved. Primary topics are: Methods and Apparatus for Studying Crystallization and Dissolution in Ultrasonic Fields; A Brief Review of Work on the Interaction of Ultrasonics with Crystallizing or Dissolving Material; Crystallization Processes in Organic Compounds; Effects of Various Agents on Nucleation in an Ultrasonic Field; The Growth and Dissolution of Monocrystals.

65 pages **A Special Research Report** **$12.50**

CRYSTAL CHEMISTRY OF LARGE-CATION SILICATES

by N.V. Belov, et. al.

An expansion of the basic lectures which Academician Belov delivered in the United States — updated for the English edition. A lucid presentation by one of the world's greatest crystallographers of the systematics of silicates with Na, K, Ca, and other large cations — The Second "Chapter" of the crystal chemistry of silicates. Papers exclusively by Belov are: V.I. Vernadskii and Silicate Crystal Chemistry; The Second "Chapter" of Silicate Crystal Chemistry; Isomorphism Relations between Zirconium and Titanium; Oxygen-Silicon Chains and Ribbons in the Second "Chapter" of the Crystal Chemistry of Silicates; The Crystal Structure of Rhodonite $MnS.O_3$ Oxygen-Silicon Networks Based on Wollanstonite Chains and Xonotlite; and Molecular Sieves. The basic text is appended with 16 pertinent papers by Prof. Belov and his colleagues, reprinted from the cover-to-cover translation journals.

168 pages **$12.50**

CONTENTS UPON REQUEST

SOVIET ATOMIC ENERGY

A translation of **ATOMNAYA ÉNERGIYA**
A publication of the Academy of Sciences of the USSR

Vol. 15, No. 5 November, 1963

CONTENTS

	PAGE ENG.	PAGE RUSS.
The Effect of a Strong Magnetic Field on the Magnetohydrodynamic Stability of Plasma and the Containment of Charged Particles in the "Tokamak"—E. P. Gorbunov and K. A. Razumova	1105	363
Methods for the Calculation of the Radiational Thermal Output in the Body and Shielding of a Nuclear Reactor—D. L. Broder and K. K. Popkov	1113	370
Measurement of the Thermal Neutron Density Distribution Along the Radius of Sleeve-Shaped Fuel Elements—V. F. Belkin, B. P. Kochurov, and O. V. Shvedov	1121	377
Calculation of γ-Ray Energy Absorption in Heterogeneous Macro-Systems—B. M. Terent'ev, V. A. Él'tekov, and D. I. Golenko	1127	382
Measurement of Neutron Tissue Dose Outside Reactor Shielding—I. B. Keirim-Markus, V. T. Korneev, V. V. Markelov, and L. N. Uspenskii	1132	386
Kinetics of the Swelling Produced in Fissionable Materials by the Separation of the Gaseous Phase from a Supersaturated Solid Solution—V. M. Agranovich, E. Ya. Mikhlin, and L. P. Semenov	1140	393
Theory of the Coalescence of Gaseous Pores Under Swelling Conditions—L. P. Semenov	1155	404
LETTERS TO THE EDITOR		
The Motion of Isolated Charged Particles in a Magnetic Field with Helical Symmetry—V. M. Balebanov, B. I. Volkov, V. B. Glasko, A. L. Groshev, V. V. Kuznetsov, A. G. Sveshnikov, and N. N. Semashko	1162	409
Inelastic Scattering of 14-MeV Neutrons by Light Nuclei—E. M. Oparin, A. I. Saukov, and R. S. Shuvalov	1165	411
On the Design of a Neutron Spin Rotator—Yu. V. Taran	1168	413
Measurement of the U^{238} and Th^{232} Capture Cross Sections for Neutrons with Energies of 5-200 keV—V. A. Tolstikov, L. E. Sherman, and Yu. Ya. Stavisskii	1170	414
Cross Sections of the Inelastic Scattering of Neutrons with Energies of 0.4—1.2 MeV on Medium and Light Nuclei—N. P. Glazkov	1173	416
Dependence of the Mean Kinetic Energy of Fragments on the Fissionable Nucleus Mass—V. N. Okolovich, V. I. Bol'shov, L. D. Gordeeva, and G. N. Smirenkin	1177	419
Energy Distribution of γ-Radiation in a Material Medium—A. M. Sazonov and V. I. Sirvidas	1179	420
Obtaining the Radioactive Isotope Be^7 from Cyclotron Targets—I. F. Kolosova and I. V. Kolosov	1182	422
The Solubility of Uranium Tetrafluoride in Aqueous Solutions of Acids—Yu. A. Luk'yanychev and N. S. Nikolaev	1184	423

(continued)

Annual Subscription: $95 **Single Issue: $30** **Single Article: $15**

CONTENTS (continued)

	PAGE ENG.	PAGE RUSS.
An Apparatus for Determining the Solubility of Radioactive Substances at Elevated Temperatures and Pressures—V. V. Ivanenko, G. N. Kolodin, B. N. Melent'ev, and L. A. Pamfilova. . . .	1188	426
The Preparation of Certain Sulfides of Thorium by the Interaction of ThO_2 with Hydrogen Sulfide—G. V. Samsonov and G. D. Dubrovskaya	1191	428
Estimation of the Dose of Neutron Irradiation Capable of Changing the Mechanical Properties of Pure Metals—V. K. Adamovich	1194	430
Aerial Surveys of Uranium Deposits in Wooded Regions—V. I. Balabanov and A. L. Kovalevskii.	1197	432
NEWS OF SCIENCE AND TECHNOLOGY		
Conference on Reactions of Complex Nuclei—S. M. Polikanov.	1201	435
Conference on Interactions of High-Energy Photons—B. B. Govorkov and A. I. Lebedev	1202	436
The Second European "Vakuum" Symposium—E. Fischer	1206	438
Modernization of the VVR-S Reactor	1209	439
Brief Communications	1213	442
Commissioning of the World's First Reactor Power Station with an Organic-Moderator and Organic-Coolant Reactor—Yu. Arkhangel'skii and I. Kovalev.	1215	443
BIBLIOGRAPHY	1216	444

THE EFFECT OF A STRONG MAGNETIC FIELD ON THE MAGNETOHYDRODYNAMIC STABILITY OF PLASMA AND THE CONTAINMENT OF CHARGED PARTICLES IN THE "TOKAMAK"

E. P. Gorbunov and K. A. Razumova

Translated from Atomnaya Énergiya, Vol. 15, No. 5,
pp. 363-369, November, 1963
Original article submitted November 24, 1962

Results of an investigation of plasma in the toroidal apparatus TM-2 in a strong longitudinal magnetic field (up to 22 kOe) are described. It is shown that increasing the magnetic field sharply decreases the low frequency oscillations in the oscillograms of the loop voltage and discharge current derivative, and also weakens the interaction between the plasma and the walls of the discharge chamber.

For a large enough ratio of the longitudinal field intensity to the intensity of the current self-field, oscillations are not observed. According to radiointerferometric measurements, the mean electron density in this case hardly alters during the course of the operations. The conductivity reaches a value of about 10^{16} cgs.

1. Introduction

Studies of electrodeless discharges in a strong longitudinal magnetic field, carried out on the stellarator [1-3] and the "Tokamak"[4], have shown that in such systems the plasma becomes unstable for currents appreciably less than the critical current of Shafranov-Kruskal. It was established by a microwave probe method that the charged particles passed anomalously quickly from the body of the chamber to the walls.

In one of the most recent experiments carried out on the stellarator [5], it was shown that the electron density fall-off rate in the plasma was proportional to 1/H, where H is the intensity of the longitudinal magnetic field. The inclusion of supplementary stellarator windings did not alter this rate, although it reduced the amplitude of regular oscillations. The maximum value of the density was substantially higher for large magnetic fields. All this led to the conclusion that current-bearing plasma in a strong longitudinal magnetic field diffuses to the walls at an anomalously high rate from the very beginning of the process.

According to Spittser this increase in diffusion may be caused by the setting up of ionic waves.

A series of experiments on the "Tokamak" [6, 7] cast doubt on the existence of increased diffusion to the chamber walls. An explanation of the nature of the observed oscillations and the anomalously swift movement of particles from the current-bearing plasma stabilized by a strong longitudinal magnetic field constitutes a most important problem.

2. Experimental Arrangement

The measurements were carried out in the toroidal chamber TM-2 with a strong longitudinal magnetic field. The electrical scheme of the set-up is given in [8]. The vacuum chamber, as usual, was made of copper with two transverse and one longitudinal insulated joint. The inner diameter of the chamber was 25 cm and the outer 80 cm. Inside was located a bellows liner of stainless steel capable of independent evacuation.

The discharge aperture was limited by one stainless steel diaphragm with aperture diameter 16 cm. The center of the aperture was displaced 5 mm outwards from the chamber axis. The outer part of the diaphragm on the side bombarded by electrons was covered by a tungsten layer 0.5 mm thick. The liner was degassed by heating and discharges twice per minute.

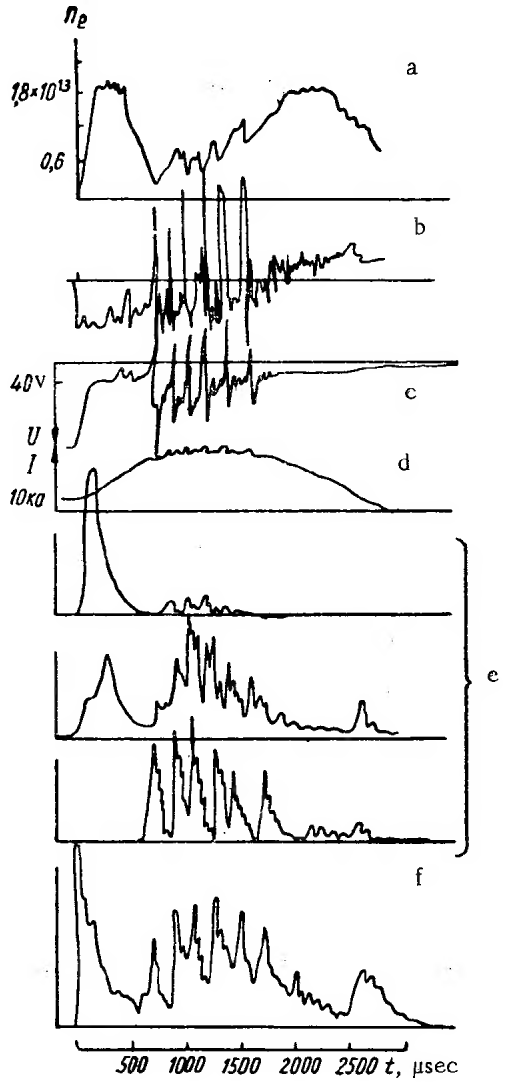

Fig. 1. Oscillograms for a typical unstable arrangement with $p = 5 \cdot 10^{-4}$ mm Hg; $I_{init} = 2.6 \cdot 10^7$ amp/sec ($E_{init} = 0.15$ V/cm), longitudinal magnetic field intensity H = 11 koe: 1) mean electron density; b) probe signal measuring the derivative of the azimuthal magnetic field; c) loop voltage; d) discharge current; e) light intensity of the spectral lines of hydrogen H_β (λ = 4860 A), carbon CII (λ = 4650 − 60 A), chromium CrI (λ = 4252 A); f) integrated intensity of illumination in the visible part of the spectrum, measured by photomultiplier.

The primary winding of the transformer was connected so that all the change in resistance of the gaseous loop showed up in the loop voltage, while the current in the majority of cases had a sinusoidal form. Hence we used the initial value of the gas current derivative as a parameter characterizing energy imparted to the discharge, rather than the electric field strength.

The discharge parameters could be changed within the following limits: initial hydrogen pressure p from $5 \cdot 10^{-4}$ to $3 \cdot 10^{-3}$ mm Hg; initial current derivative $\dot{I}_{init}$ from $0.2 \cdot 10^7$ to $8 \cdot 10^7$ amp/sec (electric field intensity E_{init} immediately after breakdown from 0.08 to 0.25 V/cm); longitudinal magnetic field intensity from 5 to 22 kOe.

Leakage fields within the chamber were not specially measured. They were apparently determined by the leakage field from the current in the liner and the field from the backward loop of the magnetic windings. The direction of the current in the backward windings was chosen so that the force acting on the plasma loop was directed towards the center of the torus.

The current, voltage, and light intensity of hydrogen and impurity lines were measured; hard X-radiation with quantum energy greater than 200 keV was recorded.* The fluctuating magnetic field was measured with the help of four coils disposed outside the liner at the inner surface of the copper chamber.

The method of determining the mean electron density in the plasma in "Tokamak" systems was described in [9]. Measurement was carried out in the millimeter wavelength range by radiointerferometry in the manner proposed by Warton for the study of plasma.

3. Description of a Characteristic Discharge Set-Up

Figure 1 shows typical discharge oscillograms for an arrangement with a fairly small magnetic field. The value of the mean electron density was calculated on the assumption that the plasma filled the whole inner aperture of the diaphragm evenly. A discharge of this kind may be separated into two characteristic stages in time.

After discharge in the gas, there are no strong oscillations in the circuit voltage for 500-800 μsec, although small fluctuations are observed in the magnetic probe. The mean electron density reaches a maximum value and for some time remains almost constant, while the spectral lines H_β and CIII are excited and then extinguished.

The second stage is characterized by the appearance of sharp oscillations in all the oscillograms, an increase in the light intensity of the impurity lines, and a fall-off in electron density followed by a fresh rise. The good synchronization of the separate sharp breaks in the oscillograms of the loop voltage and the magnetic probe with the bright flaring up of the wall material spectral lines leads to the suggestion that the second rise in the electron density is linked with interaction between the plasma and the discharge chamber walls.

* The hard X-radiation was measured by V. V. Matveev, A. D. Sokolov, and L. A. Suchkov.

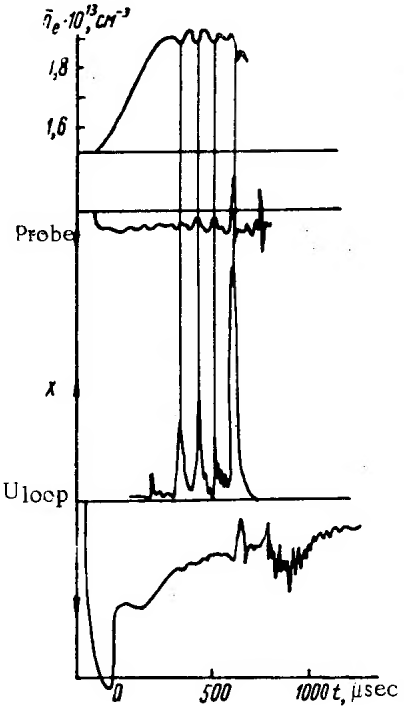

Fig. 2. Correlation between oscillations in electron density, magnetic probe, x-ray intensity, and loop voltage ($p = 0.9 \cdot 10^{-3}$ mm Hg; $I_{init} = 1.8 \cdot 10^7$ amp/sec ($E_{init} = 0.1$ V/cm); H = 11 koe).

After some thousands of discharges the side of the diaphragm farther from the axis of the torus appeared considerably fused, and in places scorched with uniform indentations. The results of measuring the space distribution of x-ray intensity leads to the conclusion that the outer edge of the diaphram is the chief source of the radiation. In the oscillogram the change in x-ray intensity during the process takes the form of surges synchronized with the oscillations on the probes (Fig. 2), breaking out before the appearance of the strong vibrations in the circuit voltage. The larger the magnetic field, the longer the x-rays continue and the greater is their intensity. The same is observed on lowering the longitudinal electric field. On increasing the hydrogen pressure or adding a certain percentage of other gases (helium or argon) to the hydrogen the x-ray output rises appreciably. Thus the x-ray intensity appears greater under those conditions for which the oscillations have lower amplitudes and appear later.

With increasing longitudinal magnetic field (Fig. 3) the oscillations and the second maximum in the mean electron density appear later. For an initial current derivative $\dot{I}_{init} = 1.8 \cdot 10^7$ amp/sec and longitudinal magnetic field $H \geq 16$ kOe oscillations in the loop voltage are not seen at all. The hard X radiation is observed in these conditions up to the end of the current, and the mean electron density hardly changes during the whole operation. In this case the integrated light intensity in the visible region, after an initial surge at the beginning of the discharge, fell considerably towards the end. This is apparently linked with a reduction in the interaction between the plasma pinch and the chamber walls.

The absolute magnitude of the mean electron density on the flat part of the curve differs from the maximum possible magnitude (ionic contribution drawn from regions near the walls in the "shade" of the diaphragm included) by three-five times. This discrepancy can be completely explained as being due to neutral-hydrogen atoms leaving in the process of dissociation and ionization at the wall.

There remains the uncertain question of what determines the fall in electron density which coincides in time with the growth of oscillations in the magnetic probes.

The microwave interferometer measures the phase shift of electromagnetic waves passing through the plasma. This shift appears in time form on the oscillogram. It depends not only on the electron density $\overline{n_e}$ but also on the length of the beam path in the plasma. The following explanations of the observed radiointerferometer results are thus possible:

1) A significant reduction of the phase shift in the discharge process may be caused by a change in the concentration of charged particles in a constant plasma-occupied volume. For this the life-time of the charged particles seems to be several orders less than the classical. Noting a similar phenomenon in stellarator-type systems, the authors of [1, 2, 5] came to the conclusion that for ohmic heating in electrodeless systems with strong magnetic fields there was an anomalously swift diffusion of plasma across the magnetic field.

For a magnetic field of 22 kOe the electron density falls slowly during the course of the discharge. If we suppose that the electron density curve forms part of an exponential, the life-time τ of the electrons is 3-4 msec for this case. It is interesting to compare this value of τ with those corresponding to the Bohm diffusion coefficient ($D \simeq 0.6 \cdot 10^6 \; T_e/H$, cm^2/sec) and the diffusion coefficient obtained in stellarator experiments ($D \simeq 2 \cdot 10^4 \; T_e/H$ cm^2/sec) [5]. In these empirical formulas T_e is expressed in electron volts and H in kilo-oersteds. For the first case the quantity $\tau = (1/d)(a/2.4)^2$ in the TM-2 should be about 1 msec and for the second 0.3-0.4 msec (in these calculations the electron temperature is taken as 50 eV and the radius of the plasma pinch a = 8 cm).

As shown in [5], in stellarator V-3 the maximum value of the mean electron density depends substantially on the longitudinal magnetic field strength. From this fact we may conclude that the anomalously rapid passing out of

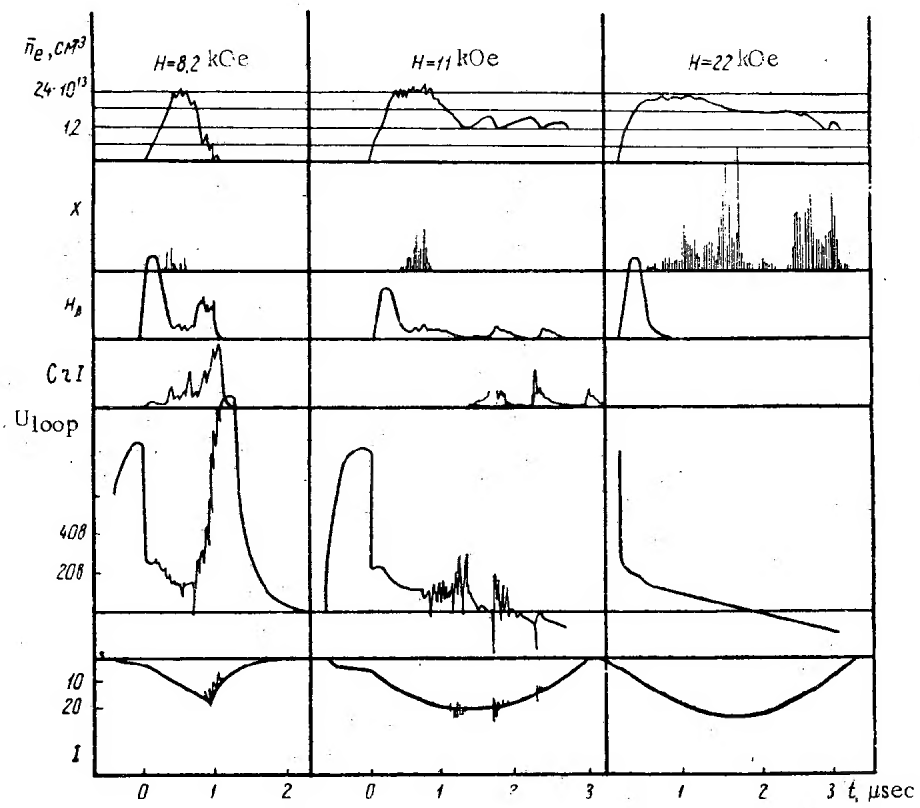

Fig. 3. Oscillograms of electron density, hard x-ray intensity, spectral line intensity of hydrogen H_β (λ = 4860 A) and chromium CrI (λ = 4254 A), loop voltage and gas current (in kA) for three arrangements with different longitudinal magnetic field intensities ($p = 0.9 \cdot 10^{-3}$ mm Hg; $\dot{I}_{init} = 1.8 \cdot 10^7$ amp/sec; E_{init} = 0.1 V/cm).

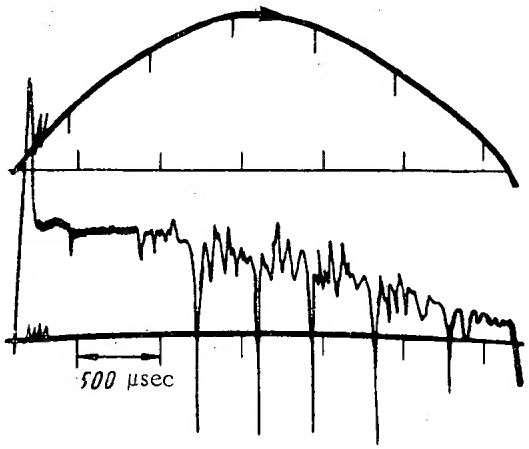

Fig. 4. Example of a voltage oscillogram with regular oscillations in the form of short-term negative throws (above: oscillogram of current discharge) for initial hydrogen pressure (with small additions of argon – about 3%) $p = 1.4 \cdot 10^{-3}$ mm Hg; $\dot{I}_{init} = 2.6 \cdot 10^7$ amp/sec (E_{init} = 0.15 V/cm); H = 15 koe.

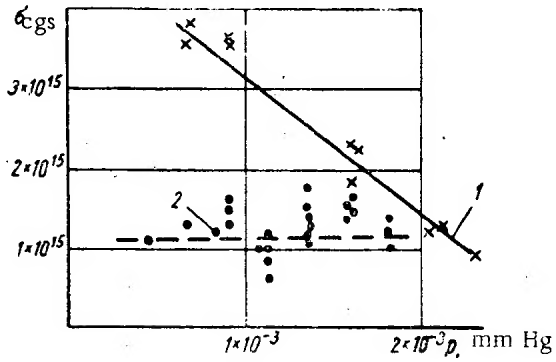

Fig. 5. Mean conductivity σ at the moment of maximum current as a function of initial hydrogen pressure: 1) no voltage oscillations throughout the process, $\dot{I}_{init} = 1.8 \cdot 10^7$ amp/sec (E_{init} = 0.1 V/cm), H = 16 koe; 2) clearly unstable arrangement: $\dot{I}_{init} = 2.6 \cdot 10^7$ amp/sec (E_{init} = 0.15 V/cm), H = 14 koe.

particles takes place from the very beginning of the process. In our experiments the maximum electron density does not depend on the magnetic field intensity. All this makes one doubt the correctness of the hypothesis regarding the determining role of anomalous plasma diffusion in systems with strong longitudinal magnetic fields.

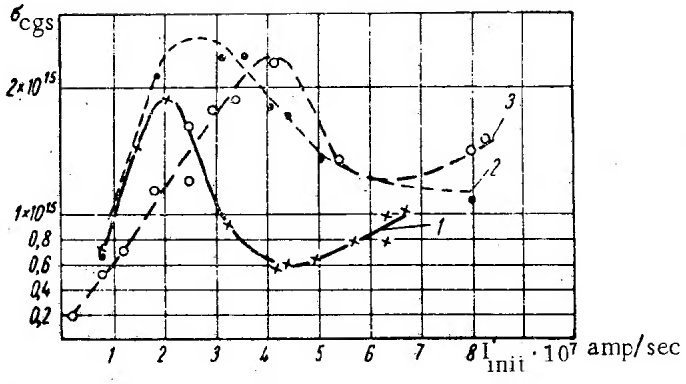

Fig. 6. Mean conductivity calculated at the moment of maximum current as a function of the initial current derivative. 1) $p = 6.5 \cdot 10^{-4}$ mm Hg, H = 11 kOe; 2) $p = 6.5 \cdot 10^{-4}$ mm Hg, H = 22 kOe; 3) $p = 1 \cdot 10^{-3}$ mm Hg, H = 22 kOe.

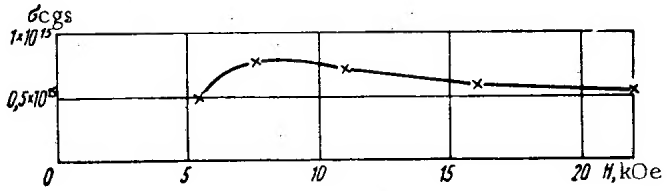

Fig. 7. Mean conductivity calculated at the moment of maximum current as a function of the magnetic field strength for $p = 1 \cdot 10^{-3}$ mm Hg; $\dot{I}_{init} = 0.8 \cdot 10^7$ amp/sec (E_{init} = 0.009 V/cm).

2) If the electrons leave only from the outer regions of the discharge, the effective radius of the plasma falls. A reduction of phase shift will also be observed in the radiointerferometer on account of the diminution of plasma volume at constant concentration. Such a phenomenon may take place not only on account of anomalous diffusion in the colder outer parts of the plasma but also because of the interaction between the plasma pinch surface and the discharge chamber walls, which is determined by magnetohydrodynamic instability.

3) If the effective radius of the plasma is much less than the inner dimensions of the diaphragm, small changes in the outside radius of the pinch will lead to a marked change in the length of the microwave path in the plasma. A displacement of the current pinch was actually observed in the "Tokamak-2" [10].

The electron density was measured with one vertical channel at the center of the chamber. No special investigations of the electron density distribution with respect to cross-section were carried out, so that at the moment we have insufficient facts by which to assert preference for any one of the three suggested explanations for the interferometric observations.

4. Oscillations in the Plasma

For arrangements in which the loop voltage remains smooth during the whole process, oscillations of comparatively small amplitude in the magnetic probe and uneven output of hard x-rays show that in such cases also the plasma is unstable, although it interacts with the walls less strongly. For less stable discharge systems there are moments [of time] when the oscillations grow rapidly in amplitude, or even change their qualitative character. The moment at which appreciable oscillations begin at the magnetic probe coincides with the beginning of weak oscillations in voltage. The moment at which very strong oscillations appear coincides with the cessation of X radiation, the appearance of negative throws in the loop voltage, and bright flashes of the spectral lines of the wall material (see Figs. 1 and 2).

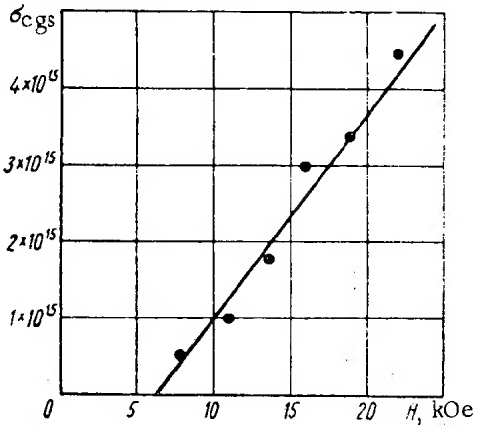

Fig. 8. Mean conductivity calculated at the moment of maximum current as a function of magnetic field intensity for $p = 1 \cdot 10^{-3}$ mm Hg; $\dot{I}_{init} = 1.8 \cdot 10^7$ amp/sec ($E_{init} = 0.1$ V/cm).

The sharp drops in voltage (Fig. 4), in some cases leading to a sign reversal, correspond to an increase in the current derivative. This may be explained by a rapid drop in the induction of the current pinch, for example, during a short-term widening of the current flow region.

In [7] the conclusion was reached that the low frequency plasma oscillations observed in the "Tokamak", determining the whole behavior of the discharge, had a magnetohydrodynamic nature. This hypothesis was confirmed by the existence of a correlation between the bursts of hard X radiation and the oscillations in the probes, and also by the cessation of X radiation on the appearance of sharp surges on the loop voltage oscillograms. Actually, the effectiveness of the interaction of electrons with small scale fluctuations must fall rapidly with increasing electron velocity, and relativistic electrons must intereact essentially only with the magnetic field of the current, which does not cause them to pass out to the outer wall of the chamber. Thus the separate bursts of X radiation must correspond to large scale displacements of the plasma pinch.

5. Conductivity of the Plasma

Careful consideration of the processes taking place in a plasma for various external discharge parameters (see Fig. 3) leads to the conclusion that the magnetohydrodynamic instability arising in the plasma influences its activity to a marked extent.

Figure 5 shows the relation between the mean* conductivity at the moment of maximum current and the ini-initial hydrogen pressure for cases with and without voltage oscillations. In the first case the energy reaching one particle drops with increase in the total number of particles, which leads to a drop in conductivity. In the second case the interaction with the walls, to which the instability arising in the plasma leads, takes away a significant part of the energy to the wall, so that the change in the number of particles taking part in the discharge has little effect on the mean conductivity.

Figure 6† shows the relation between the mean conductivity at the moment of maximum current and the value of the initial current derivative. Curves are given for various values of initial hydrogen pressure and longitudinal magnetic field. The first steep rise in the curve ends when, for the given magnetic field, there is a substantial interaction of the plasma with the wall due to the hydromagnetic oscillations arising. Calculation of the energy balance shows that the heating of the particles in this part of the curve expends about 30% of the energy put into the discharge. The second part of the curve is characterized by a drop in conductivity as the energy contributed grows. Here there occurs an increase in the amplitude of the oscillations in the plasma, and its interaction with the walls increases. Naturally that part of the energy going into heat in this case rapidly drops. The third part of the curve is characterized by a growth in conductivity with a rise in the amount of energy, but considerably more slowly than in the first part. Less than 1% of the energy is here used in heating the plasma.

If in the arrangement without substantial oscillations in voltage the magnetohydrodynamic instabilities do not lead to marked energy loss, the conductivity of the plasma must depend slightly on the longitudinal magnetic field. This is confirmed by Fig. 7. The slight fall in σ for increasing magnetic field may perhaps be linked with a change in the leakage magnetic field intensity, which leads to a displacement of the equilibrium position of the plasma pinch in the chamber. For unstable arrangements, that is, those with large initial current derivative, a linear rise in the mean conductivity with increasing longitudinal magnetic field strength is observed (Fig. 8).

6. Arrangement without Voltage Oscillations

In discharges with parameters corresponding to the first rise in the curve of Fig. 6 there are no oscillations in the oscillograms of voltage and current derivative. The conductivity of the plasma depends in a reasonable way on the initial concentration of particles and the energy imparted to the discharge.

* Mean conductivity here and later means conductivity calculated on the assumption that the current flows evenly throughout the whole cross section of the aperture in the diaphragm.

† Figures 6-8 relate to experiments with somewhat less discharge aperture and worse vacuum conditions. This has no effect on the qualitative discharge characteristics, but leads to a smaller conductivity at maximum current.

In such systems the mean conductivity at the moment of maximum current reaches the value $5 \cdot 10^{15}$ cgs. A considerable induction shift of the current relative to the voltage is observed, corresponding to a mean inductance of 1.0-1.2 μH during the discharge. It is only possible to explain this value of inductance if one assumes that the current flows not through the whole cross section of the diaphragm aperture but through a narrower channel, the actual conductivity when not being less than 10^{16} cgs. For a Maxwellian electron velocity distribution this would correspond to an electron temperature of $T_e \simeq 100$ eV.

The existence of a Maxwellian electron velocity distribution in the plasma may raise doubts, as we do not know the part of the current determined by escaping electrons. According to a simple calculation [11], the energy of the escaping electrons in our apparatus cannot exceed a few MeV. If the acceleration process is similar to that proposed in [12], then for our parameters a substantial part of all the electrons (0.1%) must be accelerated to such energies in a time of the order of 1 msec, and this may give a current of 10-20 kamp. In actuality, however, fast electrons do not apparently determine all the discharge current. This follows from the fact that in arrangements with large voltage oscillations hard X radiation, as shown earlier, vanishes immediately after the first voltage surge but the conductivity remains practically the same as it was up to the appearance of oscillations. Beside this, a coarse calculation of the relativistic electron current by the intensity of hard X radiation shows that it is negligibly small (less than 100 amp). Probably something interferes with the electron acceleration. This is indicated by the anomalous dependence of the hard X-ray output (over 200 keV) on the parameters of the discharge described in Section 3. What part of the current is determined by the direct motion of low energy electrons cannot at present be stated.

Let us suppose that the conductivity is not determined by escaping electrons, and consider the energy balance without voltage oscillations. In time t, energy W(eV) reaches one particle in the plasma. Towards the end of this time interval the plasma conductivity reaches a magnitude corresponding to electron temperature T_e. The "energetic" containment time $\tau_W = tT_e/W - T_e$ equals 300-400 μsec on condition that all the original energy is carried by particles to the wall. Probably, of course, a substantial part of the energy inparted to the discharge passes out in the irradiation of impurity atoms and ions. However even such an energetic containment time has, for our conditions, the same order as the theoretical time for the equalization of the temperatures of the electronic and ionic components. It is therefore to be expected that the temperature of the ions will be close to the that of the electrons if the phenomenon of charge exchange does not play a significant part in the heat exchange process.

7. Conclusions

Summarizing the results thus set out, we establish the following conclusions:

1) The low frequency oscillations excited in the discharge to a great extent determine its characteristics. Correlation of the oscillations with surges in x-ray intensity confirm their magnetohydrodynamic nature.

2) Up to the appearance of the oscillations in the discharge, the following processes appear to be observed. Hydrogen is being ionized all the time its lines are showing. The moment the H_β line disappears, the electron density stops growing and from then on stays constant. Escaping electrons are accelerated up to energies of some MeV and pass out to the outer wall of the diaphragm. At the end of the hydrogen ionization the conductivity begins to increase with time, while the part of the energy transferred to the plasma forms some tens of a percent of the energy imparted to the discharge. The plasma interacts comparatively weakly with the walls, but the observed oscillations in the magnetic field of the current and the unevenness in time of the x-ray output do now allow the discharge to be considered completely stable.

3) After the appearance of the oscillations in loop voltage and current derivative, the picture change sharply. The magnetohydrodynamic instabilities, developing large amplitudes, lead to a strong interaction with the walls. The spectral lines of the wall material and the gases adsorbed thereon make their appearance. Electrons accelerated to large energies as a result of large scale displacements of the plasma pinch hurl themselves into the diaphragm wall. Thereupon it appears that conditions for effective electron acceleration are no longer found in the unstable plasma, and the plasma conductivity ceases to increase. The character of the dependence of the mean conductivity on the initial gas pressure and the energy imparted to the discharge shows that this energy is not accumulated in the plasma, but is given up at the diaphragm and the discharge chamber walls.

4) For sufficiently large containing magnetic fields the voltage and current derivative remain smooth throughout the process. If we suppose that the velocity distribution of electrons is close to Maxwellian, the electron temperature is of the order of 100 eV. The electron density in such arrangements scarcely alters up to the end of the

current flow. The dependence of its maximum on the longitudinal magnetic field strength seems extremely slight. All this casts doubt upon the existing idea that in longitudinal current discharges, stabilized by a strong magnetic field, the reduction in phase shift measured by the radiointerferometer indicates a substantial rise in the diffusion of charged particles to the chamber walls. At present we have no grounds for supposing the existence of such diffusion, although there is also no conclusive proof of its absence.

In conclusion the authors express gratitude to L. A. Artsimovich for valuable discussions and interest in the work, and also to their unfailing assistants, A. A. Kondrat'ev, L. S. Efremov, G. N. Ploskirev, and E. Yu. Frolov, who performed a great part of the technical work. The work was carried out under the initiative and immediate direction of Natan Aronovich Yavlinskii.

LITERATURE CITED

1. Kur et al. In the book: Transactions of the Second International Conference for the Peaceful Uses of Atomic Energy. Collected reports of foreign scientists, Vol. 1, Atomizdat, Moscow (1959), p. 523.
2. R. Ellis, L. Goldberg, and J. Gorman, Phys. of Fluids, 3, 468 (1960).
3. W. Bernstein, A. Kranz, and F. Tenney, Phys. of Fluids, 3, 1019 (1960).
4. E. P. Gorbunov et al. "Zh. tekh. fiz.," 30, 1152 (1960).
5. V. Stodiek et al. Report No. 10 131, presented to the International Conference on Plasma Physics and Controlled Thermonuclear Synthesis, Salzburg, MAGATÉ (1961).
6. E. P. Gorbunov et al. Report No. 10/223, presented to the International Conference on Plasma Physics and Controlled Thermonuclear Synthesis, Salzburg, MAGATÉ (1961).
7. D. P. Ivanov and K. A. Razumova. Report No. 10 222, presented to the International Conference on Plasma Physics and Controlled Thermonuclear Synthesis, Salzburg, MAGATÉ (1961).
8. V. S. Vasil'evskii et al. "Zh. tekhn. fiz.," 30, 1137 (1960).
9. E. P. Gorbunov, In the collection: Diagnostics of Plasma, Moscow, Gosatomizdat (1963), p. 68 (in the press).
10. L. A. Artsimovich and K. B. Kartashov, "Dokl. AN SSSR," 146, No. 6 (1962).
11. E. Meservey and L. Goldberg, Phys. of Fluids, 4, 1307 (1961).
12. Dreiser. See [1], p. 170.

METHODS FOR THE CALCULATION OF THE RADIATIONAL THERMAL OUTPUT IN THE BODY AND SHIELDING OF A NUCLEAR REACTOR

D. L. Broder and K. K. Popkov

Translated from Atomnaya Énergiya, Vol. 15, No. 5,
pp. 370-376, November-1963
Original article submitted November 1, 1962

The radiational thermal output in the body and protective shields of energy-producing reactors is very dangerous, since it can lead to the explosion of these reactors. In order to lower the amount of heat escaping into the body and the most strongly stressed structural sections of reactors, heat screens are usually used.

In the present article we describe methods for the calculations needed in the design of thermal shields. Expressions are given that can be used for the calculation of the thermal output due to the penetrating radiation in various shielding setups, including those with the most commonly used geometry.

The absorption of neutrons and γ radiation heats the body of reactor, the shield, and also the protecting structure that is in the field of radiation. In powerful nuclear reactors, the energy flux in the body of the reactor reaches 10^{13}-10^{14} Mev/cm^2 · sec, and so the specific power of the thermal output often reaches several watts per cm^3, and it can even attain the value of 10^2 W/cm^3 in shields in the active zone.

For thick-walled reactor bodies, designed for a pressure of 100 atm or higher, intense radiation could cause supplementary thermal stresses which must be taken into account in strength calculations.

In the determination of radiational thermal output, we must take into account 1) the γ radiation of the fission products, 2) the capture γ radiation generated in the structural and protective materials (those in the body of the reactor included), and 3) the reaction $B^{10}(n, \alpha)Li^7$ in boron-containing material.

Other processes, in particular γ-radiation generated by the inelastic scattering of fast neutrons or the losses in the elastic scattering of neutrons by the relatively heavy nuclei of iron, contribute only insignificantly to the thermal output, and so their effects can be neglected. With these simplifications, the total thermal output Q is the sum of two terms, the first of which Q_γ is due to the absorption of γ radiation and the second Q_α to the absorption of α-particles generated by the reaction $B^{10}(n, \alpha)Li^7$:

$$Q = Q_\gamma + Q_\alpha \quad \text{W/cm}^3. \tag{1}$$

The determination of the γ component of the thermal output can be reduced to the calculation of the energy-space distribution of the γ radiation flux. If $I_\gamma(E, \mathbf{r})\,dE$ is the strength of the γ radiation energy in the interval from E to E + dE at the point $\mathbf{r}$, then the specific thermal output $Q_\gamma(\mathbf{r})$ can be calculated from the formula

$$Q_\gamma(\mathbf{r}) = k \int_E I_\gamma(\mathbf{r}, E)\,\mu_n(\mathbf{r}, E)\,dE, \tag{2}$$

where $\mu_n(\mathbf{r}, E)$ is the linear energy-absorption coefficient for the γ radiation of energy E at the point $\mathbf{r}$; k is a proportionality coefficient determined by the dimensions of the quantities in the expression (2):

$$k = 1.6 \cdot 10^{-13} \text{ W-sec/MeV} = 3.82 \cdot 10^{-14} \text{ cal/MeV}.$$

In practical calculations, the integral in (2) is replaced by the sum

$$Q_\gamma(\mathbf{r}) = k \sum_E \varphi_\gamma(\mathbf{r},\ E)\, E\mu_n\ (\mathbf{r},\ E), \tag{3}$$

where $\varphi_\gamma(\mathbf{r}, E)$ is the scalar flux of the γ-radiation of energy E at the point $\mathbf{r}$. The sources of γ radiation can be divided into two classes: primary sources, related directly to the fission process, and secondary sources originating with the interactions of neutrons with nuclei of elements in the heat-transfer agent, in the moderator, and also in the structural materials of the reactor and shield. In the present work, we are interested in instantaneous and delayed γ radiation (primary radiation) and in capture γ radiation (secondary radiation).

The calculation of the scalar energy flux of γ radiation φ_γ (see the diagram) reduces mathematically to the calculation of the integral

$$\varphi_\gamma^E E = E \int_{V_s} \frac{q_\gamma^E(\mathbf{r}_s)\, e^{-\mu_s(E)\,\delta_s - \mu_m(E)\,\delta_m} B(E, \delta_s, \delta_m)}{4\pi\,(\mathbf{r}_m - \mathbf{r}_s)^2}\, dV_s, \tag{4}$$

where $q_\gamma^E(\mathbf{r}_s)$ is the distribution function of the specific source strength of γ radiation of energy E; $\mu_s E$ and $\mu_m(E)$ are the linear attenuation coefficients of γ radiation of energy E in the source and shield material respectively; $B(E, \delta_s, \delta_m)$ is a measure of the accumulation of the energy of scattered γ-radiation of energy E in the material of the sources (in the region δ_s) and in the material of the shields (in the region δ_m). The integration it taken over the volume of the sources V_s.

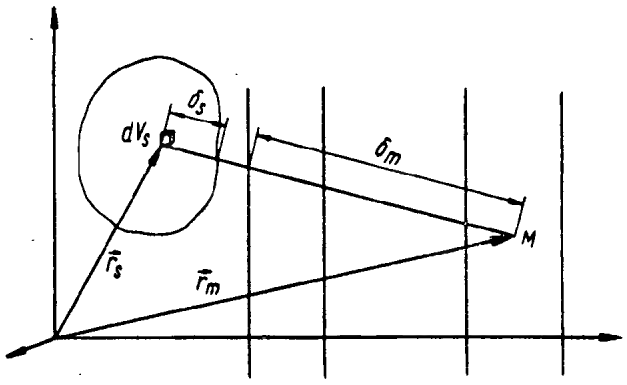

Location of radiation sources in shielding layers.

The space-distribution of the specific strength of the primary γ-radiation sources is completely determined by the integral of the fissions $\xi_f(\mathbf{r}_s)$:

$$\xi_f(\mathbf{r}_s) = \int_E nv(\mathbf{r}_s, E)\, \Sigma_f(\mathbf{r}_s,\ E)\, dE = 3{,}1 \cdot 10^{10} p(\mathbf{r}_s) \quad \text{graduations/cm}^3\text{-sec}, \tag{5}$$

where $nv(\mathbf{r}_s, E)\, dE$ is the flux of neutrons with energy between E and E + dE at the point $\mathbf{r}_s$; $\Sigma_f(\mathbf{r}_s, E)$ is the macroscopic cross section of nuclear fission corresponding to the neutron heating energy E at the point $\mathbf{r}_s$; $p(\mathbf{r}_s)$ is the specific thermal power at the point $\mathbf{r}_s$ in W/cm^3. In some cases it can be assumed that $p(\mathbf{r}_s) = P/V_{a,z} = \text{const}$ (here P is the thermal power of the reactor and $V_{a,z}$ is the volume of the active zone). Knowing the value of $\xi_f(\mathbf{r}_s)$, we can calculate the specific strength of the sources of the primary (instantaneous and delayed) γ radiation $q_{\gamma 1}^E(\mathbf{r}_s)$. If the reactor has been operating for a long period with constant power,* then

$$q_{\gamma 1}^E(\mathbf{r}_s) = \xi_f(\mathbf{r}_s)\, \nu_\gamma S_\gamma(E), \tag{6}$$

where ν_γ is the number of photons of instantaneous and delayed γ radiation referred to a single fission ($\nu_\gamma = 14.7$ [1]) and $S_\gamma(E)$ is the share of γ quanta of energy E in the spectrum of the primary γ radiation. Values of the product $\nu_\gamma\, S_\gamma(E)$ obtained from [1] and [2] for various energies are given in Table 1.

The specific source strengths of capture γ radiation $q_{\gamma 2}^E(\mathbf{r}_s)$ can be calculated if the space energy distributions of the neutrons and the dependence of the radiation capture on the energy are known. In this case, the capture integral $\xi_c^i(\mathbf{r}_s)$ for the ith isotope can be obtained from the formula

* The specific source strength for the delayed γ-radiation is determined from the integral of the fissions $\xi_f(\mathbf{r}_s, t)$ and is specified for any instant of time. In a reactor operating with constant power, the specific source strength for the delayed radiation depends only on the time t_a of operation of the reactor. In practical calculations it is usually assumed that $t_a \to \infty$.

TABLE 1. The Energy Spectrum of Instantaneous and Delayed γ-Radiation

Energy of γ-radiation E_γ (MeV)	$\nu_\gamma S_\gamma(E)$, ν-quanta/fission	Energy of γ-radiation E_γ (MeV)	$\nu_\gamma S_\gamma(E)$, ν-quanta/fission
0.5	4.7	4.0	0.065
1.0	6.4	4.5	0.024
1.5	1.34	5.0	0.019
2.0	1.17	5.5	0.017
2.5	0.71	6.0	0.007
3.0	0.162	6.5	0.004
3.5	0.062		

$$\xi_c^i(\mathbf{r}_s) = \int_E^\infty nv(\mathbf{r}_s, E)\,\Sigma_\gamma^i(\mathbf{r}_s, E)\,dE, \tag{7}$$

where $\Sigma_\gamma^i(\mathbf{r}_s, E)$ is the macroscopic cross section of radiation capture of neutrons of energy E for the ith isotope.

The quantity $q_{\gamma 2}^E(\mathbf{r}_s)$ is obtained from the relation

$$q_{\gamma 2}^E(\mathbf{r}_s) = \sum_i \xi_c^i(\mathbf{r}_s)\,S_{\gamma c}^i(E), \tag{8}$$

where $S_{\gamma c}^i(E)$ is the mean number of γ quanta of energy E generated by the absorption of a single neutron by a nucleus of the ith isotope. Table 2 gives values of $S_{\gamma c}^i(E)$ taken from [3].

The main difficulty in the calculation of sources of capture γ-radiation is the determination of the space energy distribution of the neutrons, i.e., the function $nv(\mathbf{r}_s, E)$ in the expression in (5).

Recently, in the calculation of neutron distribution in shielding, the multigroup method [4] has often been used, in which the neutron spectrum is divided into several energy groups. Within each group, all the characteristics of the materials under consideration are assumed to be independent of the energy. For every ith group of neutrons, we can write the differential equation in the diffusion form

$$\frac{1}{r^\alpha}\cdot\frac{d}{dr}\left(r^\alpha D_j\frac{d\varphi_j}{dr}\right) - \sum_j \varphi_j = -f_j(r), \tag{9}$$

where $\alpha = 0$ for plane geometry, $\alpha = 1$ for cylindrical geometry, and $\alpha = 2$ for spherical geometry; φ_j is the distribution function for neutrons of the jth group; D_j the effective diffusion coefficient for neutrons of the jth group; Σ_j the effective cross section of departure of neutrons from the jth group. The right-hand side of (9) determines the sources of neutrons of the jth group.

The multigroup method is discussed in more detail in [4-7]. In [4], a seven-group method is proposed for the calculation of biological shielding in the diffusion-growth approximation. The results of using this method are found to be in satisfactory agreement with the experimental results given in [4], and this method can thus be recommended for engineering calculations.

Knowing the space neutron-energy distribution we can calculate the capture integral (7):

$$\xi_c^i(\mathbf{r}) = \sum_{j=1}^n nv_j(\mathbf{r})\,\Sigma_\gamma^{ji}(\mathbf{r}),$$

where $\Sigma_\gamma^{ji}(\mathbf{r})$ is the mean macroscopic cross section of radiation capture of neutrons of the jth group by nuclei of the ith isotope.

Table 3 gives the means with respect to the energy of the cross sections of radiation capture for some elements for the seven-group calculation. The table gives the cross sections of the seventh (thermal) group averaged over the Maxwellian spectrum for the normal temperature 20°. If this last condition is not satisfied, then we must introduce a temperature correction. In practical calculations, we can assume [10] that

$$\sigma_\gamma(T) = \sigma_\gamma(T_0)\sqrt{\frac{T_0}{T}}, \tag{10}$$

where $\sigma_\gamma(T)$ and $\sigma_\gamma(T_0)$ are the cross sections of radiation capture for the absolute temperatures T and T_0 of the material.

It must be noted here, however, that absorption (stronger for lower energies) displaces the maximum of the Maxwellian distribution into the region of higher energies. This effect can be taken into account in the calculations by introducing into the formula (10), in place of the actual temperature T, an effective temperature T_n for the

TABLE 2. Mean Number of γ -Quanta of Energy E Generated by the Absorption of a Single Neutron by Various Elements $S^{i}_{\gamma c}(E)$, γ -quanta/capture

Element	Energy interval, MeV						
	0–1	1–2	2–3	3–5	5–7	7–9	>9
H	0	0	1.00	0	0	0	0
Li	0	0	0	0	~0.40	~0.60	0
Be	0	0	0	0.54	0.73	0	0
B^{10}	0	0	0	>1.10	>0.28	>0.06	0.008
Cr	>0.85	0.41	0.21	0.12	0.23	0.39	0.064
Mn	>1.25	0.91	0.60	0.50	0.34	0.47	0
Fe	>0.75	0.60	0.27	0.23	0.25	0.38	0.024
Ni	>0.84	0.40	0.23	0.23	0.34	0.68	0.008
Mo	>1.37	>0.48	–	0.84	0.26	0.03	0.0003
Pb	0	0	0	0	0.07	0.93	0
U^{238}	2.54	1.78	0.91	0.34	0	0	0

TABLE 3. Seven-Group Cross Sections of Radiation Capture for Some Elements, Barn

Element	Energy Interval						
	I (∞–1.5 MeV)	II (0.9–1.5 MeV)	III (0.9 MeV–45 keV)	IV (45–3 keV)	V (3 keV–3 eV)	VI (3.3 eV–E_{gr})	VII (E_{gr}–0)
H	–	–	–	0.02285	0.02368	0.0382	0.178
Al	0.0837	0.0343	0.03738	0.02366	0.02370	0.0271	0.124
Si	0.089	0.035	0.02133	0.02252	0.02506	0.0201	0.0863
B*	0.0899	0.0663	0.0828	0.799	8.22	84.9	484.7
Mn	0.0230	0.02327	0.02471	0.157	0.455	1.58	7.11
Ti	0.0340	0.02142	0.02205	0.02682	0.0675	0.690	3.125
Fe	0.0224	0.02262	0.02313	0.02893	0.0454	0.305	1.336
Cr	0.0235	0.02488	0.02662	0.0436	0.0367	0.366	1.67
Ni	0.0220	0.02965	0.0109	0.0155	0.0362	0.576	2.58
U^{238}	0.088	0.115	0.115	0.44	5.39	0.251	1.48

* For boron, the cross sections are given for the reaction $B^{10}(n, \alpha)Li^{7}$, taking into account the isotope composition of the natural mixture.

neutron gas. From the empirical formulas in [11], the value of T_n for light materials ($A < 25$) is found to be

$$T_n = T_0 \left[1 + 0{,}91 A \frac{\sigma_c (kT_0)}{\sigma_s (1\text{eV})} \right]; \tag{11}$$

while for heavy materials it is

$$T_n = T_0 \left[1 + 0{,}6 A \frac{\sigma_c (kT_0)}{\sigma_s (1\text{eV})} \right], \tag{12}$$

where $\sigma_c(kT_0)$ is the absorption cross section for neutron energy kT_0, $\sigma_s(1\text{ eV})$ is the scattering cross section for neutrons with energy 1 eV. The formulas (11) and (12) yield correct results for $0 < A\ \sigma_c(kT_0)/\sigma_s(1\text{ eV}) < 0.5$.

The next step in the calculation of the thermal output is the determination of the total intensity of γ radiation of various energies at the points under consideration, i.e., the calculation of the integral (4). In most cases this calculation, for reactor shields and bodies, can be carried out with the assumption that plane geometry can be used. Since the shield thickness is usually considerably smaller than the radius of the active zone, this zone can be considered to be a radiating half-space with shielding. In this case, neglecting the accumulation of scattered γ radiation in the active zone, we obtain for steel shields, in agreement with [12],

$$(q^{E}_{\gamma} E)_l = \frac{q^{E}_{\gamma} E}{2\mu^{E}_{s}} \sum_{j=1}^{2} A^{\text{Fe}}_{j}(E) \cdot E_2 \left[\left(1 + \alpha^{\text{Fe}}_{l}(E)\right) \sum_{i} \mu_i r_i \right], \tag{13}$$

where q_γ^E is the mean, through the volume of the active zone, of the specific source strength of γ radiation of energy E, μ_s^E is the linear coefficient of attenuation for γ radiation of energy E in the active zone, $\sum_i \mu_i x_i$ is the thickness of the shielding layers (along relaxation paths) between the surface of the active zone and the point under consideration, and $E_n(x) = x^{n-1}\int_x^\infty \frac{e^{-t}}{t^n}\,dt$ is the exponential-integral function [12].

It should be noted that, in calculations of thermal output, the energy factor for the accumulation of scattered γ radiation must be used in the determination of the γ radiation flux. In (13) an exponential approximation for the accumulation factor was used [13, 14]:

$$B(\mu x) = \sum_{j=1}^{2} A_j(E)\, e^{-\mu x \alpha_j(E)}. \tag{14}$$

Tables of graphs of the values of $A_j(E)$ and $\alpha_j(E)$ are given in many references [2, 12-16].

The neglect of the accumulation factor for the scattered γ radiation in the active zone lowers the values of $(\varphi_\gamma^E E)_1$ by up to 40%. By using the results in [17, 18], we can obtain a formula for numerical calculations in which this accumulation is taken into account. The substitution in (4) of the accumulation factor expressed as the sum (see [17] and [18] and (14)).

$$B(E,\ \delta_s,\ \delta_m) = B_s(E,\ \mu_s\delta_s) + B_m(E,\ \mu_s\delta_s + \mu_m\delta_m) - B_m(E,\ \mu_s\delta_s) =$$
$$= \sum_{j=1}^{2} A_j^s(E)\, e^{-\mu_s\delta_s\alpha_j^s(E)} + \sum_{j=1}^{2} A_j^m(E)\, e^{-(\mu_s\delta_s+\mu_m\delta_m)\cdot\alpha_j^m(E)} - \sum_{j=1}^{2} A_j^m(E)\, e^{-\mu_s\delta_s\alpha_j^m(E)},$$

yields

$$(\varphi_\gamma^E E)_I = \frac{q_\gamma^E E}{2\mu_s}\sum_{j=1}^{2}\left\{\frac{A_j^s(E)}{1+\alpha_j^s(E)}E_2\Big(\sum_i \mu_i x_i\Big) + \frac{A_j^{Fe}(E)}{1+\alpha_j^{Fe}(E)}E_2\Big[\Big(1+\alpha_j^{Fe}(E)\Big)\sum_i \mu_i x_i\Big]\right.$$
$$\left. - A_j^{Fe}(E)\,E_2\Big[\Big(1+\alpha_j^{Fe}(E)\Big)\sum_i \mu_i x\Big]\right\}. \tag{15}$$

In most cases, the distribution function for the sources of capture γ radiation for steel shields surrounded by moderator can be expressed in the form of the exponential sum

$$q_\gamma^E(x) = q_\gamma^{E'} e^{\Sigma' x} + q_\gamma^{E''} e^{-\Sigma'' x}, \tag{16}$$

where x is a coordinate measured from the shield surface nearest to the active zone.

Thus the strength of capture γ radiation of energy E from the kth shield at the point under consideration, separated from the source layer by a shield of total thickness $\sum_i \mu_i^E x_i$ (along relaxation paths), can be calculated from the formulas

$$(\varphi_\gamma^E E)_k = (\varphi_\gamma^{E'} E)_k + (\varphi_\gamma^{E''} E)_k; \tag{17}$$

$$\varphi_\gamma^{E'} = -\frac{q_\gamma^{E'}}{2\Sigma'}\sum_{j=1}^{2} A_j^{Fe}\left\{e^{\Sigma'\left(d+\frac{\sum \mu_i x_i}{\mu_s}\right)}E_1\left\langle\left[(1+\alpha_j^{Fe}) + \frac{\Sigma'}{\mu_s}\right]\sum_i \mu_i x_i\right\rangle\right.$$
$$- e^{\Sigma' d}E_1\Big[(1+\alpha_j^{Fe})\sum_i \mu_i x_i\Big] - e^{\Sigma'\left(d+\frac{\sum \mu_i x_i}{\mu_s}\right)}E_1\left\langle\left[(1+\alpha_j^{Fe}) + \frac{\Sigma'}{\mu_s}\right]\Big(\mu_s d + \sum_i \mu_i x_i\Big)\right\rangle$$
$$\left. + E_1\Big[(1+\alpha_j^{Fe})(\mu_s d + \sum_i \mu_i x_i)\Big]\right\};$$

(18)

$$\varphi_\gamma^{E''} = \frac{q_\gamma^{E''}}{2\Sigma''} \sum_{j=1}^{2} A_j^{Fe} \left\{ e^{-\Sigma''\left(d+\frac{\sum_i \mu_i x_i}{\mu_s}\right)} E_1 \left\langle \left[(1+\alpha_j^{Fe}) - \frac{\Sigma''}{\mu_s} \right] \sum_i \mu_i x_i \right\rangle \right.$$

$$- e^{-\Sigma'' d} E_1 \left[(1+\alpha_j^{Fe}) \sum_i \mu_i x_i \right] - e^{-\Sigma''\left(d+\frac{\sum_i \mu_i x_i}{\mu_s}\right)} E_1 \left\langle \left[(1+\alpha_j^{Fe}) - \frac{\Sigma''}{\mu_s} \right] \left(\mu_s d + \sum_i \mu_i x_i \right) \right\rangle$$

$$\left. + E_1 \left[(1+\alpha_j^{Fe}) \left(\mu_s d + \sum_i \mu_i x_i \right) \right] \right\}, \tag{19}$$

where μ_s is the linear attenuation coefficient of γ radiation in the material of the layer-source, $\underline{k}$ is the thickness of the layer source. For thin shields, neglecting the variation of the function $q_\gamma(x)$, we obtain

$$q_\gamma^E(x) = \overline{q_\gamma^E} = \text{const} = \frac{\int_{R_1}^{R_2} q_\gamma(r)\, 2\pi r dr}{2\pi \int_{R_1}^{R_2} r dr} = \frac{2}{R_2^2 - R_1^2} \int_{R_1}^{R_2} q_\gamma(r)\, r dr, \tag{20}$$

where R_1 and R_2 are the radii of the internal and external surfaces of the layer source and $r = R_1 + x$. For the $\underline{k}$th shield we have

$$(\varphi_\gamma^E E)_k = \frac{\overline{q_\gamma^E} E}{2\mu_s} \sum_{j=1}^{2} \frac{A_j^{Fe}}{1+\alpha_j^{Fe}} \left\{ E_2 \left[(1+\alpha_j^{Fe}) \sum_i \mu_i x_i \right] - E_2 \left[(1+\alpha_j^{Fe}) \left(\sum_i \mu_i x_i + \mu_s d \right) \right] \right\}. \tag{21}$$

This formula can also be used for the calculation of the radiation flux from thick shields if $q_\gamma(x)$ is expressed as a step function.

In the determination of the strength of γ radiation generated by the absorption of neutrons in thin layers of water ($\mu_s d > 2$), the radiating layer can be considered to be nonabsorbing. In this case

$$(\varphi_\gamma^E E)_k = \frac{\overline{q_\gamma^E}\, dE}{2} \sum_{j=1}^{2} A_j^{Fe} E_1 \left[(1+\alpha_j^{Fe}) \sum_i \mu_i^E x_i \right]. \tag{22}$$

For thick layers ($\mu_s d > 2$), we must use formulas similar to (17)-(19) and (21). For example, for the exponent $q(x) = q' e^{\Sigma' x}$ we have

$$(\varphi_\gamma^E E)_k = \frac{q'_\gamma E}{2\Sigma'} \sum_{j=1}^{2} A_j^{Fe} \left\{ e^{\Sigma' d} E_1 \left[(1+\alpha_j^{Fe}) \sum_i \mu_i x_i \right] \right.$$

$$- e^{\left[\frac{(1+\alpha_j^{Fe}) \sum_i \mu_i x_i}{\mu_s} + d\right]\Sigma'} E_1 \left[(1+\alpha_j^{Fe}) \sum_i \mu_i x_i \left(1 + \frac{\Sigma'}{\mu_s} \right) \right] - E_1 \left[(1+\alpha_j^{Fe}) \sum_i \mu_i x_i + \mu_s d \right]$$

$$\left. + e^{\left[\frac{(1+\alpha_j^{Fe}) \sum_i \mu_i x_i}{\mu_s} + d\right]\Sigma'} E_1 \left\langle \left[(1+\alpha_j^{Fe}) \sum_i \mu_i x_i + \mu_s d \right] \left(1 + \frac{\Sigma'}{\mu_s} \right) \right\rangle \right\}. \tag{23}$$

For a uniform distribution, i.e., $q(x) = \overline{q}_\gamma = \text{const}$, we have

$$(\varphi_\gamma^E E)_k = \frac{\overline{q_\gamma^E} E}{2\mu_s} \sum_{j=1}^{2} A_j^{Fe} \left\{ E_2 \left[(1+\alpha_j^{Fe}) \sum_i \mu_i x_i \right] - E_2 \left[(1+\alpha_j^{Fe}) \sum_i \mu_i x_i + \mu_s d \right] \right\}. \tag{24}$$

The strength of capture γ-radiation $(\varphi_\gamma^E E)_{II}$ at the point under consideration coming from all layers is obtained as a sum:

$$(\varphi_\gamma^E E)_{II} = \sum_k (\varphi_\gamma^E E)_k, \tag{25}$$

where k is the number of layers, excluding the layer containing the point under consideration. The contribution $(\varphi_\gamma^E E)_{III}$ of the capture γ-radiation from this layer can be obtained by using the formulas given below: for a point at a distance x from the surface of a layer with constant specific γ-radiation source strength we have q_γ^E

$$(\varphi_\gamma^E E)_{III} = \frac{\overline{q_\gamma^E} E}{2\mu_s} \sum_{j=1}^{2} \frac{A_j}{\pm \alpha_j} \{2 - E_2[(1+\alpha_j)\mu_s x] - E_2[(1+\alpha_j)\mu_s (d-x)]\}; \tag{26}$$

for a layer with an exponential distribution $q_\gamma(x) = q_0 e^{-\Sigma x}$

$$(\varphi_\gamma^E E)_{III} = \frac{q_0 E}{2\Sigma} \sum_{j=1}^{2} A \Big\{ -e^{-\Sigma x} \left\{ \ln \left| \frac{\mu_j - \Sigma}{\mu_j} \right| - e^{\Sigma x} E_1(\mu_j x) + E_1[(\mu_j - \Sigma) x] \right\} + e^{\Sigma x} \left\{ \ln \left| \frac{\mu_j + \Sigma}{\mu_j} \right| - e^{-\Sigma(d-x)} E_1[\mu_j (d-x)] + E_1[(\mu_j + \Sigma)(d-x)] \right\} \Big\}, \tag{27}$$

where $\mu_j = \mu(1 + \alpha_j)$.

In many cases, we can use a simplified formula [19] obtained under the assumption that the accumulation factor is linear: $B(\mu x) = 1 + \beta\mu x$. For the exponent $q(x) = q_0 e^{-\Sigma x}$

$$(\varphi_\gamma^E E)_{III} = \frac{q_0 E}{2} \Big\{ \beta \left[\frac{e^{-\Sigma x}}{\mu} \frac{e^{-\mu x}}{-\Sigma} + e^{-\Sigma d} \frac{e^{\Sigma(d-x)} - e^{-\mu(d-x)}}{\mu + \Sigma} \right] + \frac{e^{\Sigma x}}{\Sigma} \left\{ \ln \left| \frac{\mu + \Sigma}{\mu} \right| - e^{-\Sigma(d-x)} E_1[\mu(d-x)] + E_1[(\mu + \Sigma)(d-x)] \right\} - \frac{e^{-\Sigma x}}{\Sigma} \left\{ \ln \left| \frac{\mu - \Sigma}{\mu} \right| - e^{\Sigma x} E_1(\mu x) + E_1[(\mu - \Sigma) x] \right\} \Big\}. \tag{28}$$

The total strength $\varphi_\gamma^E E$, occurring in the formula (3), is obtained for each point for which the calculation is performed in the form of a sum

$$\varphi_\gamma^E E = (\varphi_\gamma^E E)_I + (\varphi_\gamma^E E)_{II} + (\varphi_\gamma^E E)_{III}. \tag{29}$$

The thermal output Q_α due to the absorption of α-particles with a probability of 0.94 as a result of the reaction $B^{10}(n, \alpha)Li^7$ is given by the formula

$$Q_\alpha = kE_\alpha \sum_{j=1}^{7} n v_j \Sigma_j^\alpha, \tag{30}$$

where Σ_j^α is the macroscopic reaction cross section for neutrons of the jth group (see Table 3); E_α is the energy of an α-particle equal to 2.31 MeV.

During the reaction $B^{10}(n, \alpha)Li^7$, in addition to an α-particle, a γ-quantum of energy 0.478 MeV is also emitted, which must also be taken into account in the calculations.

The method described above can be used in the calculation of the thermal output in the body and in other structural parts of nuclear reactors with an error of less then 30%.

LITERATURE CITED

1. Reactor Physics Constants, ANL-5800 (1958).
2. G. Eterington, Nuclear Engineering Handbook. McGraw-Hill (1958).
3. E. Troubetzkoy and H. Goldstein, Nucleonics, 18, No. 11, 171 (1960).
4. D. L. Broder and others. Atomnaya Énergiya, 12, 129 (1962).
5. G. I. Marchuk, Numerical Methods for Nuclear-Reactor Calculations [in Russian], Atomizdat, Moscow (1958).

6. D. L. Broder and K. K. Popkov, Inzh-fiz. Zh., No. 12, 118 (1961).
7. G. I. Marchuk, Methods for Nuclear-Reactor Calculations [in Russian], Gosatomizdat, Moscow (1961).
8. M. Clark, Nucl. Engng. 6, No. 56 (1961).
9. O. A. Barsukov and V. S. Avzyanov, Atomnaya Énergiya, 10, 478 (1961).
10. Merrei, Nuclear-Reactor Physics [Russian translation], Izd-vo inostr. lit., Moscow (1960).
11. E. R. Cohen, Report No. 611 presented by the USA at the Second International Conference on the Peaceful Uses of Atomic Energy (Geneva, 1958).
12. The Shielding of Nuclear Reactors [in Russian], Izd-vo inostr. lit., Moscow (1958).
13. G. Gol'dshtein, The Fundamentals of Reactor Shielding [in Russian], Gosatomizdat, Moscow (1961).
14. H. Goldstein and J. Wilkins, Calculation of Penetration of Gamma-Rays, NDA Report NYO-3015 (1954).

All abbreviations of periodicals in the above bibliography are letter-by-letter transliterations of the abbreviations as given in the original Russian journal. *Some or all of this periodical literature may well be available in English translation.* A complete list of the cover-to-cover English translations appears at the back of this issue.

MEASUREMENT OF THE THERMAL NEUTRON DENSITY DISTRIBUTION ALONG THE RADIUS OF SLEEVE-SHAPED FUEL ELEMENTS

V. F. Belkin, B. P. Kochurov, and O. V. Shvedov

Translated from Atomnaya Énergiya, Vol. 15, No. 5
pp. 377-381, November, 1963
Original article submitted March 14, 1963

This article is devoted to an experimental investigation of the thermal neutron density distribution along the radius of sleeve-shaped fuel elements consisting of natural uranium and an organic coolant, monoisopropyldiphenyl. The thermal neutron density distribution for 23 types of fuel element was measured by using the activation method. The theoretical neutron density distributions were determined for these fuel elements by solving the single-velocity kinetic equation by means of an electronic computer. The experimental and theoretical results are given in the form of neutron density distribution graphs, screening numbers, and neutron density jumps in the outside coolant layer.

Introduction

The tendency to increase the coolant temperature without substantially increasing the pressure with the aim of producing efficient power reactors brought about the use of coolants consisting of organic liquids with high melting points.

The thermodynamic and structural requirements imposed on systems with natural uranium (as the fissionable material) and an organic coolant led to the development of multilayer fuel elements, to which the calculation methods suitable for simpler types of fuel element cannot be applied [1, 2]. This makes it necessary to use more complex calculation methods, which must be checked experimentally.

Experimental Equipment

The thermal neutron density distribution was measured in fuel element mock-ups (fuel assemblies) whose length was 75 cm. An assembly consisted of the following elements (Fig. 1). The sleeve 1, made of natural metallic uranium (with a density of 18.7 g/cm^3), was encased between the outside and inside aluminum jackets, 2 and 3, respectively. A magnesium displacer 4, was provided at the center of the assembly. The inside layer of the monoisopropyldiphenyl coolant 5 (whose density was 0.986 g/cm^3) was poured between the outside surface of the magnesium displacer and the inside jacket of the uranium sleeve. The outside layer 6 of monoisoprophyldiphenyl was poured between the outside jacket of the uranium sleeve and the screening Avial tube 7. An air gap 9, was provided between the outside Avial jacket 8 of the assembly and the screening Avial tube. (In some experiments, monoisopropyldiphenyl was replaced by water.) The dimensions of all the fuel assemblies were the same: the inside diameter of the uranium sleeves was 30 mm, the air gap was 3 mm, the thickness of the outside Avial jacket was 2 mm, and the thickness of the screening Avial tubes and of the uranium sleeve jackets was 1 mm.

The fuel assemblies were characterized by the following dimensions: the outside diameter of the uranium sleeves, the diameter of the magnesium displacer and, correspondingly, the thickness of the inside monoisopropyldiphenyl layer, and the thickness of the outside monoisopropyldiphenyl layer.

Each assembly was given a code designation which indicated the outside diameter of the uranium sleeve, the thickness of the outside monoisopropyldiphenyl layer, and the diameter of the magnesium displacer. For instance, in the 54-1.5-20 assembly, the outside diameter of the uranium sleeve was 54 mm, the thickness of the outside monoisopropyldiphenyl layer was 1.5 mm, and the diameter of the magnesium displacer was 20 mm. If the displacer was not provided, then, depending on the material with which the inside cavity was filled, the last figure was replaced by the letter A (air) or M (monoisopropyldiphenyl).

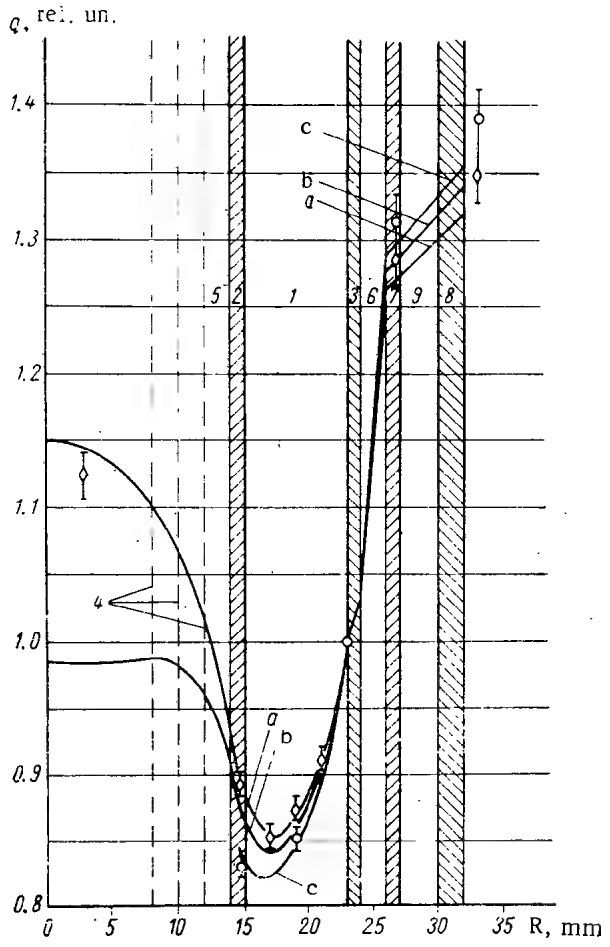

Fig. 1. Thermal neutron density distribution q along the radius R of the assemblies (the theoretical results are given by the curves, while the points represent the experimental results). a) For the 46-2-M assembly; b) 46-2-16 assembly; c) 46-2-A;) and ○) experimental values for the 46-2-M and 46-2-A assemblies, respectively.

The neutron density distribution was measured by means of detectors with a diameter of 4.2 mm and a thickness of 0.4 mm, which consisted of a mixture of a transparent plastic and dysprosium oxide (with a density of ~ 3 mg/cm^2). For the installation of the detectors, grooves into which uranium prisms with detectors were inserted during the experiment were milled in the uranium sleeves. The slits in the prisms which were not occupied by detectors were filled with uranium plates. The other detectors were placed in the recesses of the aluminum jackets and tubes and also in the grooves of the magnesium displacer. The spacing of the detectors is indicated by the positions of the experimental points in Figs. 1-3.

The detector activity was measured by means of an automatic eight-channel counting device. The assemblies were irradiated in the A–O channel of a heavy-water reactor [3] in a flux of 10^9 neutrons/cm^2 sec. There was an air gap between the outside Avial jacket of the assembly and heavy water, since the inside diameter of the AO channel was ~100 mm. The position of the detectors during the activation approximately coincided with the center of the reactor core. The cadmium ratio for dysprosium was not less than 100, so that the detectors recorded only thermal neutrons. The moderator temperature was 293°K.

Experimental Results

Figures 1-3 show typical thermal neutron density distributions along the assembly radius, which were obtained experimentally and by solving the kinetic equation by means of a computer. The assemblies whose neutron densities are given in the same figure differed from each other only by the dimension of the inside monoisopropyldiphenyl layer. In certain assembly variants, the magnesium displacer was not provided, and the inside hollow space of the uranium sleeve was filled with monoisopropropyldiphenyl or air.

Table 1 provides the values of the screening number Q,* which were obtained by using different methods: 1) processing our experimental data; 2) processing the results of the numerical solution of the kinetic equation; 3) using the data provided in [1-2].

Table 2 provides the values of the neutron density jump β, defined as the ratio of the neutron density at the outside surface of the outside layer of monoisopropyldiphenyl or water to the neutron density at the surface of the uranium sleeve. Since detectors could not be installed at the outside surface of the outside monoisopropyldiphenyl layer under our experimental conditions, the experimental values in the determination of β were corrected in correspondence with the neutron density curves obtained by solving the kinetic equation. With an allowance for

* The value of Q is given by $Q^{-1} = \frac{\int_{R_i}^{R_0} q(r)\, r dr}{q(R_0) \int_{R_i}^{R_0} r dr}$, where R_0 and R_i are the outside and inside radii of the uranium sleeve.

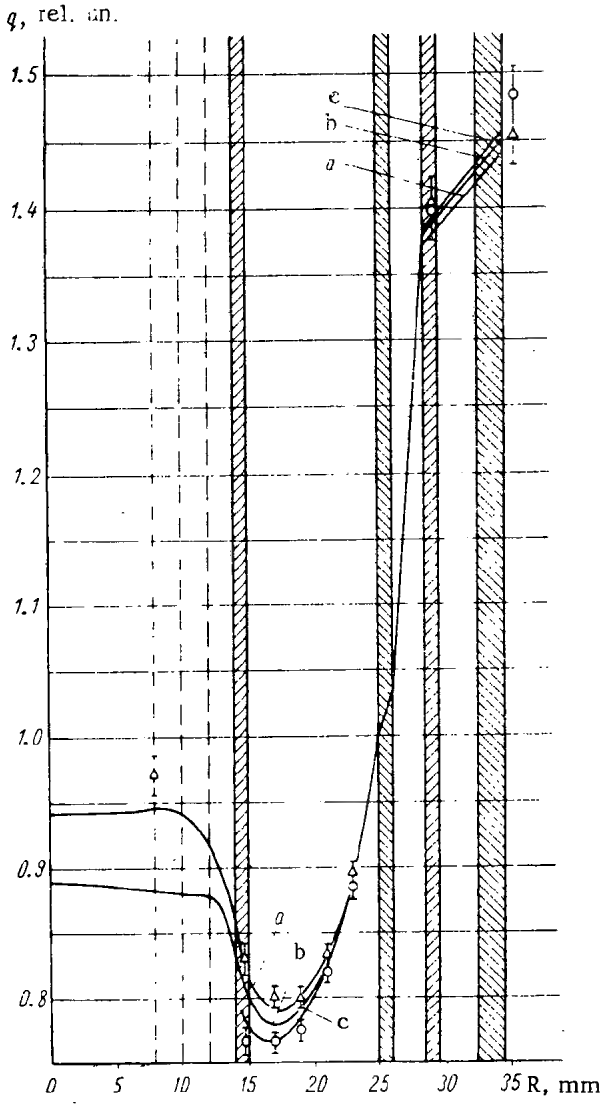

Fig. 2. Thermal neutron density distribution along the radius of the assemblies (the curves represent the theoretical results, while the points represent the experimental results). a) For the 50-2.5-16 assembly; b) 50-2.5-24 assembly; c) 50-2.5-A assembly; Δ) and ○) experimental values for the 50-2.5-16 and 50-2.5-B assemblies, respectively.

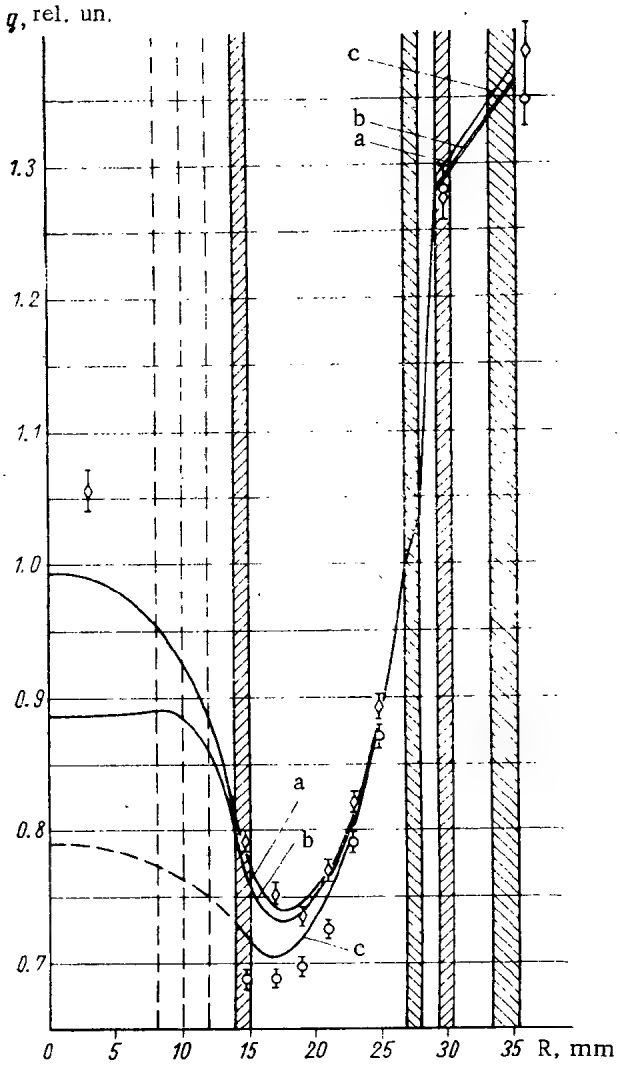

Fig. 3. Thermal neutron density distribution along the radius of the assemblies (the curves represent the theoretical results, while the points represent the experimental results). a) For the 54-1.5-M; b) 54-1.5-16 assembly; c) 54-1.5-A assembly; Δ) and ○) experimental values for the 54-1.5-M and 54-1.5-A assemblies, respectively.

inaccuracies in mounting the detectors, the errors in measuring the distributions and jumps of neutron density were equal to 1-1.5%.

The theoretical neutron density distributions were obtained by solving the single-velocity kinetic equation for the multizone Wigner-Zeitz cell. The calculations were performed according to the program composed by F. M. Filler and T. D. Bogdanova. By preliminary calculations, the dimensions of the equivalent cells for each assembly were determined under the assumption that the neutron distribution in the internal monoisopropyldiphenyl layer is close to the experimental distribution. In this, the sources of thermal neutrons in monoisopropyldiphenyl were assumed to be 4.77 times as strong as in D_2O.

It was assumed that the neutrons have a Maxwellian distribution, the mean effective temperature T_n of which may depend on the coordinates. The temperature T_n^m of neutrons in the moderator was assumed to be equal to the temperature T_n^0 of heavy water, while the temperature of neutrons in uranium was assumed to be $T_n^U = 1.3\ T_n^0$ on the

TABLE 1. Screening Numbers

Assembly type	Q		
	experiment	calculation	data borrowed from [1, 2]
54-1.5-B	1.279	1.261	1.271
54-1.5-24	1.251	1.248	
54-1.5-20	1.239	1.242	
54-1.5-16	1.227	1.238	
54-1.5-M	1.218	1.231	
50-2.5-B	1.199	1.197	1.216
50-2.5-24	1.187	1.188	
50-2.5-20	1.176	1.183	
50-2.5-16	1.166	1.179	
50-2.5-M	1.162		
46-2.0-B	1.135	1.147	1.164
46-2.0-24	1.130	1.137	
46-2.0-20	1.125	1.134	
46-2.0-16	1.120	1.131	
46-2.0-M	1.113	1.119	

TABLE 2. Neutron Density Jump β at the Outside Layers of Monoisopropyldiphenyl and Water

Assembly type	β		Layer thickness, mm
	experiment	calculation	
54-1.5-A	1.270	1.288	1.45±0.05
54-1.5-24	1.292	1.284	1.45±0.05
54-1.5-20	1.284	1.282	1.45±0.05
54-1.5-16	1.262	1.280	1.45±0.05
54-1.5-M	1.268	1.276	1.45±0.05
50-1.5-A	1.300		1.55±0.05
50-1.5-24	1.275	1.272	1.55±0.05
50-2.5-A	1.391	1.383	2.55±0.10
50-2.5-24	1.411	1.378	2.55±0.10
50-2.5-20	1.402	1.375	2.55±0.10
50-2.5-16	1.398	1.372	2.55±0.10
50-3.5-B	1.479		3.50±0.10
50-3.5-24	1.464	1.483	3.50±0.10
50-3.5-M	1.473		3.50±0.10
50-3.5-A*	1.527		3.50±0.10
50-3.5-M*	1.535		3.50±0.10
46-2-A	1.306	1.288	2.00±0.10
46-2-24	1.305	1.283	2.00±0.10
46-2-20	1.282	1.279	2.00±0.10
46-2-16	1.290	1.277	2.00±0.10
46-2-M	1.280	1.262	2.00±0.10
46-2-A*	1.349		2.00±0.10
46-2-M*	1.294		2.00±0.10

* The outside monoisopropyldiphenyl layer was replaced by water.

basis of preliminary calculations [4, 5]. A good agreement between the experimental and theoretical values of the screening number was observed in this case.

The scattering cross section Σ_{tr}^{m} of monoisopropyldiphenyl depends rather heavily on the neutron temperature (in [7], this dependence was determined experimentally: $\gamma_{tr}^{m} \sim v^{1.58} \pm 0.12$ in the temperature range from 18 to 250°C). From the preliminary calculations, it follows that much lower β values are obtained for $T_n^m = T_n^U = 1.3$. Satisfactory agreement with experimental data is obtained if the T_n^m value is assumed to be close to T_n^0. The value of β only slightly depends on the equivalent cell's dimensions and the filling of the inside space of the lump with monoisopropyldiphenyl. Some of the results of preliminary calculations are given in Tables 3 and 4.

TABLE 3. Dependence of β on Σ_{tr}^{M} and the Thickness t of the D_2O Layer for a Cell with a 50-25-20 Assembly*

t, cm	Σ_{tr}^{M}, cm^{-1}				
	1.81	2.00	2.20	2.26	2.50
5	1.311	1.336	1.361	1.375	1.400
6	—	1.341	1.367	—	1.405

* Σ_{tr}^{M} (293°K) = 2.32 cm^{-1}.

TABLE 4. Dependence of Q and β on T_n^U for a Cell with a 50-2.5 A Assembly

Q			β		
$T_n^U = T_n^0$	$T_n^U = 1.3T_n^0$	experiment	$T_n^U = T_n^0$	$T_n^U = 1.3T_n^0$	experiment
1.230	1.197	1.199	1.424	1.383	1.391

TABLE 5. Effect of the Aluminum Layer on β

Calculation	Assembly		
	46-2-B	50-2.5-A	54-2.5-A
With aluminum	1.288	1.383	1.290
Without aluminum	1.301	1.401	1.306
Air gap	1.276	--	--

In order to determine the effect of the aluminum layer between uranium and the outside coolant layer, we performed several calculations for the cases where the monoisopropyldiphenyl layer was in close contact with uranium and where aluminum was replaced by an air gap. As can be seen from Table 5, β somewhat increases in the first case and decreases in the second case.

It should be noted that a certain increase in the theoretical neutron density in approaching the assembly center is observed in the case of hollow slugs. For instance, calculations of a cell with a 54-1.5-A assembly, where a material with a very small cross section (Σ = 0.0025) was placed in the hollow space inside the uranium sleeve, have shown that the neutron density near the assembly axis increases by approximately 12% in comparison with the minimum neutron density (see the dashed curve in Fig. 3). It can be assumed that this effect is caused by the anisotropy of the angular distribution of neutrons [8].

For assemblies without a coolant inside the neutron sleeve, the screening number Q is also determined by using the equation [1, 2]

$$Q = 1 + \frac{\Sigma_a}{\Sigma} A \left[1 + \alpha \frac{\Sigma_s}{\Sigma} + \gamma \left(\frac{\Sigma_s}{\Sigma} \right)^2 \right].$$

Here A, α, and γ are tabular functions of $(2V^U/S_{out}^U)\Sigma^U$.

The calculations were performed for the following cross sections (cm^{-1}):

$$\Sigma_s^U = 0.392; \quad \Sigma_a^U = 0.275;$$
$$\Sigma_s^{Al} = 0.0842; \quad \Sigma_a^{Al} = 0.0108;$$
$$\Sigma_s^{Mg} = 0.1546; \quad \Sigma_a^{Mg} = 0.0021;$$
$$\Sigma_s^M = 2.26; \quad \Sigma_a^M = 0.011;$$
$$\Sigma_s^{D_2O} = 0.397; \quad \Sigma_a^{D_2O} = 0.001.$$

In this, the absorption cross sections were averaged with respect to the Maxwellian spectrum:

$$\overline{\sigma_a} = \frac{\int \sigma_a(x)\, xe^{-x}\, dx}{\int xe^{-x}\, dx},$$

where $x = E/kT_0$.

It should be noted that the distribution of the neutron density, i.e., of the value of $\int n(E)\,dE$ is determined in measurements (see, for instance, [6]) as well as in calculations with the accepted averaging. Therefore, in using the obtained results for calculating the thermal utilization factor, one should use the absorption cross sections for a constant temperature, for instance, T_n^U, introducing, however, temperature corrections for the deviation from the 1/v law.

For assemblies with uranium sleeves whose outside diameters were 4.6, 5.0, and 5.4 cm, the thickness of the heavy water layer was equal to 5, 5.5, and 6 cm, respectively. Thus, the measurements performed and comparisons between the experimental and theoretical results have shown that the experimental neutron density distribution in fuel elements of heavy-water reactors with organic coolants are in agreement with the calculation results for the single-velocity model with $T_n^U = 1.3\ T_n^0$ and $T_n^m = T_n^0$.

LITERATURE CITED

1. A. D. Galanin, In the coll.: Neutron Physics [in Russian], Gosatomizdat, Moscow (1961), p. 125.
2. A. Amouyal, P. Benoist, and J. Horowitz, J. Nucl. Energy, 6, 79 (1957).
3. V. V. Goncharov et al. In the book: Transactions of the Second International Conference on the Peaceful Uses of Atomic Energy. Reports by Soviet Scientists. Vol. 2, Atomizdat, Moscow (1959), p. 243.
4. P. P. Blagovol, In the coll.: Neutron Physics [in Russian], Gosatomizdat, Moscow (1961), p. 56.
5. V. I. Mostovoi et al. In the book: Transactions of the Second International Conference on the Peaceful Uses of Atomic Energy. Reports by Soviet Scientists. Vol. 2, Atomizdat, Moscow (1959), p. 546.
6. R. Deutsch, Nucl. Sci. and Engng, 10, 400 (1961).
7. L. N. Yurova et al. Atomnaya Énergiya, 12, 331 (1962).
8. K. Case, F. de Hoffman, and G. Placzek, Introduction to the Theory of Neutron Diffusion, I. Los Alamos (1953).

All abbreviations of periodicals in the above bibliography are letter-by-letter transliterations of the abbreviations as given in the original Russian journal. *Some or all of this periodical literature may well be available in English translation.* A complete list of the cover-to-cover English translations appears at the back of this issue.

CALCULATION OF γ-RAY ENERGY ABSORPTION IN HETEROGENEOUS MACRO-SYSTEMS

B. M. Terent'ev, V. A. Él'tekov, and D. I. Dolenko

Translated from Atomnaya Énergiya, Vol. 15, No. 5,
pp. 382-286, November, 1963
Original article submitted January 8, 1963

By means of the Monte-Carlo method, a determination was made of the fraction of γ-ray energy absorbed in the elements of a complex heterogeneous system formed by a cylindrical, irradiated water-equivalent mass, cylindrical γ-ray sources located inside or outside the mass, and units of auxiliary equipment. From the results, various energy efficiencies (e.e) were determined depending on the γ radiation from particular systems which were models of radiochemical equipment. Results from corresponding experiments were in good agreement with the calculated data. The program enabled one to find the e.e. for arbitrary macro-systems of a similar type.

One of the problems which arise in the carrying out of any radiochemical, radiobiological, and some medical, investigations is the determination of total absorbed γ-ray energy in the irradiated system. This quantity may be obtained by integration of the absorbed doses in some volume, but determining the latter, even by approximate methods [1], presents great difficulty, especially in the case of heterogeneous media, because of the necessity for taking multiple scattering into account.

A semi-empirical method has been given [2] for the direct determination of total absorbed energy. This method was based on an analytic determination of the primary, attenuated γ-ray flux escaping from the system (without considering scattering) and the introduction, after comparison with experimental results, of a correction factor (build-up factor for total flux). This method is very satisfactory for doing engineering physics calculations, but it is impossible to apply it universally since it is difficult to extrapolate data for a system with small dimensions to a large-scale system.

An exact analytic solution for the problem of finding both the absorbed dose field and the total absorbed γ-ray energy is possible through the kinetic equation for γ-quanta [3], but the techniques for solution have not yet been completely developed. In cases of complex geometry, it is more convenient to use the Monte-Carlo method which has been used before [4] for the computation of a similar set of problems.

In this paper, the method and results are given for a Monte-Carlo computation of the absorbed energy distribution among system components which was performed on the "Strela-3" computer. The calculations deal with models of two typical radiochemical apparatuses of the "tubular heat exchanger" (Fig. 1a) and "fractionating still" (Fig. 1b) types which are finite heterogeneous systems. Some of the calculated results are compared with experimental data which was obtained with the K-60,000 equipment described in [5]. The initial energy for all quanta was assumed to be 1.25 MeV (the average energy of the Co^{60} γ-ray spectrum). The scattering of quanta with energies less than 0.01 MeV was not considered since the probability of their absorption greatly exceeds the probabilities for all the other processes. In the range 1.25-0.01 MeV, only Compton scattering and photo-absorption play an important role. The mathematical simulation of a γ-quantum history was carried out in three steps:

1) the simulation of the creation of a quantum, which occurred uniformly over the entire volume of the source with uniform distribution in direction;

2) simulation of the quantum trajectory, which was in the form of a broken line within the finite heterogeneous system;

3) simulation of Compton scattering, which corresponded to the deflection points in the trajectory, and of photo-absorption which corresponded to the end of the trajectory.

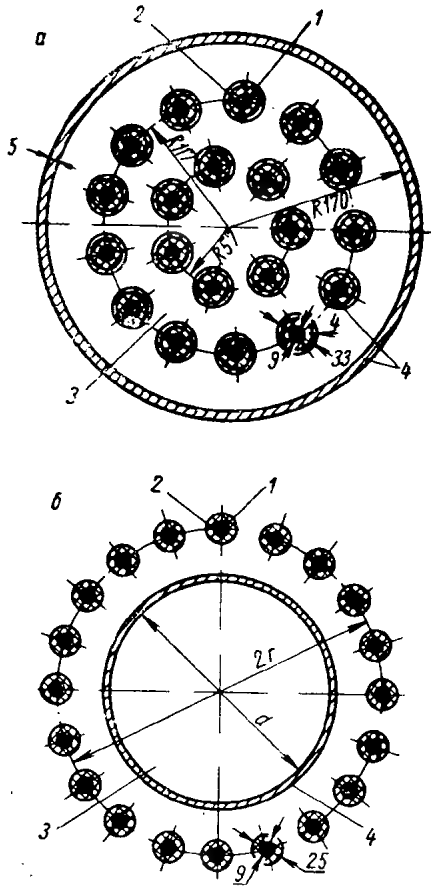

Fig. 1. Diagrams of models (dimensions given in mm): 1) source; 2) irradiator; 3) irradiated liquid; 4) model walls.

The amount of energy transferred to matter by the quanta was summed separately for each material in the system and obtained from the machine in relative units (Tables 1, 2).

The problem of γ-ray penetration was solved similarly [4].

The entire volume of the "heat exchanger" was subdivided into a number of regions occupied by different materials. We indicate the cylindrical regions occupied by the source material by $P_0^{m}k$. In this notation, m_1 is the source number in the inner row ($m_1 = 1,2,\ldots, M_1$), and m_2 is the source number in the outer row ($m_2 = 1,2,\ldots, M_2$). In our case, $M_1 = 7$ and $M_2 = 13$.

Let b_0 be the radius of the cylindrical regions. The annular coaxial cylinders which surround a source are indicated by $P_1^{m}k$ ($i = 1,2,\ldots, I-1$) and their outer radii by b_i.

We consider a_k to be the distance from the axis of a source in the kth row to the central z axis. The external walls of the heat exchanger, which are also in the form of cylindrical layers, are indicated by Q_j, and their outer radii by c_j ($j = 3,4,\ldots, J-1$).

The remaining volume, which is subdivided into three additional regions: the cylinder Q_0 of radius c_0 which contains no sources the axis of this cylinder coincides with the z axis ($c_0 \leq a_1 - b_{I-1}$), the annular cylinders Q_k ($k = 1, 2$) from which are removed the regions consisting of the sources in the kth row together with their surrounding materials, the outer radius c_1 of region Q_1 satisfying the condition $a_1 + b_{I-1} \leq c_1 \leq a_2 - b_{I-1}$, and the outer radius c_2 of region Q_2 equaling the distance from the z axis to the outer wall of the heat exchanger.

Thus, we have to do with two types of regions (see Tables 1, 2): the regions $P_i^{(m_k)}$, where $i = 0,1,2,\ldots, I-1$, and the regions Q_j where $j = 0,1,\ldots, J-1$.

The height of the heat exchanger is indicated by 2h. The probabilities of Compton scattering w_1 and photo-absorption w_2 equal

$$w_1 = \sigma\mu^{-1};\ w_2 = \tau\mu^{-1}\quad (w_1 + w_2 = 1),$$

where σ and τ are the γ-ray linear attenuation coefficients for Compton scattering and photo-absorption, respectively. Moreover, in the expressions for σ and τ, the values which they took at the ends of the straight-line sections of the trajectory were used. The value of τ (in cm^{-1}) was approximated for each material by the formula

$$\tau = R\alpha^S + T,$$

where $\alpha = E/mc^2$, which holds for a range of E from 0.02 to 2 MeV according to tests that were made. The values of the constants R, S, T are given in Table 1. The method of calculation of the quantity σ and of the quantum energy loss through scattering did not differ from that described in [4].

The program was constructed so that it could be used for apparatus of arbitrary dimensions having a similar type of configuration. In particular, the same program was used in this work for the calculation of the distribution of absorbed energy in the heat exchanger and in the still. In addition, the values of I and J are limited by the requirements $I \leq 9$, $J \leq 6$.

The results of the computations together with the original data for the heat exchanger are shown in Tables 1, 2, and they enable one to determine a number of quantities which are of practical interest, particularly the energy efficiencies for the model given. Thus, the e.e. of the system, η_c, which is equal to the ratio of the γ-ray energy absorbed in the liquid, i.e., in all the regions Q_j ($j = 0, 1, 2$), to the energy produced in the sources, is expressed

TABLE 1. Distribution of Relative Absorbed γ-Ray Energy A and Relative Energy Loss L, % (regions P_i)

Region characteristic		0	1	2	3	4	5	6	7	8
		Cobalt	Aluminum	Air	Steel	Air	Steel	Air	Brass	Plexiglas
b, cm		0.450	0.575	0.650	0.725	1.200	1.275	1.340	1.445	1.625
$-\ln R$		4.05	8.50	18.0	4.48	18.0	4.48	18.0	3.85	16.6
$-S$		2.99	3.30	3.25	3.04	3.25	3.04	3.25	2.93	3.23
$T \cdot 10^3$		1.3	0.1	0	1.3	0	1.3	0	0.7	0
$D \cdot 10$		6.00	1.95	0.001	5.50	0.001	5.50	0.001	6.10	0.81
A	$k = k_0$, $m = 1$	11.9±1.3 12.8±1.2	0.9±0.4 2.2±0.5	0 0	1.7±0.5 1.8±0.5	0 0	2.1±0.6 2.0±0.5	0 0	3.2±0.7 2.4±0.5	0.2±0.2 0.4±0.2
	$k = k_0$, $m \neq 1$	1.7±0.5 0.3±0.2	0.1±0.1 0.1±0.1	0 0	0.4±0.3 0.4±0.2	0 0	0.7±0.3 1.0±0.3	0 0	2.1±0.6 1.4±0.4	0.2±0.2 0.5±0.2
	$k \neq k_0$	0.9±0.4 0.3±0.2	0.2±0.2 0.1±0.1	0 0	0.5±0.3 0.3±0.2	0 0	1.5±0.5 0.2±0.2	0 0	1.2±0.4 1.0±0.3	0.5±0.3 0.6±0.3
L	$k = k_0$, $m = 1$	1.4±0.5 1.5±0.4	0 0.3±0.2	0 0.2±0.2	0 0	0.5±0.3 1.4±0.4	0 0.1±0.1	0 0.2±0.2	0.3±0.2 0.7±0.3	0.3±0.2 0.5±0.2
	$k = k_0$, $m \neq 1$	0.3±0.2 0.5±0.2	0 0	0.1±0.1 0	0 0	0 0.5±0.2	0 0.2±0.2	0.4±0.3 0.2±0.2	0.3±0.2 0	0 0
	$k \neq k_0$	0 0	0.3±0.2 0	0 0	0.1±0.1 0	0.7±0.3 0.6±0.3	0 0	0.2±0.2 0.3±0.2	0.3±0.2 0	0.2±0.2 0.7±0.3

Note: In the columns where values are given for A and L, the upper row of data refers to the case where the energy is produced in inner row sources, and the lower row to the case where the energy is produced in the outer row sources. The calculation of D was done as in [4].

TABLE 2. Distribution of Relative Absorbed γ-Ray Energy A and Relative Energy Loss L, % (regions Q_j)

Region characteristic	0	1	2	3	4	5
	water	water	water	plexiglas	air	brass
c, cm	4.0	10.0	17.07	17.37	17.46	17.59
$-\ln R$	11.3	11.3	11.3	16.6	18.0	3.85
$-S$	3.25	3.25	3.25	3.23	3.25	2.93
$T \cdot 10^3$	0	0	0	0	0	0.7
$D \cdot 10$	0.827	0.827	0.827	0.810	0.001	6.10
A	4.4±0.8 0.9±0.3	9.4±1.1 3.3±0.6	6.4±1.0 11.1±1.1	0.1±0.1 0.1±0.1	0 0	1.4±0.5 1.0±0.3
L	3.1±0.7 0.7±0.3	6.3±1.0 3.4±0.6	5.5±0.9 8.3±1.0	0 0.1±0.1	0.2±0.2 0.2±0.2	0 0.1±0.1

through the corresponding ratios η_{c_1} and η_{n_2} for the case where the energy is produced in only one source of the inner and outer rows, respectively, in the following manner:

$$\eta_c = \frac{M_1\eta_{c1} + M_2\eta_{c2}}{M_1 + M_2}.$$

It is easy to see from Tables 1, 2 that

$$\eta_{c1} = (20.4 \pm 1.6)\%\ *; \quad \eta_{c2} = (15.3 \pm 1.2)\%.$$

* Here and in the following, we give the standard error.

TABLE 3. Absorption A and Loss L of Energy (in %) for Source and Irradiator in a Vacuum (regions P_i)

Region characteristic	0	1	2	3	4	5	All P_i
A	10.3±0.7	1.7±0.3	0	2.2±0.3	0	1.7±0.3	15.9±0.8
L	1.6±0.3	0.3±0.1	0.2±0.1	0.4±0.1	0.8±0.2	0.1±0.1	3.4±0.4

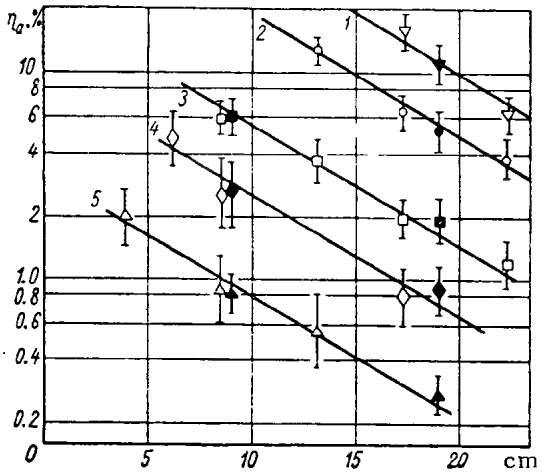

Fig. 2. Dependence of apparatus e.e., η_a, on source distance from the axis of the apparatus (solid points are experimental values; open points are computed data). Numbers on the curves indicate values of V in liters: 1) 24; 2) 14; 3) 4.8; 4) 2.2; 5) 0.63.

Consequently, $\eta_c = (17.1 \pm 1.0)\%$. We also computed the e.e. of the source, η_s, and of the irradiator, η_r (see Fig. 1). The quantities $_s$ and $\eta_s \cdot \eta_r$ are determined by the ratio of γ-ray energy flux escaping from the surface of the source (irradiator) to the energy produced when the source (source with irradiator) is located in a vacuum. The values obtained were: $\eta_s = (88.68 \pm 0.21)\%$, $\eta_r = (94.9 \pm 1.2)\%$. This indicates that, regardless of the construction of equipment and irradiator, one can use no more than ~89% of the γ-ray energy emitted by the given source. Similarly, for fixed irradiator construction, the maximum fraction of usable γ-ray energy amounts to $\eta_s \cdot \eta_r = 84\%$. The distribution of absorbed γ-ray energy when the source and irradiator are located in a vacuum is shown in Table 3.

One can experimentally determine the e.e. for the apparatus η_a, i.e., the ratio of the energy absorbed in the liquid to the energy flux escaping from the irradiator when it, and the source, are in a vacuum. The experiment, which was carried out by means of ferrosulfate dosimetry, gave the following value for η_a.

$$\eta_a = \frac{7\eta_{a1} + 13\eta_{a2}}{20} = (22 \pm 2)\%.$$

Here, η_{a_1} and η_{a_2} are the e.e. of the apparatus for the case where energy is produced only in one of the sources in the inner and outer rows, respectively ($\eta_{a_1} = (23 \pm 0.2)\%$, $\eta_{a_2} = (21 \pm 2)\%$.

From the definitions given for the different e.e., it follows that $\eta_s \eta_r \eta_a = \eta_c$. From that, on the basis of our calculations, one can obtain the values

$$\eta_a = (20.3 \pm 1.1)\%; \quad \eta_{a1} = (24.2 \pm 1.7)\%;$$
$$\eta_{a2} = (18.2 \pm 1.4)\%.$$

As can be seen, the experimental and calculated results are in satisfactory agreement.

Experiment, the Monte-Carlo calculations, showed that the quantities η_{a_1} and η_{a_2} for the heat exchanger model remained constant within the limits of statistical error when all the sources, except for one or two in the various rows, were removed from the model. This situation is explained by the small amount of mutual shielding of the irradiators. Further, in that model, the quantity $1-\eta_s$ equals within 10% the ratio of the absorbed radiation energy $A(P_0^{1k})$ to the energy produced for a given source (see Tables 1, 2). In other words, the fraction of back-scattered energy reflected from the liquid and the irradiator was small. With the same precision $A(P_0^{1k}) \approx \xi \tilde{A}(P_0^{1k})$, where $\tilde{A}$ is a quantity which is computed without taking multiple scattering into account, and ξ is the average fractional energy loss which a quantum experiences as the result of a single interaction with matter. For an initial energy of 1.25 MeV, ξ equals 0.47 for almost all materials. It appears that for the given source dimensions, a quantum undergoes, in the main, no more than one interaction within it.

For the model of the fractionating still (see Fig. 1b), the quantity η_a was determined both experimentally and by the Monte-Carlo method for several values of the diameter d and the distance 2r between the axes of two

diametrically opposed sources. As Fig. 2 indicates, the experimentally determined values of η_a are in good agreement with those obtained by the Monte-Carlo method in this case. Within the limits of error indicated in Fig. 2, they are approximated by the empirical formula

$$\eta_a = 51{,}7 \cdot V \cdot \exp(-0{,}135 \cdot r),$$

where V is the volume of the apparatus in liters; r is given in centimeters.

Analysis of the results indicated that the statistical accuracy of the results was satisfactory with the simulation of 200-300 trajectories. Exactly that number of histories was carried out for the solution of each version. Since the source was the same in all versions, and the determination of source e.e. was involved in each version, then the most precise value was obtained for the magnitude of source e.e. (the result of 10,085 histories).

Note that the computing time for the history of a single quantum on "Strela-3" was ~4 sec for the heat exchanger and ~2 sec for the fractionating still.

With an existing program, the Monte-Carlo method makes it possible to obtain various dara with respect to apparatus of arbitrary dimensions. The accumulation of such data enables one to expand considerably the applicable region of the semi-empirical method [2]. Through this same method, there exists a real possibility for solving problems of optimal construction of equipment and of the optimal number of sources and their activities.

The authors thank A. Kh. Breger for his constant concern for this work; they also wish to thank B. I. Vainshtein, N. A. Krasnoshchekov, and N. P. Syrkus for making experimental data available and for participating in discussions.

LITERATURE CITED

1. T. Rockwell, Nuclear Reactor Shielding [in Russian], Izd-vo inostr. lit., Moscow (1958); G. V. Gorshkov, Gamma Radiation from Radioactive Materials and the Fundamentals of Radiation Shielding Calculations [in Russian], Izd-vo AN SSSR, Moscow (1959); O . I. Leipunskii, B. V. Novozhilov, and V. N. Sakharov, Propagation of Gamma Quanta in Matter [in Russian], Fizmatgiz, Moscow (1960).
2. A. Kh. Breger, V. I. Vainshtein, L. S. Guzei, Yu. S. Ryabukhin, and N. P. Syrkus, Dokl. AN SSSR, 131, 1308 (1960); Proceedings of the Tashkent Conference on the Peaceful Uses of Atomic Energy [in Russian], Vol. II, Izd-vo AN UzSSR, Tashkent (1960), p. 123.
3. V. S. Galishev, V. I. Ogievetskii, and A. N. Orlov, Usp. fiz. nauk, 61, 161 (1957).
4. V. A. Él'tekov, B. M. Terent'ev, and D. I. Golenko, Zh. vychisl. matem. i matem. fiz., 1, 1089 (1961).
5. A. Kh. Breger, V. B. Osipov, and V. A. Gol'din, Atomnaya Énergiya, 8, 441 (1960).

All abbreviations of periodicals in the above bibliography are letter-by-letter transliterations of the abbreviations as given in the original Russian journal. *Some or all of this periodical literature may well be available in English translation.* A complete list of the cover-to-cover English translations appears at the back of this issue.

MEASUREMENT OF NEUTRON TISSUE DOSE OUTSIDE REACTOR SHIELDING

I. B. Keirim-Markus, V. T. Korneev, V. V. Markelov, and L. N. Uspenskii

Translated from Atomnaya Énergiya, Vol. 15, No. 5, pp. 386-393, November, 1963
Original article submitted January 12, 1963

RUS instruments, developed by the authors, are described that enable one to measure the flux and tissue dose rate of intermediate neutrons, which make a significant contribution to neutron tissue dose outside reactor shielding. The neutron dose composition was investigated in experiments at the IRT-1000 reactor, and it was shown that it depends essentially on shielding composition. It was established that the neutron tissue dose computed from readings taken with the RPN-1 instrument were actually too low by a factor amounting to one and one half outside water shielding and to five outside concrete shielding.

Thermal, intermediate, and fast neutrons each make their contribution to the neutron tissue dose outside reactor shielding. The quality of the shielding is often checked with an RPN-1 instrument which detects only thermal and fast neutrons, and thereby, the contribution of intermediate neutrons to tissue dose is not taken into account. This is associated not only with the unsatisfactory development of the intermediate neutron dosimetry problem, but also with the absence of the necessary instruments [1]. The creation of the RUS* instruments [2, 3] make it possible to partially eliminate the gap and to evaluate the intermediate neutron contribution to tissue dose outside shielding.

The RUS instruments have two scintillation counters T_1 and T mounted on an FÉU-35 (Fig. 1) and meant for the detection of slow neutrons. The zinc sulphide phosphor, 7 cm^2 in area and containing natural boron or B^{10}, which was used in [4] was used as a scintillator. It is also possible to use the T-1 phosphor [5]. The scintillation counter T is a compressed disk 1.2 mm thick containing 0.5 g ZnS–Ag, B and 1 g of plastic which contains 7 mg/cm^2 of boron, and which is approximately ten times more efficient than T_1. Depending on the discrimination level, one pulse from the counter T corresponds to 0.3-1.5 thermal neut/cm^2. This counter is practically insensitive to γ-radiation (Co^{60}) up to 0.1 r/sec. By means of a Pu^{239} check source mounted in the rotating cover of the counter, the calibration of the instrument is checked at the time of measurement.

In the main, the detection of intermediate neutrons by the RUS instruments is based on two well known principles [1, 6], one of which consists of shielding the scintillator by a cadmium layer 0.3-0.5 mm thick as a result of which the detector T becomes insensitive to thermal neutrons but detects neutrons of intermediate energies (above 0.4-0.5 eV). For Fermi spectrum neutrons ($\sim E_n^{-1}$), the efficiency of a thin boron detector covered by a cadmium filter is 25 times lower than the efficiency of the unfiltered detector for thermal neutron detection [1] in calculations based on unit flux. Actually, the ratio of the average efficiencies of such a detector for detecting the intermediate neutrons of a Fermi spectrum (ε_i) and for detecting thermal neutrons (ε_T) is

$$\frac{\varepsilon_i}{\varepsilon_T} = \frac{1.128 \int_{0.4}^{5\cdot 10^5} \frac{\sigma\, dE}{E}}{\sigma_T \int_{0.4}^{5\cdot 10^5} \frac{dE}{E}} = \frac{1}{25},$$

*RUS-2 (USD), RUS-3, RUS-4, and RUS-5 instruments were exhibited at the Exhibition of the Achievements of the National Economy of the USSR in 1957.

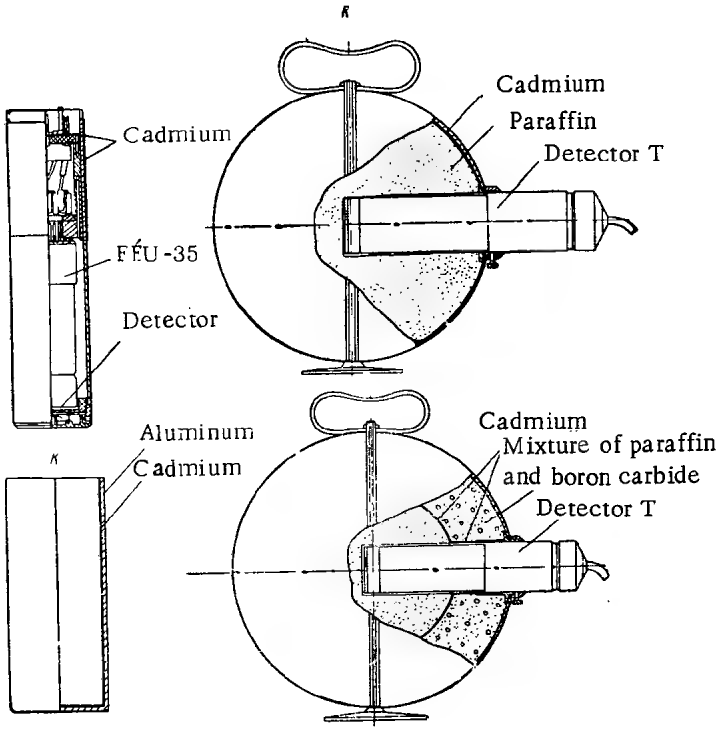

Fig. 1. Neutron detectors of the RUS-5 instrument: T) slow neutron scintillation counter; K) cadmium cover; R) moderator for measuring intermediate and fast neutron flux; D) moderator for measuring intermediate and fast neutron dose.

since the integral in the denominator equals 14, and the ratio of the magnitude of the resonance integral to the magnitude of the thermal neutron capture cross section for thin detectors (1/v type) is 0.5.

Thus, by placing the detector T, without the cadmium cover, in a thermal neutron flux of known density Φ_T cm$^{-2}\cdot$sec^{-1}, one can calibrate the detector with cadmium cover as an intermediate neutron dosimeter. Since a flux of 300 Fermi spectrum intermediate neutrons per cm^2 produces a maximum tissue dose of 1 μrem [1], then the neutron tissue dose rate measured by the instrument will be defined by the ratio $25\cdot\Phi_T/300 = \Phi_T/12$ μrem/sec. A similar relation is valid for lithium detectors and other detectors which are based on the use of nuclear reaction with a cross section $\sigma \sim E_n^{-\frac{1}{2}} \sim 1/v$.

If the detector is not thin, i.e., thermal neutron absorption is large, then an intermediate neutron dosimeter calibrated by the method presented above will overestimate the magnitude of the tissue dose by a factor $\sigma_T n(1-e^{-\sigma_T n})^{-1}$, where n is the number of boron (lithium, etc.) atoms per cm^2 for the effective thickness of the detector. This factor is 1.17 for the detector T. The specified method of calibration is valid under the condition that the intermediate neutron spectrum actually obeys the $\sim E_n^{-1}$ law. This condition is fulfilled sufficiently well in a number of cases [7, 8]. However, if the shielding contains materials with a large slow neutron capture cross sections, then the Fermi spectrum is depressed in the low-energy region and the calibration factor for the detector turns out to be too low. The maximum tissue dose per neutron, averaged over the actual spectrum, thereby increases.

Previously, it was difficult to estimate the error which was introduced by the deviation of the actual neutron spectrum outside the reactor shielding from the $\sim E_n^{-1}$ spectrum assumed in the calculations. From a comparison of the readings from this detector with the results of neutron tissue dose measurements made with other instruments in various radiation fields, it is clear that this error does not exceed 30% (an example of such a comparison is given below).

The second principle of intermediate neutron detection which was used in the development of the detectors is based on neutron moderation. One of the moderators is in the form of a cadmium-covered polyethylene sphere 210 mm in diameter into which the detector T is introduced (see Fig. 1). The dimensions of the moderator are so chosen

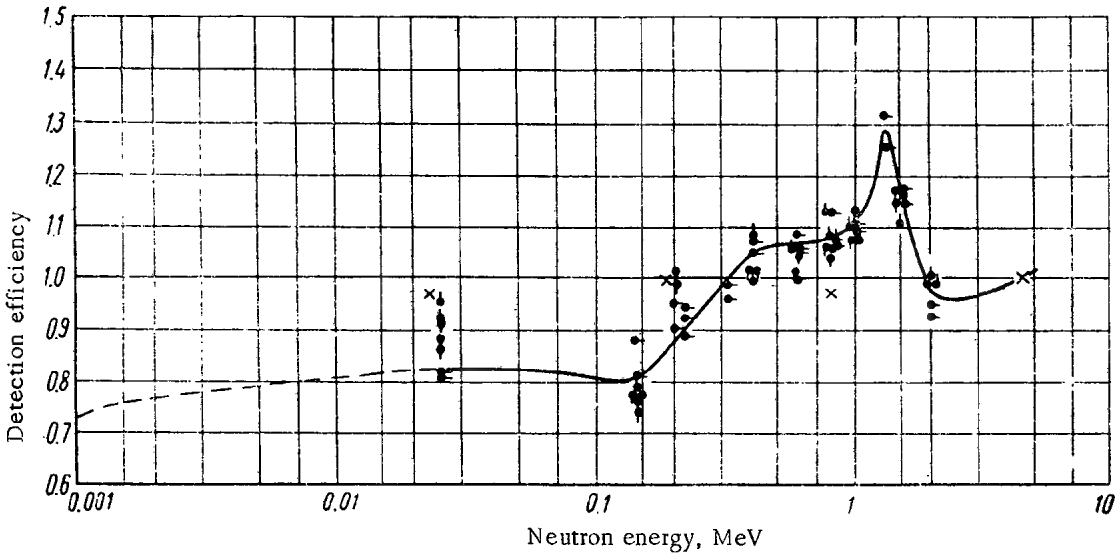

Fig. 2. Dependence of detector R efficiency on neutron energy.

that the efficiency of the scintillation counter with moderator (detector R) is independent of neutron energy, at least within the range from 25 keV to 5 MeV (with an accuracy of ±20%). The detector operates like a "long" counter of intermediate and fast neutrons with isotropic efficiency.

Curves are given in Fig. 2 for the dependence of detector R efficiency on neutron energy which were obtained in 1958 with photoneutron sources that were compared with the USSR standard, and which were refined in 1959 with monoenergetic neutrons from a Van de Graaf generator. Detector R exhibits a lesser dependence of efficiency on energy as compared with detectors using cylindrical paraffin moderators 62 and 50-75 mm thick [9, 10].

The configuration of the moderator for the fast and intermediate dosimeter of the RUS-3 instrument (detector D), selected with the help of photoneutron sources, is in the form of a drop-shaped paraffin mass (250 mm in diameter). Within it is a concentrically located paraffin-filled cadmium shell 150 mm in diameter. The variation of this dosimeter with hardness is shown in Fig. 3.

In 1959, additional measurements were made a Van de Graaf generator which made it possible to select improved moderator configurations. The dimensions of the internal sphere in detector D of the RUS-4 and RUS-5 instruments were not changed, but the external absorbing layer was increased to a diameter of 300 mm and it was filled with a mixture of paraffin and boron carbide (in a ratio of 10 : 4 by weight).

As can be seen from Fig. 3, the variation with hardness of detector D in the RUS-4 and RUS-5 instruments does not exceed ±30% in the energy range 0.1-5 MeV. The dosimeter posesses an increased efficiency for the detection of neutrons with energies below 0.1 MeV. The mean efficiency for the detection of Fermi spectrum neutrons is overestimated by approximately 30%. Such a discrepancy is permissable since 43% of the maximum tissue dose from the intermediate neutrons in the Fermi spectrum falls in the energy range 0.1-0.5 MeV, and only 20% in the region below 1 keV [11]. The variation with hardness of detector D is considerable better than that for detectors with paraffin cylinders 115 mm thick or with paraffin spheres 255 mm in diameter [9].

Measurements of neutron flux and tissue does outside reactor shielding were made with detector T in conjunction with moderators and cadmium filters. Thermal neutron flux density Φ_T was recorded by detector T without cadmium filter, neglecting possible changes in neutron temperature. The thermal neutron tissue dose rate P_T was determined from the relation 1100 neut/cm^2-sec ~ μrem/sec [1]. The intermediate neutron tissue dose rate P_I was measured by detector P (counter T with cadmium shield) which was calibrated by the method given above. The intermediate and fast neutron flux density (Φ_{I+F}) was determined from the readings of the detector R. The total neutron flux density Φ was determined from the sum of the quantities measured by detectors T and R.

The intermediate and fast neutron tissue dose rate P_{I+F} was measured with detector D which was calibrated by means of a Po–Be source. Calibration was made on the basis that neut/cm^2-sec was equivalent to 1 μrem/sec. The total neutron tissue dose rate P was determined from the sum of the measurements with detectors T and D. The fast neutron tissue dose rate P_F (neutrons with energies $E_n > 1.5$ MeV) was estimated with the RPN-1 instrument

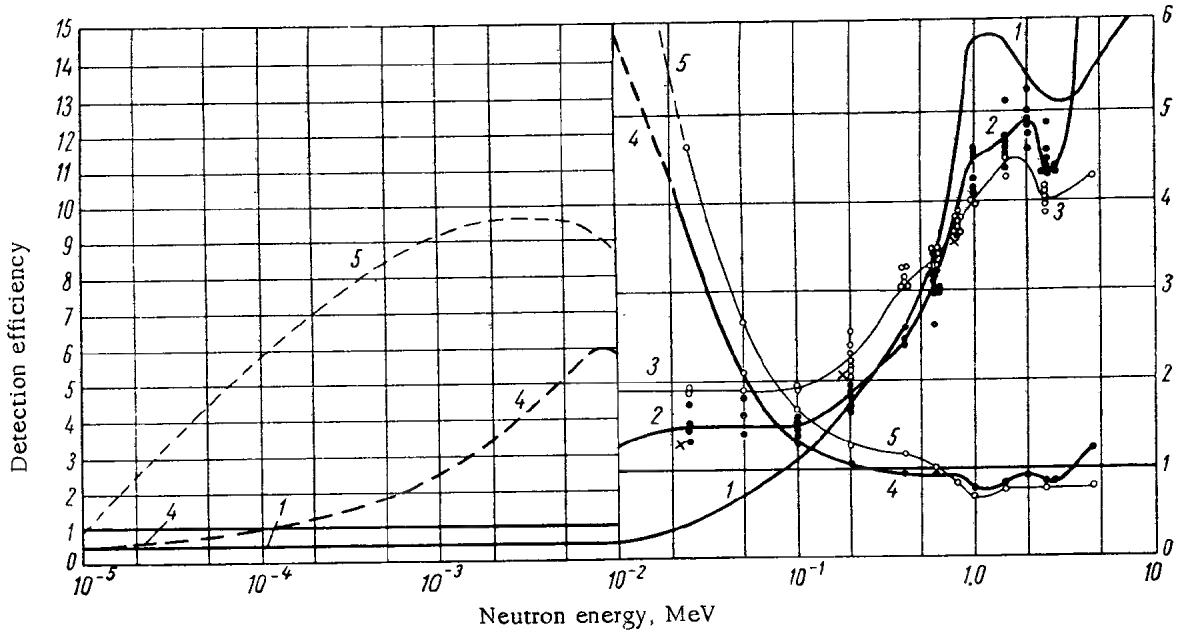

Fig. 3. Dependence of detector D efficiency on neutron energy: 1) maximum tissue dose per unit neutron flux, $\times 0.72 \cdot 10^{-8}$ rem/neut-cm^{-2} [1, 2]; 2) neutron detection efficiency of detector D in RUS-4 and RUS-5 instruments; 3) neutron detection efficiency of detector D for the RUS-3; 4); 4) variation with hardness of detector D in the RUS-4 and RUS-5 instruments; 5) variation with hardness of detector D for the RUS-3.

which was calibrated simultaneously with detector D and which discriminated against as much as 50 μc/sec of Co^{60} γ-radiation. It was assumed that 25 neut/cm^2-sec corresponded to 1 μrem/sec for flux densities measured with the RPN-1.

Besides neutron flux density Φ and neutron tissue dose rate P, the measurements made it possible to determine the contribution to the tissue dose from thermal, intermediate, and fast* neutrons recorded by the RPN-1 instrument. In addition, from the specific absorbed dose (P/Φ), the mean neutron energy outside the shielding (averaged over dose contributions) was determined by means of curve 1 (see Fig. 3). The error in the measurements was determined by the variation with hardness of the detectors, and did not exceed ±25%. The presence of accompanying radiation (γ-radiation, intermediate neutrons during thermal neutron measurements, etc.) in no case gave an error larger than 3%. The statistical errors of the measurements also did not exceed 3% except in cases where very small neutron fluxes were recorded (especially with the RPN-1 instrument).

The results of measurements made at the IRT-1000 reactor of the I. V. Kurchatov Institute of Atomic Energy [12] operating at a thermal power of 1 MW are given in Table 1 for the points shown in Fig. 4. The shielding of IRT reactors, which are quite common both in the USSR and abroad, is characteristic, within known factors, for many industrial and research reactors. Therefore, the results and the comparison of the readings of the various detectors are of rather great interest.

The data in Table 1 indicates that the neutron tissue dose rate at the time of measurement was much less than the permissable limit in all irradiated reactor locations.

The quality of neutron shielding is usually determined by the attenuation of a flux of fast neutrons with energies of several MeV. However, one should consider the fact that the build-up of intermediate and thermal neutrons in the outer shield layers also plays an important role in the formation of the dose field outside shielding. The fact that the contribution of intermediate neutrons is considerable is worthy of attention. Thus, when the shield consists of concrete (see Fig. 4 and Table 1, points 1-5), 50-60% of the tissue dose is contributed by intermediate neutrons, and the contribution of intermediate and fast neutrons amounts to 90-98%. Outside shielding with a high hydrogen content (points 12-14), 35-40% of the tissue dose is contributed by intermediate neutrons, and 35-65% by intermediate

* Here, and in the following, fast neutrons are considered to be those neutrons with energies above 1.5 MeV.

TABLE 1. Results of Neutron Tissue Dose Measurements Outside the Shielding of an IRT Reactor (location of measurements shown in Fig. 4)

Measurement location	Therman neutrons			Intermediate neutrons		Intermediate and fast neutrons					Fast neutrons			Neutrons of all energies			
	T			P		R	D		R and P		RPN-1			T and R	T and	T, and R	
	Φ_T	P_T		P_I		Φ_{I+F}	P_{I+F}		P_{I+F}	E_n	Φ_F	P_F		Φ	P	P/Φ	E_p
	neuts/cm^{-2}·sec	rem/sec	%	μrem/sec	%	neuts/cm^{-2}·sec	rem/sec	%	rem-cm^{-2}	keV	neuts/cm^{-2}·sec	keV	%	neuts/cm^{-2}·sec	μrem/sec	rem-cm^{-2}/neut	keV
1	25	0.023	11	0.12	60	23	0.18	90	$8\cdot10^{-9}$	100	1	0.04	20	48	0.20	$4\cdot10^{-9}$	40
2	10	0.009	7	0.068	52	5.8	0.12	92	$2\cdot10^{-8}$	400	<1	<0.04	—	16	0.13	$8\cdot10^{-9}$	100
3	2.6	$2.3\cdot10^{-3}$	4	0.033	51	1.5	0.062	96	$4\cdot10^{-8}$	1000	<1	<0.04	—	4.1	0.065	$1.6\cdot10^{-8}$	300
4	0.4	$3.6\cdot10^{-4}$	3	$6.5\cdot10^{-3}$	46	0.6	0.014	97	$2\cdot10^{-8}$	400	<1	<0.04	—	1	0.014	$1.4\cdot10^{-8}$	200
5	1.3	$1.2\cdot10^{-3}$	2	0.035	51	1.3	0.068	98	$5\cdot10^{-8}$	>1000	<1	<0.04	—	2.6	0.069	$2.7\cdot10^{-8}$	600
6	2500	2.3	24	3.3	35	210	7.2	76	$3.5\cdot10^{-8}$	900	—	—	—	2700	9.5	$3.5\cdot10^{-9}$	30
7	3.9	$3.5\cdot10^{-3}$	5	0.029	39	1.9	0.072	96	$4\cdot10^{-8}$	1000	<1	<0,04	—	6.8	0.075	$1.3\cdot10^{-8}$	200
8	50	0,045	13	0.17	47	19	0.31	87	$1.5\cdot10^{-8}$	250	<1	<0,04	<11	69	0.36	$5.2\cdot10^{-9}$	60
9	0.6	$5\cdot10^{-4}$	—	0.003	—	<0.05	<0.01	—	—	—	<1	—	—	0.6	$>5\cdot10^{-4}$	—	—
9a	2.0	$2\cdot10^{-3}$	—	0.003	—	<0.05	<0.01	—	—	—	<1	—	—	2	> 0.002	—	—
10	0.75	$7\cdot10^{-4}$	—	0.004	—	<0.05	0.031	—	—	—	<1	—	—	0.75	0.036	—	—
11	6900	6.2	16	24	62	1700	33	84	$2\cdot10^{-8}$	400	230	9.2	24	8600	39	$4.5\cdot10^{-9}$	45
12	810	0.74	24	1.8	58	97	2.4	76	$2.5\cdot10^{-8}$	600	10	0.40	13	910	3.1	$3.4\cdot10^{-9}$	30
13	620	0.56	40	0.50	36	47	0.80	57	$1.5\cdot10^{-8}$	250	8	0.32	23	670	1.4	$2.1\cdot10^{-9}$	15
14	880	0.80	33	1.0	42	97	16	67	$1.5\cdot10^{-8}$	250	12	0.48	20	980	2.4	$2.5\cdot10^{-9}$	20
15	1650	1.5	4	33	97	160	32	94	$2\cdot10^{-8}$	400	380	15	44	1800	34	$1.9\cdot10^{-8}$	350
16	>19 000	>17	>4	330	<82	15 000	380	<95	$2.5\cdot10^{-8}$	600	2800	110	28	>34 000	>400	—	—
17	11 500	10.5	23	22	49	2100	34	76	$1.5\cdot10^{-8}$	250	300	12	27	14 000	45	$3.2\cdot10^{-9}$	30

Note: The increase in neutron tissue dose rate at points 11-17 may have been caused both by streaming through the plugs closing the vertical channels and by lowering of the water level in the pool at the time of measurement.

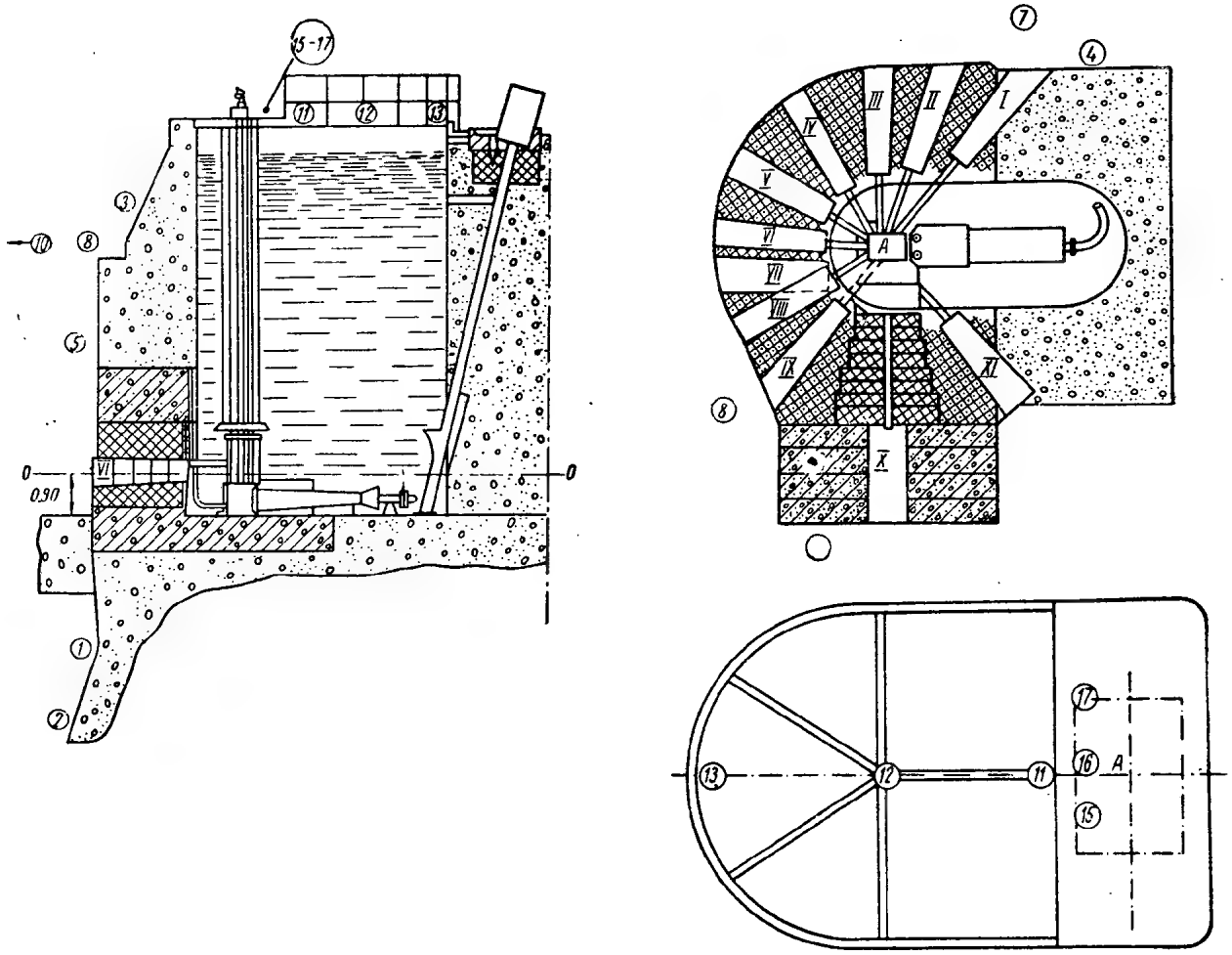

Fig. 4. Location of neutron tissue dose rate measurements outside the shielding of an IRT-1000 reactor: a) vertical section; b) horizontal section through center of the core; c) plan of the reactor pool (A is the reactor core); 1) at a pump location close to the shielding, ~ 5 m from the core (concrete external shielding layer); 2) the same location, 6-7 m from the core; 3) on the second floor close to the shield, ~ 5.5 m from the core (concrete external shielding layer); 4) close to the shield at the first horizontal channel, 4 m from the core (concrete external shielding layer); 5) above the fourth horizontal channel, 4 m from the core (concrete external shielding layer); 6) beside the open thermal column channel (the channel was especially opened for making the measurement); 7) in a working area with gate open on the first channel, in which thermal neutrons and γ-rays are absorbed; 8) staircase area on the second floor while the thermal column channel was open (the channel was specially opened at the time of measurement); 9) in the working position of a console operator; 9a) in the working position of a console operator with the thermal column channel open; 10) room No. 8, one of the laboratories on the second floow, 20-25 m from the core; 11) above the surface of the pool, beside the shielding control system area (water shielding); 12) above the central part of the pool; 13) above the far end of the pool; 14) at the pool intake on the third floor; 15) above the vertical biologic channel; 16) above the fifteenth vertical channel; 17) above the first vertical channel.

and fast neutrons with energies up to 1.5 MeV. Therefore, the relative contribution of the three parts of the neutron spectrum depends significantly on the composition of the shielding, or, more precisely, on the composition of the external layer several relaxation lengths thick.

On the basis of a generalization of a number of experimental results, Table 2 gives the approximate composition of neutron dose for three types of shielding materials. The range of values shown in the table reflects the variations in neutron dose composition from point to point outside actual reactor shielding but does not include the error

TABLE 2. Composition of the Dose from Neutron Radiation Outside Reactor Shielding (in percent of tissue dose from neutrons of all energies)

Shielding type	Neutrons			
	thermal	inter-mediate	intermediate plus fast < 1.5 MeV	fast > 1.5 MeV
I. Concrete	4-10	50-60	70-85	10-20
II. With high hydrogen content (water, polyethylene)	20-40	30-60	35-65	15-25
III. Containing slow neutron absorbers	2-10	60-80	70-90	5-20

which may be introduced by the variation with hardness of the instruments used. From this data, it follows that neutron dose measurements outside reactor shielding with an RPN-1 instrument, which detects only thermal and fast neutrons, lead to an underestimate of the total neutron tissue dose by one and one half to the times. Consequently, it is necessary to apply a correction factor to the measurements with an RPN-1, increasing the tissue dose values obtained by five times for type I, by one and one half times for type II and by ten times for type III shielding (see Table 2).

Comparing the results in Table 2 with the estimates in [6], one is convinced that, according to the calculations for water or concrete shielding 50 cm thick, the contribution of intermediate neutrons to tissue dose is less than outside the shielding of an actual reactor although the calculations [6, 8] correctly indicate a lower value of intermediate neutron contribution for water shielding. From Table 1, one can also see that the results of the measurements with detector P deviate slightly from the difference of the readings from detectors D and B (points 1, 11-14) and are 1.3-1.8 times less than those of detector D which, in contrast to detector P, overestimate the intermediate neutron tissue dose rate. From such an analysis, it follows that detector P can be used as a crude intermediate neutron dosimeter suitable for measurements outside reactor shielding.

Using the principles on which the creation of detector P was based, one can adapt the RPN-1 instrument for intermediate neutron dosimetry. Generally, any sufficiently sensitive slow neutron detector, based on the use of nuclear reactions with cross section $\sim E_n^{-\frac{1}{2}}$, can be used as an intermediate neutron dosimeter if the detector is surrounded by a thermal neutron absorber. One can calibrate such a dosimeter by the method given above.

Personnel dosimeters for intermediate neutrons can also be produced by a similar method.

The method presented for the analysis of neutron dose composition makes it possible to determine rapidly the dose contribution of the three neutron groups. By employing a larger number of neutron absorbers and moderators with different, but known, spectral characteristics, one can obtain more detailed information about the neutron dose composition or energy spectrum using a system of equations of the form: $N_i = \Sigma_j \varepsilon_{ij} \varphi_j$, where N_i is the counting rate of the ith counter; ε_{ij} is the mean efficiency (or dose sensitivity) of the ith counter for the jth portion of the neutron spectrum; φ_j is the neutron flux or tissue dose rate in the jth portion of the spectrum. Such a method offers additional possibilities for studying the composition of neutron radiation.

The authors wish to thank I. E. Kutikov for taking upon himself the task of calibrating the photoneutron sources, Yu. F. Chernilin for providing such favorable conditions for carrying out the measurements, and L. N. Smirennii, A. N. Serbinov, O. O. Lashuk, and A. A. Kutuzov for helping to calibrate the RUS detectors.

LITERATURE CITED

1. A. G. Istomina and I. B. Keirim-Markus, Atomnaya Énergiya, 8, 239 (1960).
2. I. B. Keirim-Markus et al. Atomnaya Énergiya, 4, 218 (1958); I. B. Keirim-Markus, et al. Pribory i tekhnika éksperimenta, No. 5, 35 (1960); No. 1, 86 (1961).
3. U. Ya. Margulis, Shielding Against the Action of Penetrating Radiation [in Russian], Gosatomizdat, Moscow (1961), p. 61.
4. I. B. Keirim-Markus and A. P. Pesotskaya, A Collection of Radiochemical and Dosimetric Techniques [in Russian], Medgiz, Moscow (1959), p. 311.

5. T. V. Timofeeva, Atomnaya Énergiya, 3, 156 (1957); Izv. AN SSSR, ser. fiz., 22, 14 (1958).
6. O. I. Leipunskii, Atomnaya Énergiya, 12, 216 (1962).
7. IRE Trans. Nucl. Sci., NS-8, No. 3, 35 (1961).
8. J. Brown and R. Nilson, Collected Papers of the Symposium on Selected Problems in Dosimetry [in Russian], Gosatomizdat, Moscow (1961), p. 209.
9. J. de Pangher, J. Nucl. Instrum. and Methods, 5, No. 8, 61 (1959).
10. R. Wallace et al. Collected Papers of the Symposium on Selected Problems in Dosimetry [in Russian], Gosatomizdat, Moscow (1962), p. 97.
11. O. I. Leipunskii, in: Instruments and Methods for Radiation Analysis [in Russian], No. 3, Gosatomizdat, Moscow p. 97.
12. V. V. Goncharov et al. Proceedings of the Second International Conference on the Peaceful Uses of Atomic Energy [in Russian], Dokl. sov. uchenykh. Vol. 2, Atomizdat, Moscow (1959), p. 243.

All abbreviations of periodicals in the above bibliography are letter-by-letter transliterations of the abbreviations as given in the original Russian journal. ***Some or all of this periodical literature may well be available in English translation.*** **A complete list of the cover-to-cover English translations appears at the back of this issue.**

KINETICS OF THE SWELLING PRODUCED IN FISSIONABLE MATERIALS BY THE SEPARATION OF THE GASEOUS PHASE FROM A SUPERSATURATED SOLID SOLUTION

V. M. Agranovich, É. Ya. Mikhlin, and L. P. Semenov

Translated from Atomnaya Énergiya, Vol. 15, No. 5,
pp. 393-403, November, 1963
Original article submitted August 16, 1962

When fissionable materials are irradiated with neutrons, under certain conditions a supersaturated solution of inert gases is formed. There is intensive separation of the gaseous phase, accompanied by the formation and subsequent growth of a large number of gas pores. In the present work, making quite general assumptions regarding the manner in which the gas pores are produced, we investigate the kinetics of the diffusion process of their formation and growth, resulting both from the color of the material under the effect of the gas pressure in the pores and from a mechanism related to the diffusion of vacancies to the pores. In the latter case it is assumed that the influx of vacancies to a pore is correlated with the influx of gas atoms in such a way that the pressure of the gas in the pore is brought essentially into equilibrium with the pressure caused by surface tension. We obtain an asymptotic solution of this problem and find the asymptotic behavior of the number of pores and their average dimensions, as well as the asymptotic law governing the increase in volume (the swelling).

1. Introduction and Statement of the Problem

Considerable attention has been devoted in recent years to the swelling of fissionable materials as a result of irradiation, since it is just this phenomenon that prevents high burn-up at high temperatures and thus creates difficulties in the economically expedient utilization of nuclear energy. The work "swelling" generally denotes a considerable increase in the volume of the fissionable material which takes place at high temperatures either during the process of irradiation or after a prior low-temperature irradiation. The mechanism of swelling is very complicated. The phenomenon is evidently caused by a number of processes whose relative complexity results both from the properties of the material and from the conditions of irradiation. Unfortunately, the experimental data accumulated so far are insufficient for drawing unequivocal conclusions as to what processes are responsible for the swelling of a given material under a particular set of conditions. Nevertheless, definite ideas have been developed by this time with regard to the essential nature of the processes taking place in swelling. Thus, for example, the role played by the diffusion of gaseous fission products has been generally recognized. As the gas atoms diffuse, they enter the pores that may be formed in the material during irradiation or during the annealing process taking place after irradiation. In certain cases these pores exist in the material even before irradiation. In the present study we shall consider only the increase produced in the volume of the material by the growth of the gas pores. The question of what contribution to the swelling is made by the expansion of the lattice resulting from "solid" fission products* and by the bursting of the grain boundaries, as well as by many other factors, will not be considered in the present article.

* It should be noted in passing that the increase in volume produced by nongaseous fission products is not a linear function of burn-up and can be considered approximately linear only for sufficiently low burn-up values. If the nonlinearity of the volume increase is taken into consideration, we find that its values are somewhat lower than those obtained by the linear approximation. These considerations are fairly obvious and are mentioned here only because they have not yet been reflected in the studies devoted to swelling. In such studies, the swelling caused by solid fragments is usually characterized by the ratio of volume increase to burn-up, that is, a linear relationship is implicitly assumed. Such an approach, however, may cause serious misunderstandings. Thus, for example, it is stated in [3] that for UO_2 the results of theoretical estimates of this ratio (1-1.5% uranium atoms fissioned) do not agree with the experimental value which amounts to 1/3% for 1% uranium atoms fissioned when the burn-up value is 52%. But there is no con-

A very important question for the entire problem of gas swelling is what mechanisms produce the growth in the gas pores. According to one idea [1], the gas accumulated in the pores produces a considerable pressure in them, to that there is a deformation of the material caused by its creep. From this point of view, the swelling is related chiefly to the decrease in the creep resistance of the material as the temperature increases.

In [2] the kinetics of swelling is considered on the basis of the above-described ideas. In order to simplify the calculations, the authors neglected the time needed for the diffusion of a gaseous fragment into the pores and assumed that the bubbles form a rectangular lattice. The swelling value was defined as the increase in the volume of a sphere with a radius of $(3/4\pi n)^{1/3}$, where n is the pore concentration at the center of which is a spherical bubble. It was taken into consideration that a plastic zone may be formed around the bubble at stresses above the yield point; in addition, a correction was made for the fact that the ideal gas equation could not be used for small bubbles, since the gas pressure in these may be high. In the calculations the authors used the creep constants obtained from tests made on large specimens of unirradiated uranium. They found, however, that their volume increase values in the 450-650°C region were lower than those experimentally observed.

In [4], using a model that assumed that pores were already present in the homogeneous fissionable material, equations were formulated that made it possible to describe the kinetics of the diffusion and accumulation of gaseouse fragments in the pores and the growth of the pores under the influence of the pressure produced by the gas. It was assumed that the deformation of the material around a pore may result both from plastic flow and from creep. In that study we introduced the concept of the time required for the start of the swelling and showed that the burn-up during the time preceding the start of the swelling could serve as a criterion for judging porous fissionable materials from the viewpoint of their susceptibility to swelling. The time required for the start of the swelling was found to be function of the burn-up rate.

Another view of the mechanism of swelling is based on the assumption that the gas pressure in a bubble is essentially balanced by the surface tension, so that the growth of the bubble takes place not because of any creep deformation or plastic flow in the material but because of the influx of vacancies into the pore [5].

We consider below the problem of swelling in a material when the generation of pores is taken into account. For the sake of simplicity, we shall assume that all the pores are spherical and that a gaseous fragment that has reached the surface of the pore is retained by it, while the flow of fragments out of the pore may be neglected. We are interested in the volume increase that results from the growth of the gas pores and has the form

$$\Delta V = \frac{4\pi}{3} \int_0^\infty \varrho^3 f(\varrho, t)\, d\varrho. \tag{1}$$

Here $f(\rho, t)$ is the function describing the pore distribution according to size at time t; ρ is the radius of the pore. Thus, the total number of pores is

$$N(t) = \int_0^\infty f(\varrho, t)\, d\varrho. \tag{2}$$

The function $f(\rho, t)$ satisfies the continuity equation

$$\frac{\partial f}{\partial t} + \operatorname{div}(f v_\rho) = \Psi(\varrho, t), \tag{3}$$

where $v_\rho = d\rho/dt$ is the velocity of displacement of the pores in size space; $\Psi(\rho, t)$ is the rate of generation of pores with radius ρ at time t. The change produced in the function (ρ, t) by the coalescence of pores will be neglected. It is assumed, moreover, that the medium is homogeneous and that there are no temperature gradients.

---

tradiction here. The fact is simply that for such high burn-up values the increase in volume can no longer be considered a linear function of burn-up. The value of 1/3% for 1% uranium atoms fissioned, found for this burn-up value, does not in fact characterize the variation in the volume increase as a function of burn-up; it merely indicates that at a concrete burn-up value of 52% the UO_2 volume has increased by 17%.

Let us assume that all pores have radius ρ_0 when they are generated. Then

$$\Psi(\varrho, t) = \psi(t)\,\delta(\varrho - \varrho_0). \tag{4}$$

In order to make clear the nature of the function $\psi(t)$ we must consider the mechanism of gas-bubble generation. Unfortunately, at present this question is by no means adquately understood, and here we shall confine ourselves to describing the fundamental ideas that exist today. In general, pores may be produced in either a heterogeneous or a homogeneous manner. Thus, for example, there may be heterogeneous generation of pores along lines of dislocation, at inclusions of a second phase, at fission peaks, etc. In the latter case, in particular, the rate of pore generation is determined by the burn-up rate and is not directly related to the supersaturation of a solid solution by fission products. The homogeneous generation of pores may be important in cases where the concentration c(t) of the gas dissolved in the material is far higher than the equilibrium concentration. The appearance of nucleation centers in this case is determined by the probability of the formation of a complex consisting of some number l of gas atoms, where l must be such that the complex will have a sufficiently long lifetime and be able to capture $l + 1$ gas atoms. It is quite clear that the rate of formation of the nucleation centers of the new phase will increase as the concentration of gaseous fragments in the crystal increases and will evidently be especially large near lines of dislocation, where, in accordance with the calculations of Greenwood et al. [6], the concentration of fission fragments may be about 10^5 times as high as elsewhere in the lattice. Different mechanisms of pore generation, in general, lead to different types of variation of $\psi(t)$ as a function of c(t). However, without analyzing the microscopic processes leading to the formation of pores, we may use the following expansion, which enables us to represent a fairly wide class of functions:

$$\psi(t) = \sum_{l=1}^{\infty} \xi_l (c - c_0)^l, \tag{5}$$

where c_0 is the equilibrium concentration of gas in the material.† Using Eq. (5), according to which the rate of formation of pores with an initial radius ρ_0 at time t is determined by the concentration of gaseous fragments at that time, we assume that the interval of time in which a center matures to a micropore of radius ρ_0 (see Section 4) is small in comparison with the characteristic time during which the concentration c(t) of gaseous fission fragments changes substantially.‡ In this connection, it should be noted that the way in which c(t) varies with time is considerably affected by the experimental conditions. Thus, for example, if the conditions are such that the formation of gaseous fragments begins at some instant of time t = 0 and then continues at a fixed rate, the concentration c(t) will first increase to some maximum value and then gradually decrease. In this case, the characteristic time may be taken to be the time required for c(t) to reach its maximum value. Evidently this time depends not only on the coefficients of diffusion of the gaseous fragments, but also on the rate of formation of fission fragments, etc.** For this process the gas concentration c(t) satisfies the equation

$$\frac{dc}{dt} = a - 4\pi D c(t) \int_0^{\infty} \varrho f(\varrho, t)\, d\varrho, \tag{6}$$

where a is the rate of formation of gaseous fragments per unit of volume and D is their coefficient of diffusion. The system of equations (3), (5), and (6), together with the equation for the determination of v_ρ makes it possible to solve completely the problem of the swelling of fissionable materials, using fairly general assumptions on the nature of the generation and growth of pores (the actual form of the equation for determining v_ρ depends upon the mechanism of pore growth).

† In the stages of swelling that interest us the gas concentration c(t) is considerably higher than its equilibrium value c_0; consequently, we shall hereafter neglect c_0 in comparison with c(t). For the same reason, processes of the coalescence type [7] do not play an significant role under these circumstances (high degree of supersaturation). The latter statement does not apply to the conditions that may arise during the last stages of annealing, when $c(t) \approx c_0$, which was the case considered in [8].

‡ From the assumption we have made, it is clear that the quantity ρ_0 should define a minimum pore dimension such that the fragments contained in the pore may already be regarded as a gas.

** For a more detailed discussion of the applicability of the expansion (5), see Section 4.

2. Swelling Caused by the Diffusion of Vacancies

Let us consider the kinetics of swelling on the assumption that the growth of gas pores takes place as a result of the diffusion of vacancies to a pore, this diffusion being correlated with the influx of gas atoms in such a way that the pressure of the gas in the pore is approximately equal to the pressure produced by surface-tension forces.

In general, the pressure p of the gas in a pore is balanced by the pressure of surface tension and the stresses in the material, so that when there is mechanical equilibrium,

$$p = \frac{2\gamma}{\rho} + \sigma_{\rho\rho}. \tag{7}$$

where γ is the coefficient of surface tension and $\sigma_{\rho\rho}$ is the component of the tensor of the stresses on the surface of the pore.†† Consequently, the theory developed in this section corresponds to the case where $\sigma_{\rho\rho} \ll \gamma/\rho$, so that

$$p = \frac{2\gamma}{\rho}. \tag{8}$$

This is characteristic for sufficiently small pores, as well as in the cases when the intensive diffusion of vacancies to the pores prevents the establishment of any significant stresses around them.

In order to make allowance in the case of small bubbles for the deviation of the gas from the ideal case, we shall use the following equation of state:

$$p\,[V(t) - V_0 m(t)] = m(t)\,kT, \tag{9}$$

where V(t) and m(t) are, respectively, the volume of the pore and the number of gas atoms in it at some instant of time t; V_0 is a volume of the same order of magnitude as the volume of a gas atom; T is the absolute temperature. Substituting (8) into this, we differentiate the resulting equation with respect to time. Since

$$\frac{dm}{dt} = 4\pi D \rho(t)\, c(t), \tag{10}$$

we find

$$v_\rho = \frac{d\rho}{dt} = \rho_0 B(T)\, c(t)\, \Omega^{-1}\left(\frac{\rho}{\rho_0}\right), \tag{11}$$

$$B(T) = \frac{3}{4}\frac{DkT}{\gamma\rho_0};\quad \Omega\left(\frac{\rho}{\rho_0}\right) = \frac{1 + \frac{3}{2}\frac{x_k\rho_0}{\rho}}{\left(1 + \frac{x_k\rho_0}{\rho}\right)^2};\quad x_k = \frac{2\gamma V_0}{kT\rho_0}. \tag{12}$$

Here $x_k\rho_0$ is a critical pore radius such that when $\rho \gg x_k\rho_0$, the gas in the pore may be regarded as ideal, but when $\rho \leq x_k\rho_0$, the deviation of the gas from the ideal case must be taken into account.

We introduce the dimensionless variables

$$x = \frac{\rho}{\rho_0},\quad \Phi = B\int_0^t c(t)\,dt. \tag{13}$$

In terms of these variables, Eq. (3) becomes

$$\frac{\partial f}{\partial t} + \frac{\partial}{\partial x}\left(f\frac{1}{\Omega}\right) = \varphi(\Phi)\,\delta(x-1). \tag{14}$$

Here

$$\varphi(\Phi) = \sum_{l=1}^{\infty}\frac{\xi_l}{\rho_0 B}\,c^{l-1}(\Phi). \tag{15}$$

The solution of Eq. (14) is readily found by means of the Laplace transform:

$$f(\Phi, x) = \begin{cases} 0(x-\Gamma(x))\,\varphi[\Phi-\Gamma(x)]\,\Omega(x), & \Phi > \Gamma(x) \\ 0, & \Phi < \Gamma(x). \end{cases} \tag{16}$$

where

$$0(x) = \begin{cases} 1, & x > 0 \\ 0, & x < 0 \end{cases}; \quad \Gamma(x) = \int_0^x \Omega(x)\,dx. \tag{17}$$

The resulting expression for $f(\Phi, x)$, together with Eqs. (12) and (17), allows us to assign a simple physical meaning to the quantities $\Gamma(x)$ and $\Phi - \Gamma(x)$. If Φ is dimensionless "time," then $\Gamma(x)$ may be regarded as the age of a pore of radius x expressed in the same dimensionless units as Φ. Then the quantity $\Phi - \Gamma(x)$ represents the moment of generation of the pores which have radius x at time Φ. Using such an interpretation of these quantities, we can readily convince ourselves that the function (16) we found for the size distribution of pores is in complete conformity with the physics of the process we are considering. Indeed, it follows from Eq. (16) that the number of pores with radius x [having age $\Gamma(x)$] at time Φ is determined by the pore generation which took place at time $\Phi - \Gamma(x)$. Substituting (16) into (6) and taking (13) into account, we obtain the following integro-differential equation for finding the concentration $c(\Phi)$:

$$Bc(\Phi)\frac{dc}{d\Phi} = a - 4\pi D c(\Phi) Q_0^2 \int_0^\Phi x(\Phi - y)\,\varphi(y)\,dy. \tag{18}$$

Thus, the problem of finding the distribution function $f(\rho, t)$ reduces essentially to the solution of this nonlinear equation. It is impossible to solve this analytically over the entire range of values of Φ. However, in view of the fact that what is of greatest practical interest is the behavior of the distribution function for large values of time, we shall now try to find an asymptotic form $\varphi(\Phi)$. For large values of Φ the expression $c(\Phi)\,dc/d\Phi$ appearing in Eq. (18) becomes much less than a.†† On the other hand, for large values of Φ the quantity $c(\Phi)$ decreases as Φ increases, so that the function $\varphi(\Phi)$ is approximately equal to the first nonzero term of the sum (15). (The subscript of this term will hereafter be denoted by l_1.) In accordance with (5) and (15) the quantity l_1 may take on the values 1, 2, 3, etc. If $l_1 = 1$, the asymptotic behavior of $\varphi(\Phi)$ is readily found from Eq. (15):

$$\varphi(\Phi) = \frac{\xi_1}{BQ_0} = \text{const}. \tag{19}$$

When $l_1 \neq 1$, the asymptotic behavior of $\varphi(\Phi)$ can be determined by simply considering the equation obtained from (18) for large values of Φ (see Appendix I, 1):

$$\frac{a}{q_{l_1}}\varphi^{\frac{1}{l_1-1}}(\Phi) = H\Phi + \int_{\Phi_1}^\Phi (\Phi - y + 1)\,\varphi(y)\,dy, \tag{20}$$

where

$$q_{l_1} = 4\pi D Q_0^2 \left[\frac{BQ_0}{\xi_{l_1}}\right]^{\frac{1}{l_1-1}}; \quad H = \int_0^{\Phi_1} \varphi(y)\,dy. \tag{21}$$

The solution of this equation is of the following form (see Appendix I, 2):

†† We shall assume that the asymptotic behavior of $\varphi(\Phi)$ begins when $\Phi \geq \Phi_1$. Moreover, Φ_1 must be such that the average pore size $\frac{1}{N}\int_1^\infty x f(x, \Phi)\,dx$ corresponding to it is much greater than x_k.

$$\left.\begin{aligned} \varphi(\Phi) &= \left(\frac{a}{2q_2}\right)^{1/2} \frac{1}{\Phi[\ln \Phi]^{1/2}}, \quad l_1 = 2; \\ \varphi(\Phi) &= \left(\frac{q_{l_1} N}{a}\right)^{1-l_1} \frac{1}{\Phi^{l_1-1}}; \\ N &= H + \int_{\Phi_1}^{\Phi} \varphi(y)\, dy, \qquad l_1 \geqslant 3. \end{aligned}\right\} \tag{22}$$

Knowing the asymptotic behavior of $\varphi(\Phi)$, we can show that for large values of time $B\left|c(\Phi)dc/d\Phi\right|$ is in fact less than a.

To make it clear how the distribution function varies as a function of time, let us consider the quantity $d[x_{max} - \bar{x}(\Phi)]/d\Phi$ for large values of Φ, where, in accordance with Eqs. (16) and (I. 3), the maximum bubble size is

$$x_{max}(\Phi) = \Phi, \tag{23}$$

and

$$\bar{x}(\Phi) = \frac{1}{N(\Phi)} \int_0^{\infty} x f(x, \Phi)\, dx. \tag{24}$$

Using (2), (16), (19), (20), and (22), we find that for large values of Φ

$$\frac{d}{d\Phi}(x_{max} - \bar{x}) = \begin{cases} 0, & l_1 \geqslant 3 \\ 0, & l_1 = 2 \\ \frac{1}{2}, & l_1 = 1. \end{cases}$$

Thus, for $l_1 \geq 2$, the quantities x_{max} and $\bar{x}$ increase at a uniform rate as Φ increases. Under these conditions the curve of the distribution function is displaced parallel to the x-axis without any significant changes in shape. For $l_1 = 1$, $\bar{x}$ increases more slowly than x_{max}. The reason for this is that the graph of the distribution function not only shifts along the x-axis but also rises somewhat in the region of small values of $\bar{x}$. This is understandable, since for large values of Φ the generation of pores for the case $l_1 - 1$ will be more intensive than for the case $l \geq 2$, as a result of which the relative contribution of the pores with small radius will become greater.

Using (13), (15), (19), and (22), we find the following relationship between Φ and t for large values of time:

$$\left.\begin{aligned} \Phi &= \left(\frac{3aB^2}{2\pi D \xi_1 \varrho_0}\right)^{1/3} t^{1/3}, \quad l_1 = 1; \\ \Phi^2 [\ln \Phi]^{1/2} &= \left(\frac{aB^3}{2\pi D \varrho_0 \xi_2}\right)^{1/2} t, \quad l_1 = 2; \\ \Phi &= \left(\frac{aB}{2\pi D \varrho_0^2 N}\right)^{1/2} t^{1/2}, \quad l_1 \geqslant 3. \end{aligned}\right\} \tag{25}$$

Knowing the asymptotic form of the functions $f(x, \Phi)$ and $\Phi(t)$, we can now find the law governing the variation of volume as a function of time for large values of t:

$$\left.\begin{aligned} \Delta V &= \frac{4\pi}{3} \varrho_0^3 \left(\frac{\xi_1}{4B}\right)\left(\frac{3B^2}{4\pi D \xi_1 \varrho_0}\right)^{4/3} (at)^{4/3}, \; l_1 = 1; \\ \Delta V &= \frac{4\pi}{3} \varrho_0^4 \left(\frac{2a}{q_2}\right)^{1/2} \Phi^3 [\ln \Phi]^{1/2}, \; l_1 = 2; \\ \Delta V &= \frac{\varrho_0}{3} \left(\frac{2B^3}{\pi D^3 N}\right)^{1/2} (at)^{3/2}, \; l_1 \geqslant 3. \end{aligned}\right\}$$

Taking account of formula (25) for $l_1 = 2$, we can easily see that ΔV will increase as a function of time somewhat more slowly than $t^{3/2}$ and more rapidly than t. It can be shown that for sufficiently large time values of the total

number of pores N(t) will increase with time as $t^{1/3}$ if $l_1 = 1$ and somewhat more slowly than $t^{1/3}$ if $l_1 = 2$. For $l_1 \geq 3$, from some moment on we will have $N(t) \approx$ const.

3. Swelling Caused by the Creep of the Material

In this section we shall calculate the amount of swelling caused by the creep of the material taking place under the influence of the gas pressure in the pores. In calculating the quantity v_ρ that appears in Eq. (3), we assume that the material is homogeneous and that the distance between pores is large in comparison with their dimensions. Then the distribution of the stresses around a pore may be regarded as spherically symmetrical. In this case the non-diagonal components $\sigma_{\theta\varphi}$, $\sigma_{\theta r}$, $\sigma_{\varphi r}$ of the stress tensor are equal to zero, and $\sigma_{\theta\theta} = \sigma_{\varphi\varphi}$. In order to describe the process of creep in the material we use the following material we use the following formula relating the creep rate $\varepsilon_{rr} = dv_r/dr$ to the intensity of the tangential stresses $\sigma_{\theta\theta} - \sigma_{rr}$:

$$\varepsilon_{rr} = -\frac{(\sigma_{\theta\theta} - \sigma_{rr})^n}{A}, \tag{27}$$

where A and n are constants determined by the properties of the material, the temperature, etc. Since the creep deformation is not related to the change in volume, we find for the radial component of the deformation rate **v**:

$$\operatorname{div} \mathbf{v} = \frac{dv_r}{dr} + 2\frac{v_r}{r} = 0, \tag{28}$$

and hence

$$v_r = \frac{\text{const}}{r^2}. \tag{29}$$

The stresses σ_{rr} and $\sigma_{\theta\theta}$ satisfy the equilibrium equation

$$\frac{d\sigma_{rr}}{dr} + 2\frac{\sigma_{rr} - \sigma_{\theta\theta}}{r} = 0 \tag{30}$$

with the boundary conditions

$$\sigma_{rr}|_{r=\rho} = -p, \quad \sigma_{rr}|_{r=\infty} = 0. \tag{31}$$

Solving this equation and taking Eq. (27) and (29) into account, we find that

$$v_\rho = \frac{1}{2}\left(\frac{3}{2n}\right)^n \varrho \frac{p^n}{A}. \tag{32}$$

Assuming that the gas in a pore satisfies the equation of state of an ideal gas

$$\frac{4\pi}{3}\varrho^3 p = m(t)\, kT, \tag{33}$$

we find

$$\left(\frac{d\varrho^{3n}}{dt}\right)^{1/n} = \frac{9kT}{8\pi n}\left(\frac{3n}{2A}\right)^{1/n} m(t). \tag{34}$$

Taking account of (10), we differentiate Eq. (34) with respect to time:

$$\frac{d}{dt}\left(\frac{d\varrho^{3n}}{dt}\right)^{1/n} = \frac{(3n+1)(3n)^{1/n}}{(n+1)}\varrho_0^2 B\varrho c(t), \tag{35}$$

where

$$B = \frac{9kTD\nu}{2(2A)^{1/n}(3n+1)\varrho_0^2}, \quad \nu = \frac{n+1}{n}. \tag{36}$$

This equation describes the increase in the pore radius ρ as a function of the creep strength of the material, the velocity with which the gas flows into the pores, and the time t.

We introduce the dimensionless variables

$$x = \frac{\varrho}{\varrho_0}, \quad \Phi = B^{1/\nu} \int_0^t c^{1/\nu}(t)\, dt. \tag{37}$$

In terms of these variables, Eq. (35) may be written in the form (see Appendix II. 1):

$$x^{2/\nu} - 1 = \frac{2}{\nu} \int_{\Phi_0}^{\Phi} s^{1/\nu}(\Phi') \times \left[1 - \frac{c(\Phi_0)}{c(\Phi')} \cdot \frac{s(\Phi_0)}{s(\Phi')} x^{-(3n+1)}(\Phi') \right]^{1/\nu} d\Phi', \tag{38}$$

where

$$s(\Phi) = 1 + \frac{1}{c(\Phi)} \sum_{j=1}^{\infty} \frac{(-1)^j}{(3n+1)^j} \cdot \frac{d^j c[\Phi(\varrho)]}{(d \ln \varrho)^j}; \tag{39}$$

$\Phi_0 = \Phi(t_0)$ (here t_0 is the time at which the pore was generated). Equation (38), which defines the variation of x as a function of Φ, is very complicated. The situation is simplified, however, by the fact that – as will be proved later – in Eq. (38), for $\Phi \gg \Phi_0$, we may assume approximately that

$$s(\Phi) = s_0 = \text{const} \tag{40}$$

and neglect the quantity $\frac{c(\Phi_0)}{c(\Phi)} \cdot \frac{s(\Phi_0)}{s(\Phi)} x^{-(3n+1)}(\Phi)$ in comparison with unity. Using this approximation, we find

$$x^{2/\nu} - 1 = \frac{2}{\nu} s_0^{1/\nu} (\Phi - \Phi_0). \tag{41}$$

Since we assumed that all the pores have the same radius ρ_0 when they are generated, it follows that the equation of continuity for all $\rho \neq \rho_0$ has the form

$$\frac{\partial f}{\partial t} + \frac{\partial}{\partial \varrho}(f v_\rho) = 0. \tag{42}$$

Consequently the number of pores of radius at time t is equal to the number of pores of radius1 at the t_0. If we take t and t_0 (instead of t and x) as the variables in Eq. (42), the distribution function $F(t, t_0)$ is equal to the number of pores formed at the moment t_0, i.e.,

$$F(t, t_0)\, dt_0 = \psi(t_0)\, dt_0. \tag{43}$$

The distribution function $F(t, t_0)$ is evidently related to $f(\rho, t)$ by the formula

$$F(t, t_0)\, dt_0 = f(\varrho, t)\, d\varrho. \tag{44}$$

Substituting (43) into (6) and making use of Eq. (37), we find that the gas concentration $c(\Phi)$ satisfies the following equation:

$$B^{1/\nu} c^{1/\nu} \frac{dc}{d\Phi} + a = 4\pi D \varrho_0 c(\Phi) \int_0^{\Phi} x(\Phi, \Phi_0)\, \varphi(\Phi_0)\, d\Phi_0, \tag{45}$$

where

$$\varphi(\Phi) = \sum_{l=1}^{\infty} B^{-1/\nu} \xi_l c^{l-1/\nu}(\Phi). \tag{46}$$

This equation cannot be solved over the entire range of the values of the argument Φ. We shall therefore try to find the asymptotic behavior of $\varphi(\Phi)$. By a process of reasoning similar to that of Section 2 [see the part following Eq. (18)], we can reduce the problem of finding the asymptotic behavior of $\varphi(\Phi)$ to the solution of the following integral equation:

$$\left(\frac{\nu}{2}\right)^{\nu/2}\beta_{l_1}=\sqrt{s_0}\,\varphi^{\frac{\nu}{\nu l_1-1}}(\Phi)\times\left[E\Phi^{\nu/2}+\int\limits_{\Phi_1}^{\Phi}\left(\Phi-y+\frac{\nu}{2}s_0^{-1/\nu}\right)^{\nu/2}\varphi(y)\,dy\right] \tag{47}$$

where

$$\beta_{l_1}=\frac{a}{4\pi D\varrho_0}\left(\frac{\xi_{l_1}}{B^{1/\nu}}\right)^{\frac{\nu}{\nu l_1-1}},\quad E=\int\limits_0^{\Phi_1}\varphi(y)\,dy. \tag{48}$$

The solutions of Eq. (47) for different values of l_1 are of the following form (for a more detailed discussion see Appendix II. 2).

$$\left.\begin{aligned}
&\varphi(\Phi)=\left(\frac{\left(\frac{\nu}{2}\right)^{\nu/2}\beta_{l_1}}{\sqrt{s_0}\,\Gamma_{\nu,f}}\right)^{\frac{2f}{\nu+2}}\Phi^{-f},\quad \nu l_1<3;\\
&\Gamma_{\nu,f}=\int\limits_0^1(1-t)^{\nu/2}t^{-f}\,dt,\quad f=\frac{\left(\frac{\nu}{2}+1\right)}{\left(\frac{\nu}{\nu l_1-1}+1\right)};\\
&\varphi(\Phi)=\left(\frac{2\beta_{l_1}}{\sqrt{s_0}(\nu+2)}\cdot\frac{1}{\ln\Phi}\right)^{\frac{2}{\nu+2}}\left(\frac{\nu}{2\Phi}\right),\\
&\nu l_1=3.\\
&\varphi(\Phi)=\left(\frac{\beta_{l_1}}{N\sqrt{s_0}}\right)^{\frac{\nu l_1-1}{\nu}}\left(\frac{\nu}{2\Phi}\right)^{\frac{\nu l_1-1}{2}}.\\
&\nu l_1>3.
\end{aligned}\right\} \tag{49}$$

The asymptotic expressions found for $\varphi(\Phi)$ enable us to determine the accuracy of the approximation we used for $x(\Phi)$ [see Eq. (41)] and to find the constant s_0. For this purpose we set up the relationship between the gas concentration $c(\Phi)$ in the material and the "time" Φ for large values of Φ. In accordance with (46) and (49), we find

$$\left.\begin{aligned}
&c(\Phi)=\left[\frac{B^{1/\nu}}{\xi_{l_1}}\left(\frac{\left(\frac{\nu}{2}\right)^{\nu/2}\beta_{l_1}}{\sqrt{s_0}\,\Gamma_{\nu,f}}\right)^{\frac{2f}{\nu+2}}\frac{1}{\Phi^f}\right]^{\frac{\nu}{\nu l_1-1}},\\
&\nu l_1<3;\\
&c(\Phi)=\left(\frac{\nu B^{1/\nu}}{2\xi_{l_1}}\right)^{\nu/2}\left(\frac{2\beta_{l_1}}{\sqrt{s_0}(\nu+2)}\right)^{\frac{\nu}{\nu+2}}\\
&\times\frac{1}{\Phi^{\nu/2}[\ln\Phi]^{\frac{\nu}{\nu+2}}},\quad \nu l_1=3;\\
&c(\Phi)=\left(\frac{a}{4\pi D\varrho_0\sqrt{s_0}N}\right)\left(\frac{\nu}{2\Phi}\right)^{\nu/2},\\
&\nu l_1>3.
\end{aligned}\right\} \tag{50}$$

Substituting (50) into (39) and taking (21) into account, we find that for values satisfying the inequalities $\Phi\gg\Phi_1$, $\Phi_1<\Phi_0<\Phi$, we have

$$s(\Phi)\cong s_0-\frac{\nu}{2}\cdot\frac{1}{\left[(3n+1)\frac{\nu}{2}+1\right]}\cdot\frac{\Phi_0}{\Phi},\quad \nu l_1\geqslant 3, \tag{51a}$$

where

$$s_0=1+\frac{1}{3n};\quad s(\Phi_0)\cong 1, \tag{51b}$$

and

$$s(\Phi) \cong s_0 - \frac{2f}{(\nu l_1 - 1)\left(3n + \frac{2}{\nu} + 1\right)} \cdot \frac{\Phi_0}{\Phi}, \quad \nu l_1 < 3, \tag{51c}$$

where

$$s_0 = 1 + \frac{1}{\nu l_1 n}; \quad s(\Phi_0) \cong 1. \tag{51d}$$

Taking (34) into account, we can show that for $\Phi_0 < \Phi_1$ we have $s(\Phi) \approx s_0$, $s(\Phi_0) \approx 1$. In deriving Eq. (41), we considered $s(\Phi)$ = const. It follows from formulas (51a, b, c, d) that this is valid for values of Φ sufficiently large in comparison with Φ_0. Since the value of n in (27) is usually greater than or equal to unity, it follows that the greater the value of n the more accurately the function $s(\Phi)$ may be replaced by s_0 = const. At the same time, we can easily convince ourselves that for $\Phi >> \Phi_0$, the contribution of the discarded terms to the integral in formula (38) is small.

In the region of Φ_0 values close to Φ, Eq. (41) must, in general, be replaced by a more exact relation. However, since the gas concentration $c(\Phi)$ decreases monotonically for large values of Φ [see Eq. (50)] and is small for $\Phi >> \Phi_1$, while the radius of a gas pore for Φ_0 values close to Φ does not increase substantially in a time interval $t - t_0$, it follows that for large values of Φ the Φ_0 values close to Φ make only an extremely small contribution to the integral in Eq. (47). The function $x(\Phi)$, defined in Eq. (41), may therefore be substituted into this integral with satisfactory accuracy. Knowing the asymptotic behavior of $c(\Phi)$, we can show that for sufficiently large time values the quantity $|dc/dt|$ does, in fact, become less than a.

If we now use (37) and (50), we can easily establish an explicit relationship between Φ and t for $\Phi >> \Phi_1$. By simple calculations it can be shown that

$$\left.\begin{aligned} t &= \frac{\nu}{\frac{3}{2}\nu + 1 - f}\left[\frac{\xi_{l_1}}{B^{l_1}}\left(\frac{\left(\frac{\nu}{2}\right)^{\nu/2}\beta_{l_1}}{\sqrt{s_0}\,\Gamma_{\nu,f}}\right)^{-\frac{2f}{\nu+2}}\right]^{\frac{1}{\nu l_1 - 1}} \Phi^{\frac{f}{\nu l_1 - 1}+1}, \quad \nu l_1 < 3; \\ t &= \frac{2}{3}\left(\frac{2\xi_{l_1}}{\nu B^{l_1}}\right)^{1/2}\left(\frac{(\nu+2)\sqrt{s_0}\ln\Phi}{2\beta_{l_1}}\right)^{\frac{1}{\nu+2}} \Phi^{3/2}, \quad \nu l_1 = 3; \\ t &= \frac{2}{3}\sqrt{\frac{2}{\nu}}\left(\frac{4\pi D\varrho_0\sqrt{s_0}N}{aB}\right)^{1/\nu}\Phi^{3/2}, \quad \nu l_1 > 3. \end{aligned}\right\} \tag{52}$$

Knowing the asymptotic form of the functions $\varphi(\Phi)$ and $\Phi(t)$ [see (1), (41), (49), and (52)], we can find the following rule for the variation of the volume as a function of time for large values of t:

$$\left.\begin{aligned} \Delta V &= \left(\frac{3\nu + 2 - 2f}{\nu^2}\right)^{\nu} \times \frac{aBs_0\varrho_0^2\Gamma_{3\nu,f}}{3D\Gamma_{\nu,f}} t^{\nu}, \quad \nu l_1 < 3; \\ \Delta V &= \left(\frac{3}{\nu}\right)^{\nu}\frac{aBs_0\varrho_0^2}{3D}t^{\nu}, \quad \nu l_1 \geqslant 3. \end{aligned}\right\} \tag{53}$$

Thus, regardless of the value of l_1 — that is, essentially independently of the law of generation of the gas pores — the increase in volume for large values of t is proportional to t^{ν}, where $\nu = (n + 1)/1$ depends only on the creep law.

In conclusion, let us study how the distribution function varies as a function of time. For this purpose we shall consider $d/d\Phi\,(x_{max} - \overline{x})$ for large Φ, where the maximum bubble dimension is

$$x_{max}(\Phi) \cong \sqrt{s_0}\left(\frac{2}{\nu}\Phi\right)^{\nu/2}, \tag{54}$$

and

$$\bar{x}(\Phi) = \frac{1}{N(\Phi)} \int_0^\infty x f(x, \Phi)\, dx. \tag{55}$$

Using (2), (47), and (49), we find that for large Φ

$$\frac{d}{d\Phi}(x_{\max} - \bar{x}) = \begin{cases} 0, & \nu l_1 \geqslant 3; \\ \left(\frac{2}{\nu}\right)^{\frac{\nu}{2}-1} f \sqrt{s_0}\, \Phi^{\frac{\nu}{2}-1}, & \nu l_1 < 3. \end{cases} \tag{56}$$

It is clear from this that for the case $\nu l_1 \geq 3$, both $\bar{x}$ and x_{max} increase at equal rates as Φ increases. The distribution curve is displaced parallel to the x-axis, with no special changes in shape, for increasing Φ. In the case $\nu l_1 < 3$, the value of $\bar{x}$ increases more slowly than x_{max} as Φ increases. The reason for this is that the distribution curve not only is displaced along the x-axis but also becomes higher for small values of x. This is understandable, since for small νl_1 there is no substantial amount of pore generation even for large values of Φ; as a result the relative contribution made by pores of small radius becomes larger.

4. Some Remarks

Let us consider in more detail than we did in Section 1 the assumption on which we based our use of expansion (5), according to which the rate of generation of pores time t is determined by the concentration of dissolved gas at that instant. Since the quantity v_ρ in Eq. (3) in Sections 2 and 3 was determined, in particular, by using the equation of state of the gas, the value of ρ_0 cannot strictly speaking, be taken equal to the radius of the nucleation center and should instead define the dimension of a pore for which the above-mentioned definition of v_ρ would already have been valid. On the other hand if v_ρ is defined in such a way as to assume the form of (11), and hence (32), only for sufficiently large values of ρ, while for small values of ρ it would correctly represent the rate of growth of a nucleation center, then ρ_0 could be taken to mean the minimum dimension for a stable center. The use of the expansion (5) is justified if during the time it takes to generate a new center the concentration of gas atoms outside the pore varies little. Thus, if we assume that the error introduced by the approximate calculation of v_ρ is small, then ρ_0 may be taken to mean the dimension of a stable center. In the contrary case, ρ_0 should be taken to mean the radius of pore that is minimum in the above-described sense. In order to justify the use of the expansion (5), the gas concentration outside the pores must vary little during the time that a center matures into a pore of radius ρ_0 (at least during the time when intensive pore formation is going on, that is, before the gas concentration has become fairly high).

The number of gas atoms that have been united with a center during the time interval τ from the moment t_0, when it was formed until the moment when it is converted into a pore of radius ρ_0 is

$$m_0 = 4\pi D \int_0^\tau c(t_0 + t')\, \varrho(t')\, dt' \approx 4\pi D c(t_0) \int_0^\tau \varrho(t')\, dt', \tag{57}$$

since, by assumption, the gas concentration c(t) changes little in time τ. Neglecting the dimensions of the center, we shall take $\rho(t) = \alpha t^{n_1}$, where $n_1 > 0$. Then we evidently have

$$m_0 = 4\pi D c(t_0) \frac{\alpha}{n_1+1} \tau^{n_1+1} = \frac{4\pi D c(t_0)}{n_1+1} \tau \varrho_0, \tag{58}$$

since, by assumption, $\rho_0 = \alpha \tau^{n_1}$. On the other hand,

$$m_0 \cong \frac{pV}{kT} \cong \frac{2\gamma}{\varrho_0} \frac{4}{3} \frac{\pi \varrho_0^3}{kT}. \tag{59}$$

Equating the two expressions for m_0, we find that

‡‡ As is shown by estimates, this requirement is satisfied over a very wide range of conditions.

$$\tau(t_0) \approx \frac{2\gamma\varrho_0(n_1+1)}{3DkTc(t_0)}. \tag{60}$$

The condition under which formula (5) may be used in the present case is

$$\frac{\tau\left|\frac{dc}{dt}\right|}{c} \ll 1. \tag{61}$$

For larger time values (asymptotic behavior), when c(t) decreases as (const/t^{s_1}), $s_1 < 1$ [see formulas (15), (25), (50), and (52)], we have

$$\frac{\tau\left|\frac{dc}{dt}\right|}{c} = \frac{s_1\tau}{t} - \frac{\beta}{t^{1-s_1}}, \tag{62}$$

where β = const.

Therefore Eq. (61) is satisfied for sufficiently large values of time, and thus the use of formula (5) in this case is justified. As for the other, smaller values of values of t, the region of greatest interest here is that of maximum values of c(t), when the quantity $\tau(t_0)$ is small, in accordance with (60). For a more detailed study of the inequality (61) in the range of small values of t, we must know the variation of c(t) for these values of t; however, this is not taken up in the present study. In addition to the above remarks, we may point out that in Eq. (6) we ignored the variation in c(t) caused by the formation of nucleation centers (pores of radius ρ_0). In order to take this variation into account, we should add to the right-hand side of Eq. (6) a term $\psi(t)m_0$, where m_0 is the number of gas atoms in a pore of radius ρ_0. It is easy to show, however, that for sufficiently large time values this term tends to zero ($m_0\psi(t) << a$) and may be ignored in the study of swelling for large values of t.

Conclusion

On the basis of the above, we may conclude that the kinetics of swelling depend essentially both on the mechanism of nucleation-center formation and on the mechanism of pore growth. If the pore growth is caused by the diffusion of vacancies, then for sufficiently large time values the variation in volume will obey one of the following three laws:

$$\Delta V \sim t^{4/3};\ \Delta V \sim t^{3/2};$$
$$\Delta V \sim \Phi^3[\ln\Phi]^{1/2},\quad t \sim \Phi^2[\ln\Phi]^{1/2},$$

that is, it will be determined by the mechanism of generation of gas pores. If the pores grow through the mechanism of creep, the variation of volume as a function of time will follow the law

$$\Delta V \sim t^{\nu},\quad \nu = \frac{n+1}{n}$$

for large time values and will not depend upon the mechanism of pore generation.

Thus, the experimental investigation of swelling kinetics for large time values would make it possible to draw some conclusions regarding the mechanism of growth of gas pores and – if this growth is casued by a diffusion influx of vacancies – on the nature of the pore generation as well.

In addition, the results obtained indicate that the swelling value is not a linear function of burn-up. Consequently, it will not be entirely correct to characterize the susceptibility of a material to swelling by the ratio of volume increase to the burn-up value reached, although this is still found fairly often in the literature.

The authors thank O. D. Kazachkovskii, S. T. Konobeevskii, and A. I. Leipunskii for their evaluation of results.

Appendix I

1. Derivation of Eq. (20). In accordance with what was stated above for large values of $\Phi(\Phi > \Phi_1)$, Eq. (18) becomes

$$\frac{a}{q_{l_1}}\varphi^{\frac{1}{1-l_1}}(\Phi)=\int_{\Phi_1}^{\Phi}x(\Phi-y)\varphi(y)\,dy+\lambda(\Phi), \tag{I. 1}$$

where

$$\lambda(\Phi)=\int_{0}^{\Phi_1}x(\Phi-y)\varphi(y)\,dy. \tag{I. 2}$$

in order to solve Eq. (I. 1) we must find an explicit formula for $x = x(\Phi - y)$. For large values of $x\,(x >> x_k)$ we find, using Eq. (12) and (17), that

$$x=\Phi-y+1. \tag{I. 3}$$

Since for the large values of Φ that interest us the average pore dimension is considerably greater than x_k, it follows that we may substitute the value of $\underline{x}$, found from Eq. (I. 3) into the integral appearing Eq. (I. 1). Since for $\Phi > \Phi_1$ the relation

$$\lambda(\Phi)=\int_{0}^{\Phi_1}x(\Phi-y)\varphi(y)\,dy=x(\Phi)\int_{0}^{\Phi_1}\varphi(y)\,dy=H\Phi, \tag{I. 4}$$

holds, we finally obtain the equation defining the asymptotic behavior of the function $\varphi(\Phi)$:

$$\frac{a}{q_{l_1}}\varphi^{\frac{1}{1-l_1}}(\Phi)=H\Phi+\int_{\Phi_1}^{\Phi}(\Phi-y+1)\varphi(y)\,dy. \tag{I. 5}$$

2. Solution of Eq. (20). We shall find the asymptotic form of the solution for $l_1 = 2$. Since $\varphi(\Phi)$ is a decreasing function, it follows that if we neglect the quantity $(1 - y)$ in comparison with Φ in Eq. (20) and differentiate (20) with respect to Φ, we obtain

$$-\frac{a}{q_2}\cdot\frac{1}{(\Phi\varphi)^3}\cdot\frac{d}{d\Phi}(\Phi\varphi)=\frac{1}{\Phi}. \tag{I. 6}$$

The solution of this equation is of the form

$$\varphi(\Phi)=\left(\frac{a}{2q_2}\right)^{1/2}\frac{1}{\Phi\,[\ln\Phi]^{1/2}}. \tag{I. 7}$$

By means of the solution so obtained, we can show that the relative contribution of the terms neglected in Eq. (20) is $\sim 1/\ln\Phi$ and therefore they may be neglected for large values of Φ.

Similarly, neglecting the quantity $(1 - y)$ in comparison with Φ under the integral sign, for the case $l_1 \geq 3$, we find that

$$\frac{a}{q_{l_1}}\varphi^{\frac{1}{1-l_1}}(\Phi)=\left(H+\int_{\Phi_1}^{\Phi}\varphi(y)\,dy\right)\Phi=N(\Phi)\,\Phi. \tag{I. 8}$$

It should be noted that $\rho_0 N$ is the total number of pores. For large Φ and $l_1 \geq 2$, as can be shown by using (I. 8), the value $N(\Phi)$ is approximately constant. Therefore, from Eq. (I. 7), we find the asymptotic behavior of $\varphi(\Phi)$:

$$\varphi(\Phi)=\left(\frac{q_{l_1}N}{a}\right)^{1-l_1}\frac{1}{\Phi^{\frac{1}{l_1-1}}}. \tag{I. 9}$$

Substituting (I. 9) into (20), we can convince ourselves that we are justified in neglecting the quantity $(1 - y)$ under the integral sign in comparison with Φ.

Appendix II

1. Derivation of Eq. (38). Solving Eq. (35) with the initial conditions

$$\left.\frac{d\varrho}{dt}\right|_{t=t_0}=0, \quad \varrho(t_0)=\varrho_0, \tag{II. 1}$$

we obtain

$$\left(\frac{d\varrho^{3n}}{dt}\right)^{\nu}=(3n)^{\nu}\varrho_0^2 B\left[\varrho^{3n+1}c(t)\,s(t)-\varrho_0^{3n+1}c(t_0)\,s(t_0)\right], \tag{II. 2}$$

where s(t) is defined by Eq. (39). In the dimensionless variables $\underline{x}$ and Φ this equation becomes

$$\frac{1}{3n}\left(\frac{dx^{3n}}{d\Phi}\right)=\left[x^{3n+1}s(\Phi)-\frac{c(\Phi)}{c(\Phi_0)}\,s(\Phi_0)\right]^{1/\nu}. \tag{II. 3}$$

Integrating this with respect to Φ, we obtain Eq. (38).

2. Solution of Eq. (47). The first case is $l_1 < 3/\nu$. We shall try to find the asymptotic solution of Eq. (47) in the form

$$\varphi(\Phi)=\frac{\Delta}{\Phi^f}. \tag{II. 4}$$

Substituting (II. 4), we find

$$\left(\frac{\nu}{2}\right)^{\nu/2} s_0^{-1/2}\beta_{l_1}\cong(\Delta\Phi^{-f})^{\frac{\nu}{\nu l_1-1}+1} \times\Phi^{1+\frac{\nu}{2}}\int_{\Phi_1/\Phi}^{1}(1-t)^{\nu/2}t^{-f}\,dt. \tag{II. 5}$$

An analysis of this equation shows that the quantity $\varphi(\Phi)$ defined by Eq. (II. 4) will be a solution of (II. 5) if

$$\Delta=\left[\frac{\left(\frac{\nu}{2}\right)^{\nu/2}\beta_{l_1}}{\sqrt{s_0}\,\Gamma_{\nu,f}}\right]^{\frac{2f}{\nu+2}}. \tag{II. 6}$$

From Eq. (48) it is clear that $f < 1$. Consequently the integral in Eq. (II. 5) is convergent, and since $\Phi >> \Phi_1$, we replaced it by $\int_0^1$ in calculating Δ.

The second case is $l_1 = 3/\nu$. We expand the expression $\left(\Phi-y+\frac{\nu}{2}s_0^{-1/\nu}\right)^{\nu/2}$ appearing under the integral sign in Eq. (47) into a power series in $\left(y-\frac{\nu}{2}s_0^{-1/\nu}\right)$ and retain only the zeroth term. We thus obtain

$$s_0^{-1/2}\left(\frac{\nu}{2}\right)^{\nu/2}\beta_{l_1}=(\Phi\varphi)^{\nu/2}\left[E+\int_{\Phi_1}^{\Phi}\varphi(y)\,dy\right]. \tag{II. 7}$$

Differentiating Eq. (II. 7) with respect to Φ, we find

$$s_0^{-1/2}\left(\frac{\nu}{2}\right)^{\frac{\nu}{2}+1}\beta_{l_1}\frac{d}{d\Phi}(\Phi\varphi)=-\frac{(\Phi\varphi)^{\frac{\nu}{2}+2}}{\Phi}. \tag{II. 8}$$

The solution of this equation is of the form

$$\varphi(\Phi)=\left[\frac{2\beta_{l_1}}{\sqrt{s_0}\,(\nu+2)}\cdot\frac{1}{\ln\Phi}\right]^{\frac{2}{\nu+2}}\left(\frac{\nu}{2\Phi}\right). \tag{II. 9}$$

Using (II. 9), we can show that if the following term in the expansion of the function $\left(\Phi - y + \frac{\nu}{2} s_0^{-1/\nu}\right)^{\nu/2}$ is taken into account, the contribution to the integral in Eq. (47) is $1/\ln \Phi$ times the contribution made by the zeroth term of the expansion.

The third case is $l_1 > 3/\nu$. Expanding the function $\left(\Phi - y + \frac{\nu}{2} s_0^{-1/\nu}\right)^{\nu/2}$ appearing in Eq. (47) into a power series in $\left(y - \frac{\nu}{2} s_0^{-1/\nu}\right)$ as in the second case, and retaining only the zeroth term of the expansion, we obtain

$$s_0^{-1/2} \left(\frac{\nu}{2}\right)^{\nu/2} \beta_{l_1} = N(\Phi)\, \Phi^{\nu/2}\, \varphi^{\frac{\nu}{\nu l_1 - 1}}(\Phi), \tag{II. 10}$$

where

$$N(\Phi) = E + \int_{\Phi_1}^{\Phi} \varphi(y)\, dy \tag{II. 11}$$

is the total number of pores in 1 cm^3. A study of Eq. (II. 10) shows that as Φ increases, the function $\varphi(\Phi)$ tends to zero faster than $1/\Phi$. Therefore, in formula (II. 11), for $\Phi > \Phi_1$, the upper limit may be replaced by infinity. Then N = const in the asymptotic case, and for the asymptotic behavior of $\varphi(\Phi)$ we obtain the formula

$$\varphi(\Phi) = \left(\frac{\beta_{l_1}}{N \sqrt{s_0}}\right)^{\frac{\nu l_1 - 1}{\nu}} \left(\frac{\nu}{2\Phi}\right)^{\frac{\nu l_1 - 1}{2}}. \tag{II. 12}$$

Using (II. 12), we can show in a similar manner that for large values of Φ the contribution of the subsequent terms of the expansion of the function $\left(\Phi - y + \frac{\nu}{2} s_0^{-1/\nu}\right)^{\nu/2}$ is negligible.

LITERATURE CITED

1. Pugh, In Proceedings of the International Conference on the Peaceful Uses of Atomic Energy (Geneva, 1955) [in Russian], Vol. 7, Goskhimizdat, Moscow (1958), p. 535.
2. Wyatt, et al. In Proceedings of the Second International Conference on the Peaceful Uses of Atomic Energy [in Russian]. Reports of Non-Soviet Scientists, Vol. 6, Atomizdat, Moscow (1959), p. 356.
3. W. Barney, Report No. 615, presented by the United States at the Second International Conference of Peaceful Uses of Atomic Energy (Geneva, 1958).
4. V. M. Agranovich and É. Ya. Mikhlin, Atomnaya Énergiya, 12, 395 (1962).
5. S. Pugh, J. Nucl. Materials, 4, 177 (1961).
6. I. Greenwood et al., J. Nucl. Materials, 1, 305 (1959).
7. I. L. Lifshits and V. V. Slezov, Zh. éksperim. i teor. fiz., 35, 479 (1958).
8. I. Greenwood and A. Boltax, J. Nucl. Materials, 5, 234 (1962).

All abbreviations of periodicals in the above bibliography are letter-by-letter transliterations of the abbreviations as given in the original Russian journal. *Some or all of this periodical literature may well be available in English translation.* A complete list of the cover-to-cover English translations appears at the back of this issue.

THEORY OF THE COALESCENCE OF GASEOUS PORES UNDER SWELLING CONDITIONS

L. P. Semenov

Translated from Atomnaya Énergiya, Vol. 15, No. 5,
pp. 404-408, November, 1963
Original article submitted December 27, 1962

In the last stage of decomposition of a supersaturated solid solution, an important role is played by diffusion of "grains of a new phase" through the solution (coalescence). In the present paper, a study is made of the kinetics of the process under gas swelling conditions, where the grains of the new phase are pores, saturated with an inert gas. Here, a study is made of two cases: 1) the total amount of gas in the system is constant (annealing conditions), and 2) the total amount of gas in the system increases with time.

An asymptotic solution is obtained for the problem. The asymptotic behavior of the number of pores, and of their mean dimensions, is found, as well as the asymptotic increase in volume.

Introduction. Formulation of Problem

The decay of a supersaturated solid solution is accompanied by the formation and subsequent growth of a large number of grains of a new phase. Intense decomposition of the supersaturated solution usually occurs in the first stage, where the supersaturation is large, so that there is a considerable probability of forming a seed of the new phase with greater than the critical dimension. In the second stage, where the supersaturation is already small, there is little probability of a new phase being formed as a result of fluctuations of the thermodynamically stable centers. Under these conditions, a very important role begins to be played by diffusional redistribution of material over the grains through the solution. This redistribution of the dimensions of the grains of the new phase, which is accompanied by the growth of large grains as a result of dissolving the small grains, and is known as coalescence, has been discussed repeatedly in the literature [1-4]. The most consistent theoretical study of coalescence kinetics has been made in [3].

It should be noted that it has been assumed in all the work done in this direction that the density of grains of the new phase is constant, and is independent of the number of particles in it. Along with this, it is interesting to consider coalescence under conditions where the density of the new phase is variable, and is essentially determined by the number of particles in it. This is the case in fissionable materials that have been subjected to prolonged irradiation at quite high temperatures, as well as under annealing conditions at high temperatures, after an irradiation previously carried out at low temperature. In this case, a large number of pores of different dimensions, filled with inert gases, is formed in the material [5, 6], and these are regarded as grins of a new phase, in which the particle density is determined, in particular by the number of particles in a pore. Both under annealing conditions, and under favorable conditions with continuous high temperature irradiation [7], the concentration of the inert gas dissolved in the lattice of the fissonable material quickly drops, for large times, to a value at which redistribution processes begin to play an appreciable role. For practical purposes, it always possible under these conditions to neglect the birth of gaseous pores.

It follows from what has been said above that the function $f(r, t)$ giving the distribution of pore dimensions r at the instant of time t in the first stage of the phase transformation satisfies the continuity equation

$$\frac{\partial f}{\partial t} + \operatorname{div}(f v_r) = 0 \tag{1}$$

with the initial condition

$$f(r, 0) = f_0(r), \tag{2}$$

where $v_r = dr/dt$ is the rate of directed motion of the pores in dimension space. The initial distribution function $f_0(r)$ is assumed to be known. Any change in the distribution function, resulting from the pores uniting, is neglected. The function $f(r, t)$ is normalized to the total number of pores N(t) per unit volume.

To make a concrete formulation of the problem, it is necessary to find the law giving the change in radius of the gas pores. The rate at which gas particles are transferred through an interface is, generally speaking, determined by the concentration gradients of the gas and the vacancies at the pore surface, and by the elastic properties of the lattice. If the concentration of gas in the material is considerably less than the concentration of gas inside the pores, then, under quasi-stationary conditions, the flux of gas atoms through the surface of the pore is given by the expression

$$\frac{dn}{dt} = 4\pi Dr\,(c - c_r), \tag{3}$$

where D is the diffusion coefficient c is the mean gas concentration in the lattice, and c_r is the equilibrium gas concentration at the pore surface, which is related to the pressure in the pore by the equation [8]

$$c_r = \frac{P}{kT}\, e^{-\psi/kT}, \tag{4}$$

where P is the gas pressure in the pore. It is assumed here that the gas in the pore obeys the equation of state of an ideal gas,

$$\frac{4\pi}{3}\, r^3 P = nkT. \tag{5}$$

In a state of mechanical equilibrium, the pressure P is balanced by the surface tension pressure and the elastic stresses in the material:

$$P = \frac{2\gamma}{r} + \sigma_{rr}, \tag{6}$$

where γ is the surface tension coefficient, and σ_{rr} is the diagonal component of the stress tensor at the pore surface. However, if the diffusional processes that remove distortions in the lattice are very intense, the elastic stresses in the material have practically no effect on the redistribution. In this case,

$$P \cong \frac{2\gamma}{r}. \tag{7}$$

Experimental and theoretical studies [6, 9] give reason to assume that in some cases, at high temperatures, because of active diffusion of vacancies which produces rapid relaxation of local stresses in the lattice, the gas pressure in the pore at any instant of time is given with sufficient accuracy by Eq. (7). Using this fact, and bearing in mind Eqs. (3), (4), and (5), we find that

$$\frac{dr}{dt} = \frac{R_k}{2t_0 c_0}\left(c - \frac{R_k c_0}{r}\right), \tag{8}$$

where

$$R_k = \frac{2\gamma}{kTc_0}\, e^{-\psi/kT}; \quad t_0 = \frac{R_k^2}{3D}\, e^{\psi/kT}; \quad c_0 = c\,(0). \tag{9}$$

We introduce the dimensionless variables

$$R = \frac{r}{R_k}, \quad \Delta = \frac{c}{c_0}, \quad \tau = \frac{t}{t_0}. \tag{10}$$

In these variables, Eq. (8) takes the form

$$\frac{dR^2}{d\tau} = (\Delta R - 1). \tag{11}$$

To this equation must be added the law of conservation of matter

$$1 + q_0\tau = \frac{c_0}{Q_0}\Delta + \nu\int_0^\infty R^2 f(R, \tau)\, dR. \tag{12}$$

In the last expression, q_0 is the rate of birth of gas atoms, and Q_0 is the total amount of gas in the material at $\tau = 0$, and

$$\nu = \frac{4\pi c_0}{3Q_0} R_k^3 (\psi kT). \tag{13}$$

Equations (1), (11), and (12), with the initial condition (2), permit a complete solution to be made of the problem of coalescence of gas pores.

Coalescence of Gas Pores in Annealing

In this case, $q_0 = 0$ in Eq. (12). Unfortunately, it is impossible to find an exact analytical solution of the above system of equations for the whole range of times. In view of this, it is of interest to find the asymptotic behavior of the functions $f(R, \tau)$, and $\Delta(\tau)$, and of the mean pore radius $\bar{R}(\tau)$. To this end, we make use of the method developed in [3]. Introduce the new function

$$v = \Delta R \tag{14}$$

and the new "time"

$$y = 2\ln\frac{1}{\Delta} \tag{15}$$

($y = 0$, when $\Delta = 1$; and $y \to \infty$, when $\Delta \to 0$). Substituting (14) and (15) in (11), we obtain

$$\frac{dv^2}{dy} = \beta(y)\,(v - 1) - v^2, \tag{16}$$

where

$$\beta(y) = \frac{d\tau}{d(\Delta^{-2})}. \tag{17}$$

The graphical dependence of the rate dv^2/dy on v for any values of the time is of the form of the parabola shown in the figure. Using the fact that $v(a, y)_{y=0} = a$, the integral in Eq. (12) may be written in terms of the initial distribution function. As a result, we obtain

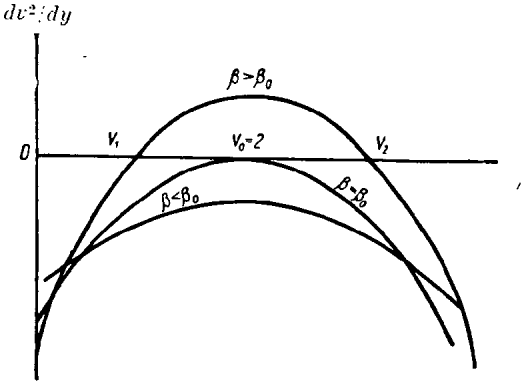

Change in the rate dv^2/dy as a function of v.

$$1 = \frac{c_0}{Q_0} e^{-y/2} + \nu e^y \int_{a_0(y)}^\infty v^2(a, y) f_0(a)\, da. \tag{18}$$

Here, $a_0(y)$ is the solution of the equation $v(a_0, y) = 0$. The physical meaning of $a_0(y)$ is that it is the lower limit of the dimensions of the original pores that have not yet dissolved up to the instant of time y.

In the following analysis, we assume that $\beta(y)$ approaches $\beta_\infty = \text{const}$ for infinitely increasing y. Three cases should be distinguished here: $\beta_\infty < \beta_0$; 2) $\beta_\infty > \beta_0$; 3) $\beta_\infty = \beta_0$.

In the first case, the rate of motion of the pores in the space of the dimensions v is everywhere negative. This means that all the points v move in the direction of reducing their dimensions, and disappear at the origin of coordinates. Thus, the amount of gas in the pores approaches zero as $\nu \to \infty$, at

the same time that the total number of particles in the system remains finite, so that that the law of conservation of matter [Eq. (18)] is violated.

For the case where $\beta_\infty > \beta_0$, only those pores remain in the solution as $y \to \infty$, which originally had dimensions greater than v_1. Here, the amount of gas in the pores will increase without limit with increase in y:

$$ve^y \int_{a_0}^{\infty} v^2(a, y) f_0(a)\, da \to vv_2^2 e^y \int_{v_1}^{\infty} f_0(a)\, da \to \text{const}\, e^y \to \infty,$$

and, hence, the law of conservation of matter is again violated.

Consider, finally, the case where $\beta_\infty = \beta_0$. Note, as follows from the analysis given above, the β can only approach β_0 from below, i.e.,

$$\beta(y) = \beta_0 (1 - \Theta^2(y)). \tag{19}$$

A similar analysis of Eq. (16) using (19) shows that

$$\Theta(y) \to \frac{1}{y}, \quad y \to \infty \tag{20}$$

and, hence,

$$\beta(y) = \beta_0 \left(1 - \frac{1}{y^2}\right). \tag{21}$$

We now set up a relation between the concentration of gas atoms in the material and the time τ for large times ($\tau \to \infty$). Substituting (21) in (17), and using (15), we find that

$$\Delta(\tau) = 2\tau^{-1/2} \left\{1 - \frac{1}{8\left[\ln\left(\frac{\tau^{1/2}}{2}\right)\right]^2} + \dots\right\}. \tag{22}$$

As we have already pointed out, redistribution of the pores in dimensions occurs in the coalescence process. The question arises in this connection, what number of gas pores will be found in an element of dimension space at the end of an arbitrarily long time interval τ. The distribution function in the variables v and y will, for large y ($y \to \infty$), everywhere, except for a small region in the vicinity of the point $v_0 = 2$, satisfy the equation*

$$\frac{\partial \varphi}{\partial y} - \frac{\partial}{\partial v}\left(\varphi \frac{(v-2)^2}{2v}\right) = 0. \tag{23}$$

Solving Eq. (23), we obtain

$$\varphi(v, y) = 2v \frac{\xi(y+X)}{(v-2)^2}, \quad v < v_0; \tag{24}$$

$$X(v) = \int_0^v \frac{2v\, dv}{(v-2)^2} = 2\ln(2-v) - \frac{4}{v-2} - \ln \tag{25}$$

It may be shown that the asymptotic probability of finding a pore with the dimension of $v > v_0$, is equal to zero.

To find the unknown function $\xi(y + X)$ in Eq. (24), we make use of the law of conservation of matter

$$1 = ve^y \int_0^\infty v^2(X)\, \xi(X + y)\, dX. \tag{26}$$

As a result, we obtain

* It is obvious that $\varphi(v, y)dv = f(R, \tau)dR$.

$$\xi(y+X)=\left[\int_0^\infty v^2(X)\,e^{-X}\,dX\right]^{-1}\exp(-y-X). \tag{27}$$

Thus, in the annealing case, the asymptotic distribution function

$$\varphi(v,\ y)=$$

$$=\left[\nu\int_0^\infty v^2(X)\,e^{-X}\,dX\right]^{-1}\frac{2v}{(v-2)^2}\exp(-y-X) \tag{28}$$

is independent of the initial distribution of the pore dimensions.

The total number of pores per unit volume of material when $\tau \to \infty$ is equal to

$$N(\tau)=\int_0^2\varphi(v,\ y)\,dv=\left[\nu\int_0^\infty v^2(X)\,e^{-X}\,dX\right]^{-1}\frac{4}{\tau}. \tag{29}$$

Note that the important characteristic of the coalescence process is the behavior with time of the mean pore radius. Since, for the conditions under discussion, the total surface of the gas pores is constant at large times, and the mean pore radius in v-space may be found from the condition

$$\int_0^\infty(v-1)\,\varphi(v,\ y)\,dv=0,$$

from which

$$\bar v=1,\quad \bar R=\frac{1}{\Lambda}=\frac{\tau^{1/2}}{2}\left(1+\frac{1}{8\ln^2\left(\frac{\tau^{1/2}}{2}\right)}+\cdots\right). \tag{30}$$

It should be kept in mind that in Eq. (30) the second term will only be small in comparison with the first for the condition

$$(\ln\tau)^2\gg 1,\quad \tau\gg 1,\quad R\gg R_k. \tag{31}$$

In conclusion, we turn our attention to the fact that coalescence of gas pores is usually accompanied by an increase in volume of the whole sample. This is due to the fact that the flow into the pores of vacancies occurring in the lattice, which tends to remove the local stresses around the pores, is made up for by the same amount of vacancies coming inside the material from the surface. Assuming that the change in volume of the material is exactly equal to the change in volume of the gas pores, we obtain for large times ($\tau \to \infty$)

$$\frac{\Delta V}{V_0}=\frac{2\pi}{3}\tau^{1/2}R_k^3\int_0^\infty v^3(X)\,\xi(X)\,dX-\frac{4\pi}{3}\int_0^\infty v^3 f_0(v)\,dv, \tag{32}$$

where V_0 is the original volume of the sample.

Coalescence when Particles are Being Born Continuously

For coalescence when particles are being born continuously, we have $q_0 \neq 0$ in Eq. (12). In proceeding to a discussion of the pore distribution mechanism under conditions where particles are being born continuously in the lattice, we assume, as in the preceding section, that the function $\beta(y)$ approaches a constant limit β_∞ as y increases without limit, which cannot be less than β_0, since otherwise the law of conservation of matter [Eq. (12)] would be violated.

Taking $\beta = \beta_\infty$ in Eq. (17), we find that the concentration of gas particles in the lattice varies with time as $\tau \to \infty$, according to the law

$$\Delta(\tau)=\left(\frac{\beta_\infty}{\tau}\right)^{1/2}. \tag{33}$$

We use this result to find the unknown quantity β_∞. Substituting (33) in the law of conservation of matter gives the asymptotic equation

$$q_0 = \frac{\nu}{\beta_\infty}\int_0^\infty v^2\varphi(v, y)\,dv. \tag{34}$$

Equation (34) may be used to find the value of β_∞. It is very complicated, and it is impossible to make an exact solution without knowing the initial distribution function. Nevertheless, a number of conclusions may be drawn regarding coalescence under conditions where gas atoms are being continuously produced in the lattice. A detailed study shows that $\beta_\infty > \beta_0$. This fact is responsible for the peculiar nature of the coalescence under the conditions being discussed ($q_0 \neq 0$). Note first of all that in this case, at some instant of time τ_0, a range δv (which increases with time to the value $\beta_\infty\sqrt{1-4/\beta_\infty}$) occurs in the values of v, in which the rate of change of the pore dimensions in v-space is positive. This means that as $\tau \to \infty$, a finite number of grains of the new phase will remain undissolved in the solid solution, i.e., gas pores having the asymptotic dimension $v_2(q_0)$. It follows from this that

$$q_0\beta_\infty = \nu v_2^2 N(q_0). \tag{35}$$

The value of $\tau_0(q_0)$ is found from the condition

$$\beta(\tau_0) = \beta_0 = 4. \tag{36}$$

We find from Eq. (35) that

$$\beta_\infty = \frac{\left(1+\frac{q_0}{\nu N(q_0)}\right)^2}{\frac{q_0}{\nu N(q_0)}}. \tag{37}$$

It appears at first glance that if $q_0 \to 0$, $\beta_\infty \to \infty$, and thus, the agreement between the results of the present and the preceding section no longer exists. However, this contradiction may easily be got rid of if it is borne in mind that β_∞ is only reached asymptotically.

Reducing q_0 increases the time interval τ_0 required for the curve showing the function $dv^2/dy = \Phi(v, y)$ to touch the v axis at the point $v_0 = 2$ as it moves in the direction of positive values of dv^2/dy. Here, the number of points that have been able to cross the vicinity of the point $v_0 = 2$, and, in the final count, disappear at the origin of coordinates, increases, while the number of points $N(q_0)$ "captured" asymptotically at the point v_2 decreases correspondingly. In the limit, when $q_0 \to 0$, we have $v_2 \to v_1 \to v_0$, and contact at the point $v_0 = 2$ only occurs asymptotically, i.e., $N(q_0) \to 0$, $q_0 \to 0$, $\tau \to \infty$. On the other hand, an increase in q_0 is accompanied by a decrease in τ_0, and, hence, by an increase in $N(q_0)$. Since the value of $N(q_0)$ cannot be greater than the original number of pores, we have $N(q) \to N_0 q_0/\nu$ for large values of q_0.

In a way similar to what was done in the preceding section, we now find the change in volume of the material as a function of time for large times:

$$\frac{\Delta V}{V_0} = B\tau^{3/2} - \frac{4\pi}{3}\int_0^\infty v^3 f_0(v)\,dv. \tag{38}$$

Comparing this expression with the corresponding formulas of [7], we see that taking account of coalescence does not change the asymptotic character of the relation between the volume change and the time. It follows from the arguments given above that the role of coalescence when particles are being born continuously is simply that of redistributing the pores in dimensions, with the result that the pores having an original dimension less than some critical value are dissolved, while the pores remaining in the solution equalize their dimensions asymptotically. In this case, the total number of pores decreases, which, however, has no effect on the relation between the volume change and the time.

Note that for the conditions under discussion, the mean pore dimension in v-space for $q_0 \neq 0$ is asymptotically equal to

$$\bar{v} = \left(1 + \frac{q_0}{vN(q_0)}\right). \tag{39}$$

In conclusion, the author expresses his gratitude to V. M. Agranovich for discussion of the results of the work and valuable comments, as well as to É. Ya. Mikhlin and Yu. V. Konobeev for useful discussions.

LITERATURE CITED

1. O. M. Todes, Zh. fiz. khim., 20, 630 (1946).
2. O. M. Todes and V. V. Khrushchev, Zh. fiz. khim., 21, 302 (1947).
3. I. M. Lifshits and V. V. Slezov, Zh. éksperim. i teor. fiz. 35, 479 (1958).
4. C. Wagner, Z. Elektrochem., 65, 581 (1961).
5. Berns, In the book: Transactions of the Second International Conference on the Peaceful Uses of Atomic Energy [in Russian], selected papers by foreign scientists, Vol. 6, Moscow, Atomizdat (1959), p. 325.
6. S. Pugh, J. Nucl. Mat., 4, 177 (1961).
7. V. M. Agranovich, É. Ya. Mikhlin, and L. P. Semenov, Atomnaya énergiya, 15, 393 (1963).
8. G. Greenwood and A. Boltax, J. Nucl. Mat., 5, 234 (1962).
9. G. Greenwood, A. Foreman, and O. Rimmer, J. Nucl. Mat., 1, 305 (1959).

THE MOTION OF ISOLATED CHARGED PARTICLES IN A MAGNETIC FIELD WITH HELICAL SYMMETRY

V. M. Balebanov, V. I. Volkov, V. B. Glasko, A. L. Groshev,
V. V. Kuznetsov, A. G. Sveshnikov, and N. N. Semashko

Translated from Atomnaya Énergiya, Vol. 15, No. 5,
pp. 409-410, November, 1963
Original article submitted March 13, 1963

In this paper we consider the possibility of stabilizing a plasma in a magnetic mirror trap with the help of helical stellarator windings. In contrast to the case of a toroidal stellarator, in which changing deflection and the radius-dependence of the spacing between lines of force produces stabilization, in the case of an open-ended magnetic mirror trap stabilization can only occur as a result of the drift of the particles. We shall call the particle drift "useful" [1] if it leads to stabilization. (The direction of drift in this connection is opposite to the direction of particle rotation).

Let us consider the motion of particles in a magnetic field produced by current I passing through a triple spiral winding with radius a and pitch L. In addition to this let there be a homogeneous longitudinal field of intensity H_0. We shall neglect the effect of the mirrors, assuming that the trap can be made sufficiently long. It may be expected that particles injected in such a field inside the separatrix [2] will not come out at the side walls along the lines of force. In what follows we shall consider predominantly particles injected inside the separatrix.

Study of the equations of motion in the drift approximation shows that actually in the central region the particles move on surfaces which for small values of the Larmor radius R_L almost coincide with the magnetic surfaces encircling the axis. For large values of R_L the surfaces in which motion takes place are turned through 60° with respect to the magnetic surfaces, but they remain closed.

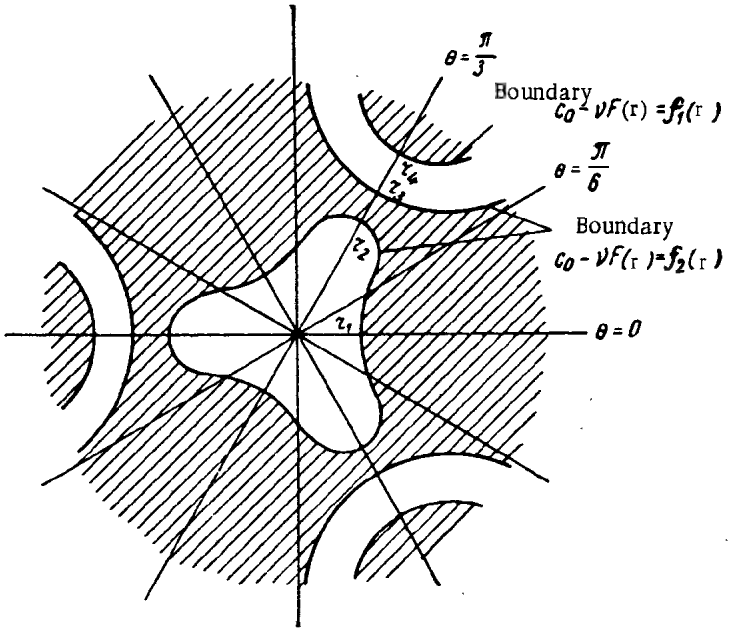

Fig. 1. Regions in which the plasma can be absolutely contained (shaded region forbidden); $\theta = \varphi - az$; $\nu = \cos\theta$.

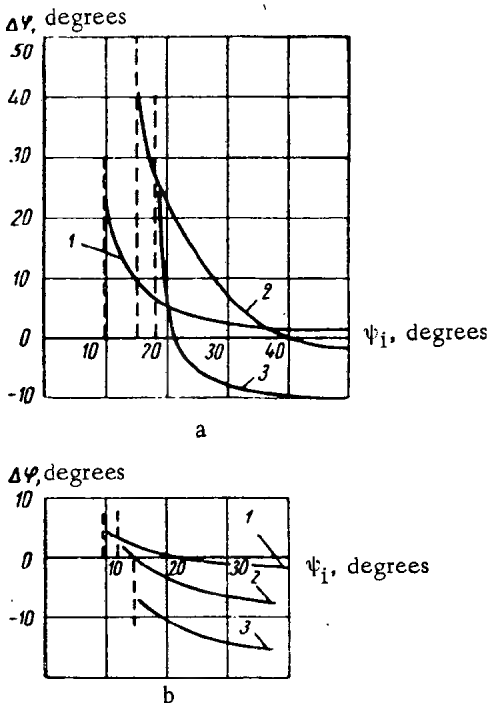

Fig. 2. Drift angle corresponding to the pitch of the helical winding as a function of the injection angle ψ_i for $\gamma = 0.5$, $r_0 = 0.2$ (a) $R_L = 0.2$; b) $R_L = 0.1$): 1) a = 2; 2) a = 1.3; 3) a = 1.

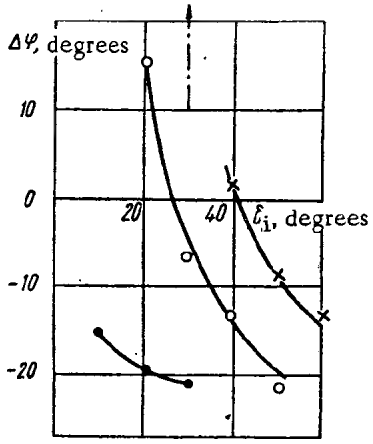

Fig. 3. Drift angle as a function of the injection angle of particles δ_i for large R_L near the separatrix ($r_0 = 0.7$, $R_L = 0.2$, $\alpha = 1$, $\gamma = 0.08$; arrow shows emergence from wall): ● – $\varphi_0 = 0$; ○ – $\varphi_0 = 30°$; × – $\varphi_0 = 60°$.

The exact equations of motion also give regions in which a particle may be found [3]. In the case of helical symmetry it may be shown that these regions may have radial gaps, or, alternatively, may be closed around the axis, depending on the initial conditions (Fig. 1).

The sign of the azimuthal drift of the particles may be determined if the magnetic field is known as a function of the coordinates. This function is given in [2]. If we limit consideration to the first harmonic and to the first term in the series of Bessel functions, then in a cylindrical system of coordinates the square of the field may be written in the form

$$H^2 = H_0^2 \left[1 + 6\alpha\gamma \left(\frac{r}{a}\right)^3 \cos 3(\varphi - \alpha z) + 36\gamma^2 \left(\frac{r}{a}\right)^4 \right],$$

where $\alpha = \frac{2\pi a}{L}$, $\gamma = \frac{2I}{HI_0 a}$.

From this equation it is clear that for small radii the field increases with radius in some azimuths and falls in others. Hence particles moving inside the separatrix and going around the axis of the system must experience a change in the sign of the azimuthal drift. The sign of the total drift may be determined on solving the equations of motion of the particles in such a field.

The motion of the particles was investigated both in the drift approximation, where an analytical relation between the drift of the particles and the field parameters is obtained, and by way of numerical integration of the exact equations of motion. The solution of the drift equations shows that the relations between the angle of drift of the particles and the injection angle ψ_i (Fig. 2) is analogous to the relation in [4] for a corrugated field. However, in the case of a helical field the positions of the transition points between "useful" and "harmful" drift depends on the pitch of the spiral winding. With increasing pitch these points move to the left (see Fig. 2a). The shift to the left also takes place on reducing the Larmor radius (see Fig. 2b). On increasing the current I or the injection radius r_0 the transition point does not move, but the steepness of the curves increases sharply. The left-hand boundary of the region of "useful" drift is determined by reflection from the field maximum. (It must be noted that the curves of Fig. 2 are constructed for injection at the field minimum.) The left-hand boundary moves to the right with increase of γ, r_0 and α.

Calculations of particle motion on a high-speed digital computer showed that the drift theory gives the correct form of the relation between total drift and the field parameters and injection conditions. However the numerical

value of the drift given by the computer differs somewhat from the value obtained in the drift approximation. This is apparently linked with the fact that for the values of Larmor radius considered ($R_L/a = 0.2$) the drift equations are insufficiently accurate.

Numerical integration of the equations of motion was also carried out in a series of cases in which reflections of particles take place from the field maximum. The injection points were chosen close to the separatrix, both inside and outside. The total drift in the majority of cases had negative sign. In certain variants particles were observed to leave at the side walls (Fig. 3).

The calculation shows that in a field with helical symmetry inside the separatrix "useful" drift only takes place for particles with large Larmor orbits in a narrow range of injection angles. On going across to smaller Larmor orbits ($R_L/a \leq 0.1$) the region of "useful" drift vanishes. This shows that for small Larmor orbits the stabilization effect cannot exist.

LITERATURE CITED

1. V. Balebanov et al., J. Nucl. Energy, 5, 205 (1963).
2. A. I. Morozov and L. S. Solov'ev, Zh. tekh. fiz., 30, 271 (1960).
3. V. M. Balebanov et al., Report No. 10/211 presented to the International Conference on Plasma Physics and Control of Thermonuclear Synthesis, Salzburg, MAGATÉ (1961).
4. A. I. Morozov and L. S. Solov'ev, Zh. tekh. fiz., 30, 261 (1960).

INELASTIC SCATTERING OF 14-MeV NEUTRONS BY LIGHT NUCLEI

E. M. Oparin, A. I. Saukov, and R. S. Shuvalov

Translated from Atomnaya Énergiya, Vol. 15, No. 5,
pp. 411-413, November, 1963
Original article submitted March 25, 1963

Calculations of the passage of neutrons through thick layers of various materials are made more difficult by the lack of necessary data on the spectra of fast neutrons inelastically scattered by light nuclei with atomic weights ranging from 6 to 16. Some information of the spectra obtained when neutrons are scattered by beryllium and carbon is given in [1-3]. It is impossible to base the calculations on the temperatures of scattered neutrons for energies of 0.5-4.0 MeV, measured in [4], since in the scattering of neutrons with energies higher than 10 MeV a considerable role is played by the processes of direct interaction of neutrons with the individual nucleons of the nucleus. This leads to a substantial increase in the average energy of the inelastically scattered neutrons.

The present paper concerns the study of the spectra of neutrons inelastically scattered by lithium, beryllium, boron, carbon, nitrogen, and oxygen for an incident-neutron energy of 14 MeV. The experimental procedure, based on measurement of the flight time, is similar to that described in [5]. The geometry of the experiment is shown in Fig. 1.

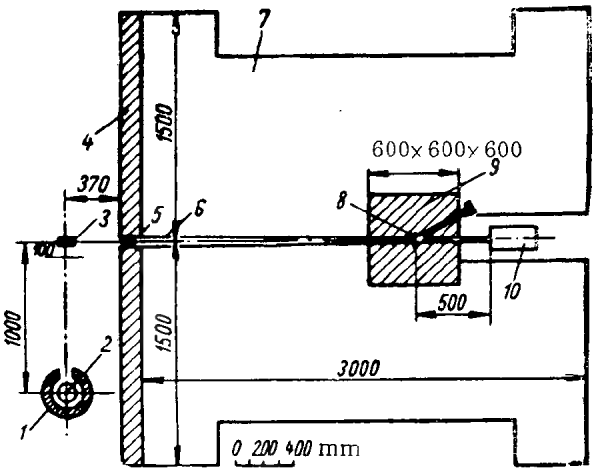

Fig. 1. Geometry of the experiment: 1) Lead shield; 2) neutron detector; 3) specimen under investigation; 4) lead; 5) monitor; 6) collimator; 7) water shield; 8) tritium target; 9) cast-iron cube; 10) alpha counter.

As the neutron detector we used a plastic scintillator 100 mm high and 100 mm in diameter, with an FÉU-36 photomultiplier. The resolution time of the apparatus (2τ), determined from the gamma peak, was $3.5 \cdot 10^{-9}$ sec. When neutrons were recorded, this time was increased to $5.4 \cdot 10^{-9}$ sec. The increase was the finite time of neutron flight through the detector and also to the smaller number of pulses and their greater amplitude dispersion in the scintillator used. We used 60 × 100 × 100 mm specimens made of the following materials: lithium hydride (LiH), beryllium, carbon (graphite), boron carbide (B_4C), melamine ($C_6H_6N_6$), and water. Since the measurements were made at an angle of 90° to the original neutron beam, the presence of hydrogen in the compounds studied left the measurement results unaffected, within the limits of experimental error. The use of shielding made it possible to obtain an effect-to-background of about 3-4 in the region of the elastic-scattering peak at a counting rate of 20-25 pulses per minute.

Figure 2 shows the observed dN/dt spectra of the scattered neutrons at an energy of 14 MeV. Since the resolving power of the equipment was insufficient to distinguish the peak of the elastically scattered neutrons from the spectrum of inelastically scattered neutrons, this distinction was made by using data on the energies of the first states of the B^{11}, C^{12}, N^{14} and O^{16} nuclei given in [6]. For each nucleus the number of neutrons scattered with the excitation of a specific level of the nucleus was taken to be proportional to $e^{-E_i/\theta}$, where E_i is the energy of the level, and θ is an empirical parameter so chosen that the energy of the neutrons, averaged over all possible excited states of a given nucleus, will be equal to the average neutron energy E_{av}, found from the experimental spectrum

$$E_{av} = \frac{\sum_i E_i e^{-\frac{E_i}{\theta}}}{\sum_i e^{-\frac{E_i}{\theta}}},$$

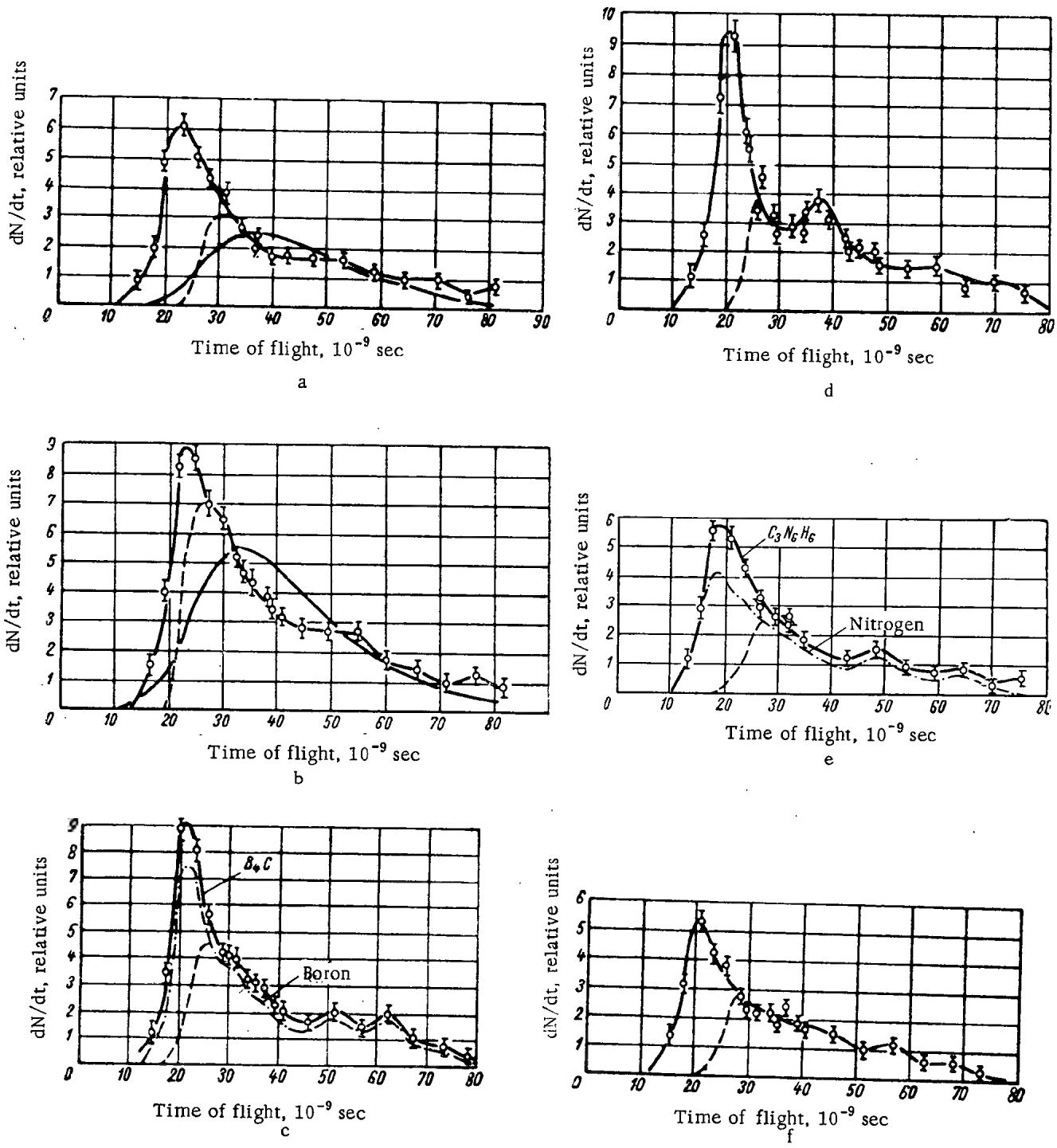

Fig. 2. Time spectra of neutrons scattered by lithium (a), beryllium (b), boron (c), carbon (d), nitrogen (e), and oxygen (f). (The dot-and-dash curves on graphs c and e represent the spectra for boron and nitrogen; the dashed curves on all the graphs represent the parts of the spectra corresponding to inelastic scattering.)

where E_i' is the scattered-neutron energy corresponding to the excitation of the given level. In order to determine the experimental value of E_{av}, we first made an approximate distinction between the elastic and inelastic portions of the spectrum on the assumption that the initial section of the spectrum, corresponding to inelastic scattering, has the shape of a Gaussian curve with a peak in the region of the first levels. After selecting the value of θ, we constructed a time spectrum of the neutrons, taking the resolving power of the apparatus into account. In the final construction of the spectrum of inelastically scattered neutrons, we used only the initial portion of the calculated spectrum.

Data on the Spectra of Neutrons Inelastically Scattered by a Number of Nuclei

Energy range, MeV	Relative number of scattered neutrons, %								
	Li	Be			B	C		N	O
		1	2	3		1	4		
>8.5	—	17	19	15	28	—	—	18	—
8.5—6.0	18	23	21	19	21	34	39	24	27
6.0—4.5	24	19	17	12	16	16	23	19	20
4.5—3.0	22	16	16	19	13	23	20	15	21
3.0—2.0	21	14	16	19	11	16	20	16	19
2.0—1.5	16	11	11	16	10	11	9	7	13
Error	±3.0	±2.0	—	—	±3.5	±3.0	—	±4.5	±3.0

Note. Columns 1, 2, 3, and 4 include data from the following studies: present study [7], [9], and [8], respectively.

When neutrons are scattered by beryllium through the (n, 2N) process, the picture is more complicated, and therefore, when a distinction was made between the elastic and inelastic types of scattering, the dashed curves in Fig. 2 were so drawn as to make the ratio of the areas under the curves correspond to the known cross sections of elastic and inelastic scattering by beryllium, on the assumption that there was spherical symmetry in the angular distribution of the neutrons produced by the (n, 2n) reaction. The first excited level of lithium had a very low excitation energy (470 keV), and it was therefore included in the elastic scattering. This assumption is completely acceptable for calculations of the passage of neutrons through a substance. In Figs. 2a, b we show by solid curves (without dots) not only the experimental curves but also the spectra of inelastically scattered neutrons, calculated on the assumption that the spectrum is Maxwellian at a temperature $T = 2E_{av}$. As can be seen from these figures, the temperature curves corresponding to the statistical model differ considerably from the experimental curves.

The final results of the measurements are shown in the table, which gives the relative number of neutrons in various energy ranges in comparison with the data of other studies [7-9]. It can be seen that the results of the different measurements are in satisfactory agreement.

LITERATURE CITED

1. J. Anderson, Phys. Rev., III, 572 (1958).
2. D. Hughes and R. Schwartz, Neutron Cross Sections. Supplement I. (1957).
3. I. V. Gordeev et al., Handbook of Nuclear Physics Constants for Reactor Design [in Russian] (1960).
4. E. Craves and L. Rosen, Phys. Rev., 89, 343 (1953).
5. V. I. Strizhak, V. V. Bobyr', and L. Ya. Grona, Zh. éksperim. i teor. fiz., 40, 725 (1961).
6. Nuclear Physics, V, 11 (1959).
7. E. Remy and K. Winter, Nuovo cimento, IX, 664 (1958).
8. J. Singlatary and D. Wood, Phys. Rev., 114, 1595 (1959).
9. L. Rosen and L. Stewart, Phys. Rev., 107, 824 (1957).

ON THE DESIGN OF A NEUTRON SPIN ROTATOR

Yu. V. Taran

Translated from Atomnaya Énergiya, Vol. 15, No. 5,
pp. 413-414, November, 1963
Original article submitted April 3, 1963

In a number of experiments with polarized thermal and resonance neutrons it is required to change the adiabatic direction of the polarization vector of a neutron beam with respect to some given direction (for example, the nuclear polarization vector). The adiabatic rotation of the neutron polarization vector through a given angle may be effected by means of a rotating magnetic field. Such a device is called a spin rotator. From the adiabaticity criterion proposed by Hughes [1] it follows that the frequency of Larmor precession $\omega_L = \gamma H_0$ of the magnetic moment of a neutron must be greater than the frequency of the rotating magnetic field ω_0, that is, $\omega_L = k\omega_0$, where $k \gg 1$. In this case the spin of the neutron will follow the field adiabatically. Obviously, the criterion for nonadiabaticity will be the inequality $\omega_L \ll \omega_0$.

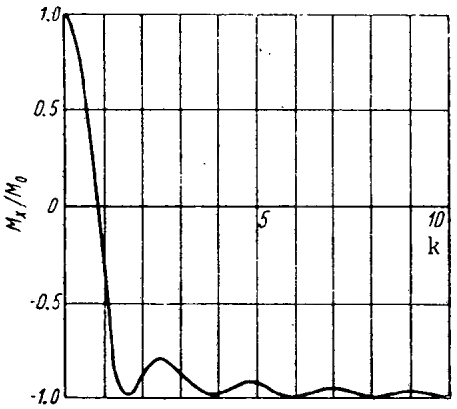

Variation of M_x/M_0 as a function of $k = \omega_L/\omega_0$.

In the design and planning of a spin rotator for resonance neutrons the question of what value the coefficient k will have is extremely important.

In order to determine this coefficient, let us consider the behavior of the spin of a neutron entering a rotating magnetic field. We shall consider a coordinate system bound to the moving neutron, with nonrotating axes. Let the z-axis be directed along the neutron velocity vector, which is perpendicular to the direction of the magnetic field. Let the polarization of the neutron at time $t = 0$ be given by the boundary conditions M_x/M_0, $M_y = M_z = 0$, where M_x, M_y, M_z are the components of angular momentum.. We shall represent the rotating magnetic field as follows:

$$H_x = H_0 \cos \omega_0 t,\ H_y = H_0 \sin \omega_0 t,\ H_z = 0. \tag{1}$$

The equation for the angular momentum was given by Halpern [2]:

$$\frac{d\mathbf{M}}{dt} = \gamma [\mathbf{MH}], \tag{2}$$

where γ is the gyromagnetic ratio of the neutron. The solution of Eq. (2) was found by Newton and Kittel [3]. We are interested in the behavior of the projection of the angular momentum, M_x. For $t = \pi/\omega_0$ (rotation through 180°) we find

$$M_x/M_0 = -(1+k^2)^{-1}\left[k^2 + \cos \pi (1+k^2)^{1/2}\right]. \tag{3}$$

The value of M_x/M_0 as a function of $k = \omega_L\ \omega_0$ is shown in the figure.

The value of ω_0 is related to the velocity of the neutron by the formula $\omega_0 = \pi v/L$, where L is the length of the spin rotator. As can be seen from the figure, for $k \geq 10$, the neutrons with velocities below a certain critical value ($v_{cr} = \omega_L L/\pi k$) will adiabatically change the direction of their polarization by 180° without depolarization.

I take this opportunity to thank Yu. P. Dmitrevskii for his useful comments.

LITERATURE CITED

1. D. Hughes M. Burgy, Phys. Rev., 76, 1413 (1949); 81, 498 (1951).
2. O. Halpern, Phys. Rev., 59, 960 (1941).
3. R. Newton and C. Kittel, Phys. Rev., 74, 1604 (1948).

MEASUREMENT OF THE U^{238} AND Th^{232} CAPTURE CROSS SECTIONS FOR NEUTRONS WITH ENERGIES OF 5-200 keV

V. A. Tolstikov, L. E. Sherman, and Yu. Ya. Stavisskii

Translated from Atomnaya Énergiya, Vol. 15, No. 5,
pp. 414-415, November, 1963
Original article submitted February 21, 1963

There is an insufficient amount of experimental data on the neutron radiative capture cross sections of U^{238} and Th^{232} in the neutron energy region below 200 keV. Considering the great practical importance of these cross sections, the measurements described here were undertaken with the aim of more accurately determining the behavior of the cross section curves in the above energy region.

The ratios of the cross sections under investigation to the cross section of the $B^1{}_0(n, \alpha)$ reaction were measured experimentally. It was assumed that the cross section of the $B^{10}(n, \alpha)$ reaction obeys the $1/v$ law in the 1-200 keV region of energies. Th^{232} and U^{238} specimens and an ionization chamber with a B^{10} layer were simultaneously irradiated in a flux of fast neutrons. The induced β-activity in Th^{232} and U^{238} was measured by means of end-type β-counters.

The ratio of the β-counter's count to the chamber's count is proportional to the ratios of the neutron radiative capture cross sections of Th^{23} (or U^{238}) to the cross section of the $B^{10}(n, \alpha)$ reaction. The normalization of the obtained dependences of the radiative capture cross section on the neutron energy was performed for E_n = 24 keV in the case of U^{238} (according to data from [1], the capture cross section was assumed to be equal to 568 ± 57 mb) and for E_n = 71.5 keV in the case of Th^{232} (according to data from [2], which were converted in connection with the change in the reference cross sections, the capture cross section of Th^{232} was assumed to be 390 ± 59 mb). In both cases, the total error was indicated in the results.

The measurements were performed by means of a Van de Graaf electrostatic accelerator, which had a maximum energy of 5 MeV. For the neutron source, we used the Li(p, n) reaction in a target consisting of thin LiF layer, which was deposited by evaporation in vacuum on the bottom of a nickel cylinder where the wall thickness was less than 0.15 mm. The water layer used for cooling the target was 0.2 mm. The annular chamber with the B^{10} layer and the annular uranium (thorium) specimens were placed at an angle of 91° with respect to the direction of the beam of accelerated protons. The specimens and the chamber were covered with a cadmium layer whose thickness was 0.5 mm. Before irradiation, thorium was chemically purified for the purpose of eliminating the natural decay products. A control specimen, which was used for checking the activity rise after purification, was prepared from purified chlorium. Natural uranium was twice subjected to chemical purification: the natural decay products were eliminated before irradiation, and the fragment activity was eliminated after irradiation. The target thickness was determined before measurements, during measurements, and after the neutrons reached the vicinity of the Li(p, n) reaction threshold. The neutrons were recorded by means of an extended counter. The normalization of the counter readings was performed with respect to the integrator of the target current. In measurements with uranium, the target thickness was 11.5 keV, while, in measurements with thorium, it was equal to 8 keV.

The scattering of energies of the neutrons with which the specimen was irradiated was due to the finite annular dimensions of the specimen and the scattering of the proton energies (caused by the nonuniform target thickness). The average scattering due to the target thickness was equal to ±4 and ±6 keV for Th^{232} and U^{238}, respectively. The scattering of the neutron energies due to the specimen's finite dimensions varied from ±1.5 keV for E_n = 5.5 keV to ±5 keV for E_n = 170 keV.

The following factors were taken into account in discussing the results of the above measurements.

1. The change in the relationship between the yields of both branches of the $B^{10}(n, \alpha)$ reaction with changes in the neutron energy. On the basis of the results given in [11], it can be shown that the efficiency of a chamber

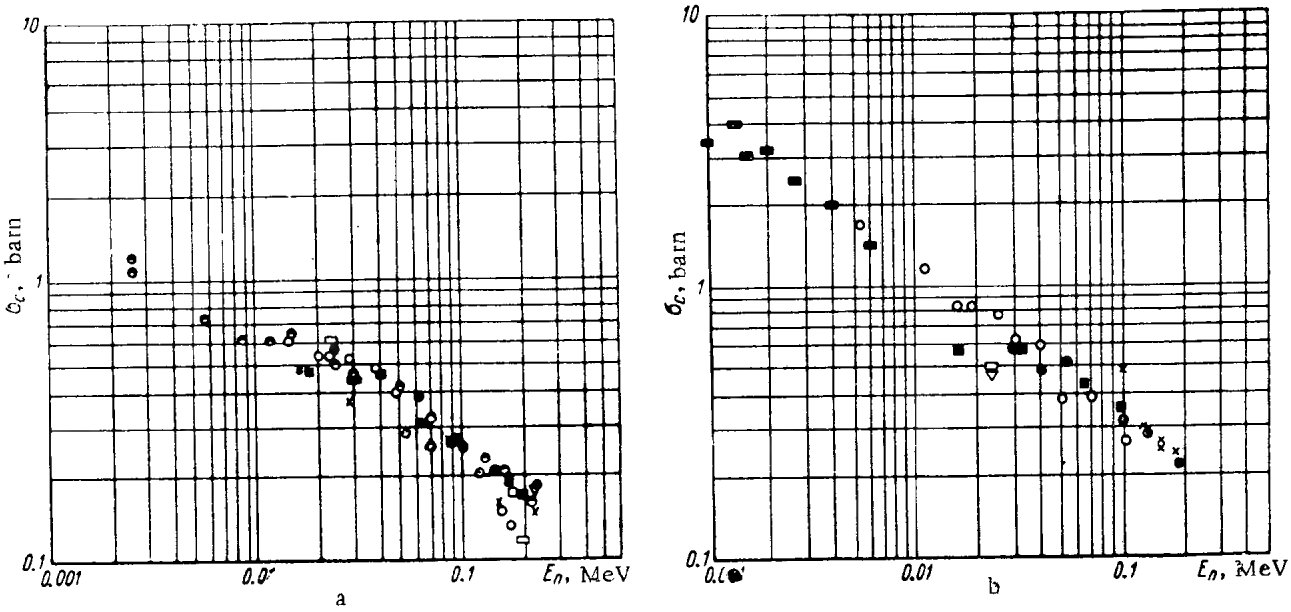

Dependence of the radiative capture cross section of U^{238} (a) and Th^{232} (b) on the neutron energy. The data are from: ○) our experiments; ●) [2]; □) [3]; ▽) [4]; ▭) [5, 10]; ○) [6]; □) [7]; ×) [8]; ■) [9].

with a B^{10} layer does not change by more than 2% as a result of this effect in the neutron energy region under investigation.

2. The contribution of neutrons which are scattered on the walls of the measuring chamber to the activation of specimens and to the count of the B^{10} chamber. It was found experimentally that this contribution was less than 1%.

3. Special attention was paid to the contribution of neutrons scattered on the target's base layer and in the material of the target structure to the boron chamber's count and the activation of U^{238} and Th^{232}. In order to reduce the amount of scattered neutrons, the entire target was made as light as possible.

The experimental determination of the contribution of scattered neutrons was performed in the following manner. The LiF target was irradiated by protons with such an energy that the flare angle of the neutron escape cone was less than 90°. In this, the boron chamber and the specimens of the materials under investigation were irradiated only with neutrons scattered on the target's base-layer. The normalization for the neutron flux was performed with respect to a long counter, which was mounted at an angle of 0° with respect to the direction of the proton beam. The thus obtained data were used for calculating the contribution of scattered neutrons in the energy region under investigation. The contributions of scattered neutrons to the boron chamber's count and the activation of uranium (thorium) were almost the same; their absolute values did not exceed 5.5%. Since the ratio of the count of the β-counter, which measured the induced activity of U^{238} (Th^{232}), to the count of the ionization chamber was determined experimentally for plotting the energetic dependence of the radiative capture cross section on the neutron energy, the effect of scattered neutrons on the measurement results was insignificant and did not exceed the limits of measurement errors.

The figure provides a comparison between our measurement results and the data by other authors.

We see that the cross sections for U^{238} which we obtained agree with the results obtained by other authors. The point at 54 keV deviates from the general smooth energy dependence of the cross section; this point lies approximately 20% below the results obtained by other authors. The points at 171 and 158 keV are also somewhat lower in comparison with those obtained by other authors. The radiative capture cross section of Th^{232} smoothly decreases with a reduction in the neutron energy. The data from [3-5] and [4-6] for energies of 17 and 24 keV, respectively, lie approximately 30% below the results of our measurements.

The authors extend their thanks to A. I. Leipunskii and O. D. Kazachkovskii for their interest in this work.

LITERATURE CITED

1. T. S. Belanova, Atomnaya Énergiya, 8, 549 (1960).
2. Yu. Ya. Stavisskii,and V. A. Tolstikov, Atomnaya Énergiya, 10, 508 (1961).
3. D. Hughes and R. Schwartz, Neutron Cross Sections, New York (1959).
4. T. S. Belanova, Dissertation (1960).
5. R. Macklin, N. Lazar, and W. Jyon, Phys. Rev., 107, 15 (1957).
6. C. Bilpuch, Z. Weston, and H. Hewson, Annal. Physics, 10, 455 (1960).
7. B. Daiven, In the book: Transactions of the Second International Conference on the Peaceful Uses of Atomic Energy. Selected reports by scientists from abroad, Vol. 2, Atomizdat, Moscow (1959), p. 233.
8. R. Hanna and B. Ross, J. Nucl. Energy, 8, 197 (1959).
9. S. Giftah, D. Okrent, and P. Moldauer, Fast Reactor Cross Sections, ANL (1960).
10. W. Jyon and R. Macklin, Phys. Rev., 114, No. 4, 1619 (1959).
11. H. Bichsel et al., Phys. Rev., 81, 456 (1951).

All abbreviations of periodicals in the above bibliography are letter-by-letter transliterations of the abbreviations as given in the original Russian journal. *Some or all of this periodical literature may well be available in English translation.* A complete list of the cover-to-cover English translations appears at the back of this issue.

CROSS SECTIONS OF THE INELASTIC SCATTERING OF NEUTRONS WITH ENERGIES OF 0.4-1.2 MeV ON MEDIUM AND LIGHT NUCLEI

N. P. Glazkov

Translated from Atomnaya Énergiya, Vol. 15, No. 5,
pp. 416-418, November, 1963
Original article submitted February 7, 1963

The method of inverse spherical geometry with a He^3-spectrometer, which was described in part I of this article, was used for measuring the inelastic scattering of neutrons on medium and light nuclei.*

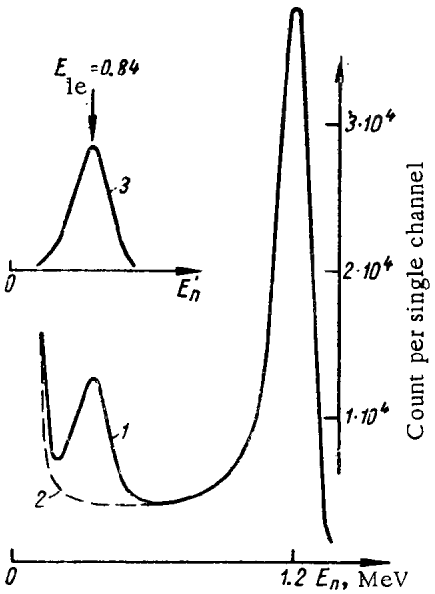

Determination of the difference spectrum for iron. 1) Spectrum of neutrons scattered on iron; 2) normalized neutron spectrum, measured without a diffuser; 3) difference spectrum for E_{1e} = 0.84 MeV.

The specific feature of the measurements described here consists in the fact that a large spread of the energy of scattered neutrons occurs due to recoil in the elastic and inelastic scattering of neutrons on light nuclei. This spread makes it difficult to analyze spectra of scattered neutrons. However, as is known, the first levels of medium and light nuclei are positioned so high and so sparsely that not more than one to two levels are actually excited in the scattering of neutrons with an energy of ~ 1 MeV, which makes it easier to separate the recoil effect from the inelastic scattering effect. Therefore, for an energy resolution of 100-150 keV of the He^3-spectrometer, the partial inelastic scattering cross sections with the excitation of individual levels can be fairly accurately determined and related to well-defined isotopes. There were only rare cases in the simultaneous excitation of very closely spaced levels where the separation of the latter was impossible, so that the cross section found was related to the entire group of the unresolved levels belonging to several isotopes.

All the inelastic scattering measurements were performed for neutron energies of 0.4, 0.6, 0.8, 1.0 and 1.2 MeV. The inelastic scattering effect was determined by subtracting the neutron spectrum measured without a diffuser from the spectrum measured with a diffuser. The normalization of spectra was performed in the vicinity of the peak corresponding to inelastically scattered neutrons (see figures).

Since the measured effects were weak, the cross sections $\sigma_{n'}$ could be calculated by using the simplified equation

$$\sigma_{n'} = \frac{1}{n\bar{l}} \cdot \frac{\int (\Delta')}{P},$$

where n is the density of nuclei in the given specimen (a natural mixture of isotopes), $\bar{l}$ is the mean free path of incident neutrons in the specimen; $\int(\Delta')$ is the partial effect or the reduced area of the peak corresponding to inelastically scattered neutrons with an allowance for the efficiency of the He^3-spectrometer, and P is the normalized total flux of incident neutrons.

The results of our experiments are given in the table. The first and the second columns of the table provide the percentage of the isotope in the diffuser material and its first levels for which the inelastic scattering effect was

* See Atomnaya Énergiya, 14, 400 (1963).

Partial and Total Cross Sections σ_n' of Inelastic Neutron Scattering on Different Nuclei (calculated for a natural mixture of isotopes), barn

Isotope percentage, %	E_{1e}, MeV	E_n, MeV				
		0,4	0,6	0,8	1,0	1,2
Ta^{181} — 100	0.137	0.95±0.10	1.35±0.15	1.45±0.15	1.55±0.15	1.10±0.15
	0.303	0.35±0.05	0.45±0.05	0.50±0.05	0.50±0.05	0.50±0.05
	0.482	—	0.30±0.05	0.50±0.05	0.55±0.05	0.60±0.06
	$\sigma_{n'}$ (total)	1.30±0.15	2.10±0.20	2.45±0.20	2.60±0.20	2.20±0.20
Ba^{135} — 7	0.49	—	<0.25	0.30±0.15	0.20±0.10	—
Ba^{137} — 11.3	0.66	—	—	<0.25	0.30±0.15	—
Ba^{136} — 8	1.04	—	—	—	—	0.15±0.10
	$\sigma_{n'}$ (total)	—	<0.25	0.40±0.20	0.50±0.25	—
I^{127} — 100	0.060	0.50±0.10	0.70±0.10	0.60±0.10	0.30±0.10	—
	0.203	0.25±0.05	0.45±0.05	0.47±0.05	0.30±0.05	—
	~0.420	—	0.17±0.10	0.28±0.15	0.47±0.15	—
	~0.630	—	—	0.28±0.10	0.48±0.10	—
	~0.744	—	—	—	0.10±0.05	—
	$\sigma_{n'}$ (total)	0.75±0.15	1.32±0.20	1.63±0.20	1.65±0.25	—
Sb^{123} — 43	0.15	0.10±0.05	0.19±0.05	0.25±0.05	0.25±0.05	0.20±0.05
Sb^{121} — 57	0.51; 0.57	—	—	0.15±0.02	0.21±0.02	0.21±0.02
	~1.0	—	—	—	—	0.30±0.10
	$\sigma_{n'}$ (total)	0.10±0.05	0.20±0.05	0.40±0.05	0.45±0.05	0.70±0.10
Sn	—	—	—	—	<0.08	<0.08
Cd	0.26; 0.30	0.11±0.02	0.27±0.03	0.30±0.03	0.18±0.02	0.14±0.02
	0.56; 0.62	—	—	0.40±0.05	0.78±0.10	0.80±0.10
	$\sigma_{n'}$ (total)	0.11±0.02	0.27±0.03	0.70±0.10	0.96±0.15	0.94±0.15
Mo	0.20	0.14±0.03	0.20±0.03	0.34±0.03	0.25±0.03	0.10±0.03
	0.53	—	0.04±0.02	0.16±0.02	0.15±0.02	0.10±0.02
	0.77; 0.87	—	—	<0.15	0.74±0.10	1.10±0.10
	$\sigma_{n'}$ (total)	0.14±0.03	0.24±0.03	0.50±0.05	1.15±0.10	1.30±0.15
Nb^{93} — 100	0.76	—	—	0.20±0.03	0.55±0.05	0.60±0.05
	0.99	—	—	—	<0.20	0.70±0.10
	$\sigma_{n'}$ (total)	—	—	0.20±0.03	0.65±0.10	1.30±0.15

TABLE (continued)

Isotope percentage, %	E_{le}, MeV	E_n, MeV				
		0.4	0.6	0.8	1.0	1.2
$Zr^{92, 94}$ — 37	0.93	—	—	—	<0.20	0.32±0.03
Sr^{87} — 7	0.39; 0.87	—	—	—	—	<0.2
$Se^{76, 78, 80}$	~0.6	—	—	0.60±0.05	0.90±0.10	1.00±0.10
$Zn^{64, 66}$	~1.0	—	—	—	<0.07	0.37±0.05
Cu^{63} — 70	0.67 0.97	— —	— —	0.10±0.05 —	0.17±0.05 0.10±0.05	0,24±0.05 0,30±0.05
	σ_n, (total)	—	—	0.10±0.05	0.27±0.05	0.54±0.05
Co^{59} — 100	1.098	—	—	—	—	<0.2
Fe^{56} — 92	0.845	—	—	—	0.28±0.03	0.52±0.05
Mn^{55} — 100	0.128 0.980	0.32±0.05 —	0.53±0.05 —	0.55±0.05 —	0.70±0,07 <0.05	0.72±0.03 0.11±0.03
	σ_n, (total)	0.32±0.05	0.53±0.05	0.55±0.05	0.75±0.07	0.83±0.10
Cr^{53} — 10	0.54; 0.97	—	—	—	<0.06	<0.06
Cl^{37} — 25	0,84	—	—	—	<0,12	<0,12
Al^{27} — 100	~0,83 1,017	— —	— —	— —	<0,05 —	0,05±0,03 0,13±0,05
	σ_n, (total)	—	—	—	<0,05	0,18±0,05
Mg^{25} — 11	0,53; 0,98	—	—	—	<0,06	<0,06
Na^{23} — 100	0,44	—	0,20±0,02	0,31±0,03	0,40±0,04	0,44±0,04
B^{10} — 20	0,723	—	—	—	<0,06	<0,06
Li^{7} — 92	0,479	—	—	<0,07	0,08±0,04	0,20±0,05

detected and measured. All the partial cross sections σ_n' were calculated for the natural mixture of isotopes. The indicated total errors ($\sim$ 15-20%) were mainly due to the statistical errors in measuring the $\int(\Delta')$ effect, the errors of the manual data on the transport cross sections σ_{tr} used for calculating the mean free path $\bar{l}$ of neutrons in the specimen, and the errors of the corrections introduced, for instance, corrections for the cross section σ_a of neutron absorption in the specimen. The indicated maximum errors (0.05-0.10 b) constitute the upper sensitivity limit of the method used ($\sim$ 1%). The data on σ_n' that are available in the literature were obtained mainly by measuring the γ-ray yields.

Our data on σ_n', based on neutron measurements, are published here for the first time; they are in good agreement with the previously known data.

DEPENDENCE OF THE MEAN KINETIC ENERGY OF FRAGMENTS ON THE FISSIONABLE NUCLEUS MASS

V. N. Okolovich, V. I. Bol'shov, L. D. Gordeeva, and G. N. Smirenkin

Translated from Atomnaya Énergiya, Vol. 15, No. 5, pp. 419-420, November, 1963
Original article submitted March 29, 1963

For the determination of the dependence of the mean kinetic energy $\bar{E}_k$ of fragments on the charge Z and the atomic weight A of fissionable nuclei. Terrell [1] proposed the relation

$$\bar{E}_K = 0{,}121\frac{Z^2}{A^{1/3}}\ \text{MeV}. \qquad (1)$$

This dependence can be explained by the fact that the kinetic energy of fragments is virtually entirely determined by the Coulomb repulsion energy after the destruction of the neck: $Z_1Z_2l^2/R \sim Z^2/A^{1/3}$. Equation (1) satisfactorily describes the experimentally detected rise in $\bar{E}_k$ with an increase in Z. At the same time, the data on $\bar{E}_k$ obtained for the neutron fission of isotopes of an element – Th^{229} and Th^{232}; U^{233} and U^{235}; Pu^{239} and Pu^{241} – indicate that there is a tendency in experiments to a change in $\bar{E}_k$ with an increase in A, which is contrary to that which could be expected according to Eq. (1). In experiments on the fission of nuclei with a larger atomic weight, a somewhat greater mean kinetic energy of fragments is observed. Although the nature of this effect is systematic, its magnitude is comparable to the errors of the measurements performed. Therefore, more accurate measurements were performed, and the casues of the deviation of $\bar{E}_k$ from the values obtained by means of Eq. (1) were analyzed. Moreover, the knowledge of the dependence of $\bar{E}_k$ on the atomic weight is necessary for discussing the very interesting problem of the energy dependence of $\bar{E}_k$ in a wide range of excitation energies when fission reactions with preliminary neutron emission occur besides fission at the maximum excitation [2].

The mean kinetic energies of the fission fragments of U^{233}, U^{235} and U^{238} under the action of neutrons are compared in the present article. In order to secure high accuracy in relative measurements of $\bar{E}_k$, we used a layer consisting of isotope mixtures in our experiments: natural uranium and uranium which has been depleted by a factor of 250 with respect to the U^{235} isotope with an addition of 1% U^{233}. The fission of U^{233} and U^{235} was caused by slow neutrons, while the fission of U^{238} was caused by fast 2 MeV neutrons. Small corrections, typical for such measurements (see, for instance [3]), were introduced into the found ratios of the mean pulse amplitudes in the ionization chamber, which were connected with the fission of different isotopes. The ratios of the mean kinetic energies for U^{233} and U^{238} and for U^{235} and U^{238} were found to be 0.9909 ± 0.0014 and 0.9938 ± 0.0018, respectively. The $\bar{E}_k$ ratio for the U^{238} fission by γ-rays and neutrons was equal to 1.000 ± 0.004 [4]. According to the data obtained, $\bar{E}_k$ monotonically rises with an increase in A. If, using small relative changes in $\bar{E}_k$ and A, this dependence is described by means of the constant factor $d\bar{E}_k/dA$, it will be equal to 0.30 ± 0.03 MeV, which would correspond to $1/\bar{E}_k \cdot d\bar{E}_k/dA = (1.9 \pm 0.2)\cdot 10^{-3}$. Equation (1) yields $1/\bar{E}_k \cdot d\bar{E}_k/dA = -1/3A \simeq -1.4\cdot 10^{-3}$, i.e., the sign is opposite to that given above.

The disagreement between Eq. (1) and the experimental results can be explained in the following manner. The fact that $\bar{E}_k$ is proportional to the $Z^2/A^{1/3}$ parameter could be considered as an indication that the critical configurations are similar at the moment of the fission of nuclei with different A values. However, such an assumption hardly corresponds to reality, if only for the reason that nuclei with different atomic weights disintegrate into fragments with different ratios of the most probable masses. Moreover, the configuration of fractionation and the effective distance between the fragments constitute specific functions of the ratio $\underline{m}$ of fragment masses, which are determined by the shell structure [5, 6]. Therefore, in describing the dependence of $\bar{E}_k$ on A, it is necessary to consider not only the change in the linear dimensions of the nucleus, which is taken into account by Eq. (1), but also the change in the most probable type of fission. Qualitatively, the influence of the latter effect can be established on the basis of the fact that the dependence of $\bar{E}_k$ on $\underline{m}$ directly in the region of the most probable modes of fractionation of the nuclei

under consideration constitutes a monotonically decreasing function. Since, with an increase in A, the most probable ratio $\tilde{m}$ of fragment masses decreases as a result of the invariance of the heavy peak's position $\tilde{A}_h \simeq 140$ on the mass yield curve, the factor which leads to an increase in $\bar{E}_k$ becomes operative.

Let us estimate the value of $1/\bar{E}_k \cdot d\bar{E}_k/dA$ using the concept of $\bar{E}_k$ as the Coulomb repulsion energy of spherical fragments in contact, one of which (the heavy one) has constant dimensions, while the other (the light one) increases as the A value of the fissionable nucleus increases. These simple calculations were performed for two modes of separation of the fissionable nucleus' charge: in proportion to the masses of the fragments formed and under the assumption that the chain lengths of β-decay are equal. The thus obtained $1/\bar{E}_k \cdot d\bar{E}_k/dA$ values were positive, but they were also much lower than the experimental value. Regardless of the latter face, the correct sign of $d\bar{E}_k/dA$ obtained within the framework of a very crude model leaves room for hope that a better agreement with experimental data will be achieved later on the basis of more accurate knowledge. However, the absence of acceptable theoretical information on the fractionation mechanism can be filled by using empirical relationships. The $d\bar{E}_k/dA$ factor in which we are interested can be represented by the following relationship:

$$\frac{d\bar{E}_\kappa}{dA} = \frac{\partial \bar{E}_\kappa}{\partial A} + \frac{\partial \bar{E}_\kappa}{\partial \tilde{m}} \cdot \frac{\partial \tilde{m}}{\partial A} ,$$

where the first term described the change in $\bar{E}_k$ with variations in the nucleus's linear dimensions, while the second term describes the variation of $\bar{E}_k$ which is due to the dependence of $\tilde{m}$ on A. According to the most accurate measurements of the dependence of E_k on the fission mode [7], the decrease in E_k with an increase in the mass A_h of a heavy fragment in the thermal neutron fission of U^{233}, U^{235} and Pu^{239} can be approximately described by a linear dependence which is characterized by the derivative $\partial E_k/\partial A_h = -1$ MeV. Hence,

$$\frac{\partial \bar{E}_\kappa}{\partial \tilde{m}} \simeq \frac{\partial E_\kappa}{\partial m}\Big|_{m=\tilde{m}} = -\frac{A}{(\tilde{m}+1)^2} \text{ MeV}.$$

By using the constancy of A_h for different fissionable nuclei from thorium to curium, we obtain $\partial m/\partial A = -m(m+1)/A$.

From the above relationships, we obtain

$$\frac{1}{\bar{E}_\kappa} \cdot \frac{d\bar{E}_\kappa}{dA} = \left(-\frac{1}{3} + \frac{\tilde{A}_h}{E_\kappa}\right)\frac{1}{A} \approx \frac{1}{2A} . \qquad (2)$$

Here, it was assumed that $\bar{E}_k = 167$ MeV, $A_h = 140$. For A = 236, $1/\bar{E}_k \cdot d\bar{E}_k/dA \simeq 2.1 \cdot 10^{-3}$, which is in good agreements with the results of the experiment performed.

Thus, the results of the above analysis and the data obtained in direct measurements indicate the existence of "fine structure" in the dependence proposed by Terrell. Although the variations of $\bar{E}_k$ with changes in A are small, it is desirable to use such a parameter which would make it possible to describe the dependence of $\bar{E}_k$ on Z and A by a single smooth curve. From relationship (2), it follows that $Z^2\sqrt{A}$ can be used as such a parameter.

The authors hereby acknowledge their indebtedness to N. S. Rabotnov for the discussion of this article.

LITERATURE CITED

1. J. Terrell, Phys. Rev., 113, 527 (1959).
2. V. N. Okolovich and G. N. Smirenkin, Atomnaya Énergiya, 13, 64 (1962).
3. V. N. Okolovich and G. N. Smirenkin, Atomnaya Énergiya, 12, 461 (1962).
4. V. N. Okolovich and G. N. Smirenkin, Zh. Éksperim. i Teor. Fiz., 43, 1861 (1962).
5. A. Cameron, Proc. of the Second UN Intern. Conf. on the Uses of Atomic Energy, Vol. 15, Geneva (1958), p p. 425.
6. W. Brunner and H. Paul, Ann. Physik, 6, 267 (1960)
7. J. Milton and J. Fraser, Phys. Rev. Let., 7, 67 (1961).

ENERGY DISTRIBUTION OF γ-RADIATION IN A MATERIAL MEDIUM

A. M. Sazonov and V. I. Sirvidas

Translated from Atomnaya Énergiya, Vol. 15, No. 5,
pp. 420-422, November, 1963
Original article submitted November 28, 1962

The mathematically rigorous solution of the problem of the transmission of γ-radiation through matter is rather complex and time-consuming in most cases. Assumptions and approximation can often be made, which provides the possibility of applying analytical methods which greatly simplify the solution of such problems.

Let us solve the equation for the energy spectrum in the approximation of small scattering angles [1]:

$$\frac{\partial I(\lambda, x)}{\partial x} = -\mu(\lambda) I(\lambda, x) + \int_{\lambda_0}^{\lambda} K(\lambda', \lambda) I(\lambda', x)\, d\lambda' \tag{1}$$

for the boundary conditions

$$I(\lambda, x)|_{x=0} = I_0(\lambda), \quad I(\lambda, x)|_{x=\infty} = 0, \tag{2}$$

where $I(\lambda, x)$ is the energy spectrum of γ-radiation at the depth x in the absorbing material medium, $\mu(\lambda)$ is the coefficient of total absorption of γ-rays with the wavelength λ, λ_0 is the wavelength of the hardest component of the primary energy spectrum, and $K(\lambda', \lambda)d\lambda'$ is the probability of the generation of a scattered γ-quantum with a with a wavelength from λ to $\lambda + d\lambda$ by a primary λ-quantum with the wavelength λ' in the process of Compton scattering (the wavelengths are expressed in Compton units).

If we introduce the function $I_1(\lambda, x) = I(\lambda, x) - I_0)\lambda)e^{-\mu(\lambda)x}$, which satisfies the homogeneous boundary conditions (2) and the nonhomogeneous Eq. (1), and use the Laplace transform

$$I_1(\lambda, x) = \frac{1}{2\pi i}\int_{\sigma-i\infty}^{\sigma+i\infty} e^{px} I_1(\lambda, p)\, dp, \quad e^{-\mu(\lambda')x} = \frac{1}{2\pi i}\int_{\sigma-i\infty}^{\sigma+i\infty} e^{px}\frac{1}{\mu(\lambda')+p}\, dp, \tag{3}$$

we can show that, under the condition

$$K(\lambda', \lambda) = \begin{cases} c & \lambda_0 < \lambda' < \lambda \\ 0 & \lambda' < \lambda \end{cases}, \tag{4}$$

$$I_1(\lambda_1 p) = C_1 \frac{e^{c\int_{\lambda_0}^{\lambda'} \frac{d\lambda'}{\mu(\lambda')+p}}}{\mu(\lambda)+p} + c\int_{\lambda_0}^{\lambda} \frac{I_0(\lambda')\, e^{c\int_{\lambda'}^{\lambda} \frac{d\lambda''}{\mu(\lambda'')+p}}}{[\mu(\lambda')+p][\mu(\lambda)+p]}\, d\lambda'. \tag{5}$$

In this, the integration constant C_1 must be chosen so that the conditions

$$\frac{1}{2\pi i}\int_{\sigma-i\infty}^{\sigma+i\infty} I_1(\lambda, p)\, dp = 0, \tag{6}$$

$$I_1(\lambda_0, x) = \frac{1}{2\pi i}\int_{\sigma-i\infty}^{\sigma+i\infty} e^{px} I_1(\lambda_0, p)\, dp = 0 \tag{7}$$

are satisfied for any x. Consequently, $I_1(\lambda_0, p) = 0$.

Condition (7) yields $C_1 = 0$. Condition (6) will certainly be satisfied, since the integration path can be closed by a semicircle with an infinitely long radius on the right, where the $I_1(\lambda, p)$ function is analytic.

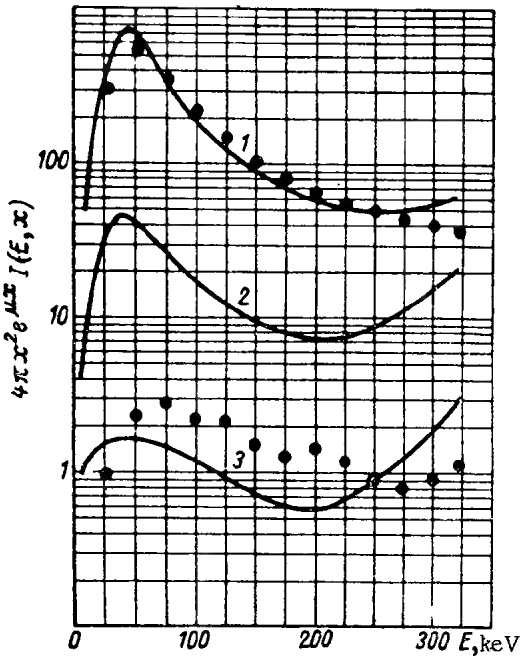

Energy distribution of Cr^{51} γ-radiation (320 keV) for the following layer depths in the sand medium: 1) 45 cm; 2) 15 cm; 3) 5 cm.

Thus,

$$I_1(\lambda_1 x) = c\int_{\lambda_0}^{\lambda} I_0(\lambda')\,d\lambda'\,\frac{1}{2\pi i}\int_{\sigma-i\infty}^{\sigma+i\infty}\frac{e^{px+c\int_{\lambda'}^{\lambda}\frac{d\lambda''}{\mu(\lambda'')+p}}}{[\mu(\lambda')+p][\mu(\lambda)+p]}\,dp \qquad (8)$$

so that the solution of the problem is reduced to the calculation of an integral of the following type:

$$J=\frac{1}{2\pi i}\int_{\sigma-i\infty}^{\sigma+i\infty}\frac{e^{px+c\int_{\lambda'}^{\lambda}\frac{d\lambda''}{\mu(\lambda'')+p}}}{[\mu(\lambda')+p]\,[\mu(\lambda)+p]}\,dp. \qquad (9)$$

On the basis of the results given in [2, 3], it can be shown that the basic contribution to integral (9) occurs near the point $p \simeq -\mu(\lambda')$. Therefore, under the condition that the absorption coefficient in the wavelength interval (λ_0, λ) is approximated by a linear function of λ in the form $\mu(\lambda) = a + \beta\lambda$, we shall write integral (9) as

$$J \cong \frac{1}{2\pi i}\left(\int_{\sigma-i\infty}^{\sigma+i\infty} e^{px-\left(\frac{c}{\beta}+1\right)\ln[\mu(\lambda')+p]}\,dp\right) \times [\mu(\lambda)-\mu(\lambda')]^{\frac{c}{\beta}-1}. \qquad (10)$$

For large x ($x \gg \mu(\lambda')^{-1}$) values,

$$J \simeq \frac{e^{-\mu(\lambda')x}\,c^{\frac{c}{\beta}}}{\Gamma\left(\frac{c}{\beta}+1\right)}[\mu(\lambda)-\mu(\lambda')]^{\frac{c}{\beta}-1}, \qquad (11)$$

where $\Gamma(c/\beta + 1)$ is the γ-function.

As a result, we obtain

$$I_1(\lambda, x) = I_0(\lambda)e^{-\mu(\lambda)x} + \frac{cx^{\frac{c}{\beta}}}{\Gamma\left(\frac{c}{\beta}+1\right)}\int_{\lambda_0}^{\lambda}\frac{I_0(\lambda')\,e^{-\mu(\lambda')x}}{[\mu(\lambda)-\mu(\lambda')]^{1-\frac{c}{\beta}}}\,d\lambda'. \qquad (12)$$

We shall now consider certain particular cases of the expression (12). The initial spectrum consists of a single-line: $I(\lambda') = I_0$ for $\lambda_0 \le \lambda' \le \lambda$. In this case,

$$U = \frac{cI_0x^{\frac{c}{\beta}}}{\Gamma\left(\frac{c}{\beta}+1\right)}\int_{\lambda_0}^{\lambda} e^{-\mu(\lambda')x}[\mu(\lambda)-\mu(\lambda')]^{\frac{c}{\beta}-1}\,d\lambda'$$

$$= \frac{cI_0x^{\frac{c}{\beta}}\cdot\beta^{\frac{c}{\beta}-1}}{\Gamma\left(\frac{c}{\beta}+1\right)}e^{-ax}(\lambda-\lambda_0)^{\frac{c}{\beta}}\int_0^1 e^{-\beta\lambda x}e^{z(\lambda-\lambda_0)x\beta}z^{\frac{c}{\beta}-1}\,dz \qquad (13)$$

for $z=\frac{\lambda-\lambda'}{\lambda-\lambda_0}$; $\lambda'=\lambda-z(\lambda-\lambda_0)$.

Introducing the hypergeometric function, we shall write Eq. (13) in the following form:

$$U=\frac{c}{\beta}\cdot\frac{x^{\frac{c}{\beta}}I_0e^{-\mu(\lambda)x}[\mu(\lambda)-\mu(\lambda_0)]^{\frac{c}{\beta}}}{\Gamma\left(\frac{c}{\beta}+1\right)}\times\frac{\Gamma\left(\frac{c}{\beta}\right)}{\Gamma\left(\frac{c}{\beta}+1\right)}F\left(\frac{c}{\beta}\left|\frac{c}{\beta}+1\right|x\beta(\lambda-\lambda_0)\right). \tag{14}$$

Under the conditions that $x[\mu(\lambda)-\mu(\lambda_0)]\gg 1$, we have

$$U\simeq\frac{c}{\beta}\cdot\frac{x^{\frac{c}{\beta}}I_0e^{-\mu(\lambda)x}}{\Gamma\left(\frac{c}{\beta}+1\right)}[\mu(\lambda)-\mu(\lambda_0)]^{\frac{c}{\beta}}\frac{e^{[\mu(\lambda)-\mu(\lambda_0)]x}}{x[\mu(\lambda)-\mu(\lambda_0)]}$$

and, finally,

$$I(\lambda,x)=I_0e^{-\mu(\lambda)x}+\frac{I_0e^{-\mu(\lambda_0)x}x^{\frac{c}{\beta}-1}}{\Gamma\left(\frac{c}{\beta}\right)}[\mu(\lambda)-\mu(\lambda_0)]^{\frac{c}{\beta}-1}. \tag{15}$$

In the case where the spectrum consists of "n" γ-lines, the initial spectrum can be approximated by the step function $I_0(\lambda')=I_k$, where k = 1,2,...,n, and the obtained expression (12) can be written thus:

$$I(\lambda,x)=I_ke^{-\mu(\lambda)x}+$$
$$+\frac{I_kx^{\frac{c}{\beta}-1}}{\Gamma\left(\frac{c}{\beta}\right)}\left\{e^{-\mu(\lambda_k)x}[\mu(\lambda)-\mu(\lambda_k)]^{\frac{c}{\beta}-1}-e^{-\mu(\lambda_{k+1})}[\mu(\lambda)-\mu(\lambda_{k+1})]^{\frac{c}{\beta}-1}\right\}. \tag{16}$$

Equations (12), (15), and (16) can be used for determining the energy distribution of γ-radiation in a material medium. The calculation accuracy depends on the energy of primary γ-radiation and the depth to which the material medium is penetrated; it increases with an increase in energy and depth.

In order to determine the limits within which expressions (12), (15), and (16) for $I(\lambda, x)$ can be applied, we performed a numberical calculation of the energy distribution of Cr^{51} γ-radiation (320 keV) in a sand medium. The figure shows the energy distribution obtained from expression (15) by converting the Compton wavelengths to energy under the condition that $c = \frac{3}{4} nZ\sigma$, where n is the number of atoms per 1 cm^3 of medium, Z is the atomic number of the medium, and σ_0 is the Thomson scattering cross section. The approximation of the sand medium's absorption coefficient by a linear function was performed by using the data from [4]. A comparison between our results and the results given in [5] showed that they are in good qualitative agreement. For illustration, the figure also shows the experimental points borrowed from [5] for x values equal to 5 and 45 cm, which were normalized for the theoretical curves.

It should be noted that the instrumental spectrum at x = 0 can be used as an approximation instead of the initial $I_0(\lambda)$ spectrum.

LITERATURE CITED

1. V. I. Ogievetskii, Zh Éksperim. i Teor. Fiz., 29, 459 (1955).
2. U. Fano, Phys. Rev., 76, 739 (1949).
3. U. Fano, J. Res. Nat. Bur. Stand., 51, 95 (1953).
4. O. I. Leipunskii, B. V. Novozhilov, and V. N. Sakharov, Distribution of Gamma-Quanta in Matter [in Russian], Fizmatgiz, Moscow (1960).
5. V. V. Matveev, A. D. Sokolov, and R. S. Shlyapnikov, Atomnaya Énergiya, No. 4, 57 (1956).

OBTAINING THE RADIOACTIVE ISOTOPE Be^7 FROM CYCLOTRON TARGETS

I. F. Kolosova and I. V. Kolosov

Translated from Atomnaya Énergiya, Vol. 15, No. 5,
pp. 422-423, November, 1963
Original article submitted February 2, 1963

At the present time the radioactive isotpoe Be^7 is obtained by irradiating a lithium target with deuterons accelerated in a cyclotron, using the nuclear reactions:

$$Li^6\ (7{,}3\%)\ (d, n)\ Be^7;$$
$$Li^7\ (92{,}7\%)\ (d, 2n)\ Be^7.$$

A number of studies of the separation of carrier-free Be^7 from cyclotron targets have been published [1-4]. The method used in [1] was selective sorption of Be^{2+} ions by a porous glass filter at a fixed pH. Another method [2] is based on the nonisomorphic coprecipitation of carrier-Be^7 on iron hydroxide when it is precipitated with ammonia. In a number of studies beryllium is extracted by means of thenoyltrifluoroacetone [3] and acetyl acetone [4].

The authors have developed a method for the separation of beryllium by thenoyltrifluoroacetone [3] which, in their opinion, gives the best results. However, quantitative isolation of beryllium could not be achieved. Particularly little success was found in the reextraction of beryllium from the organic phase and its separation from the iron. It was proposed, therefore, to vary the procedure of [2] and use the simplest reactants for the quantitative isolation of carrier-free radioactive Be^7.

Two types of target were used in the study:

1. Metallic lithium in the liquid state was poured, under a vacuum in a helium atmosphere, into a target made of electrolytic copper (depression measuring 21.5 × 62 mm^2). The target was covered at the top with tungsten foil 30 μ thick and was soldered to the base. This preparation of the target produced good thermal contact between the foil, the lithium, and the cooled backing.

2. Metallic lithium was burned, and the depression was filled with the mixture (evidently consisting of oxides and carbonates), pressing the substance carefully into place. The target was then covered with tungsten foil 50 μ thick.

In the first case the target was irradiated for 18 h at a current of 20 μA. The energy of the deuterons was 12 MeV, the irradiation area was 21.5 × 62 mm^2; in the second case the target was irradiated for 6 h at a current of 25 μA. The deuteron energy was 14.4 MeV, and the irradiation area was 80 × 10 mm^2.

The lithium used in both cases was analyzed spectrally. The purity of the lithium was 99.73%. After irradiation, the target was stored for one month. The foil was then removed, and the targets were treated with water in the first case and with dilute hydrochloric acid in the second case. Since the solubility of the irradiated lithium was low in both cases, especially at the points at which the deuteron beam had penetrated, where caked particles were observed, the target was subjected in the last stage to lengthy treatment with concentrated hydrochloric acid.

A sample was prepared from part of the irradiated lithium, and the gamma-ray spectrum of the specimen was studied in order to determine the radioactive admixtures. As the analysis showed, the activity of the target is determined chiefly by the activity of Be^7 and that of small quantities of Zn^{65}, Fe^{55}, and Fe^{59}. The gamma-ray spectrum was measured with a scintillation-type gamma spectrometer with a NaI(Tl) crystal (spectrometric method), an FEU-29 photomultiplier connected to a cathode follower, and an AADO differential analyzer. All subsequent Be^7 measurements were made with a NaI(Tl) crystal gamma-counting instrument. The dimensions of the crystal were 40 × 50 mm and the dimensions of the well inside the crystal, into which the 5 ml cuvettes containing the sample were placed, were 17 × 40 mm.

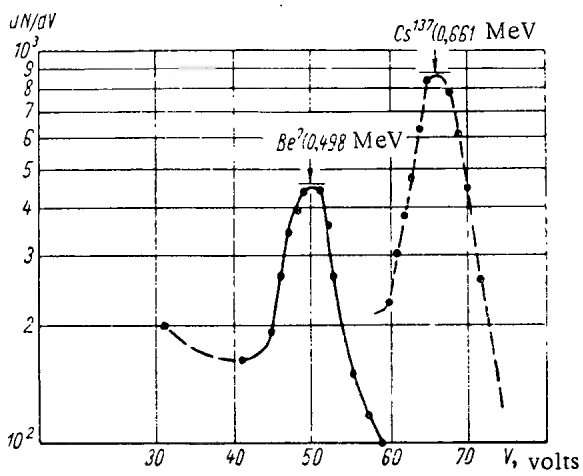

Gamma spectrum of the isolated Be^7.

After the target had been covered and its contents had been dissolved, it was decided to isolate the Be^7 on a nonisomorphic iron hydroxide carrier. For this purpose we poured the hydrochloric solution of the contents of the target into a centrifuge test tube, added a solution containing 100 mg of iron, and precipitated the iron hydroxide by means of ammonia containing no CO_3^{2-}. Under these conditions, the copper and the zinc extracted from the target backing remained in the solution. The precipitate in the cold state was separated from the solution by centrifuging and was washed three times with cold water. The wash water and the mother liquor were analyzed for Be^7. As the analysis showed, all of the Be^7 was sorbed onto the iron hydroxide. After the precipitate was dissolved in 25 ml of 8N HCl, we added 1-2 ml of 4N KCNS and extracted the iron with isopropyl ether, repeating the process eight times until all the iron was removed, as indicated by the absence of any coloring when a new batch of KCNS was added. The isotope Be^7, under these conditions, remained in the aqueous phase; an analysis of the aqueous phase for Fe^{55} and Fe^{59} yielded negative results.

In addition to Be^7 the aqueous phase contained a small amount of tungsten which had gone into solution from the foil covering the target. After evaporating this phase until a dry compound was obtained the CNS^- group was broken up, the residue was dissolved in water slightly acidified with nitric acid, and concentrated HNO_3 was used to precipitate the tungsten in the form of tungstic acid. The precipitate was separated by cenetrifuging, washed with dilute HNO_3 and checked for its Be^7 content, which was found to be very small. We then measured the spectrum of the gamma rays emitted by the solution containing Be^7 (see figure). As the analysis showed, no radioactive admixtures were found in either the low-energy or the high-energy region. Consequently, the radioactive Be^7 obtained may be regarded as radiochemically pure.

The resulting solution was evaporated in a platinum cup until a dry compound was obtained, and the latter was heated so as to remove the NO_3^- after which the residue was dissolved in a minimum amount of water, heating constantly, the K^+ was precipitated with 1-2 ml of concentrated $HClO_4$, and the mixture was left at a low temperature for 24 h. The solution was then poured off, and the precipitate was washed twice with ice-cold 0.05 M $HClO_4$; the Be^7 in the $HClO_4$ solution was diluted to a specified volume ($[H^+]$ = 0.1 M/liter), an aliquot part of the solution was taken, and the specific activity of the resulting radioactive isotope (in pulses/min · ml) was found.

In the present study we also calculated the Be^7 yield obtained by deuteron irradiation of a natural mixture of lithium isotopes in the form of Li_2O, produced by burning lithium in air. The absolute activity of the resulting Be^7 was found by comparing it with the activity of a Cs^{137} specimen determined by the beta-gamma coincenence method. It was assumed that the gamma-ray efficiency of the counter in the 0.48-0.66 MeV energy range was nearly constant. A value of (1.2 ± 0.2) μCi μA · hour was found by this method for the Be^7 yield when a thick Li_2O layer is irradiated with 13.4-MeV deuterons.

LITERATURE CITED

1. W. Garisson and J. Hamilton, Chem. Rev., 49, 237 (1951).
2. H. Heymond, W. Garisson, and J. Hamilton, J. Chem. Phys., 18, 1685 (1950).
3. R. Bolomey and L. Wish, J. Amer. Chem. Soc., 72, 4483 (1950).
4. N. P. Rudenko and A. I. Savost'yanov, Radiokhimiya, 1, 691 (1959).

All abbreviations of periodicals in the above bibliography are letter-by-letter transliterations of the abbreviations as given in the original Russian journal. *Some or all of this periodical literature may well be available in English translation.* A complete list of the cover-to-cover English translations appears at the back of this issue.

THE SOLUBILITY OF URANIUM TETRAFLUORIDE IN AQUEOUS SOLUTIONS OF ACIDS

Yu. A. Luk'yanychev and N. S. Nikolaev

Translated from Atomnaya Énergiya, Vol. 15, No. 5,
pp. 423-425, November, 1963
Original article submitted November 5, 1962

The solubility of uranium tetrafluoride in water has been determined a number of times, but the results obtained have been contradictory. The data of the various author indicate the following values for solubility at 25°C (in grams of UF_4 per liter): 0.04 [1], 0.053 [2], 0.6 [3], and 0.10 [4]. Some fragmentary information is found in the literature. Thus, for example, it is stated that in 2 N H_2SO_4 the solubility is 2.9 g/liter. In more concentrated H_2SO_4 it is lower than in the dilute acid. The dissolution mechanism is given by $UF_4 + 2H_2SO_4 = H_2[U(SO_4)_2F_2] + 2HF$. The solubility of UF_4 in 1 M and 12 M solutions of HCl [5] is equal to 1.4 g/liter and 32.5 g/liter, respectively.

In the present study, in order to explain the dissolution mechanism and also to determine the structure of the compounds in the solution, we investigated the solubility of a stable crystal hydrate of uranium tetrafluoride, $UF_4 \cdot 2.5\ H_2O$, in water and in solutions of chloric, hydrochloric, and sulfuric acids at 0 (0 ± 0.5), 25 (25 ± 0.1) and 50°C.

The crystal hydrate of uranium tetrafluoride was synthesized by a method described earlier [6]. In order to obtain acids of the required concentration, distilled acids were diluted with distilled water having a pH of 6.4-6.8.

In order to prevent acidification of the tetravalent uranium into the hexavalent state, the experiments were set up as follows: we placed an acid solution of a given concentration in a Teflon vessel, passed purified hydrogen through it for 1 h in order to force out any oxygen dissolved out of the air, and then added uranium tetrafluoride to the solution. The solution was stirred continuously for 5-6 h in a hydrogen atmosphere. When equilibrium had been reached, samples of the solution were taken, the solid phase was filtered out, and the samples were analyzed. The uranium content of the solution was determined vanadatometrically with phenyl anthranilic acid [7]. The concentration of the acid was found by direct titration with an alkali. For the solutions of UF_4 in chloric acid the pH value was also found, by means of a hydrogen electrode. A saturated calomel electrode was used as the auxiliary electrode. The following results were found:

1. Solubility of Uranium Tetrafluoride in Water, %

0°C	25°C
0.0023	0.0044
0.0027	0.0054
0.0025	0.0051
0.0025	0.0053
–	0.0046
	0.0053
Average	
0.0025 ± 0.002% or $(8.0 \pm 0.8) \cdot 10^{-5}$ M	0.0050 ± 0.0005% or $(1.6 \pm 0.1) \cdot 10^{-4}$ M

2. Solubility of Uranium Tetrafluoride in Sulfuric and Hydrochloric Acids

Concentration of H_2SO_4, M	Solubility of UF_4, g/liter	Concentration of HCl, M	Solubility of UF_4, g/liter
	at 25°C		
0.05	0.41	0.16	0.81
0.20	1.44	0.68	1.26
0.51	2.32	1.64	1.56
1.02	4.46	2.68	2.13
2.55	4.61	5.43	2.28
4.07	2.83	7.68	2.58
4.60	2.55	12.34	6.85
5.10	1.31	–	–
6.12	1.00	–	–
	at 50°C		
0.05	0.42	1.42	1.93
0.20	1.66	4.27	3.62
0.51	3.79	5.76	4.04
1.02	4.90	6.50	4.81
2.55	5.00	9.90	7.40
4.07	5.05	–	–
4.60	3.06	–	–
5.10	2.60	–	–

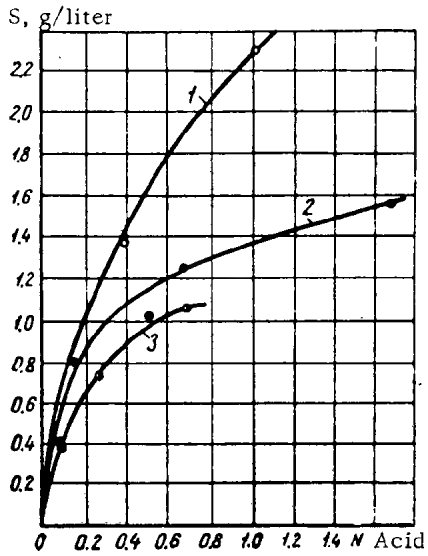

Solubility curves of UF_4 in acids at 25°C: 1) H_2SO_4; 2) HCl; 3) $HClO_4$.

The value of the solubility in water at 0°C is different from the value found earlier [1]. The data obtained at 25°C agree with the value found in [2] under similar conditions.

The solubility of $UF_4 \cdot 2.5\ H_2O$ in acids increases with increased acid concentration, but in sulfuric acid when the concentration increases beyond 3-4 M, the solubility of UF_4 decreases, probably because the complexing of uranium with the HSO_4 ion is less than with the SO_4^{2-} ion.

The process of dissolution of $UF_4 \cdot 2.5\ H_2O$ in chloric acid, as a result of the low complexing capacity of the ClO_4^- ion is caused by hydrogen ions and may be described, in the range of acid concentrations we studied, by the equation

$$UF_4 + 3H^+ \rightleftarrows UF^{3+} + 3HF.$$

The equilibrium constant of this reaction is $4.0 \cdot 10^{-8}$. The calculation method is given in [8].

Examination of the initial portions of the solubility curves (see figure) shows that up to acid concentrations of 0.1-0.2 M the curves look alike, and they begin to differ at higher concentrations. It may be assumed that in dilute acids uranium tetrafluoride is dissolved by the action of the hydrogen ions and subsequently the UF^{3+} ion radical is bound to the acid anion. As the acid concentrations increase, the curves diverge more and more. This divergence is attributable to the considerably higher dissolving action of hydrochloric and sulfuric acids in comparison with that of chloric acid, which indicates the complexing capacity of the Cl^- and SO_4^{2-} ions. The arrangement of the acids in order of increasing solubility with increasing acid concentration reflects the order of the corresponding anions as to the degree of complexing with a tetravalent atom uranium ion:

$$ClO_4^- < Cl^- < SO^{2-}.$$

TABLE 1. Calculated SP Values for UF_4

$HClO_4$ concentration, M	Found experimentally		Calculated concentrations, g-ions/liter			SP = $[U^{4+}]\cdot[F^-]^4$
	solubility of UF_4, g/liter	pH	$[U^{4+}]$	$[H^+]$	$[F^-]$	
0.09	0.421	0.93	$8.7\cdot10^{-4}$	$1.17\cdot10^{-1}$	$3.11\cdot10^{-5}$	$8.1\cdot10^{-22}$
0.27	0.74	0.59	$1.67\cdot10^{-3}$	$2.57\cdot10^{-1}$	$2.52\cdot10^{-5}$	$6.7\cdot10^{-22}$
0.52	1.01	0.40	$2.34\cdot10^{-3}$	$3.96\cdot10^{-1}$	$2.22\cdot10^{-5}$	$5.6\cdot10^{-22}$
0.69	1.04	—	$2.72\cdot10^{-3}$	$6.9\cdot10^{-1}$	$1.32\cdot10^{-5}$	$0.83\cdot10^{-22}$

TABLE 2. Solubility in Water and SP Values for a Number of Actinide Tetrafluorides

Fluorides	Solubility in water at 25°C	SP
ThF_4	0.17mg/liter [10]	$1.2\cdot10^{-29}$[10] $1.84\cdot10^{-24}$[11] $4,5\cdot10^{-26}$[8]
UF_4	0.050 g/liter [Data of the present study]	$5.3\cdot10^{22}$ [Data of the present study]
PuF_4	0.053 [2] 0.060 g/liter [12]	$6\cdot10^{-20}$[12]

From the resulting data, we can calculate the solubility product (SP) of uranium tetrafluoride. Because of the low complexing capacity of the ClO_4^- ion and because reliable data are available on the hydrogen ion concentration measured directly, the SP value was calculated only for solubility in chloric acid.

The U^{4+} concentration was calculated by the formula found earlier [8]:

$$[U^{4+}]=\frac{S}{\left(1+\frac{[F^-]}{K_{UF^{3+}}}+\ldots+\frac{[F^-]^i}{K_{iUF_i^{4-i}}}+\frac{[OH^-]}{K_{UOH^{3+}}}+\ldots+\frac{[OH^-]^q}{K_{qU^{-}(OH)_q^{4-q}}}\right)},$$

where the K's are the instability constants of the complex fluoride and hydroxo complex ions. The values of $[U^{4+}]$ calculated on the basis of the first constants for UF^{3+} and UOH^{3+} ions are shown in Table 1.

The instability constant used for the UF^{3+} ions was $6\cdot10^{-5}$ [9], and for the UOH^{3+} we used the value $4.4\cdot10^{-12}$ obtained in a solution containing fluorine ions [6]. The average SP value calculated on the basis of the instability constants of the UF^{3+} and UOH^{3+} ions was $5.3\cdot10^{-22}$.

The solubility of uranium tetrafluoride in water and the calculated SP value are shown in Table 2, together with a number of similar values for actinide tetrafluorides.

As can be seen from the table, the solubility of thorium tetrafluoride and plutonium tetrafluoride increases, even if only slightly.

LITERATURE CITED

1. J. Katz and E. Rabinowitch, Chemistry of Uranium [Russian translation], Vol. 1, Izd-vo inostr. lit., Moscow (1954), p. 303.
2. V. G. Khlopin and M. L. Yashchenko, Izv. AN SSSR, Ser. khim. 2, 87 (1942).
3. Report (B) LRG-27 (1943) (see [1]).
4. Allen, Petrow and Whitman, In "Proceedings of the Second International Conference on the Peaceful Uses of Atomic Energy." Selected Reports of Non-Soviet Scientists, Vol. 7, Atomizdat, Moscow (1959), p. 461.
5. N. P. Galkin et al., Chemistry and Technology of Fluoride Compounds of Uranium [in Russian], Moscow (1961).
6. N. S. Nikolaev and Yu. A. Luk'yanychev, Atomnaya Énergiya, 11, 67 (1961).
7. P. N. Palei, "Investigations in the Field of Geology, Chemistry, and Metallurgy." Report of the Soviet Delegation to the International Conference on the Peaceful Uses of Atomic Energy (Geneva Conference, 1955), Izd-vo AN SSSR, Moscow (1955), p. 21.

8. N. S. Nikolaev and Yu. A. Luk'yanychev, Atomnaya Énergiya, 12, 334 (1962).
9. N. S. Nikolaev and Yu. A. Luk'yanychev, Atomnaya Énergiya, 13, 179 (1962).
10. Vl. I. Spitsyn, Zh. rus. fiz-khim. o-va, 49, 357 (1917).
11. I. V. Tananaev and A. D. Vinogradova, Zh. neorganich. khim. 2, 2455 (1957).
12. C. Mandleberg, K. Francis, and R. Smith, J. Chem. Soc., 2464 (1961).

All abbreviations of periodicals in the above bibliography are letter-by-letter transliterations of the abbreviations as given in the original Russian journal. *Some or all of this periodical literature may well be available in English translation.* A complete list of the cover-to-cover English translations appears at the back of this issue.

AN APPARATUS FOR DETERMINING THE SOLUBILITY OF RADIOACTIVE SUBSTANCES AT ELEVATED TEMPERATURES AND PRESSURES

V. V. Ivanenko, G. N. Kolodin, B. N. Melent'ev, and L. A. Pamfilova

Translated from Atomnaya Énergiya, Vol. 15, No. 5, pp. 426-428, November, 1963
Original article submitted February 22, 1963

Considerable experimental difficulties are involved in determining the solubility at elevated temperatures and pressures of substances that are not readily soluble. The process of taking a sample at temperatures above the boiling point of the solution is extremely complicated and introduces distortions into the system under investigation. If, on the other hand, the sample is taken after the solution has been cooled, then the result of the determination may be incorrect, since the solubility depends on temperature and some quantity of the substance may have recipiated out of the solution.

Fig. 1. Quartz ampoule with filters.

In view of the need for sufficiently sensitive analytical methods when the substances have low solubility and of the fact that a sample taken at an elevated temperature cannot be very large in volume, the most effective method for studying the solubility is the radioactive-indicator method.

Ya. I. Olshanskii has devised an apparatus for determining the solubility of synthetic radioactive substances that are not readily soluble; with this apparatus no sample need be extracted during the experimental process. The solubility is determined by measuring the radioactivity of the solution, that is, by using the highly sensitive method of counting radioactivity.

The main part of the apparatus is a quartz ampoule in the shape of an elongated closed loop (Fig. 1). This shape makes it possible to stir the solution in the ampoule by periodically rotating the ampoule through 90° (in the plane of the loop) and returning it to the vertical position. The ampoule is equipped with two quartz filters 1, between which the substance under investigation 2, is enclosed, and with two nozzles: a for the insertion of the solid and b for the introduction of the solution. After the ampoule is filled, the nozzles are sealed. When the ampoule is rotated into a horizontal position, part of the solution flows from the right-hand side of the ampoule into the left-hand side. After the ampoule is returned to the vertical position, the solution level in the left-hand side rises by 8-10 cm above that in the right, which creates a pressure difference resulting in the filtration of the solution.* Thus, the solution circulates in the ampoule. In our experiments we used quartz ampoules that could withstand temperatures up to 200°C and solutions with pH $\leq$ 8. It is perfectly possible to use ampoules made of niobium, titanium or other materials capable of withstanding higher pressures and more alkaline solutions.

After being filled, the ampoule is held in a lead bushing and is inserted, in a rigidly fixed position, into a heater. The bushing is made of lead in order to protect the counter from the initial radioactive substance.

The heater consists of a copper tube equipped with a nichrome winding and asbestos insulation and is covered by a jacket cooled by water circulating through copper tubes soldered to the outside.

* The difference between the levels depends on the degree to which the ampoule is filled with the solution.

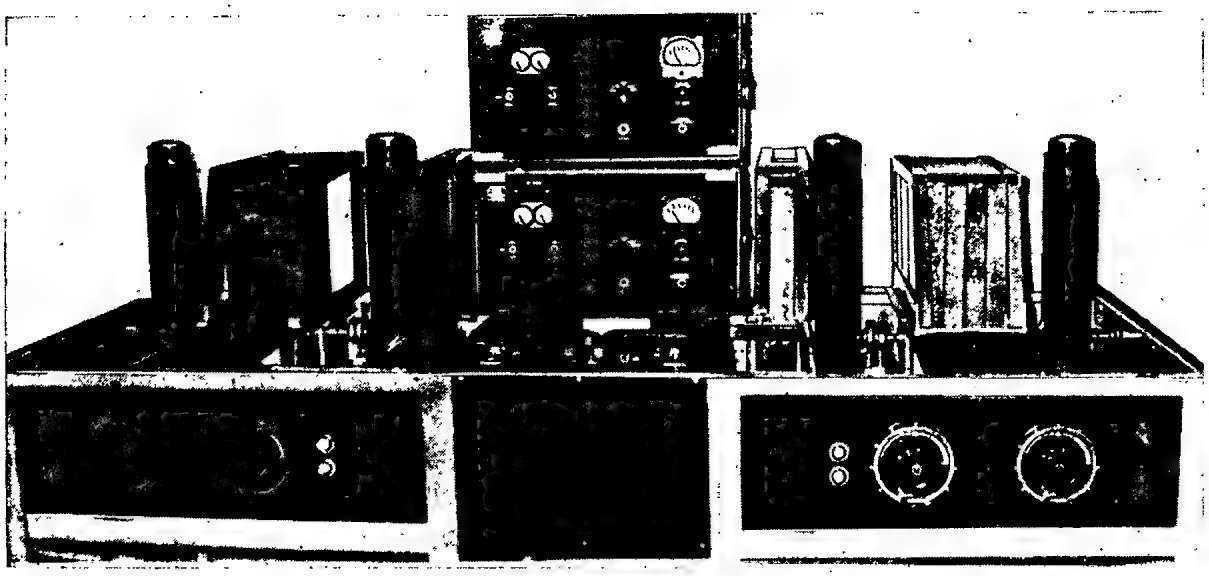

Fig. 2. Overall view of apparatus for studying the solubility of radioactive substances.

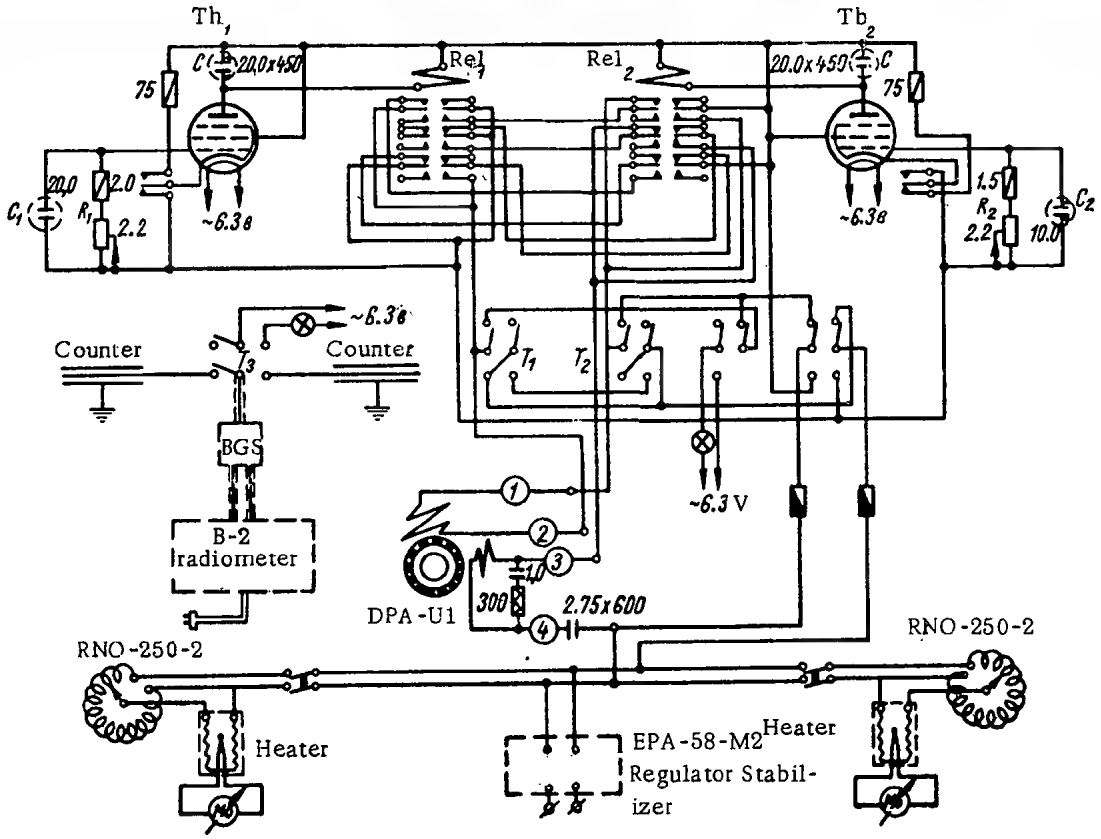

Fig. 3. Schematic of the electrical part of the apparatus.

The radioactivity of the solution is measured by a counter which is covered by a lead shield in order to reduce the external background. The solution temperature is measured by a chromel-aluminum thermocouple held inside the heater, togeteher with the ampoule, in such a way that the junction of the thermocouple is next to the filters.

The apparatus for studying the solubility has four heaters (Fig. 2) separated by blocks of lead shielding 120 mm thick. A stabilized voltage is supplied to the heaters through RNO-250-2 autotransformers which regulate the temperature. The temperature is recorded by MPP-254 millivoltmeters. The heaters are rotated two DPA-U1 motors,

which are periodically turned on by a time relay. The relay is so regulated that the heaters, together with the ampoules, are in a vertical position for five minutes and in a horizontal position for one minute.

Figure 3 shows an electrical schematic of a part of the apparatus containing two heaters. The time relay is connected to two 6P3C tubes (Tb_1 and Tb_2) and two relays (Rel_1 and Rel_2), with an actuating current of 10-20 ml and a coil resistance of 3600-4000 Ω with two rows of contacts (five contacts in each row).

The gap between the contacts is 3 mm. The relays are supplied from a 220 volt a-c source. Capacitors (C) are connected in parallel with the windings to smooth out the pulsations in the current. Circuits R_1C_1 and R_2C_2 control the times for the vertical and horizontal positions. In case of equipment failure the time relay is automatically disconnected. The motors for rotating the heaters are turned on by tumbler switches Tm_1 and Tm_2. Tumbler switch Tm_3 is designed to switch the B-2 radiometer from one counter to another.

Using the above-described apparatus, we made several series of experiments to determine the solubility of Ag_2S [1] and Fe_2O_3 [2] in aqueous solutions of varying acidity and at temperatures ranging up to 200°C.

With this apparatus the solubility can be determined by a completely automated process. It is assumed that automatic recorders will be used to record the radioactivity of the solution and automatic thermoregulators will be used for maintaining constant temperature.

LITERATURE CITED

1. Ya. I. Ol'shanskii, V. V. Ivanenko, and A. V. Khromov, Dokl. AN SSSR, No. 2, 124 (1959).
2. V. V. Ivanenko et al., In "Proceedings of the Sixth Conference on Experimental and Engineering Mineralogy and Petrography" [in Russian], Izd-vo AN SSSR, Moscow (1962), p. 96.

THE PREPARATION OF CERTAIN SULFIDES OF THORIUM BY THE INTERACTION OF ThO_2 WITH HYDROGEN SULFIDE

G. V. Samsonov and G. N. Dubrovskaya

Translated from Atomnaya Énergiya, Vol. 15, No. 5,
pp. 428-430, November, 1963
Original article submitted January 17, 1963

As was shown in [1], the higher sulfides of thorium, beginning with Th_2S_3, are semiconductors, and this fact, combined with their high thermal stability and high melting point (2200-2500°C), opens possibilities for their use in semiconductor engineering. In addition, the reaction between ThO_2 and hydrogen sulfide is of interest for the study of reactor materials.

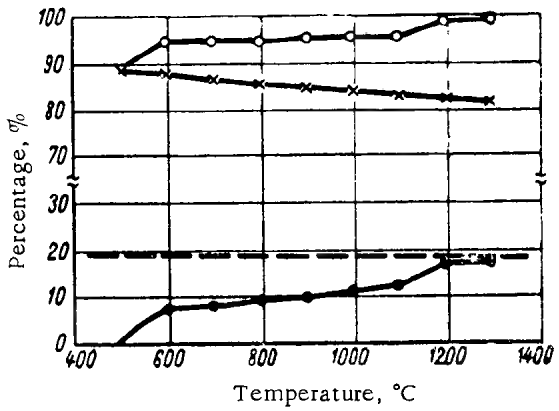

Fig. 1. Chemical composition of the products of the reaction between thorium oxide and hydrogen sulfide (in the absence of carbon) as a function of temperature. ●) S_t; ×) Th_t; ○) $Th_t + S_t$; – – –) S_t calculated for the compound $ThS_{1.7}$.

TABLE 1. Chemical and Phase Composition of the Products Obtained from the Reaction between ThO_2 and H_2S in the Absence of Carbon

Temp. °C	Chemical composition, %					Phase composition
	Th_t	S_t	S_f	$Th_t + S_t$	O (obtained by difference)	
500	88	0	0	88	12	ThO_2
600	87.5	7.2	0.2	94.7	5.3	ThO_2+ThOS
700	86.6	7.8	0.2	94.4	5.6	ThO_2+ThOS
800	85.1	9.3	0.2	94.4	5.6	ThO_2+ThOS
900	84.7	9.9	0.1	94.6	5.4	ThOS
1000	83.2	11.5	0.1	94.7	5.3	ThOS
1100	82.6	12.5	0.1	95.1	4.9	ThOS
1200	81.5	17.7	0.1	99.2	0.8	$ThS_{1.7}$
1300	81.3	17.9	0.1	99.2	0.8	$ThS_{1.7}$

No diagram of the thorium-sulfur system has been worked out, so that information on the existence of thorium-sulfur compounds is available only in preparatory studies according to which [2] the sulfides ThS, Th_2S_3, ThS_2, and Th_4S_7 exist.

The sulfides ThS and Th_2S_3 can be synthesized from metallic thorium and sulfur [3], and ThS_2 is obtained from the action of dry hydrogen sulfide on metallic thorium [4], by the treatment of ThO_2 with carbon disulfide and hydrogen [5], or by the action of hydrogen sulfide on thorium chloride [6] or its hydride [7]. The sulfide Th_4S is formed by the thermal dissociation of ThS_2 [2]. Methods of preparing the sulfides of thorium are described in [8]. All of these methods for the preparation of sulfides are concerned with the use of metallic thorium or other products which must be prepared specially from thorium oxide; moreover, the use of these methods requires special apparatus. Only one patent [9] recommends the preparation of ThS_2 by heating thorium oxide in the presence of carbon in a current of H_2S, while [10] gives preliminary data on the reaction between thorium oxide and hydrogen sulfide.

The present study investigates the reaction between thorium oxide and hydrogen sulfide in order to determine the possibility of preparing thorium sulfides from the simplest raw materials and with simple equipment.

The study used 99.8% thorium oxide, one-gram specimens of which were placed in porcelain boats in a quartz tube and were heated in a current of hydrogen sulfide which was dried by passing it through a column containing silica gel and phosphorus pentoxide. The rate of the hydrogen sulfide current was monitored with a flow meter and was about 0.2 liter/min. The products obtained by sulfidation was proved in a current of hydrogen sulfide, thoroughly

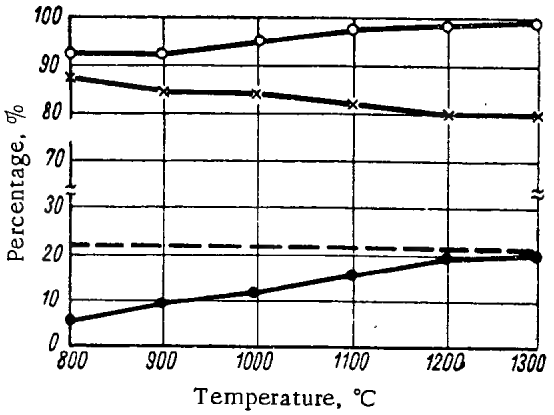

Fig. 2. Chemical composition of products obtained from the interaction of thorium oxide and hydrogen sulfide (in graphite boats), as a function of temperature over a one-hour period. (The notation is the same as in Fig. 1).

TABLE 2. Thorium Content of the Products of the Reaction between ThO_2 and H_2S in the Absence of Carbon, as a Function of Sulfidation Time

Sulfidation time, hours	Th_t, %		
	Temperature, °C		
	800	1000	1200
2	85.1	83.3	81.3
4	85.0	82.8	81.2
6	84.2	82.5	81.0

ground, removed, and tested for their total thorium content (Th_t), total sulfur content (S_t), and free sulfur content (S_f). To determine the thorium, the sulfidation products were oxidized to ThO_2 by calcining at 1000-1100°C, periodically monitoring to check the thorium content by precipitating with oxalic acid after dissolving in aqua region. To determine the total sulfur content, a 0.15-0.2 g specimen of the sulfidation product was ignited at 1200-1300°C in a 0.5 liter/min current of oxygen [11]. The combustion products were passed through a 3% H_2O_2 solution. The resulting H_2SO_4 was titrated with a 0.1 N solution of NaOH, using a mixture of methyl red and methylene blue as the indicator. The resulting method for determining the free sulfur content is based on the formation of the hyposulfate when the specimen is boiled in the presence of sodium sulfite [12].

TABLE 3. Chemical and Phase Composition of the Products obtained from the Interaction of ThO_2 and H_2S in the Presence of Carbon, for Various Temperatures and Reaction Times*

Temperature °C	Sulfidation time, hours	Chemical composition, %					Phase composition
		Th_t	S_t	S_f	$Th_t + S_t + C_t$	O (obtained by difference)	
800	1	86.8	5.02	0.20	91.92	8.17	ThO_2+ThOS
800	2	86.1	8.45	0.10	94.65	5.35	$ThS_{1.6}$+ThOS
900	1	83.3	9.65	0.15	93.05	6.95	$ThS_{1.5}$+ThOS
900	2	83.2	9.86	0.10	93.16	6.84	$ThS_{1.7}$+ThOS
1000	1	83.1	11.5	0.10	94.7	5.3	$ThS_{1.7}$+ThOS
1000	2	83.2	11.5	0.10	94.8	5.2	$ThS_{1.8}$+ThOS
1100	1	81.6	15.5	0.10	97.2	2.8	$ThS_{1.8}$+ThOS
1100	2	81.05	15.8	0.10	96.95	3.05	$ThS_{1.9}$+ThOS
1200	1	79.2	19.2	0.10	98.5	1.5	$ThS_{1.9}$+ThOS
1200	2	79.0	19.5	0.10	98.6	1.4	$ThS_{1.98}$
1300	1	79.11	19.9	0.10	99.11	0.89	$ThS_{1.98}$
1300	2	79.11	20.5	0.10	99.81	0.29	$ThS_{2.05}$

* The value of C_t was 0.1% for all products.

The results obtained by studying the reaction between ThO_2 and H_2S over a one-hour period are shown in Table 1 and Fig. 1. At 600°C the sulfur content increases rather sharply, after which it gradually approaches the calculated $ThS_{1.7}$ content. In the 900-1100°C range the oxysulfide ThOS is formed. It is only between 1200 and 1300°C that the oxygen is almost completely removed and the sulfide $ThS_{1.7}$ is formed. It has been found by x-ray analysis that the resulting product* has a hexagonal structure, the dimensions of an elementary cell being a = 11.045 kX;+ c = 3.984 kX, which is close to the tabulated data for $ThS_{1.7}$ (a = 11.041 kX, c = 3.983 kX. As can be seen from

* The x-ray investigation was made by O. P. Khorpyakov.

+1.00202 kX = 1 angstrom.

TABLE 4. Cell Periods and Density of Thorium Disulfide

Property	Experimental data	Data of [5]
Cell periods (angstroms)		
a	4.267	4.268
b	7.262	7.263
c	8.617	8.617
Calculated density, g/cm^3	7.36	7.36
Pycnometric density, g/cm^3	7.31	–

Table 2, the increased time for the sulfidation of ThO_2 by hydrogen sulfide has practically no effect on the composition of the sulfidation products. It may be assumed that the best process for obtaining $ThS_{1.7}$ is to treat the thorium dioxide with H_2S for 1-2 h. For large quantities of the reactants the sulfidation time is increased accordingly, but thorium sulfides can be produced more efficiently by this method if a rotary furnace is used. The product obtained by this process has a microhardness of 433 ± 30 kg/mm^2 (with a 10 g load), and its electrical resistivity is $3.6\text{-}7 \cdot 10^7$ ohm-cm, which is larger by two orders of magnitude than the values given in [1].

The following series of experiments was conducted under similar conditions except that instead of porcelain boats we used graphite boats with 2 g of ThO_2. The results, shown in Table 3 and Fig. 2, indicate that in the absence of carbon the reaction takes place in several stages. At the beginning, at 800-1100°C, ThOS, the yellow oxysulfide of thorium, is formed; after this the oxysulfide formation is accompanied by the formation of sulfidation products with a sulfur content gradually approaching the composition of ThS_2; finally, at 1300°C, we obtain almost pure thorium disulfide containing only a small amount of oxygen as an impurity. This product is brown in color. In order to improve the quality of the product further we used a multi-stage sulfidation process: one hour at 1000°C, one hour at 1200°C, and ten minutes at 1300°C. The resulting product was dark brown and contained 78.5% Th_t and 21.0-21.2% S_t, which is closer to composition of ThS_2, calculated as 78.5% Th and 21.5 S.

X-ray analysis showed that this product has the rhombic lattice characteristic of thorium disulfide, with elementary-cell periods and density close to those given in [13] (Table 4).

Thus, when thorium oxide reacts with hydrogen sulfide, the sulfide phases $ThS_{1.7}$ and ThS_2 are formed. These products may be used as the raw material for the preparation of lower sulfide phases of thorium. An important feature of the proposed method is the preparation of large quantities of thorium sulfides using simple equipment.

LITERATURE CITED

1. F. McTaggert, Austral. J. Chemistry, 11, 471 (1958).
2. E. Strotzer and M. Zumbusch, Z. anorgan. Chem., 247, 415 (1941).
3. G. V. Samsonov and N. M. Popova, Zh. obshch. khim., 27, 3 (1957).
4. H. Moissan and A. Etard, Comptes Rendus, 122, 573 (1896).
5. G. Seaborg and D. Katz, Actinides [Russian translation], Izd-vo inostr. lit., Moscow (1955).
6. A. Duboin, Comptes Rendus, 146, 815 (1908).
7. E. Eastman et al., J. Amer. Chem. Soc., 72, 4019 (1950).
8. G. V. Samsonov and S. V. Radzikovskaya, Usp. khim., 30, 60 (1961).
9. United States Patent No. 791466 (1949).
10. G. V. Samsonov and G. N. Dubrovskaya, Zh. prikl. khim., 36, 1623 (1963).
11. I. E. Yatsyk and L. I. Tokarev, Collection of the Scientific Proceedings of the All-Union Scientific Research Institute for the Mining and Metallurgy of Nonferrous Metals [in Russian], No. 6, 472 (1960).
12. A. I. Ponomarev, Methods for the Chemical Analysis of Minerals and Rocks [in Russian], Izd-vo AN SSSR, Moscow (1951).
13. W. Zachariasen, Acta Crystallogr., 2, 888 (1949).

ESTIMATION OF THE DOSE OF NEUTRON IRRADIATION CAPABLE OF CHANGING THE MECHANICAL PROPERTIES OF PURE METALS

V. K. Adamovich

Translated from Atomnaya Énergiya, Vol. 15, No. 5,
pp. 430-432, November, 1963
Original article submitted November 22, 1962

Up to the present time, a large number of studies (for example, [1, 2]) have been devoted to the effect of neutron irradiation on the properties of structural materials.

The quantity generally used to characterize the degree of irradiation of metals is a flux of fast neutrons with an energy in excess of some specified value (for example, 1 MeV). However, as has already been remarked in [3, 4], the fast-neutron flux cannot completely characterize the extent of the damage. For this reason, the use of a fast-neutron flux as a characteristic of irradiation conditions produces serious difficulties in the comparison of experiments in which the material has been irradiated with neutrons of different energy spectra. Even greater difficulties are encountered in the design of reactors when data obtained from experiments on irradiation of materials are used [3]. The procedure by which the neutron irradiation dose is calculated is very important in this connection.

In [3-5] it was supposed that such a dose should be represented by an amount proportional to the total number of point defects (vacancies and interstitials) formed by the neutrons when they pass through a substance.

However, the total number of point defects produced by neutrons is not adequate to indicate the extent to which the mechanical properties of a material have been changed by the irradiation, since these properties are not greatly affected by point defects in the absence of complex defects. It is true that point defects make the principal contribution to the change in such properties as electrical resistance, modulus of elasticity, etc. But even in this case the value of the neutron dose, proposed in [3-5], cannot be used to characterize the irradiation, since in calculating it the thermal and radiation annealing of point defects is left out of consideration.

In the present study we have attempted to calculate the effectiveness of the dose of neutron irradiation capable of changing the mechanical properties of metals. When a fast neutron collides with an atom, it may knock the atom out of its normal position in the crystal lattice and give it a higher energy. Thereafter the atom initially knocked out of place will move through the lattice and displace other atoms. In [6, 7] it was shown that at the end of the path of the atom initially knocked out of place there will be formed a multiple vacancy surrounded by a cloud of displaced atoms, and it is assumed that the displaced atoms regress to the polyvacancy, producing a displacement peak which constitutes a complex defect of the crystal lattice. Seeger [8] believes that in metals with a close-packed structure in which the dynamic crowdions form a stable configuration, the interstitials travel far away from the polyvacancy and do not regress but accumulate at different points or disappear through various sinks. In this case the polyvacancy is thereafter converted into a more stable cluster of vacancies. Thus, irradiation produces chiefly two kinds of defects: point defects (vacancies and interstitials) and stationary complex defects (displacement peaks, clusters of vacancies and of interstitials). The two indicated mechanisms of radiation damage enable us to find the correct explanation for the experimentally observed effects of neutron irradiation [7-9]. The picture found by direct observation of neutron-produced defects under the electron microscope [10-13] is also in good agreement with the ideas developed by Brinkman and Seeger. We shall find the effectiveness of a dose of neutron irradiation characterizing the change in the mechanical properties of metals (yield point, strength, elongation and area-reduction characteristics, toughness, critical temperature for brittleness). It is known [14] that the yield point of a polycrystalline material is found from the following formula:

$$\sigma_T = \sigma_i + K_y d^{-1/2}, \tag{1}$$

where σ_i is the frictional stress of the lattice produced by various defects which hinder the motion of dislocations in the slip plane; K_y is a coefficient characterizing the degree of spinning of the dislocations; d is the grain size.

The complex defects produced by irradiation change the frictional stress. The latter will depend only on the number of these defects [15], but the point defects will affect the degree of pinning of the dislocations. Experiments show that the change in the yield point as a result of irradiation is chiefly related to the change in the frictional stress σ_i. Thus, it has been found [16] that in copper only 10% of the total increment of the yield point can be attributed to a change in the pinning coefficient K_y, while in steels the coefficient K_y, in general, remains unchanged after irradiation [14].

Thus, the total number of complex defects produced by irradiation is a quantity which defines the change in frictional stress (and consequently the change in the yield point and other mechanical characteristics of the material). This is the quantity that should be used as a dose value in experiments investigating the effect of neutron irradiation on the change in the mechanical properties of metals.

It was pointed out earlier that in the model proposed by Seeger, in addition to the accumulation of vacancies, there are also accumulations of interstitials; however, the latter are of secondary importance in neutron irradiation effects [17]. According to Brinkman [6-7], it can be shown that both the numbers of displacement peaks and the number of vacancy accumulations produced by fast neutrons will be equal to the number of originally knocked-out atoms with energy above some threshold energy E_{th}. For displacement peaks E_{th} = 400 eV [7]; for an accumulation of vacancies E_{th} should be taken equal to $6E_d$ (here E_d is the energy required for the displacement of an atom). This follows from the fact that the atoms originally knocked out do not increase the number of vacancy accumulations if they produce mobile defects (that is, single or double vacancies), which will disappear in various sinks. On the other hand, if the atom has an energy of less than $6E_d$ it will produce only single and double vacancies. For an irradiation time t, the number of initially knocked-out atoms with energies greater than E_{th} per unit volume of the substance may be found from the formula

$$N = \int_0^t dt \int_{E_{th}/\xi(E)}^{\infty} N_0 \sigma_s(E) \frac{d[nv(E, t)]}{dE} dE, \qquad (2)$$

where N_0 is the number of atoms per unit volume of the substance; $\sigma_s(E)$ is the elastic-cross section of the material under study; $\xi(E)$ is the average logarithmic energy loss per collision; $d[nv(E, t)]/dE$ is the intensity of the neutron flux for a unit interval of neutron energy E.

It should be noted that for large doses of irradiation the number of complex defects will no longer be determined by formula (2), owing to saturation; experiments show [1] that saturation is found when one uses an integral flux of fast neutrons of the order of 10^{20} neutrons/cm^2.

In addition, the determination of the effectiveness of the neutron dose capable of changing the mechanical properties of metals is based chiefly on taking into account the complex defects produced by neutron irradiation, since the point defects have a comparatively slight effect. However, point defects are of great importance in the study of the irradiation-produced changes in such properties such as electrical resistance, modulus of elasticity, internal friction, diffusion, and a number of others. In all these cases, therefore, the number and properties of the point defects must be taken into account in determining the neutron irradiation dose.

In conclusion, the author expresses his gratitude to N. F. Pravdyuk, N. N. Ponomarev-Stepnoi, P. A. Platonov, I. A. Razov, and A. V. Efimov for their interest in the work and their comments.

LITERATURE CITED

1. Effects of Radiation on Materials [Russian translation]. Edited by J. Harwood. L., Sudpromgiz (1961).
2. The Metallurgy of Reactor Materials. Abstracts of the Battelle Institute, Vol. 2. Structural Materials and Technology of Fuel Elements. Transaltion into Russian edited by D. M. Skorov. Gosatomizdat, Moscow (1962).
3. N. N. Ponomarev-Stepnoi, Atomnaya Énergiya, 11, 184 (1961).
4. A. Rossin, Nucl. Sci. and Engrg. 9, 137 (1961).
5. C. Bruch, W. McHugh, and K. Hockenbury, J. Metals, 8, 1362 (1957).
6. J. Brinkman, J. Appl. Phys., 25, 961 (1954).

7. J. Brinkman, Amer. J. Phys., 24, 246 (1956).
8. A. Seeger Proceedings of the Second U. N. International Conference on the Peaceful Uses of Atomic Energy, Vol. 6, Geneva (1958), p. 250.
9. M. Makin and A. Mauthorpe, Acta Metallurgica, 9, 186 (1961).
10. M. Makin, A. Whapham, and F. Minter, Philos. Mag., 7, 285 (1962).
11. A. Grenall, J. Nucl. Mater., 4, 3 (1961).
12. J. Brinkman, A. Sosin, and A. Grenall, J. Nucl. Mater., 4, 332 (1961).
13. A. Hull and J. Modford, Philos. Mag., 6, 535 (1961).
14. M. Makin et al., "Proceedings of the Second International Conference on the Peaceful Uses of Atomic Energy" [Russian translation]. Selected Reports of Non-Soviet Scientists, Vol. 6, Atomizdat, Moscow (1959), p. 411.
15. A. H. Cottrell, Dislocation and Plastic Flow in Crystals [Russian translation]. Metallurgizdat, Moscow (1958), p. 157.
16. M. Makin and S. Mauthorpe, Acta Metallurgica, 9, 86 (1961).
17. M. Makin, A. Whapham, and F. Minter, Philos. Mag., 6, 63 (1961).

All abbreviations of periodicals in the above bibliography are letter-by-letter transliterations of the abbreviations as given in the original Russian journal. *Some or all of this periodical literature may well be available in English translation.* A complete list of the cover-to-cover English translations appears at the back of this issue.

AERIAL SURVEYS OF URANIUM DEPOSITS IN WOODED REGIONS

V. I. Balabanov and A. L. Kovalevskii

Translated from Atomnaya Énergiya, Vol. 15, No. 5,
pp. 432-434, November, 1963
Original article submitted January 23, 1963

Various literature references [1-3] take up the question of absorption of gamma radiation from the soil layer by forest flora. However, the biomass of forest vegetation may itself be the emitting medium. The aerial parts of the plants may contain an appreciable quantity of radium accumulated by absorption from the soil [4]. Anomalous radium contents usually found in the ash of plants growing on uranium deposits and their dispersion halos are $(0.3\text{-}10)\cdot 10^{-10}$ g/g at background (normal) contents outside the deposit boundaries of less than $(3\text{-}10)\cdot 10^{-12}$ g/g [4, 5]. In live plants, the radium content values are: anomalous $(0.3\text{-}20)\cdot 10^{-12}$ g/g, and background (q_{back}) less than $(3\text{-}2)\cdot 10^{-14}$ g/g (at 0.2 to 2.0% ash content of the live plants).

The radium content in ash of branches of such trees as birch, larch, fir, spruce are one and a half to three times that found in the soil, and less (roughly equal to the concentration in the soil) in the ash of branches of pine, cedar, aspen, willow, linden. The wood ash contains one and a half to twice the amount of radium, as a rule, as the ash of branches.

In some cases, appreciable radium anomalies are observed in plants growing on uranium ore bodies when normal uranium and radium contents prevail in the upper soil horizon. Slight radioactive anomalies have been recorded in such cases on the sunlit surface; in some places such anomalies are completely absent (cf. diagram). Accordingly, even in those cases where the upper soil horizons are depleted of radioactive elements, the plants still absorb radium intensively from the lower soil horizons (from a depth of 0.5 to 1.0 meter and lower), and gamma emission from those layers remains virtually unrecorded in an aerial gamma survey.

As calculations have indicated, anomalously high radium concentrations in the aerial parts of trees growing on uranium deposits may set up gamma-radiation anomalies as high as 0.4-0.9 μr/h at an elevation of 40-50 meters above ground level. Calculations followed the procedure described in [3] closely. It was assumed that the forest consists of three "layers:" the crown, the tree trunks, and the dead floor cover (debris on the forest floor). The crowns of the trees form a uniform top layer from H/2 to H (H being the height of the forest). The density of this layer is a function of the density of the forest and of the treetop mass (mass of the crown). A dense stand of tree crowns in a thick forest comes to 0.8-0.9 density [6], so that it is safe to assume this layer to be homogeneous. The tree trunks are visualized as the lower "layer" from 0 to H/2. The thickness of the forest stand is characterized by the specific area S_0 per tree. The forest floor-debris layer may, as we know, contain reserves of from 20 to 150 tons or more per hectare [6].

For our calculations, we took the anomalous areas within which the concentration of radioactive material $q(x, y)$ is unevenly distributed and declines toward the periphery. Proceeding from experience, the ratio q_{max}/q_{back} is assigned the value 20, so that the variation in radium concentration over the area presented by a local area may be expressed by the formula [7]:

$$q(x, y) = q_{max} \exp\left(-3\frac{x^2+y^2}{R^2}\right), \quad (1)$$

where q_{max} is the maximum concentration of radioactive material at the center of that area; R is the radius of the circular area on the boundaries of which $q(x, y) \simeq 0.05\, q_{max}$.

Formula (1) may be simplified [7] as

$$\exp\left(-3\frac{x^2+y^2}{R^2}\right) \approx \exp\left[-6\frac{h}{R^2}(r_1 - h)\right], \quad (2)$$

where r_1 is the path length of gamma photons in air; h is the height above the center of the circular area.

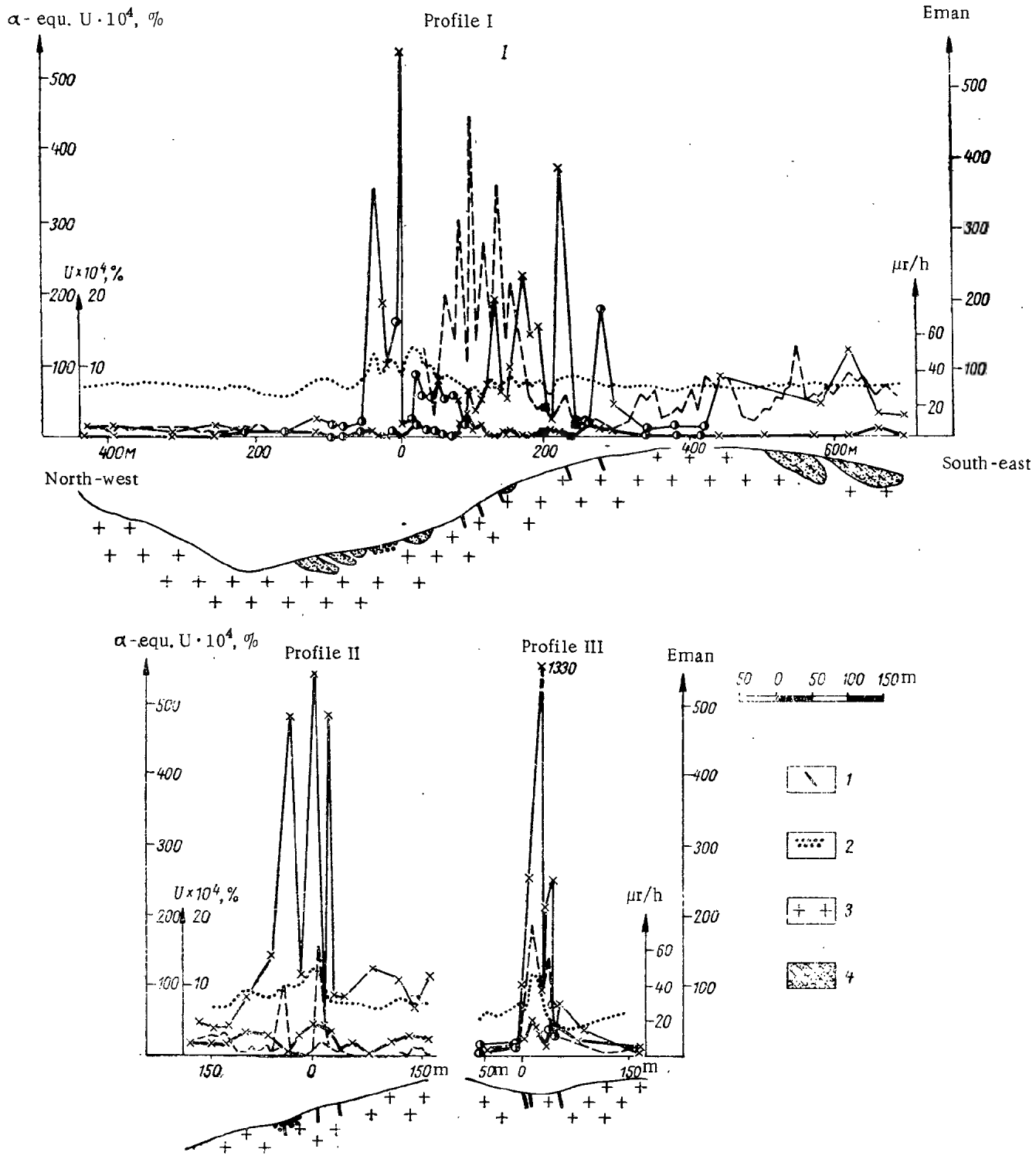

Distribution of radioactivity and of content of radioactive elements according to profiles (cf. A. L. Kovalevskii and M. S. Makarov): 1) Uraniferous ore bodies; 2) ore-body dispersion halos; 3) granites; 4) schist xenoliths; ——— α-activity of plant ash (α = equ.U 10^4%); ▬▬ uranium content in ash (× 10^4, %); ..... intensity of β + γ-emission on the sunlit surface (μr/h); – – – – concentration of radon in the soil layer (emans); ×, ○, □ sampled branches of birch, aspen, and pine, respectively. Remark. On each area, the radium content (in equilibrium uranium units) in the ash of plants with anomalous α-activity is equal to the α-activity (in equilibrium uranium units) multiplied by 1.4.

In order to determine the gamma dose rate from the crown and trunks, we made use of Yu. P. Bulashevich's formulas [8] which, after a few straightforward transformations, assume the form

$$J = J_1 - J_2,$$

where

$$J_1 = J_{0\max} \exp\left\{6\frac{h^2}{R^2}\left[\Phi\left(\mu_2 h + 6\frac{h^2}{R^2}\right) - \Phi\left(\mu_2 h + \mu_1 l + 6\frac{h^2}{R^2}\right)\right]\right\}, \quad (3)$$

$$J_2 = J_{0\max} \exp\left\{6\frac{h^2}{R^2}\cos\psi_0\left[\Phi\left(\frac{\mu_2 h + 6\frac{h^2}{R^2}}{\cos\psi_0}\right) - \Phi\left(\frac{\mu_2 h + \mu_1 l + 6\frac{h^2}{R^2}}{\cos\psi_0}\right)\right]\right\}. \quad (4)$$

Here, J_1 is the gamma emission from an infinite layer of finite thickness through an absorbing layer; J_2 is the gamma emission from a circular annulus of finite thickness through an absorbing layer in the range of angles from ψ_0 to $\pi/2$:

$$J_{0\max} = 2\pi k q_{\max} \rho;$$

$\Phi(x)$ is King's function; l is the height of the emitting object; ψ_0 is the polar angle in spherical coordinates with the center placed at the observation point (0, 0, h); μ_1 and μ_2 are the linear gamma absorption coefficients in the emitting object and in air.

To calculate the dose rate from the forest floor debris, we employed the formula [3]:

$$J = J_{0\max} \exp\left[6\frac{h^2}{R^2}\Phi\left(\frac{6h^2}{R^2} + \mu_2 h\right)\right]. \quad (5)$$

The masking effect of the upper-lying "layers" was neglected, since it failed to exceed 10-15% [2, 3].

The average parameters of a mature forest (i.e., of age 80–120 years) were assumed to be the following: H - 25 meters, S_0 - 18 m^2, volume of a single tree with crown 1.6 m^3, mass of the crown 30% of the mass of the trunk, reserves of forest floor litter 80 tons per hectare.

If the wood density is assigned the value 0.86 g/cm^3 [9], then the density of the uniform layer constituting the crown of the forest $\rho_{cr} = 1.8 \cdot 10^{-3}$ g/cm^3. On the basis of the known value for the effective mass absorption coefficient of gamma radiation, $\mu/\rho = 0.03$ cm^2/g, we obtain $\mu_{cr} = 5.5 \cdot 10^{-5}$ cm^{-1}. Assuming the undergrowth and regrowth to have a mass 30% of the total mass of the tree trunks, we find the distributed density and the absorption coefficient of the trunk layer to be: $\rho_{tr} = 6.1 \cdot 10^{-3}$ g/cm^3; $\mu_{tr} = 1.8 \cdot 10^{-4}$ cm^{-1}. The density of the floor debris is assumed equal to 0.16 g/cm^3, and hence $\mu_{fl} = 4.8 \cdot 10^{-3}$ cm^{-1}.

The distribution of radium in the crown and wood of a tree is assumed to be uniform, and the ash content to be: 0.5% for wood (including the bark), 1% for the crown, 5% for the forest floor litter; the maximum radium content in the ash being $3.4 \cdot 10^{-8}$% (equilibrium 0.1% of uranium). This radium concentration is quite common for many uranium deposits and ore showings investigated.

Clearly, as we see from the table, the gamma intensity for the conditions stipulated and due to the radium found in the aerial parts of the trees is greater than the sensitivity of currently available aero-gamma-survey meters. For the cases observed under actual field conditions, where the peak radium content in the ash of trees amounts to $1.1 \cdot 10^{-7}$%, the effect will triple that reported in the table.

The values obtained must be regarded as maximum values, requiring experimental verification, since emanation and radon loss by the live plants were not taken into account in the calculations, and neither were meterological factors. According to the data reported by M. S. Makarov and A. I. Kalabin, the emanation power of the plants is 80-100% for radon.

Because of appreciable accumulation of radium isotopes by the plants and the large emanating power, it seemed feasible to make a study of the possibilities in the ionization prospecting method for discovering radioactive ores in wooded districts.

Gamma Intensity Above the Center of the Region (peak radium content in ash $3.4 \cdot 10^{-8}$), μr/h

Area of anomalous tract, hectares	Gamma intensity at aero-gamma survey height (above the sunlit surface)	
	40 meters	50 meters
1.0	0.6	0.4
2.0	0.9	0.6

There are, then, at least three factors to be taken into consideration in any examination of the effect of the forest cover on the results of aero-gamma surveying of deposits of radioactive ores. These are:

1. Specific geochemical processes taking place in forest soils (which are generally acidic), and resulting in a drastic depletion of the yields of uraniferous ore bodies down to 0.5-1.0 meter depth and lower. This is the principal reason for the diminished effectiveness of prospecting.

2. Absorption of radium by the aerial parts of the plants, and the formation of radium biogeochemical anomalies (at a relatively slight thickness of the radium-depleted soil horizon to 1-3 meters), which might have the effect of slightly enhancing the probability of uncovering deposits of radioactive ores.

3. A negligible reduction in the effectiveness of aero-gamma surveys due to absorption of gamma radiation from the soil layer by the aerial parts of the plants.

LITERATURE CITED

1. G. N. Kotel'nikov and I. N. Kalyakin, JAE, 8, 370 (1960).
2. A. V. Matveev, JAE, 11, 550 (1961).
3. A. V. Matveev, Symposium: Problems of mining geophysics. No. 3, [in Russian], State geology press, Moscow (1961), p. 185.
4. A. L. Kovalevskii, Izvestiya Sibir. otdel. akad. nauk SSSR, No. 4, 108 (1962).
5. K. G. Kunasheva, Radium content in flora and fauna. Proceedings of the biogeochemical laboratory, Vol. 7, [in Russian], Publ. by the USSR Academy of Sciences (1944).
6. V. G. Nesterov, General forestry, Atate paper and pulp press [in Russian], (Goslesbumizdat, Moscow-Leningrad (1945), p. 45.
7. A. V. Matveev, Advances in prospecting radiometry, No. 2, 2 (1960).
8. Yu. P. Bulashevich, Trudy Gorno-geolog. inst. Ural'. filiala akad. nauk SSSR. Geofiz. sbornik, No. 2, 146 (1957).
9. N. F. Lyashenko, Handbook on lumber and woods [in Russian], State paper and pulp press, Kiev (1955).

CONFERENCE ON REACTIONS OF COMPLEX NUCLEI

Translated from Atomnaya Énergiya, Vol. 15, No. 5,
pp. 435-443, November, 1963

The III conference on reactions between complex nuclei convened in April 1963 at Pacific Grove (California, USA), under the auspices of the Lawrence Radiation Laboratory (Berkeley). Topics in scattering of heavy ions, direct reactions brought about by heavy ions, decay of compound nuclei, coulombic excitation of nuclei, and nuclear spectroscopy came under discussion in the seven sessions of the conference.

Empirical data on elastic and inelastic scattering of C, N, and O ions on various nuclei were reported in papers dealing with heavy-ion scatterin research. The data reported were compared to the results of calculations based on the optical model, and with calculations using the phase shift method (the McIntyre model). The value of applying semiclassical methods to the calculation of heavy-ion elastic scattering cross sections was underlined in the reports and in the discussion. Attention was also centered on the usefulness of the quasiclassical approach in analyzing the simplest nucleon exchange reactions in interactions involving heavy ions.

Experimental papers on the study of exchange reactions in encounters of heavy ions were directed primarily to a careful measurement of the energy distributions and angular distributions of particles emitted in heavy-ion collisions. The high resolution of the experimental equipment was a conspicuous factor in the reports.

Experiments conducted by the Bromley group at Yale University showed that an α-particle is always formed in the binary splitting of the Li^7, B^{11}, B^{10}, and Li^6 ions on various targets, while the spectrum and angular distribution of the α-particles are in accord with classical kinematical calculations which assume splitting of the ion when adjacent nuclei interact.

Detailed investigations of deuteron and proton transfer reactions in response to irradiation of C^{12} by B^{11} ions have also been carried out at Yale. The findings show that the residual nucleus is in the excited state in most cases, while selectivity is observed with respect to separate isolated levels. Experimental findings on pickup of α-particles with the formation of Li^6 as deuterons bombard various targets were reported.

Some of the papers presented accounts of investigations of neutron transfer reactions in nuclear collisions. The findings were analyzed from the viewpoint of the tunneling theory of neutron transfer.

Work on the resonance nature of the reactions $C^{12}(C^{12}\alpha)Ne^{20}$ and $C^{12}(O^{16})Mg^{24}$ was reported. This work has been carried out on tandem electrostatic generators, and the results were analyzed on the basis of current concepts on excited states of high spin for the nuclides Ne^{20} and Mg^{24}.

The high monochromaticity of the beam of ions accelerated by electrostatic generators enables researchers to study fluctuations in the cross sections of nuclear reactions, and thus to extract information on the lifetime of the compound nucleus. In this context, we might note the paper by Zucker and colleagues (Oak Ridge), in which the s statistical correlation function was employed.

The decay of compound nuclei formed in reactions with heavy ions was the subject of several papers reporting work using linear heavy-ion accelerators at the Lawrence Radiation Laboratory and at Yale University. In experiments on the study of neutron emission, the effect of the angular momentum contributed by the heavy ion is manifested rather prominently. Among the papers dealing with research on the compound nucleus, we must mention a theoretical presentation by Swiatecki et al., on equilibrium forms of a rotating charged liquid drop. Calculations indicate that the fission barrier declines drastically as a result of the nucleus rotating.

An experimental paper presented by Price et al., at Berkeley on a search for ternary fission events (fission into three equal parts) was received with keen interest. It was found that nuclides having a high value of the parameter Z^2/A obtained by irradiating Th^{232} and U^{238} with argon ions experience fission into three equal parts to a strikingly high probability. Mica detectors were employed with success in recording the fission fragments.

In addition to papers devoted to the study of the mechanism behind reactions between complex nuclei, the conference also discussed papers dealing with coulomb excitation of nuclei. The results of theoretical and experimental investigations indicate the existence of second-order effects for excitation of levels in coulombic interactions of nuclei. A detailed study of these effects opens up opportunities for measuring the quadrupole moments of nuclei existing in an excited state. Some experimental papers cited empirical results on coulomb extinction of levels of different natures (levels of rotation bands, vibration levels).

New experimental data on the rotation levels of neutron-deficient rare-earth nuclides extended the scope of the region of deformed nuclei.

Reports were presented on experimental heavy-ion research carried out at the Nuclear Reactions Laboratory of the Dubna Joint Institute. These included papers on a spontaneously fissioning isomer, delayed-proton emitters, nucleon transfer reactions, the spectra of fission fragments. Also presented were theoretical papers by B. N. Kalinkin and colleagues (Theoretical Physics Laboratory of the Dubna Joint Institute) on a study of elastic scattering of heavy ions and transfer reactions, and by V. M. Strutinskii (I. V. Kurchatov Institute of Atomic Energy) on the probability of isomerism in nuclei.

V. Gol'danskii made reports on theoretical estimates of the probability of proton radioactivity.

In speaking on the conference as a whole, we may draw the inference that the work accomplished in the last two years on the study of nuclear reactions elicited by heavy ions has undergone a significant development. The advance to high-accuracy quantitative research and consistent theoretical analysis of the data obtained are noteworthy.

S. M. Polikanov

CONFERENCE ON INTERACTIONS OF HIGH-ENERGY PHOTONS

Translated from Atomnaya Énergiya, Vol. 15, No. 5,
pp. 436-438, November, 1963

A conference on interactions involving photons with energies as high as several billion electron volts took place in January 1963 at the Massachusetts Institute of Technology (Cambridge, USA). About 300 scientists from the USA, Britain, France, Italy, and other countries were in attendance.

The conference was scheduled for the commissioning of the Cambridge 6 BeV cyclic electron accelerator. The purpose of the conference was to review theoretical and experimental advances in research on electromagnetic interactions of elementary particles in the energy region of 1 BeV and to consider the possibilites of using the photons and electrons from the Cambridge cyclic accelerator in research on the nature of the elementary particles and their interactions.

The conference was opened by reports dedicated verifying the applicability of quantum electrodynamics at small distances. From a comparison of theoretical calculations and experimental data on the anomalous magnetic moment of the μ-meson, photoproduction cross sections of $\mu^+ - \mu^-$-pairs, scattering of μ-mesons in the coulomb field of the nucleus, the production of $e^+ - e^-$-pairs at large angles, and other topics, it became clear that electrodynamics is valid at distances as short as $\lambda > (1\text{-}2) \cdot 10^{-14}$ cm. Further progress in this type of research is contingent on the successful production of fairly intense colliding electron beams. Storage of electrons and positrons in storage systems were discussed as possible solutions to this problem in reports by V. Touschek (Frascati, Italy) and V. Richter (Stanford, USA).

In the first of these papers, it was reported that research findings from the AdA storage system (Frascati, Italy) delivered to the linear electron accelerator at Orsay (France) indicate a strong dependence of the lifetime of particles in the storage ring on the total number N of stored particles. The lifetime varies from 40 h at low intensity to 6 h at $N = 4 \cdot 10^7$. At these high intensities, attempts are being made to scan the electron-positron beam system to observe the reaction $e^+ - e^- \rightarrow 2\gamma$ by recording by means of Cerenkov lead glass counters, coincidence of any two gamms photons emitted in the direction of motion of the primary particles. It is proposed to utilize the findings of these measurements to determine the dimensions of bunches of stored particles.

At Stanford, injection of a rather large number of electrons into the storage system was plagued by difficulties associated with a sharp deterioration of the vacuum, and this is apparently due to the radiation-induced decomposition of the grease used in the vacuum pumps. Decisive steps are being taken to eliminate this deficiency.

The next group of reports was devoted to a discussion of electron scattering on protons and of electromagnetic form factors of nucleons (reports by D. Jenne, R. Wilson et al.). It was noted that in $e-p$-scattering experiments radiation corrections attaining 20% in some individual cases were reliably estimated for the first time. From the new data on scattering of ~ 1.4 BeV electrons on protons, we infer that a description of the electrical and magnetic form factors of the proton requires that we take under consideration two new particles of mass about one half of, and 1.5 times greater than the large masses of ρ- and ω-mesons, in addition to taking ρ- and ω-mesons into account.

The conference devoted considerable attention to the production of mesons (π, K, η, ρ etc.) in response to real and virtual gamma quanta. The study of these processes may yield information on the electromagnetic structure of nucleons and pions, the relative parity of particles (e.g., the parity $\lambda = K$ from the reaction $\gamma + p \rightarrow \Lambda + K$), and on the coupling constants of unstable particles. For instance, an investigation of the reaction $\gamma + p \rightarrow p + \eta$ made it possible to find the ratio between alternative decay schemes of the η^0-meson, $R = \eta \rightarrow 3\pi / \eta \rightarrow 2\gamma \approx 1 \pm 0.5$. Of the experimental findings reported by this group, we must take note of a measurement of the differential cross sections of the reactions $\gamma + p \rightarrow K^+ + \Lambda^0$, $\gamma + p \rightarrow K^+ + \Sigma^0$ and measurement in the first reaction of the polarization of Λ-particles, found to be $\sim 30\%$ at $E_\gamma \approx 1$ BeV, clearly pronounced third resonance established at energy $E_\gamma \approx 1$ BeV in the total cross sections of the photoproduction cross section of π^+- and π^0-mesons on nucleons, and also measurements of the differential cross section for angle 90° in the center of mass system for elastic scattering of gamma photons in the neighborhood of the second resonance ($E_\gamma \approx 500\text{-}850$ MeV). The cross section of this reaction passes

through a clearly defined maximum, whereupon the value of the cross section at the second maximum is found to be $^2/_3$ of the cross section of the first maximum, traceable, as we know, to resonant $\pi - N$-interactions in the $(^3/_2, ^3/_2)$ state.

In the group of reports touching on the asymptotic behavior of the cross sections at high energies, methods for treating the analytic properties of the amplitudes of the processess in the plane of the complex orbital angular momenta l were developed, and experimental data bearing on the $\pi - N$, $N - N$- and $e - p$-scattering processes at the maximum presently attainable energies were discussed. The absence of any narrowing of the diffraction maximum in $\pi - N$-scattering in the energy region 10-20 BeV is at variance with the assumption that vacuum pole exchange plays the predominant role. An analysis of the $e - p$-scattering data for very low angles leads to the inference that the photon is an ordinary fundamental particle, and not a Regge pole, and that the role of two-photon exchange is insignificant in $e - p$-scattering.

The conference centered a good deal of attention on new techniques for recording elementary particles and on new devices and instrumentation.

Three papers dealt with the production of beams of monochromatic photons.

An investigation of coherent bremsstrahlung of electrons on ordered structures, i.e., crystals (ruby, etc.), pointed up the possibility of obtaining intense fluxes of quasi-monochromatic gamma photons of high energies (of energies less by a factor of 2 or 3 than the energy of the primary electron) and 50% polarized. Monochromaticity may be enhanced by improving the angular resolution.

Another method proposed for obtaining beams of monochromatic polarized gamma photons consisted in producing a head-on collision between a beam of accelerator high-energy gamma photons and a beam of laser photons. The photons scattered on the moving electrons are sharply directed backwards and, in virtue of the Doppler effect, will have a high energy (at $E_{electr} \approx 6$ BeV, $E_\gamma \approx 850$ MeV). Consideration was also given to a technique designed to monochromatize a beam of photons by monitoring coincidences between a photon and an electron radiating it in some target, with the momentum of the electron determined by means of a magnetic spectrometer. To measure the polarization of the high-energy photons, it is proposed to use photoproduction of $e^+ - e^-$-pairs, but on crystals rather than on a conventional gamma-ray converter. In addition, methods for designing sources of polarized electron beams were discussed, along with problems concerning the depolarization of electrons in the course of acceleration.

A paper presented by D. Hall provided a survey of recording equipment suitable for use on photon beams. In addition to the unique single-channel magnetic spectrometer (resolution $\delta p/p = \pm 0.007$) built at MIT, detailed discussion of the use of bubble chambers and spark chambers in synchrotron work took place. Bubble chambers feature excellent pulse resolution and spatial resolution, but their use directly in the beam is hindered by the presence of a large electron background. Careful collimation of the beam, the use of vacuum in put tubes, filtering magnets, etc., makes it possible to work with a beam of 10^4 effective photons per pulse at the present time. The use of an additional tube filled with hydrogen gas and with walls made of heavy elements, the tube being placed alongside the beam in the interior of the chamber, enabled designers to increase the allowable intensity per pulse to 10^5 effective photons.

Bubble chambers filled with high-Z substances (freon, methyl iodide, etc.) as detectors of high-energy gamma photons have gained considerably in popularity. Backing up bubble chambers at present as gamma-ray detectors and elementary-particle detectors are spark chambers. The conference heard a detailed discussion of a cylindrical spark chamber with electrodes of heavy materials encircling a hydrogen target. It has been proposed to use a chamber of this type in colliding-beam experiments.

Intense interest was shown in a report on a discharge chamber built at CERN by G. Charpak and L. Massonet. This chamber is similar to the ordinary spark chamber, but the working gas is a helium-neon mixture with a halogen gas added. This gas is added to produce a self-quenching discharge. The use of this working medium leads to a sharp decrease in operating voltage (~ 2 kV/cm), to the possibility of recording many particle tracks simultaneously, and on an increased frequency of operation (up to 10^4 operations a second). There seems to be some indication of proportionality between the brightness of a spark and completeness of the ionization of a particle track.

Some of the papers dealt with various systems for automatic scanning of 10^6 to 10^7 photographic plates from bubble chambers and spark chambers in a year, and an acoustic method for recording particle tracks in spark chambers.

Foreign Electron Accelerators and Storage Systems

Type of machine	Country, city	Maximum energy, BeV	Intensity or total current of electron beam	Remarks
Storage ring	Italy, Frascati	1.5	0.1 A	Project; injection e^+ ~ 200 μ, beam lifetime ~ 30 h at 10^{-9} mm Hg vacuum. 4 points of collisons in $e^+ - e^-$-beams
Linear accelerator	France, Orsay	1.05		In operation: before long the energy will be increased to 1.3 BeV. In two years, according to plans, a storage ring (450 MeV) will be installed.
Strong-focusing synchrotron	West Germany, Frankfurt	6		Under construction; commissioning planned for early 1964.
Synchrotron	Sweden, Lund	1.2	10^{10} electrons/sec	In operation; 6 MeV microtron injector.
Strong-focusing synchrotron	Britain, Glasfow	4	4-10 A	Project; scheduled for completion by end of 1966.
Linear accelerator	USA, Standford	40		Project; scheduled for completion by end of 1966.
Synchrotron	USA, Cornell	2.2		Now operative 1.3 BeV accelerator being redesigned; reconstruction to begin in summer of 1964; 10 BeV accelerator being planned.
Synchrotron	Japan, Tokio	0.75	10^{11} electrons/sec	In operation; plans call for increasing energy to 1.3 BeV.

Experiments now in progress on the Cambridge cyclic accelerator or being planned for that machine were discussed in the closing sessions of the conference. The principal drift of this research is to verify the applicability of quantum electrodynamics at small distances (measurements of the photoproduction cross sections of $e^+ - e^-$- and $\mu^+ - \mu^-$-paris), investigate electromagnetic form factors of the proton and structure of the photon (on the basis of $e - p$-scattering), and detect nre particles. A broad program of research using a variety of procedures to investigate such processes as photoproduction of π - and K-mesons, the Compton effect on the proton, and other subjects is also underway.

At the conclusion of the conference, the participants were briefly brought up to date on new electron accelerators and storage systems, information on which is included in the accompanying table.

B. B. Govorkov, A. I. Lebedev

THE SECOND EUROPEAN "VAKUUM" SYMPOSIUM

Translated from Atomnaya Énergiya, Vol. 15, No. 2,
pp. 438-439, November, 1963

On the initiative of the European Federation of Chemical Engineers, the second "Vakuum" symposium on vacuum technology met at Frankfurt-am-Main in June 1963. The symposium drew about 250 physicists, technicians, and engineers from the West European countries, as well as East Germany, Yugoslavia, Czechoslovakia, Hungary, and the USA.

The symposium chose as its basic topic "The physics and engineering of sorption and desorption processes at low pressures." The choice of this topic was determined by the understanding that significant advances in vacuum technology in the next two decades will be governed in large measure by research and development progress in this area.

The first batch of papers was devoted to the fundamentals of physicochemical processes involving gases and solids. Yarwood and Clans (Britain) reported on a measurement of the probability of inert-gas ions of energies ranging from 100 to 5,000 eV sticking to metal surfaces. They determined the depth of penetration of the ions, the effect of diffusion rate, and investigated the corresponding desorption processes. Measurements of gas release by pure nickel brought about by electron bombardment were carried out by Peterman (Sweden), and were shown to be of fundamental significance; how much gas issued from the surface and how much from the bulk phase of the metal was clearly distinguished in the work. Eshbach (West Germany) and colleagues reported on their measurements of the diffusion constants of hydrogen in alloyed steels. The lowest diffusion constant, according to their measurements, is obtained in the case of austenitic steel; it is approximately 10^3 greater in the case of ferritic steel. Jackel and Wagner (West Germany) determined the work function photoelectrically for tantalum and palladium, and investigated the effect of an adsorbed gas layer on the work function (under high-vacuum conditions). Junge (West Germany) carried out some interesting observations in producing a two-component semiconducting layer by separate vaporization of individual components. By appropriately choosing the temperature of the substrate, the layer to be precipitated could be obtained in the exact proportions specified, even when the rate of vaporization of the individual components contrasted sharply. Schram (France) treated the question of different determinations of physical surfaces; Gohr (West Germany) studied the "retarded condensation" of mercury; Armand and Lapujoulade (France) reported on measurements of the interaction between stainless steel and carbon monoxide at low pressures and high temperatures.

The second batch of papers dealt with partial-pressure measurements and instruments for measuring partial pressures. There is no need to emphasize the decisive significance such measurements have for research into sorption and desorption processes and ways of controlling them. Günther (West Germany) made a review presentation on this topic. He described all existing devices (omegatron, sectored-field spectrometer, time-of-flight spectrometer, resonance ion spectrometer, the mass filter quadrupole spectrometer, the cycloidal spectrometer, and the desorption spectrometer), and considered their merits, drawbacks, and potentialities for further development and improvement. In this connection, it is fitting to note that almost all partial-pressure analyses reported on at the symposium were carried out by means of omegatrons. This compact device has become, despite its limitations, a standard instrument for measuring partial pressures (down to 10^{-12} torr). However, it would still be desirable to see partial pressure measuring devices of greater sensitivity and greater speed in read-out of partial-pressure values become available on the market. Gentsch (West Germany) described a very promising omegatron which he was the first to propose, and which is capable of capturing and measuring not only resonant but also all off-resonance ions. This will enable technicians to make continuous and simultaneous measurements of both partial and total pressures and to eliminate those errors in the measurements which are due to space-charge effects. Bueltmann and Delgmann (West Germany) described an analysis they made of the residual gas in an ultrahigh-vacuum system; they used a quadrupole spectrometer in their work.

An extended survey paper on the practical observable interaction between the residual gas and solids was presented by Venema (Netherlands). The next lengthy report dealt with the effects of sorption processes in accelerators,

plasma machines, and outer-space simulators, and was delivered by Degras (France). On this point, Fischer (CERN) reported on the gas released by the vacuum chamber of a beam storage ring for 2 MeV electrons.

The technology of working and machining metal surfaces for high vacuum and ultrahigh vacuum work was described in detail in the presentation by Doray (France). Of the many techniques available for lowering desorptive power which he mentioned, we need only mention the following ones: electrolytic polishing, electrochemical formation of a "passivating layer" and building up a protective layer, tightly bound to the metal, by precipitating a metallic compound from the gaseous phase, by means of dissociation or thermal reduction. Another method for working metal surfaces, ion bombardment etching, was described by Jobin (Switzerland).

Pumps based on the sorption principle, for example the zeolite pumps in which gases are adsorbed on a ceramic presenting a high specific surface (zeolite) are coming into increasingly wider use. They usually act by lowering the pressure in the vacuum chamber from atmospheric pressure to the 10^{-2} torr required for getter-ion pumps to begin efficient operation.

Windsor (Britain) spoke on the present state of development of zeolite pumps and reported that pressures of 10^{-9} torr may be attained by using these pumps. Fischer (CERN) described measurements of the rate of evaporation of a sputtered-titanium pump; Kienel (West Germany) investigated harmful desorption of gas from getter pumps, and made some suggestions for reducing these effects. This same topic was broached by Klopfer (West Germany), who dealt with measurements of the rate of adsorption of nitrogen and carbon monoxide on titanium. He found no confirmation for the multiplicity of hypotheses holding that the rate of adsorption of excited gas molecules must be greater than that of molecules in the ground state. Farkas (Hungary) spoke on a completely new principle for attaining low pressures. The gases to be evacuated are adsorbed on a constantly freshly exposed surface of molten metal. The metal (an alkali rare earth plus an alkali metal) is then cycled in a closed loop with the aid of an electromagnetic pump.

Two papers were devoted to cold adsorption, a phenomenon of current interest which may have great significance in the performance of cryogenic pumps. Normally, a cryogenic pump operates on the condensation principle: an intensely cooled surface promotes the evacuation, so long as the partial pressure of the gas being evacuated is greater than the vapor pressure of that gas at the temperature of the cooled surface. Contrariwise, in cold adsorption the evacuating action is possible even at a pressure lower than the vapor pressure. The gas is then bound not to the bulk phase of the metal, but to a film of another substance formed simultaneously or previously. Hengevoss (Lichtenstein) reported, for example, on cold adsorption of hydrogen on an argon layer at the temperature of liquid helium (4.2°K). Degras (France) reported on a similar phenomenon observed in the case of a cold trap cooled by liquid nitrogen.

It is very difficult to avoid errors in pressure measurements using Bayard-Alpert gages. These errors, which often go beyond one order of magnitude, were mentioned by Apgar (USA) and Hoch (West Germany). Later on, Huber (Lichtenstein) mentioned, within the context of his paper, measurement of a vacuum and determination of the x-ray range of various gages in the Bayard-Alpert system as compared to Lafferty gages. Meinke (West Germany) proposed a new tube for an ionization manometer, specially designed as a standard gage. If this tube proves to have such a high stability and reproducibility of performance characteristics as is claimed, then it may well replace the McLeod manometers which are in general use as standards (in the range to 10^{-5} torr), but which are highly inconvenient in practice.

When adsorption and desorption rates are to be measured, it is often desirable to measure very slight flows of gas. A special technique has been devised for these measurements. Garbe (West Germany) studied very slight quantities of oil vapors which penetrated into an ultrahigh-vacuum system from an oil diffusion pump with an absorbent trap. Such low quantities of oil could not be successfully measured with a mass spectrometer, since they are instantly absorbed on the heating walls of the chamber. Garbe devised, for his measurements, a valve between the pump section and the chamber, and discovered an increase inpressure when the chamber was heated. Using this method, he could also prove the existence of a reverse flow of oil at the rate of 10^{10} molecules a day. Kraus (Lichtenstein) described a new device for measuring gas flow where the pressure in the volume to be measured in raised and lowered within specified limits by intermittently and briefly opening a valve controlled by a pressure gage. The frequency at which the valve is operated is a measure of the gas flow. Exact constant-pressure measurements of gas flow were also mentioned by Henri (France).

In passing, we note that French delegates astonished the audience with their proposal of a new pressure unit which they in fact used in their reports: 1 pascal = $7.5 \cdot 10^{-3}$ torr. The pascal is a new name for the pressure unit in

the MKS system: pascal-N/m^2 = kg/sec^2m. The initiative of the French on this point is consistent and to be welcomed, but we are sure that it will be a long time before that unit gets to replace the now accepted unit (torr = mm Hg).

In general, we feel free to state that the symposium provided an excellent review of the many problems associated with sorption and desorption processes, and that much new was to be gained from its sessions. We do not hesitate in affirming that the proceedings of the symposium, to be published in 1963, will be a most valuable reference for everyone active in this field.

E. Fischer (CERN, Geneva)

MODERNIZATION OF THE VVR-S REACTOR

Translated from Atomnaya Énergiya, Vol. 15, No. 2,
pp. 439-44a, November, 1963

A method has been developed at the I. V. Kurchatov Institute of Atomic Energy for effecting a significant increase in the power of standard VVR-S water-cooled water-moderated research reactors without making extensive alterations on the core.

As is generally known, reactors of this series have been installed in many research institutes throughout the USSR and other countries. Many scientists working throughout the USSR and other countries. Many scientists working with these reactors are interested in increasing the reactor power and broadening the experimental potentialities of these reactors.

The essence of the new method consists in replacing the fuel assemblies now in use with EK-10 fuel assemblies which present a more elaborate heat-transfer surface. This requires absolutely no redesigning of the reactor core.

Several variants were looked over, and the choice fell on an assembly consisting of four fuel elements of octagonal cross section, an inner round fuel element, and an aluminum jacket. The design of the proposed fuel assembly is shown in Fig. 1. The inner element may be extracted from the assembly, and experimental channels or ampules of 19 mm outer diameter may be put in its place.

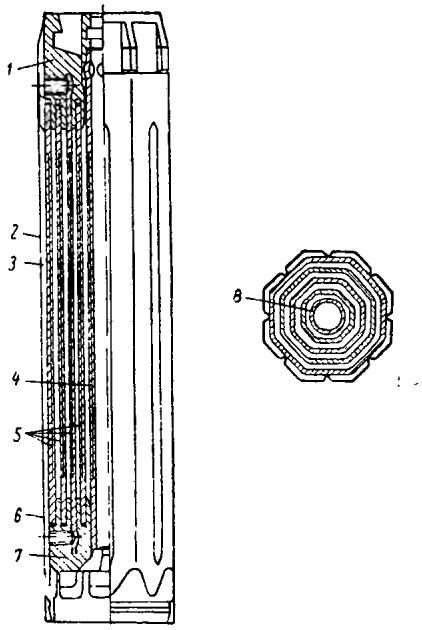

Fig. 1. Fuel assembly: 1) upper end part; 2) upper reactor lattice; 3) aluminum cladding; 4) round (inner) fuel element; 5) hexagonal fuel elements; 6) lower reactor lattice; 7) lower end-piece; 8) cross section through fuel assembly.

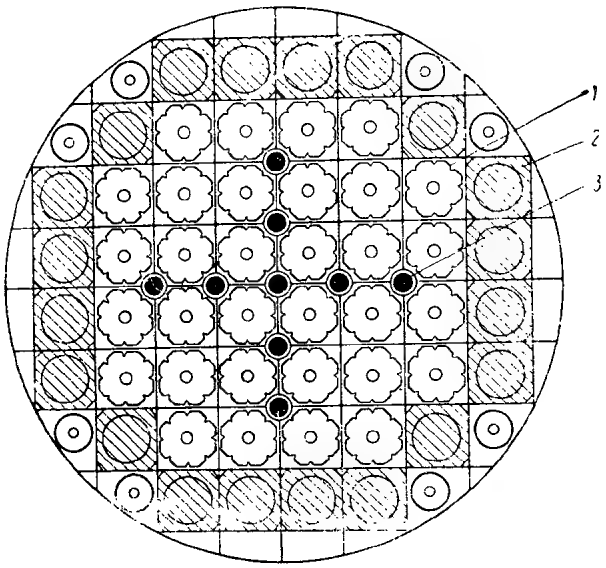

Fig. 2. Cross section through reactor core: 1) fuel assemblies; 2) metal beryllium slugs (round plug seen in center of each slug; 3) control rod and scram rod channels.

Inside the core, the walls of the fuel elements consist of three layers: an outer and inner lining of aluminum each 0.8 mm thick and a medium layer of uranium-aluminum alloy meat 0.9 mm thick. The aluminum cladding of the assembly is 0.8 mm thick. Longitudinal semicircular recesses are cut on the edges of the cladding to heighten its rigidity and hinder any closing of the gap between the cladding and the outer surface of the external fuel

element brought about by the difference in the pressures of the coolant water inside the cladding and outside. The clearing between cladding and outer fuel element is 2.7 mm. The clearances between the remaining elements are 3.0 mm. The water space encircling the inner fuel element has a variable thickness with a minimum of 2.5 mm. The end parts are so shaped as to distribute the coolant water inside the fuel assembly such that the flow will be maximized in the first two clearances starting from the exterior of the fuel element. The rate of coolant water flow between the assemblies is very slight. The arrangement of the fuel assemblies in the reactor core may be seen in Fig. 2.

Below, we list for comparison the characteristics of the present VVR-S core and the characteristics of the proposed modification.

	Assembly with EK-10 elements	New Al-clad assembly
Fraction of core volume filled with water	0.7	0.66
Heat-transfer surface, in core units, cm^2/cm^3	0.98	2.4
Core height, mm	500	700
Uranium enrichment, %	10	36
U^{235} content, g	128	180
Amount of U^{235} per square meter of heat-transfer surface, g/m^2	500	205
U^{235} concentration in core, g/liter	50	50

The new fuel assemblies display the following advantages:

1. The height of the VVR-S reactor core may be increased to 700 mm, which will raise the reactivity excess by 4%.

2. The use of the new fuel assemblies increase the heat-transfer surface per unit core volume by a factor 2.4.

3. The new fuel assemblies, as well as the assemblies with EK-10 elements, facilitate a rational utilization of the coolant. Over 90% of the coolant water passing through the core flows inside the fuel assemblies. Throttling plates mounted in the lower core lattice can serve to distribute the water through individual fuel assemblies to match the power developed in them.

4. The new fuel assemblies may be mounted in any cell of the core. This is an important point for attaining higher fuel burnup and for carrying out in-core experiments.

5. The aluminum jacket reliably protects the outer fuel element in the assembly from mechanical damage during transfer and replacement or during loading into the core.

6. Experimental channels or ampules may be inserted into the center of the new fuel assemblies to enhance the research potentialities and capabilities of the reactor. The separating adjacent fuel assemblies is available for use in experiments.

Some flaws and shortcomings might be pointed out in the new fuel assemblies too, but these do not detract from their advantages, on the whole. First, there is the need to introduce aluminum into the core as the cladding, and this has the effect of slightly reducing the volume fraction of the water; secondly, local neutron flux increases occur in the water spaces between the fuel assemblies, and these increase radial and angular nonuniformities in the heat released by elements composing the assemblies.

RFT type fuel assemblies with tubes of round cross section may be used in addition to the fuel assemblies with tubes of octagonal cross section.

The possible pile power levels attainable when the new fuel assemblies are used are determined from the following initial data:

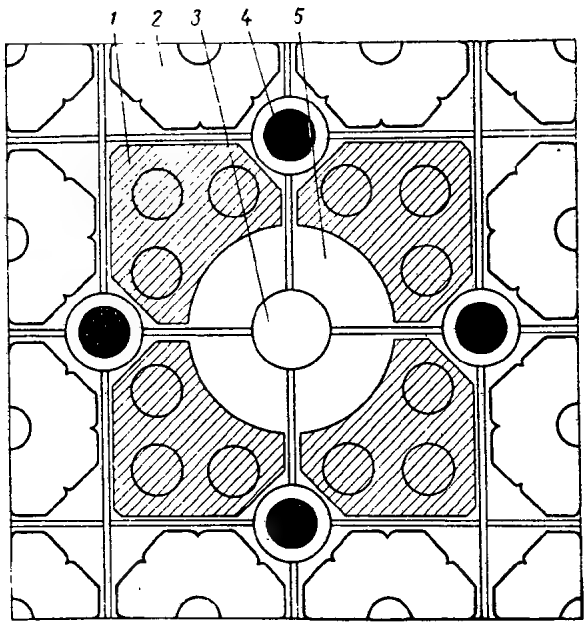

Fig. 3. In-core neutron "trap." 1) Beryllium metal slugs; 2) fuel assemblies; 3) central channel; 4) control rod and scram rod channels; 5) water space.

1. Coolant flowrate through the core at 900 m^3/h, of which 10% flows outside the fuel assemblies and beryllium slugs.

2. 2.5 m^3/h of coolant is used to cool each beryllium slug.

3. The average in-core water temperatures is 50°C.

4. The peak temperature of the fuel-element surfaces is 90°C.

5. The unevenness factors in heat release along the height of the core and over the cross sectional area of the fuel elements are 1.36 and 1.35, respectively.

For purposes of comparison, two variants in pile core loading were considered for the new fuel assemblies. The first loading pattern called for 32 fuel assemblies and 20 slugs of metallic beryllium (Fig. 2), the second for 52 fuel assemblies. Below, we list some of the computed data for these two loading latter patterns:

	Loading: 32 assemblies and 20 beryllium slugs	Loading: 32 fuel assemblies with no throttle plates	Loading: assemblies with throttle plates
Water flowrate in each assembly, m^3/h	24	15.6	16.7
Heat release unevenness factor, on core radius	1.4	1.67	1.67
Peak power, MW	8	8	11
Peak heat flow over assembly surface, $kcal/m^2 \cdot h$	$6.4 \cdot 10^5$	$4.5 \cdot 10^5$	$6.4 \cdot 10^5$
Peak thermal neutron flux, $neutrons/cm^2 \cdot sec$	$6 \cdot 10^{13}$	$6 \cdot 10^{13}$	$6 \cdot 10^{13}$

The use of the new fuel assemblies made it possible to triple the thermal flux (initial flux is $2 \cdot 10^{13}$ $neutrons/cm^2 \cdot sec$).

The presence of beryllium metal slugs in the core will, as our comparison shows, make it possible to triple the neutron flux (bringing it up to $6 \cdot 10^{13}$ neutrons/cm^2 · sec) at considerably lower reactor power. Moreover, the beryllium slugs may be used in performing experiments. For experimental work, the plug is removed and an experimental channel or ampule of 54 mm O. D. is inserted in its place.

An even greater thermal flux ($2 \cdot 10^{14}$ neutrons/cm^2 · sec) may be obtained in a neutron "trap." This trap may be set up in the center of the reactor core (Fig. 3).

When the pile power is increased above 4 MW, additional heat exchangers have to be installed and an emergency cooling system must be included.

The proposals to modernize the VVR-S reactors were worked out by R. S. Ambartsumyan, P. M. Verkhovykh, V. V. Goncharov, A. M. Glukhov, P. M. Egorenkov, L. G. Kuprievskaya, Yu. G. Nikolaev, R. F. Smirnova, Yu. F. Chernilin, and P. I. Shavrov, and were reported by V. V. Goncharov to the April 1963 Prageu conference on research reactor physics and engineering in the socialist countries. This modernization will make it possible to step up the power and to expand the experimental capabilities of VVR-S reactors without making a fundamental redesign.

BRIEF COMMUNICATIONS

Translated from Atomnaya Énergiya, Vol. 15, No. 5,
pp. 442-443, November, 1963

USSR. Industrial tests are in progress on a deep-hole SGS-1 type gamma-logging spectrometer for use in geophysical prospecting of petroleum and ore deposits. The information passed up the thin cable is automatically decoded. The deep-hole gamma-ray spectrometer may be used to determine the presence of petroleum copper, m manganese, aluminum, and rare earths in the interior of the earth.

USSR. At Frunze, a mobile "Atoms for Peace" exhibit has been open to the public for some time. The introductory section of the exhibit familiarizes visitors with the nature of the atom, the structure of nuclei, and the mechanism of atomic energy. Here we find on exhibit an operating mock-up of the world's first operative nuclear reactor electric power station, with the operating principles clarified for the layman. Visitors to the exhibited also became acquainted with reactor electric power stations of greater power output: the Siberian, Belyi Yar, and Novaya Voronezh stations. Some of the exhibits explained the achievements of Soviet science and industry in building nuclear reactors of various types. A special section, "Thermonuclear reactions: the power of the future," was devoted to work on harnessing new and inexhaustible sources of energy. The attention of visitors was drawn more particularly to materials dealing with the world's first nuclear-powered icebreaker, the LENIN. The exhibit had displays reflecting various trends in the utilization of radioactive isotopes and nuclear radiations in industry, agriculture, medicine, and displays on radiation protection techniques and instruments.

USSR. Radioisotope instruments are now entering into use in industrial enterprises and units in the Karaganda Council of the National Economy. At the Balkhash Mining and Metallurgical Combine, thickness gages are being employed to continuously measure the thickness of cold-rolled sheet, and radioisotope level gages are being used in process control operations at ore dressing plants. Radioisotope temperature controls are being used to regulate heat processes in furnaces and kilns at the Karaganda cement plant and the Dzhezkazgan mining and metallurgical combine. Far from negligible savings are expected from the use of a radioactive servoed level gage to be installed on a blast furnace at the Kazakhstanskaya Magnitka works.

USSR. An All-Union seminar on the uses of radioactive instruments in the chemical processing industry was held at Aktyubinsk. The seminar participants became familiar with experience in the use of such instruments at a chromium compounds plant where twenty production operations were successfully automated by means of radioactive instrumentation.

USSR. The biophysics laboratory of the plant protection research institute is working on the development of techniques for utilizing atomic energy, x-rays, ultraviolet rays, and other rays in the battle against crop pests. Research on the effects of ionizing radiations on microorganisms is being conducted in collaboration with the laboratory of microbiological research techniques. The outcome so far includes the isolation of new forms of microorganisms which give rise to epidemic plagues among the pest insects. The use of ionizing radiation to exterminate insects in grain stores is under study. In its efforts to find ways of using atomic energy in the fight against field pests, the laboratory is developing a new technique involving a mass resettlement of male insects subjected earlier to sex-sterilization by intense gamma exposures. Methods for producing sterile insects are being developed intensively.

USSR. A special seminar was organized at Erevan to facilitate exchanges of experience in the use of radioisotope automation and process control equipment in the chemical and oil refining industries. Twenty-three reports and communications on new types and designs of instruments and equipment based on the use of ionizing radiations were heard and discussed. Opportunities for the use of such instrumentation and the outlook for automated process control were discussed. The seminar participants displayed keen interest in an exhibit at which new isotope instruments were available for examination, along with instrument catalogs and new items in the technical literature on the uses of atomic energy in industry.

IAEA. An agreement was drawn up and signed on the building of subcritical assemblies at the Otaniemi (Finland) Technological Institute. Enriched uranium for these assemblies will be delivered from the Soviet Union.

Poland. The transistorized MSK-1 designed for individual or mass personnel monitoring of exposures to radioactive materials offers the advantages of making it possible to check out a large number of personnel in a short time immediately after completion of work. The instrument operates automatically and emits an alarm signal when hands, footwear, or clothing are exposed to radioactive materials. The MSK-1 is simple to operate and service, and is failure-proof.

COMMISSIONING OF THE WORLD'S FIRST REACTOR POWER STATION WITH AN ORGANIC-MODERATOR AND ORGANIC-COOLANT REACTOR

Translated from Atomnaya Énergiya, Vol. 15, No. 5,
p. 443, November, 1963

On August 11, 1963, a 750 kW power transportable modular nuclear power station was started up at the Atomic Reactor Research Institute (at Melekess). This power station has been baptized the ARBUS (abbreviation for "atomic reactor modular facility"); it is the prototype of a line of small electric power stations to be developed for construction in remote regions of the Soviet Union.

The physical start-up of the reactor on June 29, 1963 was preceded by the operation of bringing the electric power station to on-power operating conditions, whereby the correctness of the physical core calculations were was confirmed.

The design of the ARBUS nuclear power station, fabrication of the ancillary equipment, assembly and start-up operations were all completed within a short span of time (less than two years). The heterogeneous thermal reactor installed in the power station is both cooled and moderated by organic fluid. The reactor thermal power is 5000 kW. The reactor, steam generators, and the piping of the primary loop are made of carbon steel. The loading of the reactor core was 22.5 kg (in U^{235}). The reactor is designed to operate for two years at full power without reloading.

One outstanding feature of the power station is the capacity to recover the organic coolant used by cycling part of the coolant through a regeneration facility included in the station loop.

A team of specialists engaged in installing the ARBUS facility proceeded to carry out the program of research and compiling of operating experience on the electric power station under full-power conditions. The program also includes a study of the performance of the modular power station under autonomous conditions. The ARBUS is the world's first nuclear power facility incorporating an organic-cooled and organic-moderated reactor with regeneration of the coolant, and operating at full power.

Received, October 9, 1963

Yu. Arkhangel'skii, I. Kovalev

BIBLIOGRAPHY

NEW LITERATURE

Atomizdat Releases

Metallurgiya i metallovedenie chistykh metallov [Metallurgy and metallography of pure metals.]. No. 4. Symposium of papers edited by V. S. Emel'yanov and A. I. Evstyukhin. 1963, 252 pages, 91 kopeks.

This is a collection of 27 papers most of which were delivered at the 1961 conference of the Moscow Engineering and Physics Institute. The articles shed light on such topics as the winning of various metals and alloys and the study of their properties, with zirconium, molybdenum, niobium, nickel-chromium alloys, chromium-nickel steel, beryllium, SAP alloy, etc., considered. Methods for obtaining pure zirconium, and single crystals of niobium by zone recrystallization are discussed; the reader will find studies of the properties of chromium-nickel steel, iron, and titanium in liquid coolants; methods for obtaining and studying new structural materials, such as rhenium-carbon alloys, SAP alloys, etc., are presented. The last six articles in the collection take up techniques in experimental research on the physical properties of metals, based on the use of radioisotope practice, quantitative radiography, thermomagnetic phenomena, etc.

I. V. Koshelev. Radiometricheskaya apparatura dlya obogashcheniya uranovykh rud. 1963, 94 pages, 29 kopeks. [Radiometric equipment for uranium ore enrichment processes].

This book presents a classification and the circuitry of radiometers for use in ore-grading processes: radiometer components such as radiation detectors, RC circuits, pulse amplifiers, wave shaping circuits, pulse-height discriminators, pulse recording networks, commutating and auxiliary circuits, are discussed; radiometers with count rate recording and absolute pulse count are described; the parameters of various types of ore-grading radiometers are given.

Materialy dlya yadernykh reaktorov [Materials for nuclear engineers: Temple Press, London, 1956]. Edited by A. B. McIntosh and T. J. Heal. Translated from the English, 1963. 386 pages, 1 ruble, 89 kopeks.

This book, made up of chapters contributed by a panel of authors, briefly presents information on the physical and mechanical properties of reactor materials; emphasis is given to compatability of materials, corrosion behavior, creep resistance, and behavior under irradiation; uranium, plutonium, thorium and their alloys are discussed, along with ceramic fuel, graphite, magnesium, beryllium, zirconium, each of which is the subject of a separate chapter. The appendices to the chapters include reference tables of data on the basic properties of the materials discussed, as well as a generous bibliography.

W. R. Harper. Osnovnye printsipy reaktorov deleniya [Basic principles of fission reactors]. Translated from the English [Interscience, New York, 1961]. 1963, 304 pages, 1 ruble, 26 kopeks.

This book outlines the basic principles of the design of nuclear reactors, and discusses topics related to reactor design and performance, as well as radiation shielding. The first three chapters contain descriptions of the basic design principles of reactor electric power stations, design of a graphite-moderated experimental reactor, and development of a power reactor project; the next two chapters take up various types of nuclear fuel and the performance of fuel elements; later on we find descriptions of fast reactors, homogeneous and heterogeneous reactors. Radiation shielding, radiation safety practice, and disposal of radioactive wastes are also discussed.

Information on reactor characteristics, absorption cross sections, moderator properties, etc., appear in the appendices. A subject index appears in the back of the book.

Books Released by Other Publishers

K. P. Medvedev. Primenenie radioizotopov v koksokhimii [Use of radioisotopes in coke chemistry]. Khar'kov, Metallurgizdat, 1963. 144 pages, 60 kopeks.

This book describes the application of the tracer technique to research on the structure and properties of hard coals, their thermal decomposition mechanisms, the accumulation and transformations of radioactive and miscellaneous elements in coals. New data on the thermal decomposition process and on sintering or organic constituents of coals are included. The discussion covers possible tracer applications in automation and process control of coke production.

The list of literature references includes 127 titles.

B. M. Zlobinskii, N. S. Nemtsov. Radioaktivnye izotopy v domennom proizvodstve [Radioisotopes in blast-furnace work]. Moscow, Metallurgizdat, 1963. 96 pages, 31 kopeks.

This book discusses techniques in the application of radioactive isotopes in blast-furnace production, and safe handling of radioactive materials in blast-furnace shops. The first chapter presents a survey of research involving the use of radioisotopes in blast-furnace production inside and outside the USSR. The second chapter takes up the question of the behavior of isotopes in blast furnaces: the conversion of the isotopes into blas-furnace products, the isotope distribution in the furnace hearth and in the ladles, radioactive contamination of the lining and of the atmosphere. The third chapter is presents recommendations on the choice of radioisotopes, how to calculate radio-activity and ensure safe practices under blast-furnace work conditions.

A list of pertinent literature including 152 titles is appended to the book.

ARTICLES FROM THE PERIODICAL LITERATURE

I. Nuclear Physics

(Nuclear reactions, neutrons, fission). Nucl. Instrum. and Methods, 23, No. 1 (1963).

C. Weitkamp, 10-12. Experimental determination of the photofraction of a cylindrical NaI(Tl) crystal scintillation detector.

C. Weitkamp, 13-18. Determination of photofractions and intrinsic efficiencies of cylindrical scintillation NaI(Tl) detectors.

M. Paic et al., 19-23. Comparative measurements of neutron yield on different targets.

A. Judd, 29-35. Measurement of neutron flux by resonance activation of foils.

J. Leroy et al., 93-103. Wilson diffusion chamber measures polarization of fast neutrons.

G. Walter and A. Coche, 147-51. Organic-scintillator measurement of the slow component of light.

M. Mladenovic and Ali-El-Farash, 175-77. Fabrication of thin bea emitters by cathode sputtering.

Nucleonics, 21, No. 7 (1963).

J. Bell and P. Cheever, 58 ff. Two methods for determining the rate of Co^{60} decay.

II. Plasma Physics

Doklady akad. nauk SSSR, 150, No. 2 (1963).

V. F. Demichev and V. D. Matyukhin, 279.82. Study of the properties of fast-moving plasmoids.

Doklady akad. nauk SSSR, 150, No. 3 (1963)

A. A. Galeev, 503-506. An asymptotic method in plasma stability theory.

V. F. Demichev and V. M. Strunnikov, 523-26. Interaction between high-density plasmoids and magnetic fields.

Zhurnal tekhn. fiz., 33, No. 7 (1963).

F. M. Nekrasov, 796-75. On one class on nonlinear solutions of the kinetic equation without the collision integral.

A. V. Timofeev, 776-81. Convection of a weakly ionized plasma in a nonuniform external magnetic field.

G. M. Zaslavskii and S. S. Moiseev, 782-87. Viscous processes in relativistic magnetohydrodynamics.

Yu. A. Berezin, 788-94. On self-oscillations of a plasma ellipsoid in a time-invariant magnetic field.

V. N. Tsytovich, 795-800. Note on the theory of charges moving along a channel axis in a medium.

G. M. Zaslavskii, 801-804. Heat flow in relativistic magnetohydrodynamics.

V. I. Karpman and R. Z. Sagdeev, 805-14. Stability of the structure of a shock front propagating transverse to the magnetic field in a rarefied plasma.

E. F. Tkalich and V. S. Tkalich, 815-19. Note on the theory of stationary states of a high-temperature plasma; plasmoid with a longitudinal magnetic field.

N. A. Khizhnyak,and P. MKolesnikov, 820-22. Note on the theory of electrodynamical acceleration of plasmoids in a coaxial line.

B. P. Kononov. Investigation of the pinch process in a cross-field magnetic trap.

Ya. M. Pinskii, 864-66. Effect of collisions on electron trapping in a high-frequency field.

E. B. Sonin, 872-81. Effect of electrode sheath regions on the electrical resistivity of a weakly ionized plasma.

K. A. Lur'e, 886-89. Note on the propagation of small perturbations through a gas of finite conductivity in a magnetic field.

I. S. Baikov and R. R. Ramazashvili, 890-92. On the temperature relaxation of charged particles in a plasma.

Izvestiya akad. nauk Uzbek.SSR. Seriya fiz. matem. nauk, No. 2 (1963).

G. Ya. Umarov, 56-60. Transverse injection of plasmoids.

Izvestiya vyssh. ucheb. zaved. Radiofizika, 6, No. 2 (1963).

V. F. Aleksin and K. N. Stepanov, 297-310. Spatial correlation of electromagnetic field noise in a plasma. I.

A. A. Rukhadze, 401-403. On one mode of beam instability in a plasma.

K. N. Stepanov, 403-405. Absorption of electromagnetic waves in quasilongitudinal propagation.

Nature, 198, No. 4887 (1963).

T. McLaren et al., 1264-65. Measurement of electron temperatures in a shock tube with a double probe.

L. Heroux, 1291-93. Spectroscopic technique of electron temperature measurements in plasmas.

III. Acceleration of Charged Particles. Accelerators

Zhur. tekhn. fiz., 33, No. 7 (1963).

A. I. Zykov and E. K. Ostrovskii, 892-894. A technique for calculating buncher parameters at v_f = const.

Trudy inst. metallurgii im. Baikov, No. 12 (1963).

Yu. V. Gromov, 276-81. A new high-efficiency betatron injector.

J. Inst. Electr. Engrs., 9, No. 6 (1963).

J. Adams, 251-52. High-energy accelerators for nuclear physics research.

Nucl. Instrum. and Methods, 23, No. 1 (1963).

F. Firk et al., 141-146. Nanosecond neutron time-of-flight system for the 30 MeV linear electron accelerators.

Nukleonika, 8, No. 2 (1963).

A. A. Glazov et al., 89-100. High-frequency system for a proton accelerator, consisting of a single resonator.

IV. Nuclear Engineering. Nuclear Power

(Neutron physics. Nuclear reactor theory and calculations. Reactor design. Performance of nuclear reactors and of reactor electric power stations. Radiation shielding. Radioactive waste disposal).

Izhener.-fiz. zhur., No. 6 (1963).

J. Pearson and T. Irwin, 10-19. Analog simulation of turbulent heat exchange of liquid metals in the entrance region of tubes of non-round cross section.

Atomkernenergie, 8, No. 5 (1963).

R. Pruschek, 161-65. Calculating coolant temperature fields at the cores exit in a spherical-fuel reactor.

H. Hejtmanek, 166-68. Stability of slurry-fuel reactor.

Atomkernenergie, 8, No. 6 (1963).

E. Keberle, 204-207. Numerical determination of the shadowing effect of two cylindrical fuel elements.

W. Kohler, 208-12. Spectral distribution of epithermal and fast neutrons in the FRM reactor.

A. Mareske, 213-23. Effect of cooling system on peak reactor power in liquid-cooled reactor.

Atomwirtschaft, 8, No. 6 (1963).

J. Cretté et al., 357-66. The ESSOR experimental reactor.

K. Penster, 366-70. Engineering aspects of fuel-element guarantees.

L. Rachor, 370-72. A spherical high-temperature fuel element.

A. Finkelstein, 373-76. Development of the French experimental program.

Engineer, 215, No. 5601 (1963).

---, 1018. Modular nuclear thermionic converter facility.

Engineer, 215, No. 5604 (1963).

---, 1107-1110. Research work at Harwell.

Engineer, 216, No. 5607 (1963).

---, 4-6. Performance of the Bradwell and Berkeley reactor power stations. I.

Engineer, 216, No. 5607 (1963).

---, Performance of the Bradwell and Berkeley reactor power stations. II.

Energia nucleare, 10, No. 6 (1963).

G. Pinchera, 319-35. Heat transfer by organic fluids.

M. Silvestri and S. Villani, 336-39. Compatibility of nuclear reactor electric power stations.

Kernenergie, 6, No. 6 (1963).

P. Wenzel, 252-57. Investigations of uranium-plutonium cycles in application to water-moderated reactors.

B. Kozik, 257-63. Exact solution of the slowing-down equation for fast neutrons.

P. Liewers, 263-67. Global oscillator of the Rossendorf research reactor.

K. Fahrmann, 268-73. Shielding measurements on a VVR-S reactor.

H. Schmidt, 286-89. Large-surface area methane flow counter measures contamination by liquid radioactive wastes.

Kerntechnik, 5. No. 6 (1963).

K.-E. Betzler, 254-56. Design of the FRM reactor installation hot laboratory.

B. Schallopp, 257-65. Neutron absorbers for reactor control.

Nucl. Energy, July (1963).

D. Collins, 180-85. Prevention of leakage of fision fission products from nuclear reactors.

S. Van den Broek, 186-91. Lead shielding.

L. Gardiner, 191-95. General-purpose versatile manipulator.

N. Harris, 196-203. Survey of water-moderated USA reactors.

H. Atkins, 205-208. Maritime nuclear propulsion plants.

Nucl. Instrum. and Methods, 23, No. 1 (1963).

M. Ladu, 173-74. BF_3 response to fast neutrons in paraffin moderator.

Nucl. Sci. and Engng., 16, No. 1 (1963).

N. Katcher and W. Mackewicz, 31-38. Effect of boundary layer turbulence promoters on the local film coefficients of ML-1 fuel elements.

B. Chidley et al., 39-67. Neutron temperatures in a CANDU type power reactor.

C. Bigham et al., 68-84. Slowing-down spectrum in a CANDU type power reactor.

C. Bigham et al., 85-100. Neutron temperature distributions in a hot moderator cylinder.

J. Koppel, 101-110. Method for solving the neutron thermalization problem as a function of time.

M. Kalos, 111-117. Monte Carlo determination of flux at a point.

G. Bell et al., 118-23. Probable distribution of neutrons and precursors in a neutron-multiplying medium. II.

I. Asplund-Nilsson et al., 124-30. Absolute measurements of mean number of Cf^{252} neutrons.

R. Danofsky and R. Uhrig, 131-33. Kinetics of bound regions in the UTR-10 reactor.

J. Wilkins, 135-36. Reactor dynamics with specific reactivity and proportional energy losses.

H. Honeck and P. Michael, 140-42. Measurement of thermal diffusion coefficient.

Nucleonics, 21, No. 7 (1963).

---, 37-42. Characteristics of the Elk River boiling-water reactor.

W. Gunson et al., 43-47. Magnetohydrodynamic energy conversion.

I. Spiewak, 64-68. Large desalinization reactor based on current technology.

V. Materials for Atomic Industry

(Geology. Chemistry. Chemical Process Technology. Metallurgy).

Geokhimiya, No. 5 (1963).

R. P. Rafal'skii, 512-14. Note on conditions for migration and deposition of uranium via hydrothermal solutions, and on the role of complex formation in these processes.

G. B. Naumov, 514-18. On the role of complex formation in the transport and deposition of uranium by hydrothermal solutions.

Zhur. anal. khim., 18, No. 5 (1963).

M. K. Chmutova et al., 588-95. Solvent extraction of chelates of plutonium and other elements using N-benzoylphenylhydroxylamine.

Z. K. Karalova and A. A. Nemodruk, 615-17. Extraction-photometric determination of boron in uranium tetrafluoride.

Zhur. neorgan. khim., 8, No. 5 (1963).

V. A. Golovnya and L. K. Shubochkin, 1116-21. On the complex nature of uranyl acetates.

Zap. Vsesoyuz. mineralog. obshch., part 92, No. 2 (1963).

Yu. M. Dyshkov et al., 242-47. Pseudospherolites of uraninite.

Zap. Leningrad. gorn. inst., 45, No. 2 (1963).

Yu. N. Kapkov, 21-24. On readily soluble uranium in Sinian metamorphic rocks.

G. F. Novikov, 45-51. Note on the interpretation of gamma-ray logging charts in studying complex uranium-thorium-bearing ores.

V. A. Artsybashev, 52-60. Method for absolute measurements of the volume weight of rocks and ore by the attenuation of gamma rays in a broad beam.

V. A. Artsybashev, 61-67. Conversion factors for a quantitative interpretation of gamma-logging and gamma-logging of uraniferous ores.

Izvestiya akad. nauk SSSR, Otdel. khim. nauk, No. 4 (1963).

A. A. Tolstopyatova et al., 616-619. Catalytic properties of $-U_3O_8$ in dehydrogenation and dehydration reactions; bond energies of carbon, hydrogen, and oxygen with catalysts.

Izvestiya akad. nauk Uzbek.SSR, Seriya fiz. matem. nauk, No. 2 (1963)

S. V. Starodubtsev and A. E. Kiv, 41-43. Note on the mechanisms underlying radiation damage effect in crystals.

Trudy inst. geologii rudn. mestorozhdenii, petrografii, mineralogii i geokhimii, No. 99. Voprosy geokhimii, 5 (1963).

I. E. Smorchkov et al., 60-67. On the forms of uranium occurrence in granitoids of the Kuraminskii zone.

V. I. Danchev. On the classification of exogenetic uranium deposits.

J. Amer. Ceramic Soc., 46, No. 4 (1963).

P. Shalek, 155-160. Fabrication and properties of uranium and thorium monosulfides.

J. Nucl. Materials, 8, No. 3 (1963).

A. Accary, 281-306. Fabrication and shaping of uranium-carbon alloys.

K. Scott K. Harrison, 307-19. Research on the oxidation of uranium dioxide.

C. Motoc and I. Teodorescu, 320-28. Radiation effects in thin films.

B. Chandler et al., 329-47. Fabrication techniques and properties of beryllium oxide.

J. Nucl. Materials, 9, No. 1 (1963).

A. Boyd, 1-17. Radiolysis and pyrolysis of organic coolants.

I. Cohen and B. Schaner, 18-52. Metallographic and x-ray spectrographic investigation of the UO_2-ZrO_2 system.

A. Berndt, 53-58. Lattice constants of plutonium alloys in α-uranium at room temperature.

Y. Sokurski et al., 59-64. Anisotropy of surface properties of alpha-uranium. I. Anisotropy of cathodic etching.

H. Kelpfer, 65-84. Binary zirconium-niobium alloys for boiling-water reactors. I. II.

B. Cina, 85-100. Decomposition effects in PuO_2 after sintering.

S. Bronisz, 101-106. Mechanical properties of alpha-plutonium under compressive load.

C. Angerman, 109-110. Electron microscopy of uranium.

B. Cina, 111-113. Segregation effects in sintered UO_2-PuO_2 beads.

C. Rhodes and D. Kramer, 114-15. Note on gamma-gamma transformations in uranium with 33 a/o molybdenum.

E. Ruedl and S. Amelinckx, 116-19. Electron-microscopic investigation of dislocation lattices and radiation defects in α-uranium.

Kernenergie, 6, No. 6 (1963).

D. Naumann, 243-51. Regeneration of neutron-irradiated nuclear fuel by the halogenation method.

R. Münze and R. Reinhard, 274-76. Radiochemical studies of multiple uranium disintegration.

Nature, 198, No. 4883 (1963).

I. Mason and R. Knibbs, 850-51. Effect of crystal size on the specific thermal conductivity of irradiated polycrystalline graphite.

Nucl. Sci. and Engng., 16, No. 1 (1963).

R. Sowden and K. Francis, 1-24. Study of electrophoresis in plutonium oxide and thorium oxide slurries.

M. Lietzke et al., 25-30. Mathematical simulation of the solvent extraction of uranyl nitrate and nitric acid.

I. Amato et al., 137-40. Sintering of UO_2 in a carbon dioxide atmosphere.

Nucleonics, 21, No. 7 (1963).

D. Goslee, 48-52. Improving performance of stainless-steel-UO_2 cermet fuels.

M. Weech, 70-71. Boron permits larger reprocessing vessels.

Nukleonika, 8, No. 2 (1963)

B. Jezowska-Trzebiatowska and B. Kedzia, 100-115. Uranyl nitrate anhydrate and its spectral characteristics.

VI. Dosimetry and Radiometry. Nuclear Meteorology

Izvestiya akad. nauk SSSR. Seriya geofiz., No. 5 (1963).

Yu. A. Izrael', 818-24. Effect of microrelief of the earth's surface on the propagation of gamma radiation in the ground layer of the atmosphere.

Prikladn. geofizika, No. 36 (1963).

I. G. Dyad'kin and A. T. Lisinenkov, 233-35. Calculation of dose from a polonium-beryllium neutron source on the surface of a paraffin shield up to 60 cm thick.

Atomkernenergie, 8, No. 5 (1963).

T. Tuchscherer, 179-83. Effects of backscattering on the dose distribution from extended radiation sources.

H. Langendorff, 183-89. Note on minimum doses in chronic exposure of higher organisms to small doses of of x-rays and γ-rays.

Energia nucleare, 10, No. 6 (1963).

E. Cerrai et al., 315-18. Total radioactivity of plankton specimens collected in the Adriatic and Ligurian seas.

Nature, 198, No. 4886 (1963).

N. Jamagata, 1220-21. Contamination of leaves by fallout.

VII. Radioactive and Stable Isotopes

(Separation, production, applications)

Inzhener.-fiz. zhur., 6, No. 7 (1963).

N. B. Kondukov et al., 12-18. Investigation of parameters of particle motion in a fluidized bed by radiotracer methods. I.

Neftekhimiya, 3, No. 2 (1963).

Ya. D. Zel'venskii and V. L. Kochetkov, 285-95. Tracer study of adsorption purification of cyclohexane from benzene impurities

Tsvetnye metally, No. 4 (1963)

E. Buidosho et al., 50-55. Radiotracer study of dwell time and mixing time of material in autoclave continuous process banks in clay processing mills.

Atomkernenergie, 8, No. 6 (1963).

C. Torre, 226-31. Distribution of radioactive isotopes in ground water.

Atomwirtschaft, 8, No. 6 (1963).

---, 342-52. Nuclear engineering and the petroleum industry.

J. Leger, 376-78. Development of industrial isotope application techniques in France.

Chem. and Engng. News, 41, No. 21 (1963).

Single-state separation of radioactive isotopes by extraction.

Industries atomiques, 7, No. 5/6 (1963)

J. Kuba, 85-93. Application of radioactive isotopes in process measurement, control, and automation.

Kernenergie, 6, No. 6 (1963).

H. Westmeyer, 276-79. How to measure moisture with neutrons.

R. Schroller and H. Stiede, 279-85. Measuring moisture of molding sand with a boron counter probe.

Kerntechnik, 5, No. 6 (1963).

H. Koch and B. Koch, 248-51. Activation analysis determines purity of selenium.

H. Timm, 253-54. Novel special device hermetically seals standard aluminum irradiation capsules.

Nature, 198, No. 4882 (1963).

A. Breccia and F. Spalletti, 756-58. Rapid separation of radioisotopes by thin-layer chromatography.

Nucleonics, 21, No. 7 (1963).

D. Chleck et al., 53-55. Kryptonates: Kr^{85} becomes a universal tracer.

L. Bate, 72-75. Nucleonic techniques of oxygen analysis.

Jaderna Energie, No. 10 (1963).

Editorial: The 65th birthday of Academician Behounek.

V. Santholcer. Nuclear fallout following the tests of the 1961-1963 megaton atomic bombs.

J. Klumpar and M. Majerova, Correction for absorption in substrate in calibrating beta emitter sources in a counter of 4π geometry.

Z. Kovar. Simple calorimetric method measures x-ray dosage.

J. Benes. Isolating carrier-free Th^{234}.

M. Mozisek. New device measures mass of cord impregnating solution.

M. Podest and L. Jakesova, Note on the theory of the fabrication of compact pellets of uranium dioxide by powder metallurgy.

D. Jakes and L. Sedlakova. Note on the relations between lattice parameters and the composition of epistoichiometric uranium dioxide.

L. Jakesova. Problems in the fabrication technology of uranium monocarbide and uranium mononitride.

Z. Spurny, J. Sulcova, and J. Hruska. Chemical gamma-ray dosimeter is insensitive to neutrons.

F. Kochol. Rapid analysis of type and activity of radiographic emitters.

Soviet Journals Available in Cover-to-Cover Translation

ABBREVIATION	RUSSIAN TITLE		TITLE OF TRANSLATION	PUBLISHER	TRANSLATION Vol.	Issue	BEGAN Year
AÉ	Atomnaya énergiya		Soviet Journal of Atomic Energy	Consultants Bureau	1	1	1956
Akust. zh.	Akusticheskii zhurnal		Soviet Physics – Acoustics	American Institute of Physics	1	1	1955
Astr(on). zh(urn).	Astronomicheskii zhurnal		Soviet Astronomy – AJ	American Institute of Physics	34	1	1957
Avto(mat). svarka	Avtomaticheskaya svarka		Automatic Welding	Br. Welding Research Assn. (London)	12	1	1959
	Avtomatika i Telemekhanika		Automation and Remote Control	Instrument Society of America	27	1	1956
	Biofizika		Biophysics	National Institutes of Health**	6	1	1961
	Biokhimiya		Biochemistry	Consultants Bureau	21	1	1956
Byull. éksp(erim). biol. (i med.)	Byulleten' éksperimental'noi biologii i meditsiny		Bulletin of Experimental Biology and Medicine	Consultants Bureau	41	1	1959
DAN (SSSR) Dokl(ady) AN SSSR	Doklady Akademii Nauk SSSR	The translation of this journal is published in sections	Doklady Biological Sciences Sections (includes: Anatomy, biochemistry, biophysics, cytology, ecology, embryology, endocrinology, evolutionary morphology, genetics, histology, hydrobiology, microbiology, morphology, parasitology, physiology, zoology) — Life Sciences	National Science Foundation*	112	1	1957
			Doklady Botanical Sciences Sections (includes: Botany, phytopathology, plant anatomy, plant ecology, plant embryology, plant physiology, plant morphology) — Life Sciences	National Science Foundation*	112	1	1957
			Proceedings of the Academy of Sciences of the USSR, Section: Chemical Technology — Chemical Sciences	Consultants Bureau	106	1	1956
			Proceedings of the Academy of Sciences of the USSR, Section: Chemistry — Chemical Sciences	Consultants Bureau	106	1	1956
			Proceedings of the Academy of Sciences of the USSR, Section: Physical Chemistry — Chemical Sciences	Consultants Bureau	112	1	1957
			Doklady Earth Sciences Sections (includes: Geochemistry, geology, geophysics, hydrogeology, lithology, mineralogy, oceanology, paleontology, permafrost, petrography) — Earth Sciences	American Geological Institute	124	1	1959
			Proceedings of the Academy of Sciences of the USSR, Section: Geochemistry — Earth Sciences	Consultants Bureau	106-123	1 6	1956-1958
			Proceedings of the Academy of Sciences of the USSR, Section: Geology — Earth Sciences	Consultants Bureau	112-123	1 6	1957-1958
			Soviet Mathematics – Doklady — Mathematics	American Mathematical Society	130	1	1960
			Soviet Physics – Doklady (includes: Aerodynamics, astronomy, crystallography, cybernetics and control theory, electrical engineering, energetics, fluid mechanics, heat engineering, hydraulics, mathematical physics, mechanics, physics, technical physics, theory of elasticity sections) — Physics	American Institute of Physics	106	1	1956
	Elektrosvyaz'		Telecommunications	Am. Inst. of Electrical Engineers		1	1957
Entom(ol). oboz(r).	Entomologicheskoe obozrenie		Entomological Review	National Science Foundation**		1	1958
FMM	Fizika metallov i metallovedenie		Physics of Metals and Metallography	Acta Metallurgica	37	1	1957
FTT, Fiz. tv(erd). tela	Fizika tverdogo tela		Soviet Physics – Solid State	American Institute of Physics	5	1	1959
Fiziol. Zh(urn). SSSR	Fiziologicheskii zhurnal imeni I.M. Sechenov		Sechenov Physiological Journal USSR	National Institutes of Health**	1	1	1961
Fiziol(ogiya) rast.	Fiziologiya rastenii		Plant Physiology	National Science Foundation*	47	1	1961
	Geodeziya i aerofotosyemka		Geodesy and Aerophotography	American Geophysical Union	4	1	1957
	Geokhimiya		Geochemistry	The Geochemical Society			1962
Geol. nefti i gaza	Geologiya nefti i gaza		Petroleum Geology	Petroleum Geology	1	1	1956
	Geomagnetizm i aeronomiya		Geomagnetism and Aeronomy	American Geophysical Union	2	1	1958
	Iskusstvennye sputniki zemli		Artificial Earth Satellites	Consultants Bureau	1	1	1961
Izmerit. tekhn(ika)	Izmeritel'naya tekhnika		Measurement Techniques	Instrument Society of America	1	1	1958
					7	1	1958

Izv. AN SSSR O(td). Kh(im). N(auk)	Izvestiya Akademii Nauk SSSR: Otdelenie khimicheskikh nauk	Bulletin of the Academy of Sciences of the USSR: Division of Chemical Science	Consultants Bureau	16	1	1952
Izv. AN SSSR O(td). T(ekhn). N(auk): Metall). i top.	(see Met. i top)					
Izv. AN SSSR Ser. fiz(ich).	Izvestiya Akademii Nauk SSSR: Seriya fizicheskaya	Bulletin of the Academy of Sciences of the USSR: Physical Series	Columbia Technical Translations	18	3	1954
Izv. AN SSSR Ser. geofiz.	Izvestiya Akademii Nauk SSSR: Seriya geofizicheskaya	Bulletin of the Academy of Sciences of the USSR: Geophysics Series	American Geophysical Union	7	1	1957
Izv. AN SSSR Ser. geol.	Izvestiya Akademii Nauk SSSR: Seriya geologicheskaya	Bulletin of the Academy of Sciences of the USSR: Geologic Series	American Geological Institute	23	1	1958
Iz. Vyssh. Uch. Zav., Tekh. Teks. Prom.	Izvestiya Vysshikh Uchebnykh Zavedenii Tekhnologiya Tekstil'noi Promyshlennosti	Technology of the Textile Industry, USSR	The Textile Institute (Manchester)	4	1	1960
Kauch. i rez.	Kauchuk i rezina	Soviet Rubber Technology	Palmerton Publishing Company, Inc.	18	3	1959
	Kinetika i kataliz	Kinetics and Catalysis	Consultants Bureau	1	1	1960
	Koks i khimiya	Coke and Chemistry, USSR	Coal Tar Research Assn. (Leeds, England)		8	1959
Kolloidn. zh(urn).	Kolloidnyi zhurnal	Colloid Journal	Consultants Bureau	14	1	1952
	Kristallografiya	Soviet Physics – Crystallography	American Institute of Physics	2	1	1957
Metallov. i term.	Metallovedenie i termicheskaya obrabotka metallov	Metals Science and Heat Treatment of Metals	Acta Metallurgica	6	1	1958
	Metallurg	Metallurgist	Acta Metallurgica		1	1957
Met. i top.(gorn.)	Metallurgiya i toplivo (gornoye delo)	Russian Metallurgy and Fuels (mining)	Scientific Information Consultants, Ltd.		1	1960
Mikrobiol.	Mikrobiologiya	Microbiology	National Science Foundation*	26	1	1957
	Ogneupory	Refractories	Acta Metallurgica	25	1	1960
OS, Opt. i spektr.	Optika i spektroskopiya	Optics and Spectroscopy	American Institute of Physics	6	1	1959
Paleontol. Zh(urn)	Paleontologicheskii Zhurnal	Journal of Paleontology	American Geological Institute		1	1962
	Pochvovedenie	Soviet Soil Science	National Science Foundation**	53	1	1958
	Poroshkovaya Metallurgiya	Soviet Powder Metallury and Metal Ceramics	Consultants Bureau	2	1	1962
	Priborostroenie	Instrument Construction	Taylor and Francis, Ltd. (London)	4	1	1959
Pribory i tekhn. éks(perimenta)	Pribory i tekhnika éksperimenta	Instruments and Experimental Techniques	Instrument Society of America	3	1	1958
Prikl. matem. i mekh(an).	Prikladnaya matematika i mekhanika	Applied Mathematics and Mechanics	Am. Society of Mechanical Engineers	22	1	1958
PTE	(see Pribory i tekhn. éks.)					
	Problemy Severa	Problems of the North	National Research Council of Canada		1	1958
	Radiokhimiya	Radiochemistry	Consultants Bureau	4	1	1962
Radiotekh.	Radioteknika	Radio Engineering	Am. Institute of Electrical Engineers	16	1	1961
Radiotekhn. i élektron(ika)	Radiotekhnika i électronika	Radio Engineering and Electronic Physics	Am. Institute of Electrical Engineers	6	1	1961
	Stal'	Stal (in English)	Iron and Steel Institute	19	1	1959
	Stanki i instrument	Machines and Tooling	Production Engineering Research Assoc.	30	1	1959
Stek. i keram.	Steklo i keramika	Glass and Ceramics	Consultants Bureau	13	1	1956
Svaroch. proiz-vo	Svarochnoe proizvodstvo	Welding Production	Br. Welding Research Assn. (London)	5	4	1959
Teor. veroyat. i prim.	Teoriya veroyatnostei i ee primenenie	Theory of Probability and Its Application	Soc. for Industrial and Applied Math.	1	1	1956
Tsvet. metally	Tsvetnye metally	The Soviet Journal of Nonferrous Metals	Primary Sources	33	1	1960
UFN	Uspekhi fizicheskikh nauk	Soviet Physics – Uspekhi (partial translation)	American Institute of Physics	66	1	1958
UKh, Usp. khimii	Uspekhi khimii	Russian Chemical Reviews	Chemical Society (London)	29	1	1960
UMN	Uspekhi matematicheskaya nauk	Russian Mathematical Surveys	Cleaver-Hume Press, Ltd. (London)	15	1	1960
Vest. mashinostroeniya	Vestnik mashinostroeniya	Russian Engineering Journal	Production Engineering Research Assoc.	39	4	1959
Vop. onk(ol).	Voprosy onkologii	Problems of Oncology	National Institutes of Health**	7	1	1961
Zav(odsk). lab(oratoriya)	Zavodskaya laboratoriya	Industrial Laboratory	Instrument Society of America	24	1	1958
ZhAKh, Zh. anal(it). Khim(ii)	Zhurnal analiticheskoi khimii	Journal of Analytical Chemistry	Consultants Bureau	7	1	1952
ZhETF Zh. éksperim. i teor. fiz.	Zhurnal eksperimental'noi i teoreticheskoi fiziki	Soviet Physics – JETP	American Institute of Physics	28	1	1955
ZhFKh Zh. fiz. khimii	Zhurnal fizicheskoi khimii	Russian Journal of Physical Chemistry	Chemical Society (London)	33	7	1959
ZhNKh Zh. neorg(an). khim.	Zhurnal neorganicheskoi khimii	Journal of Inorganic Chemistry	Chemical Society (London)	4	1	1959
ZhOKh Zh. obshch. khim.	Zhurnal obshchei khimii	Journal of General Chemistry USSR	Consultants Bureau	19	1	1949
ZhPKh Zh. prikl. khim.	Zhurnal prikladnoi khimii	Journal of Applied Chemistry USSR	Consultants Bureau	23	1	1950
ZhSKh Zh. strukt(urnoi) khim.	Zhurnal strukturnoi khimii	Journal of Structural Chemistry	Consultants Bureau	1	1	1960
ZhTF	Zhurnal tekhnicheskoi fiziki	Soviet Physics – Technical Physics	American Institute of Physics	26	1	1956
Zh. tekhn. fiz.	Zhurnal vychislitel'noi matematika i matematicheskoi fiziki	U.S.S.R. Computational Mathematics and Mathematical Physics	Pergamon Press, Inc.	1	1	1962
Zh. vyssh. nervn. deyat. (im. Pavlova)	Zhurnal vysshei nervnoi deyatel'nosti (im I. P. Pavlova)	Pavlov Journal of Higher Nervous Activity	National Institutes of Health**	11	1	1961

*Sponsoring organization. Translation published by Consultants Bureau.
**Sponsoring organization. Translation published by Scripta Technica.

SOVIET MASER RESEARCH

Edited by Academician D.V. Skobel'tsyn

Reports of four coordinated researches into the theory and applications of masers for frequency standards, Conducted at the **P.N. Lebedev Physics Institute** under the guidance of **Academician A. M. Prokorov.** Transactions (Trudy) No. 21.

A THEORETICAL STUDY OF THE FREQUENCY STABILITY OF A MASER

by A. I. Oraevskii

The article presents a general analysis of the functioning of a molecular generator or maser operating with a molecular beam of "sorted" molecules. Effects of external perturbations (pressure and magnetic field effects) are treated, and the problem of hyperfine structure of the emission line is considered. Cases treated in detail are those of masers using inversion transitions in ammonia. Some comparisons between theoretical and experimental results are given for such cases.

INVESTIGATION OF THE CHARACTERISTICS OF MASERS ($J = 3, K = 3$ in ammonia $N^{14}H_3$)

by G. M. Strakhovskii and I. V. Cheremiskii

The authors report experimental investigations into the dependence of frequency and relative power of an ammonium maser, $N^{14}H_3$, on the natural frequency of the resonator, the voltage applied to the quadrupole condenser (or to a circular separation system) and the ammonia pressure in the molecular beam source. Also reported on is the dependence of frequency and relative power of a maser with two intersecting beams on ammonia pressure in the molecular beam source.

THEORY OF THE HYPERFINE STRUCTURE OF THE ROTATIONAL SPECTRA OF MOLECULES

by K. K. Svidzinskii

A theory of the hfs has been developed which allows the calculation of hyperfine effects in rotational spectra of molecules (in a nondegenerate electronic ground state) with an accuracy not lower than 10 cps. By applying methods of group theory, especially the apparatus of irreducible tensor operators and the 3nj-symbols, the calculation of hfs has been successfully simplified and standardized.

In order to provide the necessary accuracy (not lower than 10 cps), the present treatment includes, besides the usual dipole and quadrupole interactions, the magnetic octupole and the electric hexadecapole interactions. A general calculation of the energy of the spin-spin interactions of nuclei in a rotating molecule is presented, along with a general expression for the energy of the dipole I·J interaction in the asymmetric-top molecule.

THE ND_3 MASER

by N. G. Basov, V. S. Zuev, and K. K. Svidzinskii

Reports work aimed at investigating the possibility of making a maser using inversion transitions of heavy ammonia ND_3, including the accomplishment of a working model. The power output of the ND_3 maser is reported as 10^{-11} watt at 1656·18 mc ($J=6$, $K=6$ line in the inversion spectrum of ND_3). The absolute stability of the line, according to preliminary data, is of the order of 10^{-9}.

The results of calculations on the hyperfine inversion spectrum of ND_3 are given. Analysis of the hyperfine structure leads to an estimate for the absolute stability of the $J=6$, $K=6$ line ($\sim 10^{-6}$).

SOVIET MASER RESEARCH contains a unique bibliography of all work performed in the Laboratory of Oscillations FIAN, P. N. Lebedev Institute from 1935-1961, and covers topics such as: Electron paramagnetic resonance; Quantum electronics; Molecular generators and amplifiers; Time standards; Gas radiospectroscopy; Propagation of radio waves; Statistical radiophysics; Accelerators; and various other problems.

Over 200 pages | Translated from Russian | $27.50

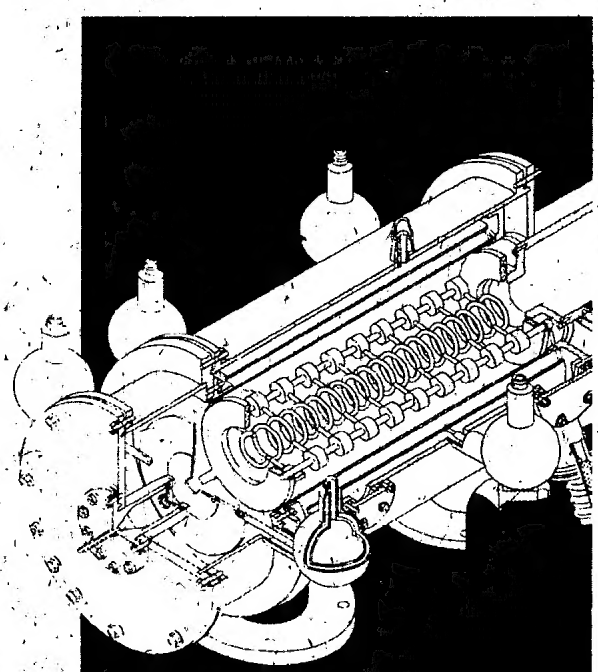

RENEWAL REMINDER

THIS VOLUME WILL SOON BE COMPLETED.

HAVE YOU PLACED YOUR RENEWAL ORDER?

Declassified and Approved For Release 2013/02/25 :
CIA-RDP10-02196R000600110003-4